

New Sand Control Design Criteria and Evaluation Testing for Steam Assisted Gravity Drainage  
(SAGD) Wellbores

by

Mahdi Mahmoudi Eshkaftaki

A thesis submitted in partial fulfillment of the requirements for the degree of

Doctor of Philosophy

in

PETROLEUM ENGINEERING

Department of Civil and Environmental Engineering

University of Alberta

## ABSTRACT

This thesis presents experimental results obtained using a novel Sand Retention Testing (SRT) facility. The testing results and interpretations provide an improved understanding of the parameters that affect sand control performance in Steam Assisted Gravity Drainage (SAGD) operations. The SRT testing data are used to develop a set of new design criteria for slotted liners based on parametric testing.

The SRT facility was designed and commissioned to address limitations in existing testing methods for sand control evaluation. The facility uses multiple slots in the slotted liner coupon instead of a single slot in the existing facilities. Measurements are also improved by obtaining pore pressures along the sand pack in addition to the pressure drop across the liner coupon to assess the retained permeability and flow convergence. More realistic methods are designed and used for sand pack preparation, fluid injection, and sample saturation than the existing practices. The testing also includes post-mortem analysis to measure fines/clay content above the screen and in the produced fluids to evaluate fines migration and the potential for pore plugging.

Slotted liner coupons in this research vary in slot size and density and are tested for select PSDs. Testing data are analyzed to evaluate existing heuristic liner design models and propose new design criteria.

Test measurements and observations indicate that the sand packs preparation procedure, injected fluid velocity, and ionic concentrations highly affect the testing results. For typical field porosities and PSDs, sand production is observed to stay within acceptable limits for the screens designed based on existing models.

Data also indicate improved retained permeability for higher slot density, which levels off at high slot densities. The optimum slot width is also determined for minimal plugging and acceptable sanding levels.

Measurements indicate that the skin buildup due to pore plugging caused by fines migration is reduced by increasing the slot width. However, the increase of the slot width beyond a certain level does not reduce the skin any further and only contributes to higher levels of sanding.

The parametric testing allows finding the limits for the slot width beyond which the plugging condition is not further improved and, at the same time, the sanding is kept within acceptable levels. These findings lead to the formulation of an optimum liner design model that would result in minimal plugging, coupled with acceptable amounts of sand production.

## **ACKNOWLEDGEMENTS**

I sincerely thank my parents, my wife, and son for their love, devotion, and continued encouragement to gain further education.

I am very thankful to my supervisor, Dr. Alireza Nouri, for giving me the opportunity to work on this project, for all of his encouragement and support, and for granting me freedom to explore my ideas.

In addition, I am very thankful to my colleague, Dr. Vahiddodin Fattahpour, for his help with this project.

I would also like to thank all my committee members, Dr. Hassan Dehghanpour, Dr. Lijun Deng, Dr. Carlos Lange, and Dr. Jalal Abedi for their valuable suggestions to improve my thesis.

I would like to acknowledge RGL reservoir management Inc. for their technical and financial support and Natural Sciences and Engineering Research Council of Canada (NSERC) for funding this project through their Collaborative Research and Development (CRD) Grants Program.

Finally, I would like to thank all those who assisted me throughout my research.

## TABLE OF CONTENTS

ABSTRACT.....	ii
ACKNOWLEDGEMENTS.....	iv
LIST OF FIGURES .....	xi
LIST OF SYMBOLS AND ABBREVIATIONS .....	xix
CHAPTER ONE: INTRODUCTION.....	1
1.1 Background .....	1
1.2 Statement of the problem.....	3
1.3 Research objectives.....	3
1.4 Research hypothesis.....	4
1.5 Research steps .....	4
1.6 Significance of the work.....	5
1.7 Thesis outline .....	6
CHAPTER TWO: LITERATURE REVIEW.....	8
2.1 Introduction.....	8
2.2 Failure mechanisms of slotted liners .....	9
2.2.1 Excessive sand production.....	9
2.2.2 Plugging.....	10
2.2.3 Steam breakthrough .....	19
2.2.4 Corrosion and erosion .....	19
2.2.5 Scaling.....	19
2.3 Design and evaluation of sand control screens.....	19
2.3.1 Particle size distribution/shape analysis.....	19
2.3.2 Sand control design.....	20
2.3.3 Screen Performance Indicators .....	25

2.3.4 Current Design Criteria for Sand Control Screens .....	26
2.5 Summary.....	27
CHAPTER THREE: OIL SAND AND COMMERCIAL SAND AND FINES CHARACTERIZATION .....	33
3.1 Introduction.....	33
3.1.1 Particle size distribution (PSD).....	33
3.1.2 Particle shape .....	33
3.1.3 Mineralogical composition .....	35
3.1.4 Particle surface texture.....	35
3.2. Particle size and shape parameters .....	35
3.2.1 Particle size description and measurement .....	36
3.2.2 Particle shape description and measurement .....	38
3.3. Particle shape and PSD of the oil sand in McMurray Formation .....	40
3.3.1 Geological description of oil sands in McMurray Formation.....	41
3.3.2 Particle size distribution of oil sands in the McMurray Formation .....	42
3.3.3 Particle size distribution of the commercial sands and fines .....	42
3.3.4 Particle shape of the oil sands in McMurray Formation.....	43
3.3.5 Particle shape of the commercial sand.....	43
3.4 Dynamic image analysis for different size groups.....	43
3.5 Mineralogy testing .....	45
3.6 Surface texture of particles .....	45
3.7 Conclusions .....	46
CHAPTER FOUR: INVESTIGATION INTO THE USE OF COMMERCIAL SANDS AND FINES TO REPLICATE OIL SANDS FOR LARGE-SCALE SAND CONTROL TESTING ..	68
4.1 Introduction.....	68
4.2 Preparation of oil sands and commercial sand samples.....	69

4.3 Replicating McMurray Formation oil sand with commercial sands and fines .....	69
4.3.1 PSD replication .....	69
4.3.2 Shape variation comparison .....	70
4.2.4 Mechanical tests .....	70
4.3 Conclusions .....	71
CHAPTER FIVE: EXPERIMENTAL SET-UP AND TESTING PROCEDURE .....	81
5.1 Introduction .....	81
5.2 Experimental set-up .....	81
5.2.1 SRT cell and accessories .....	81
5.2.2 Flow injection unit .....	82
5.2.3 Pressure and fluid flow rate measurement unit .....	82
5.2.4 Fines and sand production measurement .....	83
5.2.5 Data acquisition system .....	83
5.3 Test procedure .....	83
5.3.1 Sand pack preparation .....	83
5.3.2 Sample saturation .....	84
5.3.3 Step-rate fluid flow injection .....	84
5.3.4 Post-mortem analysis .....	85
5.3.5 Test assumptions and limitations .....	85
5.4 Test plan .....	86
5.5 SRT testing repeatability .....	87
CHAPTER SIX: AN EXPERIMENTAL INVESTIGATION OF THE EFFECT OF pH AND SALINITY ON SAND CONTROL PERFORMANCE FOR HEAVY OIL THERMAL PRODUCTION .....	94
6.1 Introduction .....	94
6.2 Composition of the produced and formation water .....	95

6.3 Effect of pH and salinity on clay/fines migration .....	96
6.4 Testing program.....	98
6.4 Results and discussions .....	98
CHAPTER SEVEN: EFFECT OF SLOT WIDTH AND DENSITY ON FINES MIGRATION AND PRODUCTION IN SAGD OPERATIONS .....	109
7.1 Introduction.....	109
7.2 Testing program.....	111
7.3 Results and discussions.....	111
7.4 Conclusions .....	114
CHAPTER EIGHT: EFFECT OF SLOT WIDTH AND DENSITY ON SAND PRODUCTION IN SAGD OPERATIONS .....	132
8.1 Introduction.....	132
8.2 Testing program.....	134
8.3 Results and Discussion .....	134
8.3 Conclusion .....	138
CHAPTER NINE: NEW CRITERIA FOR SLOTTED LINER DESIGN FOR HEAVY OIL THERMAL PRODUCTION .....	164
9.1 New design criteria for slotted liners .....	164
9.1.1 Traffic light design approach.....	165
9.1.2 Acceptable sanding limits.....	165
9.1.3 Flow performance and plugging tendency.....	166
9.1.4 Design and SRT testing assumptions.....	167
9.1.5 New criteria for slotted liner design.....	168
9.1.6 Incorporation of flow rate in the design criteria .....	169
9.2 Conclusions .....	169
CHAPTER TEN: CONCLUSIONS AND FUTURE WORKS.....	185



10.1 Main results .....	185
10.2 Main contributions .....	186
10.2.1 Sand production .....	186
10.2.2 Plugging .....	186
10.2.3 Sanding Criteria .....	187
10.3 Recommendations for further research .....	187
10.3.1 Investigate the effect of multiphase flow .....	187
10.3.2 Effect of PSD curve on sand production and plugging.....	187
10.3.3 Effect of stress on sand production and plugging.....	188
10.3.4 Effect of particle shape on sand production and plugging.....	188
10.3.5 Effect of clay composition on the pore plugging.....	188
REFERENCES .....	189
APPENDIX A: CURRENT INDUSTRIAL DESIGN PROCEDURES .....	209
A.1 Slot Width .....	209
A.2 Slot Profile .....	210
A.3 Slot Density.....	210

## LIST OF TABLES

Table 2-1. Typical chemical composition of clay, presented in percentages by weight (from Khilar and Fogler, 1998).....	29
Table 2-2. Composition of produced water for different SAGD projects (NM: Not Mentioned)	29
Table 3-1. Examples of shape factors for known shapes.....	46
Table 3-2. PSD indices and shape factors for oil sands from different depths of McMurray Formation in Well A.....	47
Table 3-3. PSD indices and shape factors for oil sands from different depths of McMurray Formation in Well B.....	48
Table 3-4. PSD indices and shape factors for the commercial sands.....	48
Table 3-5. Composition of the percentage of the clays in the fines (<44µm) of the oil sands.....	48
Table 3-6. Composition of the particle larger than 44µm in oil sands from both wells.....	49
Table 3-7. XRD results of the commercial sands. All values are in percentage.....	49
Table 4-1. Friction angle results for oil sands and the representative commercial replica. Sample names present depth and PSD class.....	73
Table 5-1. Testing plan to study the role pH and salinity on retained permeability.....	88
Table 5-2. Testing plan to study the role of slot width and slot density.....	88
Table 6-1. Composition of produced water for different SAGD projects.....	101
Table 7-1. Average pore throat size calculated based on different methods.....	116
Table 9-1. TLS color code definition for sand production and flow performance.....	171
Table A-1. The input values from the PSD curve into slot size model.....	212
Table A-2. Slot model for the four class of sand of the McMurray Formation.....	212

## LIST OF FIGURES

Figure 1-1. Different sand control screens and comparison of their OFA.....	7
Figure 1-2. Common sand control screens in SAGD wells .....	7
Figure 1-3. Different sand control screen and comparison of their OFA .....	7
Figure 2-1. Workflow of the current screen design approach .....	30
Figure 2-2. Schematic representation of deposited mineral layers: (a) silica, (b) kaolinite, (c) chlorite and (d) smectite /montmorillonite. (After Jeannin et al. 2010) .....	30
Figure 2-3. McMurray Formation water TDS in the Athabasca oil sands region, overlain on ground surface elevation (Cowie, 2013).....	31
Figure 2-4. Three mechanisms for permeability reduction caused by changing the ionic condition of the environment for clay particles: (a) Migration, (b) Swelling and (c) Swelling-induced migration (Mohan et al. 1993) .....	32
Figure 2-5. Liner damage after four years of production (After Hallman et al. 2015).....	32
Figure 3-1. The Concept of elliptical representation of a particle .....	49
Figure 3-2. Particle shape determination (sphericity, S and roundness, R) chart, modified version from Krumbein and Sloss (1963).....	50
Figure 3-3. Geological log for Well A in McMurray Formation.....	51
Figure 3-4. Comparison between the PSD from image analysis and dry sieve .....	52
Figure 3-5. PSD for oil sand samples from different depths of McMurray Formation in Well A	52
Figure 3-6. PSD for oil sand samples from different depths of McMurray Formation in Well B	53
Figure 3-7. Four Representative PSDs provided by Abram and Cain (2014) .....	53
Figure 3-8. PSD for seven different available commercial sands.....	54
Figure. 3-9. PSD for ten different available commercial fine-grained materials.....	54
Figure 3-10. Comparison between shape factors, (a) sphericity, (b) convexity and (c) aspect ratio, for commercial sands and oil sands for Well A and B .....	56
Figure 3-11. Distribution of shape factors for different particle sizes for samples from different depths of Well A and B. Legend indicates sample depth .....	57
Figure 3-12. SEM images from silts and sands from Well A and B and commercial sands .....	67
Figure 4-1. Four Representative PSD's provided by Abram and Cain (2014).....	74
Figure 4-2. Comparison between the PSD for oil sand samples (OS-A) from depth 173.47 m in Well B and commercial sand CS-C .....	74

Figure 4-3. Comparison between the convexity for an oil sand sample (OS-A) from 173.47 m depth in Well B and commercial sand type C (CS-C).....	75
Figure 4-4. Comparison between the sphericity for oil sand sample OS-A from 173.47 m depth in Well B and commercial sand CS-C .....	75
Figure 4-5. Comparison between the aspect ratio for oil sand sample OS-A from 173.47 m depth in Well B and commercial sand CS-C .....	76
Figure 4-6. Combination of the commercial sand and fine silts to duplicate four classes of oil sands presented by Abram and Cain (2014) .....	77
Figure 4-7. Comparison of shape factor distribution for different particle sizes for oil sands with the PSD of DC-II (a, c and e) and DC-III (b, d, and f) and the corresponding replicas .....	78
Figure 4-8. Direct shear testing results for (a) oil sands samples from Well A and B, (b) the commercial replica.....	79
Figure 4-9. 1D consolidation testing results for oil sands and corresponding commercial replica with the PSD of (a) DC-I, (b) DC-II, (c) DC-III, (d) DC-IV.....	80
Figure 5-1. Schematic view of different units of the SRT facility.....	89
Figure 5-2. Multi-slot coupon schematic, (a) the representation of the multi-slot coupons as a section of a 7-inch liner, (b) SPC and slot patterns of the tested coupons for pre-packed SRT tests; three SPC of 30, 42 and 54 and six slot widths of 0.018” to 0.010”, 0.022” to 0.014”, 0.026” to 0.018”, 0.030” to 0.022”, 0.032” to 0.026”, and 0.040” to 0.032” are tested. All dimensions are in inch .....	90
Figure 5-3. Multi-slot coupon with seamed slots of 0.022” to 0.014” aperture .....	90
Figure 5-4. Fitting and connection in the back of coupon for pressure measurements, the yellow tube is to take the sample of the outflow from the center slot during the tests.....	91
Figure 5-5. Injected PVs for step rate tests in pre-packed SRT tests on sand packs prepared by different PSDs: (a) DC-III and (b) DC-II .....	92
Figure 5-6. Comparison of the retained permeability for the repeated tests.....	93
Figure 5-7. Cumulative produced sand for the repeatability tests .....	93
Figure 6-1. McMurray Formation water TDS in Athabasca oil sands region, overlain on ground surface elevation (Cowie, 2013) .....	102

Figure 6-2. Three mechanisms for permeability reduction caused by changing the ionic condition of the environment for clay particles: (a) Migration, (b) Swelling and (c) Swelling-induced migration (Mohan et al. 1993) .....	102
Figure 6-3. SRT results for the constant pH value of 6.8 and different salinities: (a) retained permeability, (b) fines production, (c) pH of produced fluid and (d) D50 of produced fines for different flow rates .....	103
Figure 6-4. SRT results for the constant pH value of 7.9 and different salinities: (a) retained permeability, (b) fines production, (c) pH of produced fluid and (d) D50 of produced fines for different flow rates .....	104
Figure 6-5. SRT results for constant pH value of 8.8 and different salinities: (a) retained permeability, (b) fines production, (c) pH of produced fluid and (d) D50 of produced fines for different flow rates .....	105
Figure 6-6. SRT results for the constant salinity of 0% and different pH values: (a) retained permeability, (b) fines production, (c) pH of produced fluid and (d) D50 of produced fines for different flow rates .....	106
Figure 6-7. SRT results for the constant salinity of 0.7% and different pH values: (a) retained permeability, (b) fines production, (c) pH of produced fluid and (d) D50 of produced fines for different flow rates .....	107
Figure 6-8. SRT results for the constant salinity of 1.4% and different pH values: (a) retained permeability, (b) fines production, (c) pH of produced fluid and (d) D50 of produced fines for different flow rates .....	108
Figure 7-1. For DC-II (a) effect of slot density on the concentration of fines near the screen, (b) effect of slot width on the concentration of fines near the screen .....	117
Figure 7-2. For DC-II: (a) effect of slot density on cumulative fines production, (b) effect of slot size on cumulative fines production .....	117
Figure 7-3. For DC-II: (a) effect of slot size on fines production for different flow rates at SPC=30, (b) effect of slot size on fines production for different flow rates at SPC=42, (c) effect of slot size on fines production for different flow rates at SPC=54, (d) fines production for different flow rates and different slot density and width .....	118
Figure 7-4. For DC-II: (a) D50 of produced fines for different flow rates at SPC=30 and different slot widths, (b) D50 of produced fines for different flow rates at SPC=42 and different slot	

width, (c) D50 of produced fines for different flow rates at SPC=54 and different slot width, (d) D50 of produced fines for different flow rates and different slot density and width.....	119
Figure 7-5. For DC-III: (a) effect of slot density on the concentration of fines near the screen, (b) effect of slot width on the concentration of fines near the screen .....	120
Figure 7-6. For DC-III: (a) effect of slot density on cumulative fines production, (b) effect of slot size on cumulative fines production .....	120
Figure 7-7. For DC-III: (a) effect of slot size on fines production for different flow rates at SPC=30, (b) effect of slot size on fines production for different flow rate at SPC=42, (c) effect of slot size on fines production for different flow rates at SPC=54, and (d) fines production for different flow rates and different slot densities and widths .....	121
Figure 7-8. For DC-III: (a) D50 of produced fines for different flow rates at SPC=30 for different slot width, (b) D50 of produced fines for different flow rates at SPC=42 for different slot width, (c) D50 of produced fines for different flow rates at SPC=54 for different slot width, (d) D50 of produced fines for different flow rates and different slot density and width.....	122
Figure 7-9. Retained permeability of sand packs versus flow rate for DC-II (a) for different slot width and SPC=30, (c) for different slot width and SPC=42, (e) for different slot width and SPC=54; solid red line shows the suggested threshold for acceptable retained permeability for SRT .....	124
Figure 7-10. Retained permeability of sand packs versus flow rate for DC-III (a) for different slot width and SPC=30, (b) for different slot width and SPC=42, (c) for different slot width and SPE= 54; solid red line shows the suggested threshold for acceptable retained permeability for SRT .....	125
Figure 7-11. Retained permeability versus flow rate for DC-II (a) slot width of 0.026", (b) slot width of 0.022", (c) slot width of 0.018", (d) slot width of 0.014", (e) slot width of 0.010"; Solid red line shows the suggested threshold for acceptable retained permeability for SRT .....	128
Figure 7-12. Retained permeability versus flow rate for DC-III (a) slot width of 0.032", (b) slot width of 0.026", (c) slot width of 0.022", (d) slot width of 0.018", (e) slot width of 0.014", (f) slot width of 0.010"; Solid red line shows the suggested threshold for acceptable retained permeability for SRT .....	131

Figure 8-1. Cumulative sand production for different flow rate steps for DC-III. Green, yellow and red colors are related to Mode I, Mode II and Mode III, respectively, (a) SPC=30, (b) SPC=42, (c) SPC=54. .... 140

Figure 8-2. Cumulative sand production for different flow rate steps for DC-II. Green, yellow and red colors are related to Mode I, Mode II and Mode III, respectively, (a) SPC=30, (b) SPC=42, (c) SPC=54. .... 142

Figure 8-3. Equivalent plugging for different flow rates calculated based on the flow rate of 40 ml/hr/slot for no plugging cases..... 142

Figure 8-4. Produced sand for DC-II (a) produced sand for different slot width at constant slot density, (b) produced sand at constant slot width for different slot density; solid lines are the upper limit for acceptable sand production of 0.15 lb/sq ft and 0.12 lb/sq ft ..... 143

Figure 8-5. Produced sand for DC-III (a) produced sand for different slot width at constant slot density, (b) produced sand at constant slot width for different slot density; the solid lines show the upper limit for acceptable sand production of 0.15 lb/sq ft and 0.12 lb/sq ft, ..... 144

Figure 8-6. Comparison between the produced sand size and the slot width for DC-II; solid red line shows the slot width; dashed red line shows the 1/3 size of the slot width. (a) slot size=0.026", (b) slot size=0.022", (c) slot size=0.018", (d) slot size=0.014", (e) slot size=0.010". ..... 147

Figure 8-7. Comparison between the produced sand size and the slot width for DC-III; solid red line shows the slot width; dashed red line shows the 1/3 of the slot width. (a) slot size=0.032", (b) slot size=0.026", (c) slot size=0.022", (d) slot size=0.018", (e) slot size=0.014", (f) slot size=0.010" ..... 150

Figure 8-8. Comparison of the produced sand size distribution for different slot sizes for the coarser portion of sand pack PSD (>44µm) for DC-II; dashed line shows the sand pack PSD, (a) SPC=30, (b) SPC=42, (c) SPC=54 ..... 152

Figure 8-9. Comparison of the produced sand size distribution for different slot sizes for the coarser portion of sand pack PSD (>44µm) for DC-III; dashed line shows the sand pack PSD, (a) SPC=30, (b) SPC=42, (c) SPC=54 ..... 153

Figure 8-10. Sphericity distribution of the produced sand in comparison with the sphericity distribution of the sand pack for DC-II; solid red lines show the sphericity distribution of the sand pack. (a) SPC=30, (b) SPC=42, (c) SPC=54 ..... 155

Figure 8-11. Sphericity distribution of the produced sand in comparison with the sphericity distribution of the sand pack for DC-III; solid red lines show the sphericity distribution of the sand pack. (a) SPC=30, (b) SPC=42, (c) SPC=54 .....	156
Figure 8-12. Convexity distribution of the produced sand in comparison with the convexity of the sand pack for DC-II; solid red lines show the convexity distribution of the sand pack. (a) SPC=30, (b) SPC=42, (c) SPC=54 .....	158
Figure 8-13. Convexity distribution of the produced sand in comparison with the convexity of the sand pack for DC-III; solid red lines show the convexity distribution of the sand pack. (a)SPC=30, (b) SPC=42, (c)SPC=54 .....	160
Figure 8-14. Aspect ratio distribution of the produced sand in comparison with the aspect ratio of the sand pack for DC-II; solid red lines show the aspect ratio distribution of the sand pack. (a)SPC=30, (b) SPC=42, (c) SPC=54.....	162
Figure 8-15. Aspect ratio distribution of the produced sand in comparison with the aspect ratio of the sand pack for DC-III; solid red lines show the aspect ratio distribution of the sand pack. (a) SPC=30, (b) SPC=42, (c) SPC=54 .....	163
Figure 9-1. Schematic design of a typical SAGD producer well completion with dual tubing string completion .....	172
Figure 9-2. Linear x-axis representation of the PSD and slot sizes in tested coupons, (a) DC-II (b) DC-III.....	172
Figure 9-3. Slot window for DC-II for SPC=30, (a) sanding performance, (b) flow performance, (c) overall design window .....	173
Figure 9-4. Slot window for DC-II for SPC=42, (a) sanding performance, (b) flow performance, (c) overall design window.....	173
Figure 9-5. Slot window for DC-II for the SPC=54, (a) sanding performance, (b) flow performance, (c) overall design window .....	174
Figure 9-6. Slot window for DC-III for SPC=30, (a) sanding performance, (b) flow performance, (c) overall design window.....	174
Figure 9-7. Slot window for DC-III for SPC=42, (a) sanding performance, (b) flow performance, (c) overall design window.....	175
Figure 9-8. Slot window for DC-III for SPC=54, (a) sanding performance, (b) flow performance, (c) overall design window.....	175



Figure 9-9. Slot window for DC-II and SPC=30 for low flow rate (<0.8 bbl/day), (a) sanding performance, (b)flow performance, (c) overall design window .....	176
Figure 9-10. Slot window for DC-II and SPC=30 for moderate flow rate (0.8 bbl/day<Q<1.5 bbl/day), (a) sanding performance, (b) the flow performance, (c) the overall design window for low plugging/low flow rate.....	176
Figure 9-11. Slot window for DC-II and SPC=30 for aggressive flow rate (>1.5 bbl/day), (a) sanding performance, (b) the flow performance, (c) the overall design window .....	177
Figure 9-12. Slot window for DC-II and SPC= 42 for low flow rate (<0.8 bbl/day), (a) sanding performance, (b)flow performance, (c) overall design window .....	177
Figure 9-13. Slot window for DC-II and SPC= 42 for moderate flow rate (0.8 bbl/day<Q<1.5 bbl/day), (a) sanding performance, (b) the flow performance, (c) the overall design window for low plugging/low flow rate.....	178
Figure 9-14. Slot window for DC-II and SPC= 42 for aggressive flow rate (>1.5 bbl/day), (a) sanding performance, (b) the flow performance, (c) the overall design window .....	178
Figure 9-15. Slot window for DC-II and SPC= 54 for low flow rate (<0.8 bbl/day), (a) sanding performance, (b)flow performance, (c) overall design window .....	179
Figure 9-16. Slot window for DC-II and SPC= 54 for moderate flow rate (0.8 bbl/day<Q<1.5 bbl/day), (a) sanding performance, (b) the flow performance, (c) the overall design window ..	179
Figure 9-17. Slot window for DC-II and SPC= 54 for aggressive flow rate (>1.5 bbl/day), (a) sanding performance, (b) the flow performance, (c) the overall design window .....	180
Figure 9-18. Slot window for DC-III and SPC=30 for low flow rate (<0.8 bbl/day), (a) sanding performance, (b) flow performance, (c) the overall design window .....	180
Figure 9-19. Slot window for DC-III and SPC=30 for moderate flow rate (0.8 bbl/day<Q<1.5 bbl/day), (a) sanding performance, (b) flow performance, (c) overall design window .....	181
Figure 9-20. Slot window for DC-III and SPC=30 for aggressive flow rate (>1.5 bbl/day), (a) sanding performance, (b) flow performance, (c) overall design window.....	181
Figure 9-21. Slot window for DC-III and SPC=42 for low low flow rate (<0.8 bbl/day), (a) sanding performance, (b) flow performance, (c) the overall design window .....	182
Figure 9-22. Slot window for DC-III and SPC=42 for moderate flow rate (0.8 bbl/day<Q<1.5 bbl/day), (a) sanding performance, (b) flow performance, (c) overall design window .....	182

Figure 9-23. Slot window for DC-III and SPC=42 for aggressive flow rate ( $>1.5$  bbl/day), (a) sanding performance, (b) flow performance, (c) overall design window ..... 183

Figure 9-24. Slot window for DC-III and SPC=54 for low low flow rate ( $<0.8$  bbl/day), (a) sanding performance, (b) flow performance, (c) the overall design window ..... 183

Figure 9-25. Slot window for DC-III and SPC=54 for moderate flow rate ( $0.8$  bbl/day $<Q<1.5$  bbl/day), (a) sanding performance, (b) flow performance, (c) overall design window ..... 184

Figure 9-26. Slot window for DC-III and SPC=54 for aggressive flow rate ( $>1.5$  bbl/day), (a) sanding performance, (b) flow performance, (c) overall design window ..... 184

Figure A-1. Particle size distribution of oil sands categorized by Abram and Cain (2014); Solid lines show the upper limit of their set of PSD and dashed lines show the lower limit of their PSD in each class. Graphs show (a) the upper and lower ranges of the DC-I, (b) the upper and lower range of the DC-II, (c) the upper and lower range of the DC-III, and (d) the upper and lower range of the DC-IV. .... 213

Figure A-2. Slot window model for the different classes provided by Abram and Cain (2014) 214

## LIST OF SYMBOLS AND ABBREVIATIONS

### Symbols

a	Longest principal axis of an ellipsoid
AR50	50% Aspect ratio
b	Median principal axis of an ellipsoid
c	Shortest principal axis of an ellipsoid
Cc	Coefficient of curvature
Cu	Coefficient of uniformity
Cv	Convexity
C50	50% Convexity
DC-I	Class I oil sand for Devon Pike I
DC-II	Class II oil sand for Devon Pike I
DC-III	Class III oil sand for Devon Pike I
DC-IV	Class IV oil sand for Devon Pike I
D <sub>1</sub>	Sieve opening size that retains 1% of the particles in a sample
D <sub>5</sub>	Sieve opening size that retains 5% of the particles in a sample
D <sub>10</sub>	Sieve opening size that retains 10% of the particles in a sample
D <sub>30</sub>	Sieve opening size that retains 30% of the particles in a sample
D <sub>40</sub>	Sieve opening size that retains 40% of the particles in a sample
D <sub>50</sub>	Median size on the PSD curve
D <sub>60</sub>	Sieve opening size that retains 60% of the particles in a sample
D <sub>70</sub>	Sieve opening size that retains 70% of the particles in a sample
D <sub>90</sub>	Sieve opening size that retains 90% of the particles in a sample
d <sub>90</sub>	Sieve opening size that will just pass 90% of the particles in a sample
d <sub>30</sub>	Sieve opening size that will just pass 30% of the particles in a sample
d <sub>40</sub>	Sieve opening size that will just pass 40% of the particles in a sample
d <sub>60</sub>	Sieve opening size that will just pass 60% of the particles in a sample
d <sub>70</sub>	Sieve opening size that will just pass 70% of the particles in a sample
d <sub>10</sub>	Sieve opening size that will just pass 10% of the particles in a sample
S <sub>p</sub>	Particle surface area
S50	50% Sphericity
S	Salinity (weight percentage)
V <sub>p</sub>	Particle volume
V <sub>CH</sub>	Minimum convex volume

w Slot width (1/1000 inch)  
 $\varphi$  Sphericity

### Abbreviations

2D Two-dimensional  
3D Three-dimensional  
AER Alberta Energy Regulator  
ASW Average slot width  
CHOPS Cold heavy oil production with sand  
CSC Critical salt concentration  
CSS Cyclic steam stimulation  
DAQ Data acquisition  
DEM Discrete element method  
DIA Dynamic image analysis  
ERCB Energy Resources Conservation Board  
FCD Flow control device  
ICD Inflow control device  
IFT Inter facial tension  
LPSA Laser particle size analysis  
MMscf Million standard cubic feet  
NBT Natural bridge tendency  
NPT National pipe thread  
OCD Outflow control device  
OFA Open-to-flow area  
PPS Pre-packed screen  
PSD Particle size distribution  
PV Pore Volume  
PZC Point zero charge  
SAGD Steam Assisted Gravity Drainage  
SEM Scanning electron microscope  
SL Slotted liner  
SOR Steam-oil ratio  
SPC Slot per column (number of slot in one column of 7” liner)

SRT	Sand retention test
TDS	Total dissolved solids
THAI	Toe-to-heel air injection
TLS	Traffic light system
TOC	Total organic content
WWS	Wire Wrap Screen
XRD	X-Ray diffraction

## CHAPTER ONE: INTRODUCTION

### 1.1 Background

Alberta's oils sands are one of the largest proven oil reserves in the world of which 170 billion barrels are heavy oil (ERCB, 2011). Two types of production methods have been used to extract the oil sands reserves: surface mining and in-situ enhanced oil recovery. The area of surface mineable oil sands is only ~3% of the total oil sands area; thus, deeper resources must be recovered by in-situ techniques (CAPP, 2011). Canada will continue to rely on in-situ production techniques to recover oil sands resources well into the future (ERCB, 2011).

Steam Assisted Gravity Drainage (SAGD) is the main method for in-situ heavy oil production in Canada. This method employs two horizontal wells. High-pressure steam is injected into the upper wellbore (the injection well) to heat the heavy oil and reduce its viscosity. The heated oil and condensed water drain into the lower wellbore to be pumped out (Guo, 2014).

SAGD wells are supported against collapse by the installation of screen liners in the well, which are called sand control completions. Sand control completions are designed to prevent sand production while allowing the flow of reservoir fluids into the wellbore; allow the flow of fine materials to avoid the plugging of pore spaces behind the slots; and provide a conduit for the installation of valve tools, called flow control devices (FCDs) that operators use to control the flow of steam into the reservoir and the flow of oil into the production well. Per Kaiser et al. (2000), inflow resistance and cost, besides sanding, are primary factors in the design of sand screens for SAGD wells. Bennion et al. (2008) and Romanova et al. (2014a, 2014b) also included the plugging tendency as another important factor in their evaluation testing. All sand control completions have been shown to plug over time, contributing to the so-called 'skin'. The skin parameter represents several phenomena that impede the flow such as plugging of slots by the gradual corrosion of the liner, buildup of scale and clay in the pore space around the liner, and buildup of scale and clay inside the liner slots.

There are several types of completions that are used in SAGD applications. The main types, in order of popularity, are: slotted liners (SL), wire wrapped screen (WWS) and precise punched screen (PPS) (**Figure 1-1**).

A slotted liner is a pipe with multiple longitudinal slots spread along the length and around the circumference of the pipe (**Figure 1-2(a)**). A wire wrapped screen consists of a perforated structural pipe to provide unimpeded flow and a specially shaped wire wound around it (**Figure**

**1-2(b)**). The gaps between the wire wraps provide the sand control. A precise punched screen is composed of a perforated structural pipe and a filtration jacket with punched slots, which provide the sand filtration (**Figure 1-2(c)**).

Slotted liners have been used in oil and gas production and water wells since the early 1900's (Kobbe, 1917; Alcorn and Teague, 1937; Dean, 1938; Chenault, 1938) due to their economy and lower plugging tendency compared to other types of the screen. The main advantage of slotted liners over other standalone completions such as wire-wrapped screens and premium screens is the low cost (Petrowiki, 2013). However, slotted liners have proven to be less effective in more challenging formations with higher amounts of fines and reactive clays such as smectite and illite (Romanova et al. 2013).

The performance of slotted liners is assessed based on their ability to prevent sand production and allow the passage of flow. Screen aperture is usually considered as the main sand control parameter (Coberly 1937; Markestad et al. 1996; Meza Diaz et al. 2003; Ballard et al. 2006; Bennion et al. 2008; Chanpura et al. 2011a, 2011b, 2012b), while Open-to-Flow Area (OFA) (defined as the ratio of open area of the liner over the total area) is used as the inflow performance indicator (Tang et al. 2000; Kaiser et al. 2000; Furui et al. 2007). Conventionally, the upper bound for the slot aperture is specified based on the amount of produced sand and the lower bound is specified based on plugging tendency (Markestad et al. 1996).

Screen aperture selection for sand control applications has been studied extensively through laboratory studies (Coberly 1937; Suman et al. 1985; Markestad et al. 1996; Meza Diaz et al. 2002, 2003; Ballard et al. 1999, 2003, 2006, 2012; Bennion et al. 2008; Chanpura et al. 2011a, 2011b, 2012b) and numerical simulations (Mondal et al. 2011, 2012; Chanpura et al. 2012a). All these studies assume a value for acceptable sand production and relate one or more points on the Particle Size Distribution (PSD) to the aperture size to keep the produced sand below an acceptable limit. The produced sand is a function of screen aperture, screen profile, OFA, flow rate, formation PSD, and fluid-formation interactions. However, current design approaches are simply based on the selection of an aperture size to keep sand production below a specific limit (Markestad et al. 1996; Fermaniuk 2013). This approach neglects the dependence of produced sand on both slot width and slot density as well as on the wellbore operational conditions.

## **1.2 Statement of the problem**

Over the past few decades, considerable efforts have been made to investigate the mechanism of sanding and plugging in sand control screens. The current design practice for the slotted liner is based on specifying slot aperture windows in relation to the PSD of different sand facies within the reservoir. These slot apertures are mainly selected based on field experiences and laboratory testing and range from a minimum (e.g. 2D50) to a maximum slot width (e.g. 3.5D50) (Fermaniuk, 2013). The consideration is that a slot width smaller than the lower bound leads to severe plugging while a slot width higher than the upper bound results in severe sanding (Markestad et al. 1996). This design approach, however, does not incorporate the effect of other screen parameters such as the slot density and profile as well as the effect of the formation fluids chemistry and wellbore operation on the screen design. Further, the laboratory testing which has been used in developing these criteria use single-slot coupons (Bennion et al. 2008), which neglects the interaction between the slots.

This thesis introduces a new testing facility for sand control testing, which allows the use of multi-slot coupons that represent a portion of the actual liner. The new testing can fully capture the interaction between the slots. Further, the new testing device allows parametric testing to study the effect of screen design, operating conditions, and fluid and sand properties on the performance of sand control screens in terms of sanding and plugging. The outcome of the testing methods in this research allows the development of more objective design criteria for sand control for different types of sand media.

## **1.3 Research objectives**

The main objective of this study is to improve the current design criteria for slot width and slot density by using experimental data. The primary aim is to study the dependency of sand screen performance on the screen design parameters such as the slot width and slot density. The new criteria are based on two performance indicators (1) sand production weight; (2) retained permeability (the ratio of the near screen zone permeability to the formation permeability) as a measure of plugging tendency. Each of these performance indicators is assessed for two representative PSDs in the McMurray formation through laboratory testing for different slot widths and slot densities.



This research also aims at finding how the variations of slot width, flow rate, and slot density affect the fines movement within the sand pack. Another objective is to find how the pH and salinity of flowing fluid affect the sanding and fines migration within the sand pack.

#### **1.4 Research hypothesis**

Research hypothesis is defined as speculation of research outcomes based on physical understanding and logic. It is evident that the produced sand increases with an increase in slot width. Higher sanding is expected to improve the retained permeability of the screen. The effect of larger aperture on fines migration and slot plugging, however, is less evident as it depends also on whether the slot density is kept constant (hence higher OFA) or reduced for the larger aperture to keep the OFA constant. For constant slot density, hence larger OFA for wider slots, flow velocities behind the slots reduce for the same flow rate resulting in lower fines migration and pore plugging. For wider slots and lower slot density at constant OFA, the larger aperture results in sharper flow stream curvature behind the slots, therefore, larger pressure drops and lower retained permeability.

An increase in flow rate is anticipated to increase drag forces on fine particles leading to larger fines mobilization and transport. For smaller slot width, it is expected that the flow rate will have a smaller impact on the amounts of produced sand. The effect of flow rate is expected to increase for larger slot apertures.

The pH and salinity of flowing fluid are expected to affect the mobilization and transport of the fines in the porous medium and near the screen. Higher pH is expected to lead to deflocculation of clay particles and result in larger fines migration and fines production.

#### **1.5 Research steps**

This research is performed in the following steps:

1. Design and build a new Sand Retention Testing (SRT) facility for sand control testing, debug the testing facility, establish a standard testing procedure, verify the repeatability of the results and verify the results with current testing protocols.
2. Develop a testing matrix to study the effect of slot width, slot density, PSD, and flow rate on the performance of slotted liners.
3. Study the effect of fluid characteristics (pH and salinity) as well as fluid flow rate on fines migration, fines production and PSD of produced fines over the testing duration.

4. Study the movement of fines within the sample and analyze the pore plugging along the sample by pressure measurements at various points along the sample.
5. Develop a correlation between produced sand and retained permeability with formation PSD, slot width, and slot density.

### **1.6 Significance of the work**

This research greatly enhances the understanding of various important well completion parameters that affect optimal recovery from oil sand resources in Western Canada and around the world. Estimates indicate that 70% of the world's hydrocarbon reserves are in sand-prone reservoirs (Bianco and Halleck 2001). Sanding is estimated to cost the oil industry billions of dollars every year (Kenter and Currie 1998). Sanding erodes production equipment due to quartz abrasiveness and may lead to tubing and casing collapse, which is a safety concern as well as an economical problem. Produced sand can damage pumps and even block flow passages. Further, sanding can impact the environment due to the production of sand contaminated by the reservoir fluids. The produced sand must be cleaned or injected into deep formations, both being expensive options. On the other hand, sanding can boost productivity by removing wellbore skin developed by formation damage, wax deposition, and fines migration (Geilikman et al. 1994; Vaziri et al. 2002).

In Alberta, millions of dollars are annually spent on well interventions and remediation to increase the performance of sand control completions or recomplete the wells in which failed screens are detected. Estimates in Alberta indicate around 15-45% of wellbore costs relate to the wellbore completion (Athabasca Oil Corporation, 2015a, 2015b; Petroleum Service Association of Canada, 2015). Due to the importance of selecting appropriate cost-effective screens for the well, several evaluation and design techniques have been developed over the years.

Improper design of slotted liners can prompt a massive sand production, low flow efficiency, and severe liner erosion. Each of these problems can be extremely costly and can result in the loss of well productivity or poor well performance. A better understanding of sand control design procedure can lead to improved well completion, reduced well failures, and enhancement of wellbore performance.

This research will result in an improved understanding of the performance of slotted liners. This knowledge is used to improve the design criteria for slotted liners by including and quantifying

the effect of liner aperture, slot density, and flow rate on sand production and the plugging tendency of the liner.

## **1.7 Thesis outline**

The work in this research is divided into seven chapters:

Chapter 1 (the current chapter) provides the background and the scope of this research.

Chapter 2 contains the literature review on the screen design and evaluation methods and current testing facilities. This review presents state-of-the-art information on the factors that affect the failure mechanism and screen performance.

Chapter 3 presents a procedure for oil sand and commercial sand characterization in term of their PSD, particle shape, and composition.

Chapter 4 presents the replication of oil sands from commercial sands and fines to duplicate the PSD, particle shape, and composition for large scale testing. Also, it presents a series of mechanical tests to assess the agreement between the mechanical response of the oil sand and its commercial replica.

Chapter 5 presents the experimental setup and testing procedure for this study.

Chapter 6 presents the results of experimental work on the effect of pH and salinity on the fines mobility. This helps to understand the necessity of using realistic values for the pH and salinity of the injection fluid during the testing.

Chapter 7 presents the test results on the effect of slot size and slot density on fines migration and accumulation above the coupon.

Chapter 8 presents the sand production results and compares the PSD and shape of produced sands with those of the original sand pack. Different modes of sanding are defined and discussed in this chapter.

Chapter 9 presents a set of new design criteria to determine the optimal slot window for different slot densities and expected flow rates/plugging ratios.

Chapter 10 summarizes the major findings of this research and presents suggestions for future research on this topic.

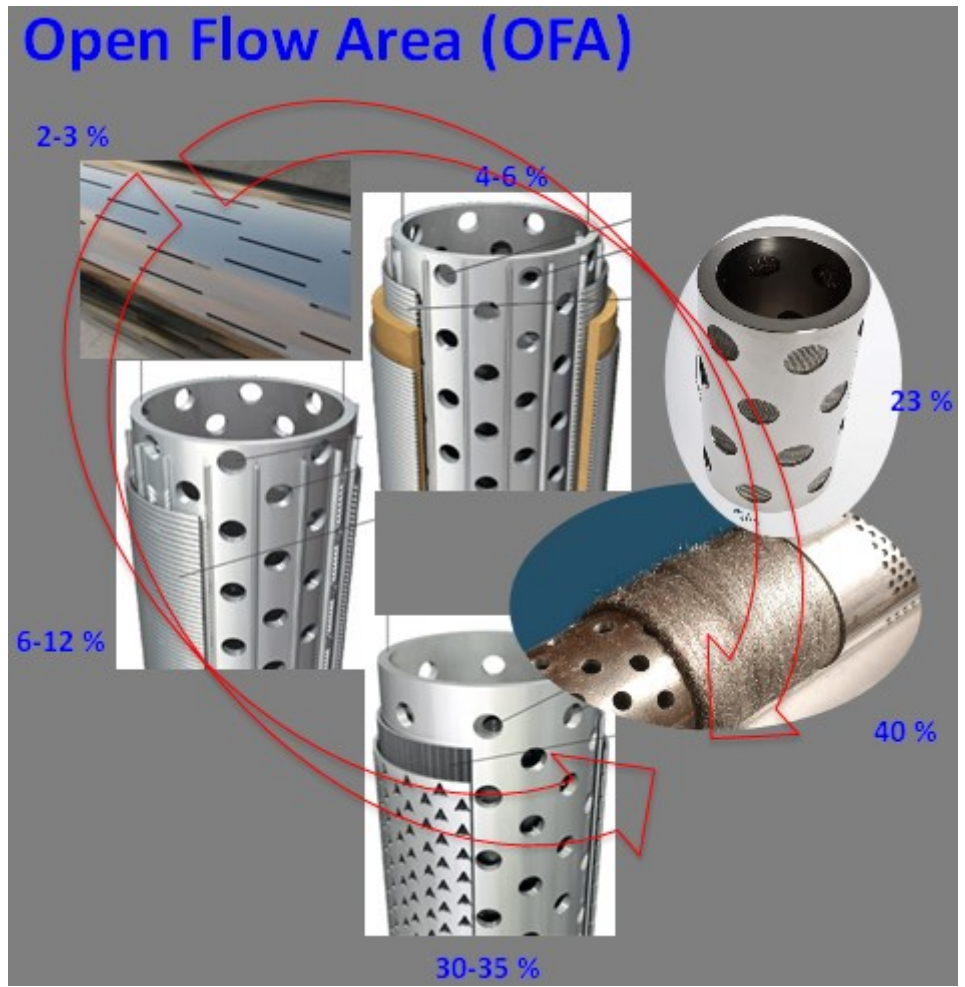


**Figure 1-1. Different sand control screens and comparison of their OFA**

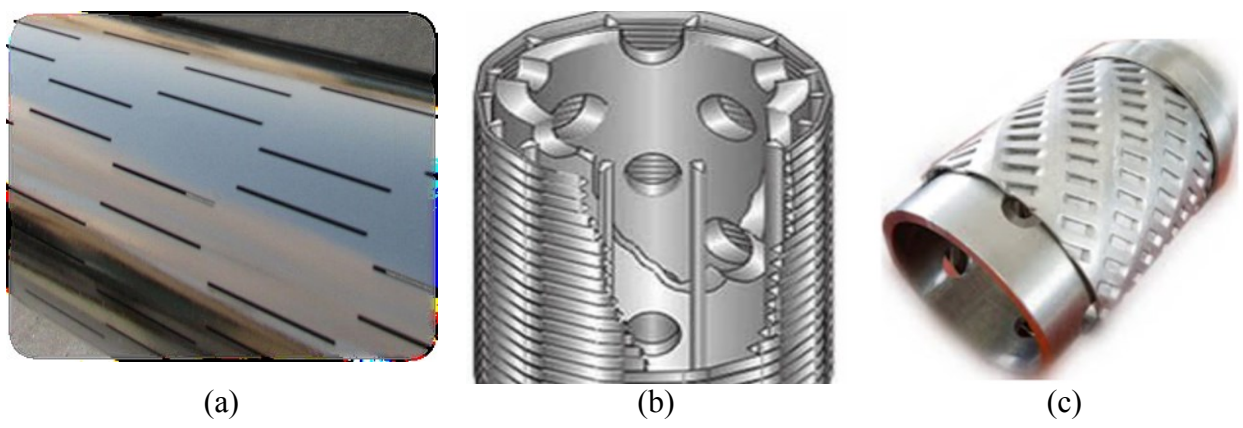


**Figure 1-2. Common sand control screens in SAGD wells**

## CHAPTER TWO: LITERATURE REVIEW

### 2.1 Introduction

Due to the unconsolidated nature of oil sands, sand control is essential for developing the oil sand resources in Western Canada. Currently three main techniques are employed to develop these resources: (1) in-situ mining for resources which are buried within the depth of ~50m, (2) primary production (Cold Heavy Oil Production with Sand (CHOPS)), and (3) thermal operations (Toe to Heel Air Injection (THAI), Cyclic Steam Stimulation (CSS), and Steam Assisted Gravity Drainage (SAGD) for deeper resources.

The focus of this research is sand control in SAGD operations. The choice of sand control technique for SAGD wells depends on site-specific conditions, operating practices, and economic considerations.

Horizontal well pad drilling is the common practice in developing heavy oil resources particularly in SAGD developments (Illfelder et al. 2011; Strobl et al. 2014). Economic considerations rule out most of the expensive sand control techniques such as gravel packing or premium and pre-packed screens. It has been widely accepted by the industry that standalone screens (such as slotted liners, wire wrapped screens and precise punched screens) are sand control methods of choice in thermal operations. However, these screens should be carefully designed for the specific formation and operational conditions.

Design procedures and criteria for standalone screens in horizontal wells for thermal operations are not unique everywhere. Kaiser et al. (2000) proposed to use sand control, inflow resistance, and cost as the main criteria for the screen design. Later the design workflow evolved to also include plugging tendency through evaluation testing (Bennion et. al. 2008; Romanova et al. 2014, 2015), joint makeup torque assessment (Bradley et al. 2005), mechanical integrity evaluation (e.g. running load limit evaluation) and thermal loads/cycles evaluation (Slack et al. 2000; Dall'Acqua et al. 2005, 2010; Xie 2006, 2015).

Mahmoudi et al. (2016) summarized the current workflow followed by the industry in the design of sand control screens for SAGD wells (**Figure 2-1**). In the current industrial workflows, the screen aperture is designed to control the amount of produced sand (Coberly 1937; Markestad et al. 1996; Meza Diaz et al. 2003; Ballard et al. 2006; Bennion et al. 2008; Chanpura et al. 2011a,

2011b, 2012b) and the flow performance requirements are achieved through the Open Flow Area (OFA) (Tang et al. 2000; Kaiser et al. 2000; Furui 2004; Furui et al. 2007). The OFA changes by the variation of the slot width and slot density.

In this research, the focus is the design criteria for slot width and slot density for slotted liners. State-of-the-art knowledge about failure mechanisms and practices for slotted liner design and evaluation are discussed in this chapter.

## **2.2 Failure mechanisms of slotted liners**

The first step in improving current practices and procedures for the design of slotted liners is to understand the failure mechanisms of slotted liners. Liner failure can be defined as the full or partial impediment to flow that leads to partial or complete loss of production (Hallman et al. 2015). Liner failure, in extreme cases, results in wellbore shut in due to significant reduction in wellbore productivity or increased risk for continued operation. Excessive sand inflow into the wellbore and plugging of the formation and screen are two of the main causes of screen failure.

### ***2.2.1 Excessive sand production***

Sand production in horizontal wells is extremely costly and has been studied for decades. It can cause significant damage, ranging from erosion and plugging of downhole pumps, tubing, and downhole valves, to the accumulation of sand in the horizontal well and surface facilities. A sand control screen acts as a barrier to the sand flow (Wan and Wang 2004). Sand production is governed by the balance between the forces that hold the sand behind the screen and the driving forces that move the sand or break the sand bridge behind the slots.

Sand inflow to the wellbore in a standalone screen for a given PSD is affected by the slot width (Coberly 1937; Suman et al. 1985; Markestad et al. 1996; Mondal et al. 2011; Chanpura et al. 2011a, and 2012a), OFA (Chanpura et al. 2012b), flow interruptions, and backflow (Ballard et al. 2006).

SAGD wells are typically low-flow-rate wells with changing water cut percentage during the lifetime of the well (Stahl et al. 2014). However, from the initial production to the late stage of the wellbore life, SAGD wells produce water beside oil. The adverse effects of water production on sand production are well documented (e.g. Wu and Tan 2001; Wu et al. 2006). Steam

breakthrough and steam flashing in production wells are also known to highly impact the sand production (Doan et al. 1999; Das 2005).

### **2.2.2 Plugging**

As discussed earlier, an ideal screen should not only stop the sand but also provide the least resistance to fluid flow. In an ideal case, the screen should have equal or higher equivalent permeability compared to the formation sand (Parlar et al. 2016).

The aim in screen design is to maintain a high retained permeability over the life cycle of the well. However, the retained permeability is adversely affected by the plugging of the slots and the pore network behind the slots. To account for the plugging effect, a plugging factor is heuristically considered in the design process (Fermaniuk 2013).

To investigate the screen effect on the fluid flow, a parameter called retained permeability is defined for the combination of the screen and the porous medium near the screen. Retained permeability is defined as the ratio of current over initial permeability in the zone around the liner where the flow velocities and path are affected by the liner. Retained permeability is typically below one due to the additional pressure drop caused by the screen installation. Ideally, the retained permeability should be equal to one, meaning that the presence of the screen does not cause an additional pressure drop.

The slot and pore space plugging reduce the retained permeability over time. The retained permeability relates to the retention mechanism of sand over the screen, the PSD of the formation sand, the OFA, the flow convergence towards the screen, and the fines movement (Markestead et al. 1996; Hodge et al. 2002).

Two zones are considered in the evolution of retained permeability over time. The first zone is inside the slots and the surface of the liner and the second zone is the formation sand near the liner.

In the first zone, the plugging is mainly dominated by scaling/fouling, a bank of sand/asphaltene deposits, corrosion, and development of a film of clay-adsorbed by the liner surface and further thickened by corrosion. In the second zone plugging is dominated by pore plugging (Rege and Fogler 1987; Taniguchi et al. 1997; Foct et al. 2004; Wakeman 2007; Gaudin et al. 2008, 2013; Jeannin et al. 2010; Tien and Bandaru 2011; Porubcan and Xu 2011; Urios et al. 2011;

Romanava et al. 2013; El Mendili et al. 2014; Xie et al. 2014; Yan et al. 2015; Sacramento et al. 2015; Ding et al. 2015a, 2015b).

Farther away from the liner in the formation, there are several impairment mechanisms such as hydrodynamic bridging, inertial impaction, interception, absorption, Brownian diffusion, and sedimentation (McDowell et al. 1986; Ives 1986; Van Oort et al. 1993, Bennion et al. 1995; Faure et al. 1997; Bedrikovetsky et al. 2002; Zhuang et al. 2004; Valdes et al. 2006; Zamani et al. 2009; Louvet et al. 2010; Sacramento et al. 2015).

Further details on the plugging mechanisms are provided herein.

### **2.2.2.1 Screen plugging**

To better understand the mechanism of plugging inside the slots, it is important to examine the deposited mineral layer over the surface of the standalone screens based on field observations (Ramonava and Ma 2013) and laboratory experiments (Bennion et al. 2008). Bennion et al. (2008) reported severe plugging caused by clay particles. Their test results showed a bank of clay particles forming and thickening over time inside the slot and over the coupon surface. Romanava et al. (2013) published a series of tests on extracted slotted liners from the McMurray formation. Their observations reveal that the materials that plug the slots are mainly clay and corrosion byproducts. It seems that clay adsorption to the carbon steel is playing an important role in the plugging observed in the slotted liner (Benion et al. 2008; Ramonava and Ma 2013). Adhesive forces in clay mixture originate from the electrostatic forces between the clay minerals and the screen materials.

The structure of the clay film formed on the surface of the liner depends on the pH level in the medium. Van Olphen (1965) explained that the Point Zero Charge (PZC, a condition when the electrical charge density on a surface of the clay particle is zero) for kaolinite is approximately at the neutral pH (pH=7), while for chlorite and bentonite at lower than the neutral pH. For pH ranges higher than PZC, charges with the opposite sign form on the faces and edge of the clay particles.

**Figure 2-2** shows a schematic of mineral deposition for silica, kaolinite, chlorite, and smectite/bentonite on a metal surface at neutral pH (pH=7) (Jeannin et al. 2010). At neutral pH (pH=7) and low ionic strength, clay deflocculation occurs resulting in clay dispersement in the medium



(**Figure 2-2(c)** and **2-2(d)**) where the opposite signs of the charges on the faces and the edges of clay platelets lead to a so-called “house of cards” structure (Jeannin et al. 2010). Whereas for kaolinite (PZC is reached at  $\text{pH} = 7$ ) at neutral pH ( $\text{pH}=7$ ), faces are neutral leading to a face-to-face stacking of the clay platelets, and the resulting deposit is a more compact film of clay (**Figure 2-2(b)**).

Adhesion and adhesive friction between the clay particles and the metal surface are described by Bowden and Tabor (1950, 1964) to be dependent on the real contact surface of the clay and the metal. The real contact surface increases by the plastic deformation of the clay. This implies that the required shear force at the metal-clay interface to separate clay particles increases as normal stress increases.

Fontaine (1954) designed a vertical adhesion test and found that the adhesion can be attributed entirely to the water film between the contact surfaces. Later Fukagawa et al. (2002) found that the adhesive stress decreases with the increase of porosity (decrease in compaction). Satomi et al. (2012) found that the roughness of the metal surface affects the adhesion between the clay and the metal surface. Kooistra et al. (1998) highlighted the effect of ionic conditions on the adhesion of the clay minerals to the metal surface.

Romanova et al. (2013) discussed the coexistence of corrosion materials and clay deposits in the slots, which leads to slot plugging. Studies have shown that the corrosion products can invade the deposited clay (Foct et al. 2004; Jeannin et al. 2010; Urios 2011). Jeannin et al. (2010) explained that the deposition of kaolinite in a compact film on the metal surface favors a local increase of  $\text{Fe}^{2+}$  at the clay-steel interface. In certain conditions, the clay film cracks due to the growth of corrosion allowing the corrosion byproducts to move into the deposited film. Such cracks allow further invasion of oxygen,  $\text{H}_2\text{S}$  and  $\text{CO}_2$  to the metal surface and progression of the corrosion. These processes seem to be highly affected by mineralogy of the clay. For instance, chlorite has a higher shield tendency than kaolinite (Jeannin et al. 2010).

Foct et al. (2004) observed that the clay particles are more adherent in the presence of fluid flow. They performed a series of in situ tests to study carbon steel corrosion due to exposure to illite/smectite-rich formations and measured an average corrosion rate of 5.2-17  $\mu\text{m}/\text{year}$ . However, the presence of fluid flow increases the rate of corrosion to as high as 39  $\mu\text{m}/\text{year}$ . The

main corrosion product was  $\text{FeO}(\text{OH})$  which is consistent with observations of Romanova et al. (2013).

Urios et al. (2011) observed that the steel corrosion produces mineralogical dissolutions (Ca phases) and precipitations (iron oxides and hydroxides), leading to a partial mixture of the clay film and corrosion products near the test coupon. They observed five distinct zones: (1) partially corroded steel, (2) corroded steel, (3) Fe-enriched layer in the formation, (4) Ca-enriched layer in the formation and (5) unaltered formation. The thickness of the altered zone was approximately 4 mm.

Foct et al. (2004) observed two distinguished layers near the steel coupon: (1) the first layer (nearly 40  $\mu\text{m}$  thick) is at the interface with steel and does not contain any Si or Al (clay free) and (2) the second layer (also around 40  $\mu\text{m}$  thick) is located at the interface with clay, and presents a high Si and Al content (mixed iron oxide and clay zone). The same zones could also be distinguished from the energy dispersive spectrometry images reported by Romanova et al. (2013).

#### **2.2.2.2 Fines migration and pore plugging**

Several experimental and numerical works have been conducted to describe the fines migration in porous media (Barkman and Davidson 1972; Abrams 1977; Ives 1986; McDowell et al. 1986; Kumar et al. 1988; Van Oort et al. 1993; Bennion et al. 1995; Faure et al. 1997; Bedrikovetsky et al. 2002, 2010; Zhuang et al. 2004; Civan 2007; Valdes and Santamarina 2006; Zamani et al. 2009; Louvet et al. 2010; Bedrikovetsky 2010; Sacramento et al. 2015). However, this review focuses only on fines migration and pore plugging studies in the SAGD context.

Valdes (2006) specified four stages of fines migration leading to pore plugging in the porous media as (1) fines generation, (2) fines mobilization, (3) fines transportation, and (4) fines entrapment. These stages are influenced by the pore structure, fines size, mineralogy and electro-chemical interaction of the fines, porous structure, and the saturating fluids. Further details on the contributing factors on fines migration and pore plugging follow.

#### **Pore structure, fines size and mechanisms of fines migration**

Sand particles in oil sands form the load-bearing skeleton. Fines are not a part of this skeleton and may be mobilized under certain conditions and transported by fluid flow. Fines may collide

with the pore walls and be trapped resulting in reduced pore throat sizes, hence, lower permeability. The interaction of particles with the pore fluids becomes significantly important for particles smaller than 10  $\mu\text{m}$  (Wakeman 2007). For these particles, electrical attraction/repulsion increases and becomes as important as the gravitational and hydrodynamic forces.

In oil sands, clay minerals act as a cementing agent, holding particles together at the particle contacts. Clay content and distribution dictate oil sand's permeability and sensitivity to ionic conditions (Gaida et al. 1985; Khilar and Fogler 1998).

The relevant particle size in fines migration is the dimension perpendicular to the longest dimension. This is because suspended particles tend to orient their largest dimension along the direction of flow (Khilar and Fogler 1998). Per experimental observations (Barkman and Davidson 1972; Abrams 1977):

1. Particles equal or larger than one-third of the average pore throat size, bridge at the pore throat.
2. Particles smaller than one-third but larger than one-seventh of the average pore throat size deposit in the pore spaces resulting in reduced effective pore/pore throat size.
3. Particles that are smaller than one-seventh of the pore throat size pass through the pores with minor or no impairments. Van Oort et al. (1993) showed that at extremely low flow rates, particles larger than one-fourteenth but smaller than one-seventh of the average pore throat can still deposit in the pore spaces.

#### **Chemical interaction between injection fluid and formation minerals/fluids**

Clay-size particles mobilize in response to electrochemical forces, while larger particles tend to preferentially migrate in response to hydrodynamic forces (Cerdeira 1988). The strength of electrochemical forces is dependent upon the fines mineralogy. Fine particles are generally kaolinite, smectite, illite, mica and quartz (Valdes 2006). The main clays in McMurray Formation are kaolinite and illite (Bennion et al. 2008). Silica ( $\text{SiO}_2$ ) and alumina ( $\text{Al}_2\text{O}_3$ ) are the main ingredients for most clay particles as summarized in **Table 2-1** (Khilar and Fogler 1998).

There have been several research studies on low-salinity water injection (Tang and Morrow 1999; McGuire et al. 2005; Buckley and Morrow 2010; Sheng 2014) and formation damage due to fines migration (Vaidya and Fogler 1992; Sheng 2014). However, few studies have been

conducted on the effect of these parameters on plugging of sand control screen. Most of SRT tests don't report the salinity and pH of their brine which makes their retained permeability results subjective.

Bennion et al. (2008) discussed the effect of pH on pressure drop across a single-slot coupon to see the possibility of acid stimulation to remove the plugging material near the screen. They found that the pressure drop is highly sensitive to the pH level of the injected fluids. They adjusted the pH level by adding only 1% or less HCl to the injected fluid and observed clay (kaolinite and illite) flocculation (aggregation) at low pH and deflocculation (dispersion) at high pH.

For kaolinite and illite, the reduction of the pH level to less than the neutral pH has been observed to reduce screen plugging (Benion et al. 2008). In SAGD, fresh steam is mixed with the formation water around the injection well. As the condensate moves toward the production well, the salinity of the condensate goes up as it picks up the formation minerals and is mixed with the high-salinity formation water with dissolved minerals in the range of 20,000 - 60,000 ppm (Bhattacharjee 2011). Further, the exposure of the condensate to solution  $H_2S$ ,  $CH_4$ , and  $CO_2$  results in a low pH value, hence a lower chance of the mobilization of formation clays in early stages around the production well (Bhattacharjee 2011). Over time, the salinity of the brine near the production well decreases gradually due to the continued production of melted bitumen and water (formation water and condensate). Additionally, the pH level gradually increases as further condensate with caustic nature (Bennion et al. 2008) is injected and ion exchange happens between the adsorbed cations and  $H^+$  in the solution (Mohan et al. 1993). At low salinity and high pH around the production well, the clay particles can mobilize (Khilar et al. 1990) and migrate towards the production well.

$Na^+$  and  $Cl^-$  (sodium and chlorides) are the dominant ions in the produced water from SAGD wells (Cowie 2013). However, bivalent cations can reduce the water sensitivity and clay migration in the medium (Khilar and Fogler 1984).

### **Composition of produced and formation water**

It is necessary to know the composition of produced and formation water before conducting a laboratory sand control or fines migration test. The interaction between the injected water,

formation water, formation clays and injected steam seems to influence the fines movement in the formation (Sheng 2014).

The composition of formation water in the oil sands reservoirs is highly variable for different formations. Cowie (2013) mapped the Total Dissolved Solids (TDS) of 355 McMurray Formation water samples in Athabasca oil sands. His study showed that McMurray Formation waters varied from non-saline (TDS < 4,000 mg/L) to brine (TDS > 100,000 mg/L) with a regional trend of high salinity at the dissolution edge of the Prairie Evaporate Formation (red shading in **Figure 2-3**). Cowie (2013) discussed the hydrological explanation for the observed variation in the TDS, which is beyond the scope of this thesis. The important conclusion is the difference in formation water's composition for different SAGD sites in Alberta. As such, any study of the effect of the formation water's composition must be done on a case-by-case basis.

Bhattacharjee (2011) characterized produced water in SAGD operations based on the amounts of dissolved solids (1,500 to 6,000 ppm TDS) and suspended solids (typically silica at 275 to 400 ppm level). Peterson (2007) concluded that produced water in Northern Alberta generally has the following characteristics:

- TDS in the range of 1,500 to 5,000
- Silica saturation up to 350 ppm
- High alkalinity and chloride (major inorganic anions)
- High sodium (major inorganic cation)
- High dissolved organic content (measured as total organic content, TOC)
- Low immiscible organic content (measured as oil and grease)
- Low hardness
- Low sulfate

Per Bennion et al. (2008), the pH of produced water in SAGD wells depends on several variables such as the caustic nature of the injected steam and steam condensate and the existence of carbon dioxide and hydrogen sulfide in the reservoir. **Table 2-2** shows several examples for the composition of the produced water for SAGD projects and indicates a pH range of 7.3 - 8.8 for these cases.

Some of above parameters (such as alkalinity of the injected steam, companion gases and additives to the injected steam) can be modified by the operator, while others relate to the original composition of the reservoir solids and fluids and cannot be changed.

### **Effect of pH and salinity on clay/fines migration**

The effects of pH and salinity on fines migration have been widely investigated to understand the mechanisms involved in low-salinity water injection (Tang and Morrow 1999; McGuire et al. 2005; Buckley and Morrow 2010; Sheng 2014) and formation damage (Vaidya and Fogler 1992). This section only focuses on studies related to the interaction of brine with clay particles under different pH conditions in sand and sandstone media.

As stated before, the main clays in McMurray Formation are kaolinite and illite (Bennion et al. 2008). These clays can become detached during aqueous flow, especially when the flowing brine becomes less saline in comparison with the formation water (Boston et al. 1969). Mohan et al. (1993) and Mohan and Fogler (1997) provided an explanation of pore blockage by clay detachment and migration. They concluded three mechanisms for permeability reduction in sandstone containing swelling (smectites and mixed-layer clays) and non-swelling (kaolinites and illites) clays (**Figure 2-4**):

1. Migration: Release of clay particles from pore walls due to the change in ionic conditions, which cause the pore blockage.
2. Swelling: Clay swelling blocks pore channels and reduces the permeability.
3. Swelling-induced migration: a change in the ionic condition causes swelling of the clays lining the pore walls which eventually dislodges the fines.

The first mechanism seems to apply to McMurray Formation oil sands where kaolinite and illite are the main minerals. Due to the high variation in the composition of produced water and depending on ionic concentrations, the tendency for fines migration can highly vary from one reservoir to another. For a better understanding of the fines migration, a detailed testing program is required for each case.

It has been shown that a Critical Salt Concentration (CSC) exists for clay particle movement in porous media (Khilar et al. 1983; Khilar and Fogler 1984; Khilar et al. 1990). If the salinity of the permeating fluid falls below the CSC, the sandstone permeability is significantly reduced

because of the detachment of clay particles from the pore walls, which block the pore throats. Khilar and Fogler (1984) found the CSC concept applies only for monovalent cations (such as  $\text{Na}^+$ ,  $\text{K}^+$ , and  $\text{Li}^+$ ) and is virtually nonexistent for cations with a valence greater than one (such as  $\text{Ca}^{2+}$ ,  $\text{Mg}^{2+}$ , and  $\text{Ba}^{2+}$ ). They observed that “water sensitivity” does not occur when bivalent salt solutions like  $\text{CaCl}_2$  and  $\text{MgCl}_2$  are used in the test (contrary to monovalent salts like  $\text{NaCl}$ ). Even for monovalent cations, the CSC depends on counter-ions. The release of clay particles is effectively prevented due to the strong ion-exchange affinity of clay for the polyvalent counter-ion.

In addition to salinity, pH could also affect the movement of clay particles in porous media. Mungan (1965), Simon et al. (1976), Kia et al. (1987) and Leone and Scott, (1988) concluded that permeability reduction due to the abrupt change in salinity does not occur in extremely acidic solutions (pH values below 2.6).

Different studies (Mungan 1965; Simon et al. 1976; Leone and Scott 1988; Vaidya and Fogler 1992) showed that dispersion of clay particles was minimized at low pH. Variation in pH was reported to impose a great change in terms of dispersion and aggregation of the clay particles in slotted liner experiments (Bennion et al. 2008).

It has been found that during the injection of a low salinity solution, the pH of effluent increases to higher levels than the initial pH value (Vaidya and Fogler 1992; Sheng 2014). The pH variation has been related to ion exchange between the adsorbed  $\text{Na}^+$  and  $\text{H}^+$  in the solution, which results in an increased  $\text{OH}^-$  concentration in the solution (i.e. pH increases) (Mohan et al. 1993). This increased pH is believed to amplify the release of fines and cause a drastic reduction in permeability.

In their variable pH fluid injection tests, Vaidya and Fogler (1992) reported small variations in permeability for pH values up to 9. Permeability reduction starts at pH values higher than 9. For  $\text{pH} > 11$ , they observed a rapid and drastic decrease in the permeability. Solution pH also affects the Inter-Facial Tension (IFT) (McGuire et al. 2005).

As Vaidya and Fogler (1992) discussed, in a system where exchangeable cations exist, the salinity and pH of the solution are expected to have interrelated effects. Therefore, to understand the combined effect of these two parameters, a test matrix is required in which both these parameters are varied.

### ***2.2.3 Steam breakthrough***

Avoiding steam breakthrough in SAGD operations is very important to reduce Steam Oil Ratio (SOR) and prevent wellbore and reservoir damage. Steam breakthrough can cause extreme erosion in the liner by allowing sands and fines at extremely high velocities into the screen slots. Typically steam trap acts as an operational control to reduce or prevent steam breakthrough from the injector well to the production well (Doan et al. 1999; Das 2005).

### ***2.2.4 Corrosion and erosion***

Corrosion of casing and downhole equipment is unavoidable due to the presence of sour gases and a variety of ions alongside hydrocarbon production (Fermaniuk et al. 2015). The corrosion has proven to be one of the contributing factors in the plugging of slotted liners (Romanova et al. 2013).

Erosion is also one of the important causes of screen failure and can be triggered by such phenomena as slot plugging and steam breakthrough. Plugging of the screen increases the flow velocity in the open slots of the screen, which in turn increases the rate of erosion (Procyk et al. 2015; Fermaniuk et al. 2015). Removal of the corrosion film on the screen exposes the metal to further corrosion/erosion leading to a so-called “hot spot” (Procyk et al. 1998; Hallman et al. 2015). **Figure 2-5** shows a damaged extracted screen by the growth of a hot spot.

### ***2.2.5 Scaling***

Scaling is caused by disruption to the chemical equilibrium of the fluid and solution ions due to physical or chemical changes leading to the precipitation of dissolved components. Scaling in downhole completion equipment has proven to play an important role in production impairment (Brown, 1998). Calcium Carbonate, silica, strontium sulfate and barium sulfate are the common scaling materials (Schulien 1997; Fermaniuk et al. 2015).

## **2.3 Design and evaluation of sand control screens**

The success of sand control technique depends on its ability to stop the flow of sand, with little resistance to the flow of fluids and fines (allowing fines to move freely and be produced). Current design approach for standalone screens is mainly based on the PSD of the reservoir sand. This section reviews several issues related to the slotted liner design.

### ***2.3.1 Particle size distribution/shape analysis***



Particle Size Distribution (PSD) is the critical input in the design of standalone screens. There are various methods for obtaining the PSD of a sand mix such as sieve analysis, Laser Diffraction Particle Size Analysis (LPSA) and Dynamic Image Analysis (DIA).

#### **2.3.1.1 Sieve analysis**

Sieve analysis is the common procedure used to determine the PSD of oil sands. Sieve analysis is performed using a column of standard sieves stacked from coarse to fine from top to bottom. Representative samples of the formation sand are poured onto the top sieve and the sieves are shaken using a mechanical shaker for a certain period.

Sieve analysis represents the second smallest dimension due to the way particles orient themselves to pass through the sieve. Sieving is the most appropriate method of PSD measurement for screen design applications (Fermaniuk 2013). However, in sieve analysis, fine particles can adhere to the surface of larger particles (Chanpura et al. 2014) and affect the measurements. Measurements could be also affected by such matters as particle's tendency to agglomerate, density and electrostatic charges (Gupta et al. 1975).

#### **2.3.1.2 Laser Diffraction Particle Size Analysis (LPSA)**

Laser Diffraction Particle Size Analysis (LPSA) is one of the common practices in determining the PSD of oil sands with the capability of identifying particles from nanometers up to millimeters in size. It determines the PSD by measuring the variation of scattered light intensity. Larger particles scatter the light at small angles and small particles scatter light at large angles. There is a relationship between particle sizes and the angle and intensity of scattered light.

This method tends to report different sizes for non-spherical particles with the same equivalent diameters (Ballard et al. 1999; Chanpura et al. 2014). Moreover, for fines and clay particles, this method is sensitive to the suspending medium (Chanpura et al. 2014).

#### **2.3.1.3 Dynamic Image Analysis (DIA)**

Dynamic Image Analysis (DIA) is based on analyzing the image of individual particles to build a conventional PSD curve. It offers more data and possibilities to describe the particles such as Martin's diameter, Feret's diameter, projected area diameter, and sieve diameter, among others.

### ***2.3.2 Sand control design***

Current design approaches for sand control screens are mainly based on the PSD of the reservoir sand. Further, the opening width and density of slots are determined based on the expected wellbore flow rate. Different matters related to the design of sand control screens are reviewed herein, with emphasis on slotted liners.

### **2.3.2.1 Numerical/analytical studies**

Some numerical and analytical techniques have been developed to predict the weight and PSD of produced sand from different screens. The analytical approaches simulate the slurry flow where the concentration of solids is low (<1%) so the particle-particle interaction can be ignored (Chanpura et al. 2012 and 2013). This assumption allows the development of an equation for the mass of produced sand based on the screen aperture and slot density. However, the development of such an equation requires the assumption that the only mechanism of particle capture is size exclusion. This assumption can be reasonable due to low solids concentration in the slurry test. Considering this assumption, Chanpura et al. (2012 and 2013) developed a mathematical relationship to predict the mass of the produced sand for wire wrapped screens and square mesh screens. Moreover, they developed a numerical technique based on Monte-Carlo simulation to predict the PSD of the produced sand.

For higher concentrations, it is not possible to develop an analytical technique due to the complexity of inter-particle interactions. Mondal et al. (2011, 2012, and 2016) developed a numerical simulation technique based on Discrete Element Method (DEM) to simulate gravitational discharge of a multi-size spherical pack through different screens.

### **2.3.2.2 Experimental studies**

Three types of testing have been employed to assess the sanding and flow reliability of the screens. The screen evaluation experiments are adopted from granular suspension flow through restriction and can be classified into three main groups, (1) slurry SRT tests, (2) pre-pack SRT tests, and (3) full-scale liner tests.

#### **Slurry SRT**

Markestad et al. (1996) built a set up using a cylindrical sand pack with linear flow from the bottom of the sample to the top towards a slotted liner coupon. They created a gap between the sand pack and the coupon to simulate the initial gap between the sand face and the liner in real

field cases. The test conditions hardly allow the flow of larger particles towards the screen as typical field flow velocities are not enough to lift larger sand particles in these experiments.

To overcome this limitation, a new slurry SRT technique was developed by Ballard et al. (1999). In this technique, a screen coupon is placed in a flow loop and a mixture of reservoir sand with low concentration is pumped towards the screen and the differential pressure across the coupon is measured. The pressure drop across the screen coupon starts with low values but drastically increases as the sand and fines accumulate over the screen due to the formation of a filter cake. Chanpura et al. (2010) selected the pressure drop of 100 psi as the maximum acceptable pressure drop across the screen.

The flow of granular media through restrictions has been studied extensively (Vitthal and Sharma 1999; Valdes and Santamarina 2006; Wakeman 2007; Porubcan and Xu 2011; Agbangla et al. 2012; Guariguta et al. 2012; Lafond et al. 2013; Xie et al. 2014). The experimental research presented in the literature is based on the flow of granular suspensions with different concentrations, through different opening sizes and shapes, with two main objectives: (1) predicting the mass and size-distribution of the produced particles, and (2) investigating the factors that influence the screen plugging.

The understanding of particle flow through an opening is necessary to better understand the mechanisms of particle capture. Vitthal and Sharma (1999) described four main particle capture mechanisms in granular flow through an opening:

1. Size exclusion happens by the capture of particles larger than the opening size. This mechanism is not concentration dependent.
2. Surface deposition is the mechanism in which the particle capture is due to the attractive forces between the particle and the opening surfaces, such as van der Waals electrostatic and hydration forces. This mechanism is highly concentration dependent.
3. Sequential bridging is described as the sequential capture of the particles where the first particle is captured by surface deposition and then subsequent particles are captured sequentially on previously deposited particles till the particles bridge across the opening. This mechanism is highly dependent on particle concentration.

4. Multi-particle bridging is mostly a physical mechanism for the case that many particles attempt to simultaneously flow through an opening. This mechanism is highly concentration dependent as well. Bridging could form even if the size of the outlet is larger than the particle size. Multi-particle bridging may be further classified into two types:

- Hydrodynamic bridging: which occurs at low particle concentrations because of the converging flow-field near the opening.
- Mechanical bridging: which occurs due to a high particle concentration.

Multi-particle bridging is inevitable, regardless of the flow-field. Mechanical multi-particle bridging is commonly referred to as arching and is the primary mechanism of jamming in the gravity discharge of granular packs through hoppers and silos.

Size exclusion and surface deposition have been widely investigated (Corapcioglu et al. 1987; Herzig et al. 1970; Rajagopalan and Tien 1979). Previous researchers physically modeled the clogging of porous media at the macroscopic scale (Ghidaglia et al. 1996; Narayan et al. 1997) and microscopic scale (Wyss et al. 2006; Agbangla et al. 2012).

Several experimental studies have concentrated on multi-particle mechanical bridging during the discharge of granular materials in either dry sand packs (Coberly 1937; To et al. 2001; To and Lai 2002; To 2005; Zurigueta et al. 2003, 2005; Janda et al. 2008; Saraf and Franklin 2011) or in the presence of fluid flow (Guariguata et al. 2012; Lafond et al. 2013). In comparison, fewer experiments have studied multi-particle hydrodynamic bridging (e.g., Ramachandran and Fogler 1999; Sharp and Adrian 2005; Valdes and Santamarina 2006; Tran et al. 2009).

At low concentration slurry flows (less than 1% solid concentration) the closure of the restriction is dominated by particle-fluid interactions. In such low concentrations, fluid-particle interactions (fluid flow path and rate) are the dominant force for the retention/size exclusion mechanism. (Ballard et al. 1999, 2006, 2016; Gillespie et al. 2000; Williams et al. 2006; Constien and Skidmore 2006; Mathisen et al. 2007; Furgier et al. 2013).

In high-concentration tests (porosity less than 50%) the jamming of the particle in the restriction is dominated by particle-particle interactions. The flow of fluid and gravity force move the particles till the flow of particles is stopped by size exclusion or bridging (Markestad et al. 1996;

Hodge et al. 2002; Meza Diaz et al. 2002, 2003; Williams et al. 2006; Bennion et al. 2008; Ballard et al. 2012, 2016).

### **Pre-packed SRT**

The main purpose of a slurry test is to simulate the gap that initially exists between the formation sand and the screen. However, in SAGD wells, due to the unconsolidated nature of the formation, the formation collapses around the liner to result in a high-porosity zone in early stages of the well operation (Boone et al. 1997; Carlson 2003). Therefore, a pre-packed SRT seems to be more representative of the actual field conditions.

In most pre-packed SRTs, a certain amount of sand is packed above a screen coupon and then some axial stress is applied. This stress is required to avoid channeling in the sand pack (Ballard et al. 2006). The main parameter to measure is the pressure drop across the coupon. Due to complexities in measuring the pressure drop across the coupon, most researchers measure the pressure drop across the sand screen and a small depth into the sand pack (Markestad et al. 1996; Ballard et al. 2012; Bennion et al. 2008; Romanova et al. 2014, 2015).

Pre-pack tests could be performed either by using actual oil sands from the reservoir, outcrop sand or commercial sand replicas. Ballard et al. (2016) obtained a good agreement between the results of pre-packed SRT tests by using reservoir sands, equivalent (i.e. same PSD) outcrop sands, and equivalent commercial sands.

Bennion et al. (2008) developed a protocol for optimum screen opening size selection/evaluation for SAGD wellbores. Their protocol is based on the testing results from pre-packed SRT. In their protocol, the cleaned sample of the reservoir sand is packed in a Hassler cell/core holder. Sand pack is pressurized axially to a stress level equivalent to the field condition. In these tests, the pressure drop across the coupon is measured along with the produced sand. Their experiments are conducted by flowing single-phase oil, two-phase oil-brine, and three-phase oil-brine-gas through the sand pack. They consider a limit for the acceptable pressure drop and sand production to evaluate different screens. The same test protocol has been applied later in tests on sand packs supported by wire wrapped screens (Romanova et al. 2013, 2014, and 2015). However, this test protocol does not account for the interaction between the slots as it uses single-slot coupons. Further, their testing does not allow the use of a coupon with a reasonable OFA.

### **Full-scale liner tests**

All pre-packed SRTs are designed for linear flow conditions. However, the flow near the screen should be radial. Some researchers have developed full-scale test apparatus to study the effect of radial flow on the screen performance.

Chenault (1938) developed a full-scale SRT apparatus to evaluate the screen flow capacity and plugging tendency. He found that a pack of high permeability sand in the space between the liner and the formation reduces or eliminates the sand inflow.

A similar set up was later used by Qi (2004) and Jin et al. (2012) to study the performance of different screens for unconsolidated heavy oil resources in China. They compared the performance of pre-packed screens with gravel pack screens. Their study indicated that properly designed pre-packed screens have a similar performance compared to gravel pack screens.

Asadi et al. (2000) developed a full-scale sand flow loop. The aim was to evaluate different stimulation techniques for plugging removal in standalone screens. Their focus was not screen evaluation testing.

#### ***2.3.3 Screen Performance Indicators***

Two main performance indicators are usually considered in sand control screen evaluation: (1) acceptable sand production; (2) acceptable retained permeability.

To quantitatively compare the capabilities of different screens for stopping the inflow of sand, a threshold for the acceptable amount of produced sand (either transient sand production or continuous sand production) should be specified. Such a threshold has been widely used to define the highest aperture size that could be used in a sand control screen (Coberly, 1937; Suman et al. 1985; Markestad et al. 1996; Tiffin et al. 1998). In most of these studies, the value of acceptable sanding threshold has not been clearly stated.

To understand the acceptable sanding threshold, the mechanisms for particle capture described by Vitthal and Sharma (1999) need to be understood. For size-exclusion, there is some initial sand production and by the capture of larger particles at the screen opening, the sand inflow stops. Due to the simplicity of this mechanism, there have been several numerical attempts to predict the produced sand weight and PSD (Chanpura et al. 2012; Mondal et al. 2014). In such a mathematical representation, the produced sand is a function of the screen opening, OFA, and

PSD. However, if the particle capture mechanism is bridging, these approaches are less effective in predicting the produced sand due to the more complex nature of the bridge formation and destabilization.

Valdes (2006) discussed the role of unconditionally stable bridges and sensitive bridges in sand production. He argued that the produced sand threshold must be divided into (1) initial produced sand (transient sand production), and (2) continuous sand production.

The acceptable sand production highly depends on operational constraints. For example, for higher rate wells, where the produced sand can be transported to the surface, the erosional resistance of the production facilities and the separator capacity will determine the acceptable sand production. For low-rate horizontal wells, sand transport to the surface due to the low flow rate is unlikely and the volume of the liner and the artificial lift requirements dictate the acceptable sand production.

Chanpura et al. (2012b) proposed 0.12-0.15 lb/ft<sup>2</sup> (pounds per square foot of liner surface area) as the threshold for initial sand production. While there is no stated limit for continuous sand production in the literature, the value of 50 gr/bbl is floating around among SAGD practitioners.

Few papers discuss an acceptable flow performance for sand control screens. Markestad et al. (1996) proposed a retained permeability of 0.5 (i.e. 50%) as an acceptable limit. Retained permeability is defined as the altered permeability of the near-screen zone over the initial permeability of the intact formation.

### ***2.3.4 Current Design Criteria for Sand Control Screens***

Due to the complex nature of the screen design and the wide range of variables that affect the sanding level, most attempts to address this problem have mainly been based on experimental results. Experimental attempts go back to early 1930's. Coberly (1937) showed that the sand retention on the slot is dictated by the coarser portion of the PSD. He concluded that the slot opening should not exceed two times of the upper 10% particle size in the PSD ( $2D_{10}$ ). Some of his tests resulted in an even more conservative limit for the slot size ( $D_{10}$ ). The difference arises from the different assumptions for the acceptable level of sand production.

Markestad et al. (1996) considered two thresholds for the acceptable opening widths ( $d_+$  and  $d_{++}$ ) where  $d_{++}$  is the extreme upper limit for slot width that should not be exceeded. The same

concept was used by Fermaniuk (2013) who specified a series of slot sizes ranging from 2D<sub>50</sub> to 3.5D<sub>50</sub> for the minimum and maximum aperture size referred sometimes as the “slot window”.

Further complexities arise in heterogeneous reservoirs where changes in the depositional environment cause drastic changes in the PSD along the wellbore. To address this problem, Markestad et al. (1996) specified a sand window for each sand facies in the reservoir. The ultimate screen aperture opening was selected by fitting one size to all the sand facies. A similar approach was adopted by Fermaniuk (2013) in selecting the slot size for slotted liners. This complexity becomes clearer in long horizontal wells where the well potentially crosses various sand facies. Mahmoudi et al. (2016) proposed a new method based on PSD mapping and used the slot window concept to select different slot sizes along the horizontal well to avoid fitting one size for the entire wellbore.

Above-mentioned discussions are valid for screens with a simple geometry such as slotted liners, wire wrapped screens, and precise punched screens. Guidelines developed for slotted liners and wire wrapped screen design are not applicable to premium mesh screens that have irregular and complex surfaces and openings (Chanpura et al. 2010).

## **2.5 Summery**

The screen design for sand production and flow performance of standalone screens has been studied extensively in the literature. Screen evaluation methods, mainly the SRT, have mostly focused on sand production and flow performance. Screen evaluation tests have been also used to address the plugging tendency and longevity of the screens. Due to the limited duration of the tests, complex phenomena such as screen plugging, corrosion, and scaling are not captured in the conventional laboratory experiments. Flow rates in these tests are usually ramped up to levels beyond typical field levels to account for the higher velocities behind the unplugged slots of the screen.

Pre-packed SRTs are widely used as a testing method for the screen design evaluation. They mimic the high porosity sand pack around the liner produced from the collapse of the gap between the sand face and the screen in the early phases of SAGD projects. During the pre-packed SRT, the main measurements are the produced solids through the screen and the pressure drop across the screen and sand pack as a function of time.



In the current test protocols of screen design for SAGD operations, which are mainly developed based on the work by Bennion et al. (2008), the maximum fluid flow rates are more than ten times of the rate expected in the field for a single slot coupon. These results need to be normalized for the OFA (O'Hara, 2015).

Pre-packed SRTs have shown that the produced sand is not only dependent on the slot aperture size but also on the flow velocity. One of the objectives of this study is to better understand this dependency and provide a correlation that relates the slot aperture size and the slot density to the amount of produced sand.

Fines migration and sand production in slotted liners and the parameters which control the size and concentration of the mobilized transported and produced solids along with the flow performance of the screen are the main focuses of this study. Fines migration is usually studied in the context of formation damage and reduced reservoir productivity. In this research, however, the focus is on its role in the screen plugging and pore plugging near the screen. Another aim is to understand the effect of fluid salinity and pH as well as the slot width and density on the mass of produced fines and entrapped fines near the screen.

In the end, the main goal of this research is to develop a new evaluation technique for the selection of the best screen for SAGD operations, by designing test conditions comparable to the SAGD operations, and by accounting for both the slot aperture and slot density in the test matrix.

**Table 2-1. Typical chemical composition of clay, presented in weight percentage (from Khilar and Fogler, 1998)**

	SiO <sub>2</sub>	Al <sub>2</sub> O <sub>3</sub>	Fe <sub>2</sub> O <sub>3</sub>	TiO <sub>2</sub>	CaO	MgO	K <sub>2</sub> O	Na <sub>2</sub> O
<b>Kaolinite</b>	40-49	35-40	0-13	0-2	0-0.8	0-0.5	0-1.0	0-2.0
<b>Illite</b>	50-56	18-31	2-5	0-0.8	0-2	1-4	4-7	0-1
<b>Chlorite</b>	31-38	18-20				35-38		
<b>Montmorlonite</b>	44-55	19-20	0-3			0-2		

**Table 2-2. Composition of produced water for different SAGD projects (NM: Not Mentioned)**

	Bhattacharjee (2011)	Hill (2012)	Hill (2012)	sand Project (2013)	Michaud (2009)	Pedenaud and Michaud (2009)	Pedenaud and Michaud (2009)	Pedenaud and Michaud (2009)	Garnache et al. (2012)	Garnache et al. (2012)	Peterson (2007)	Goodman et al. (2010)
<b>Calcium (Ca) (ppm)</b>	7	4	11	NM	2.7	3.9	22	10	2	20	1-52	
<b>Magnesium (Mg) (ppm)</b>	NM	1	5	NM	6.1	0.3	11	3	1	10	1.6-14	
<b>Barium (Ba) (ppm)</b>	0.8	NM	NM	NM	0	0.2	0	NM	NM	NM	NM	
<b>Sodium (Na) (ppm)</b>	314	NM	NM	NM	2200	706	780	1310	321	1004	130-3000	
<b>Sulfate (SO<sub>4</sub>) (ppm)</b>	107	NM	NM	NM	56	1	58	NM	NM	70	NM	
<b>Chloride (Cl) (ppm)</b>	200	NM	NM	NM	1697	930	962	2060	260	1310	48-4800	
<b>Potassium (K) (ppm)</b>	NM	NM	NM	NM	NM	NM	NM	21	18	NM	14-240	
<b>Ammonia(NH<sub>3</sub>) (ppm)</b>	NM	NM	NM	NM	NM	NM	NM	NM	NM	NM	11-64	
<b>Ammonium(NH<sub>4</sub>) (ppm)</b>	NM	NM	NM	NM	NM	NM	NM	46	66	NM	NM	
<b>Bicarbonate (HCO<sub>3</sub>) (ppm)</b>	NM	NM	NM	NM	2677	332	489	493	406	429	NM	
<b>Carbonate (CO<sub>3</sub>) (ppm)</b>	NM	NM	NM	NM	108	1	0	NM	NM	2	NM	
<b>Silica (SiO<sub>2</sub>) (ppm)</b>	NM	188	261	273	260	260	250	170	255	NM	11-260	
<b>Alkalinity (as CaCO<sub>3</sub>) (ppm)</b>	NM	173	297	257	NM	NM	NM	NM	NM	NM	140-1400	
<b>Salinity (ppm)</b>	NM	NM	NM	1	NM	NM	NM	NM	NM	NM	NM	
<b>NaCl (ppm)</b>	NM	NM	NM	NM	NM	NM	NM	3400	400	NM	NM	
<b>Hardness (as CaCO<sub>3</sub>) (ppm)</b>	22	NM	NM	6	32	11	100.9	NM	NM	NM	NM	
<b>Total Solid (TS) (ppm)</b>	NM	NM	NM	NM	NM	NM	NM	5700	2800	NM	NM	
<b>Total Dissolved Solid (TDS) (ppm)</b>	1005	1290	2870	1644	6951	2370	2585	NM	NM	3040	NM	
<b>SS (Suspended Solid) (ppm)</b>	NM	NM	NM	NM	NM	NM	NM	NM	NM	<25	NM	
<b>Total Organic Carbonate (TOC) (ppm)</b>	NM	300	350	NM	NM	NM	NM	588	596	200	170-430	
<b>Oil(ppm)</b>	NM	NM	NM	82	NM	NM	NM	NM	NM	20	NM	
<b>pH</b>	8.5	NM	NM	8	7.9	8	7.7	NM	NM	7.9	7.3-8.8	
<b>Specific Gravity</b>	1.005	NM	NM	NM	NM	NM	NM	NM	NM	NM	NM	

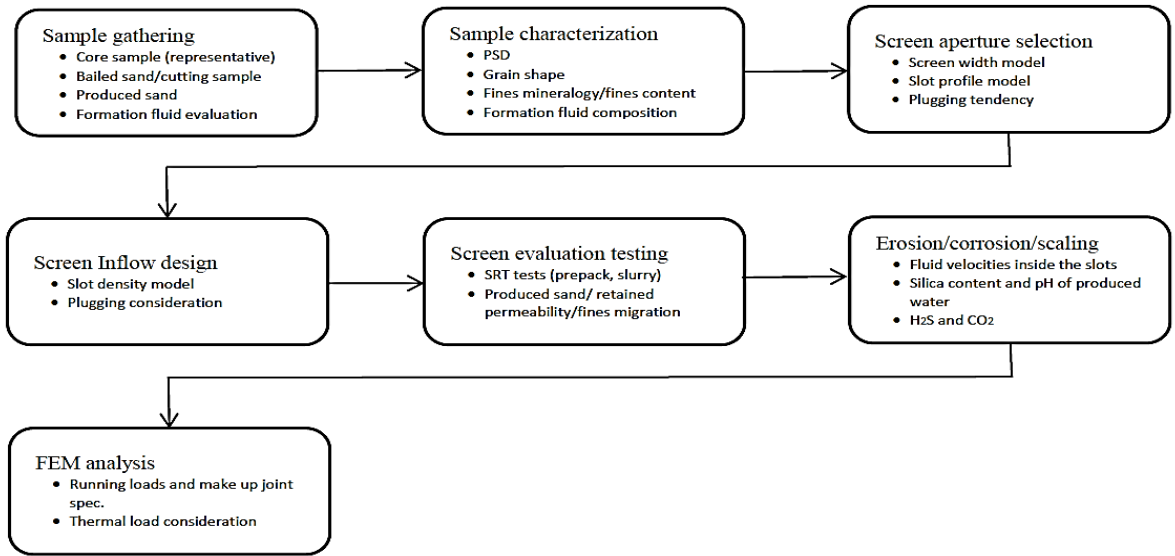


Figure 2-1. Workflow for the screen design

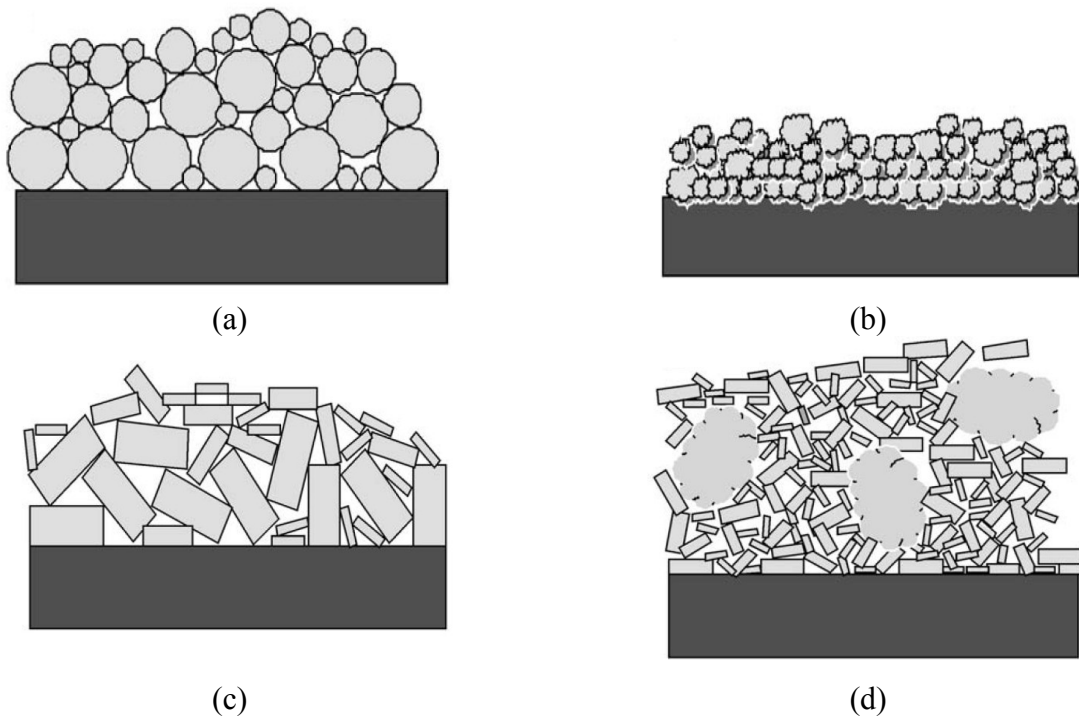


Figure 2-2. Schematic representation of deposited mineral layers: (a) silica, (b) kaolinite, (c) chlorite and (d) smectite /montmorillonite (After Jeannin et al. 2010)

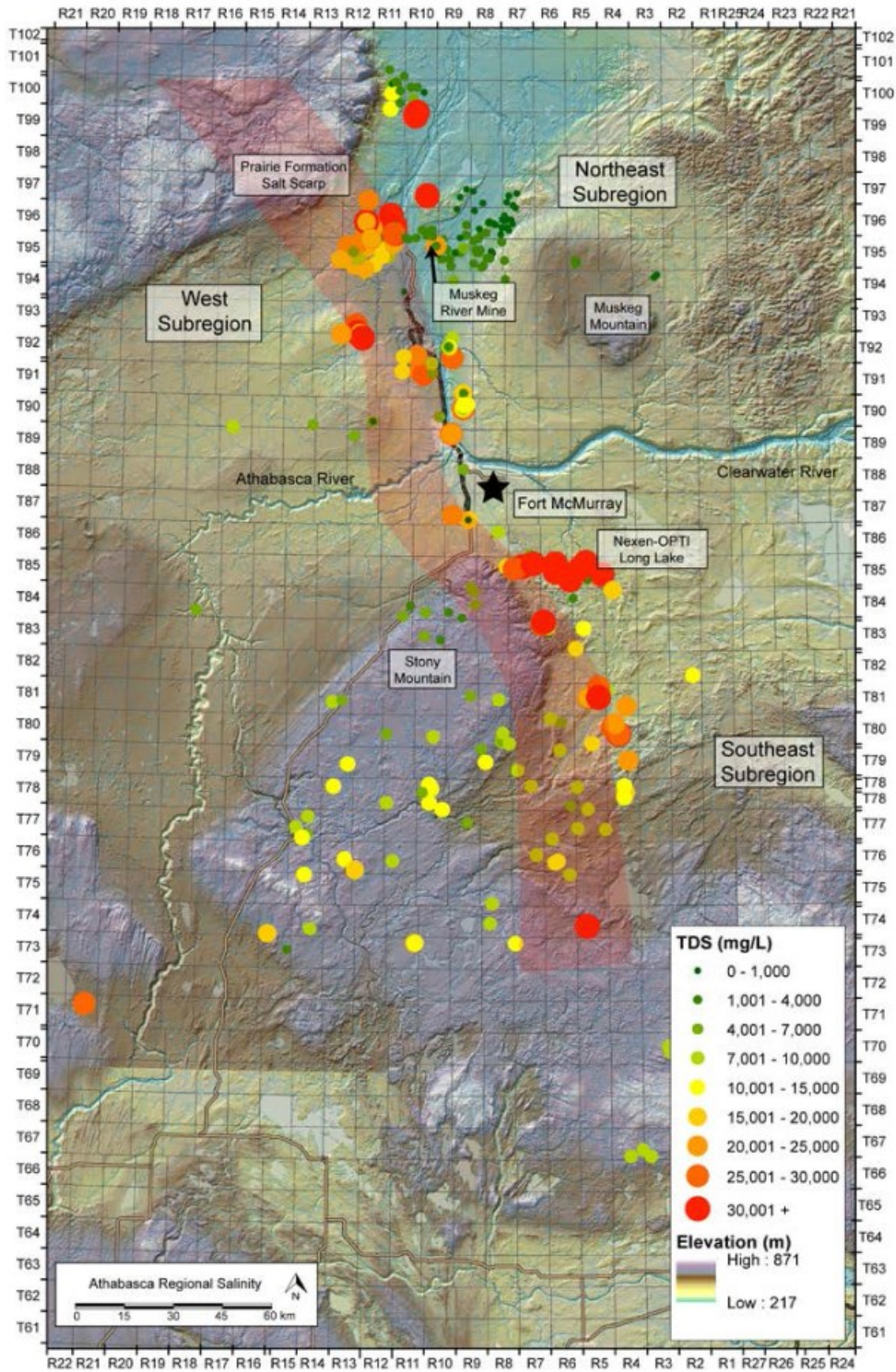
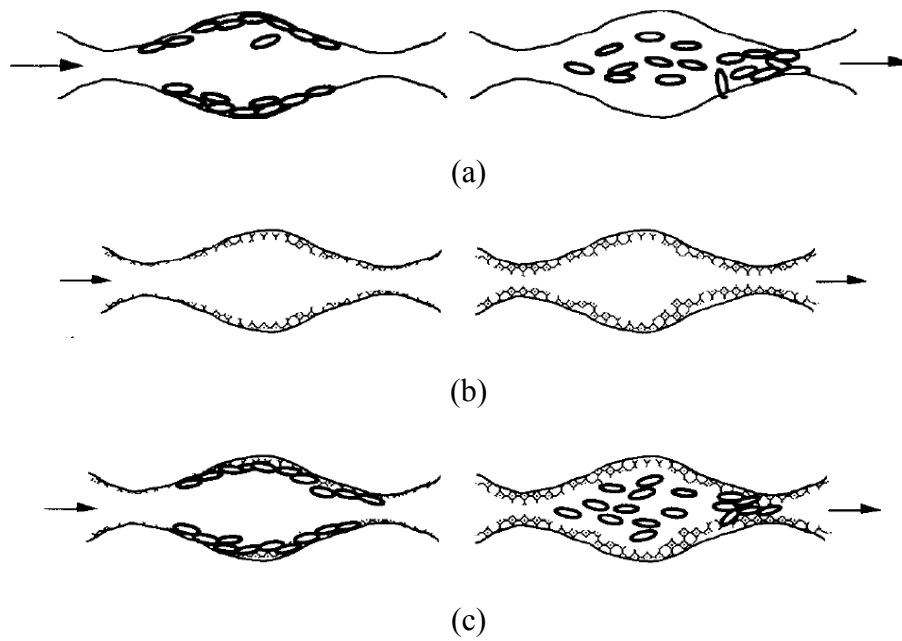


Figure 2-3. Water TDS for McMurray Formation in the Athabasca oil sands region, overlain on ground surface elevation (Cowie, 2013)



**Figure 2-4. Three mechanisms for permeability reduction caused by changing the ionic condition of the environment for clay particles: (a) migration, (b) swelling and (c) Swelling-induced migration (Mohan et al. 1993)**



**Figure 2-5. Liner damage after four years of production (After Hallman et al. 2015)**

## CHAPTER THREE: OIL SAND AND COMMERCIAL SAND AND FINES CHARACTERIZATION

### 3.1 Introduction

Particle sizes distribution (PSD), particle geometry (shape) and particle composition are fundamental characteristics of oil sand particles. From the literature, size distribution, shape, and composition of the particles influence the mechanical performance of granular media. Particle shape emerges as a significant parameter that needs to be properly characterized and documented. This chapter presents the first comprehensive characterization of the mineralogical composition, surface texture of particles, and particle shape and size distribution for commercial sands as well as samples obtained from two steam assisted gravity drainage (SAGD) wells in the McMurray Formation. It will be shown that the particle shape and size distribution of the oil sand can be closely duplicated by commercial sands.

This section is continued with a review of the role the granular characteristics on the properties of a sand pack.

#### *3.1.1 Particle size distribution (PSD)*

The PSD of oil sand controls its porosity, permeability (Miura et al. 1997) and mechanical behavior (stiffness, shear strength, and volumetric deformation). The PSD also reveals the depositional environment and the history of transported sediments (Wen et al. 2002). Holtz et al. (2010) suggested that for the same porosity, granular soils with wider PSDs possess larger internal friction angles. There is evidence that suggests the PSD influences the compressibility of granular soils (Yamamuro and Wood 2004). Several experimental attempts have been focused on relating the permeability of a sand pack to the PSD (Kovacs 1981; Vukovic and Soro 1992; Cheng and Chen 2007; Odong 2008; Koch et al. 2011). These research studies related the permeability of the sand pack to mean particle size ( $d_{50}$ ) or the  $d_{90}$  (the larger 10% in the PSD curve). Kenney and Lau (1985) proposed that the PSD determines the sensitivity of granular media to internal erosion (i.e. fines migration in the petroleum context).

#### *3.1.2 Particle shape*

Particle shape is dependent on such factors as the mineralogical composition of parent materials, the distance of sediment transport before settling, and the mechanical and chemical processes the

sediment materials undergo after settling (Wentworth 1919). Particle shape is described based on the measurements of particle's sizes in different directions, leading to the shape description by such parameters as sphericity (Fonseca, 2011), aspect ratio (Diepenbroek et al. 1992), and elongation (Sukumaran and Ashmawy 2001) among others. Each of these definitions reflects some aspects of the formation history and contributes to the overall behavior of the oil sand, from particle packing to mechanical response.

Santamarina and Cho (2004) highlighted the influence of particle sphericity on the evolution of stress-induced anisotropy and showed that angularity and roughness influence both the stiffness and the strength. Guo and Su (2007) demonstrated that angularity influences the shear strength and dilatancy of sands. Clayton et al. (2006) addressed the effect of particle geometry on the sand response in cyclic triaxial testing.

It is evident that the force distribution in porous media is not homogenous (Terzaghi 1920; Santamarina 2002; Mitchell and Soga 2004). In a granular material, forces are transmitted through a series of, so called, inter-particle force chains. Particle shape influences the geometry of inter-particle contact and consequently the distribution of the stresses at the contact (Santamarina 2002).

Spherical particles have a higher tendency to rotate under stress, as the branch vector joining the centroids of two contacting particles and the contact normal are collinear. For ellipses and ellipsoids, the branch vector and contact normal are not collinear, increasing rotational resistance. Additionally, non-convex particles are more likely to developing a greater number of contacts per particle and hence exhibit higher strength and stiffness in comparison with convex particles (Fonseca et al. 2012). In real world, particles are not perfect spheres and sphericity and convexity of particles dictate the number of contact points. The shape and structure of fine particles ( $d \leq 44\mu m$ , smaller than mesh #325) and coarse particles ( $d \geq 100\mu m$ ) affect the filtration and mechanical properties differently (Santamarina and Cho 2004).

Sands in the McMurray Formation oil sand are classified as locked sand (Dusseault and Morgensten 1979). The particle shape plays an important role in the properties of such a dense fabric. Dusseault and Morgensten (1979) reported that the locked sand has an interlocking texture with relatively long particle contacts. The contact characteristics of the material are dictated by the PSD, shape, and stress conditions. This chapter presents the characterization

technique commonly used to characterize the PSD and presents a new approach for the sand characterization.

### ***3.1.3 Mineralogical composition***

Composition and fines concentration are one of the most critical properties of oil sands as they affect the permeability and its evolution through fines migration (Vaidya and Folger 1992; Sheng 2014). The fines mineralogy of oil sands in Alberta consists mainly of kaolinite and illite. Devere-Bennett (2015) reported a compositional fraction of 64.5%, 23.3% and 11.3% for kaolinite, illite, and smectite with a minor trace of chlorite in the clay content ( $<4\mu\text{m}$ ) in oil sands samples from the McMurray Formation.

Thermal diagenesis of feldspar particles to smectite can result in a significant reduction in the permeability of oil sands (Romanova et al. 2015). Further, the formation wettability is affected by the mineralogy of solid particles, which plays an important role in the ultimate oil recovery (Teeters et al. 1989; Liu et al. 2002; Sparks et al. 2003).

### ***3.1.4 Particle surface texture***

Particle texture is a smaller scale shape descriptor than the particle shape. Wenzel (1936) described that the surface roughness affects the wettability, where rougher surface texture strengthens the wettability caused by the surface chemistry.

The texture is assessed using terms like rough or smooth which reflects the texture on the grain surface and corners. Larger particles typically show a larger variation of texture (Krinsley and Smith 1968). Santamarina and Cascante (1998) showed that surface roughness influences small-strain deformation behavior of sand packs.

SEM images are conventionally used for the texture characterization (Krinsley and Takahashi 1962; Porter 1962; Krinsley and Donahue 1968). However, there are limited methods available to quantify the surface texture of sand particles. Vallejo (1995) proposed using fractal analysis and Bowman et al. (2001) proposed using the Fourier analysis to quantify the surface texture of the particles.

## **3.2. Particle size and shape parameters**

This section reviews the measurement techniques for the PSD and particle shape analysis and presents the definition of the parameters that are used to describe the particle shape and size.



These techniques and parameters are used in subsequent sections for determining the PSD and particle shape parameters for commercial sands and oil sand samples from the McMurray Formation.

### ***3.2.1 Particle size description and measurement***

Determination of the PSD is the most common method for describing the sand in a heavy oil reservoir and used primarily for sand control design. In this section, size description, size analysis techniques, and PSD representation are discussed in detail.

#### **3.2.1.1 Particle size description (PSD)**

A spherical particle can be described by its diameter alone. However, non-spherical particles must be described by multiple length and width measures. These descriptions provide greater accuracy, but also result in greater complexity.

Particle size is a basic parameter used to characterize sand in engineering applications. Definitions of representative sizes are important in describing the 3D geometry of a given particle (Endoh 2006). Conventional techniques assume that every particle can be characterized as an equivalent sphere. The reported value is typically an equivalent diameter. These techniques essentially take the physical measured value (i.e. scattered light and settling rate) and determine the size of the sphere with the same volume or the same surface area. Problems can arise if the material contains particles with very large aspect ratios.

Particle size analysis on a complex 3D shape is a delicate task as different methods could be used to define the dimensions for particle size analysis (Al-Raoush 2007). Feret diameter is usually used to describe the particle from image analysis. The Feret diameter is defined as the distance between two parallel tangents to the particle outline. The minimum and maximum Feret diameters ( $F_{\min}$  and  $F_{\max}$  respectively) are the largest and smallest values of Feret diameter for a given outline and can be calculated from 2D laser scanning data. Feret diameter  $90^\circ$  to  $F_{\min}$  and  $F_{\max}$  and mean Feret diameter can also be used for particle size description.

Another parameter for the size analysis is the 'effective diameter'. Al-Raoush (2007) presented an approach to determine the effective diameter of a particle based on the distance between the center of gravity of the particle and the voxels on the boundary of the particle. An alternative

approach also presented by Al-Raoush (2007) was to calculate the average length of the major, intermediate and minor axis.

### **3.2.1.2 Different techniques for particle size analysis**

Laser diffraction, image analysis, particle counter, sedimentation column and dry sieve analysis have been used in determining the PSD of granular materials. Due to different physics used in each measurement, the results could be different (Ballard and Kageson-Loe 1999; Ballard and Beare 2003; Slayter et al. 2008; Zhang et al. 2014). For instance, a sieve will tend to emphasize the smallest dimension because of the way particles must orient themselves to pass through the mesh opening. A sedimentation column measures the rate of the fall of the particle through a viscous medium, with other particles and/or the container walls tending to slow their movement. Flaky or plate-like particles will orient themselves to maximize drag while settling, shifting the reported particle size toward the smaller dimension. A light scattering device will average the particle dimensions in different directions as the particles flow randomly through the light beam, producing a distribution of sizes from the smallest to the largest dimensions.

Zhang et al. (2014) presented a series of measurement from sieve analysis and laser diffraction and showed the differences between the two cases relate to the aspect ratios of the particles. For glass bead with the aspect ratio of 1.0, both sieve analysis and laser diffraction method lead to the same PSD curve. However, the gap between the dry sieve and laser diffraction PSD curves widen as the aspect ratio reduces. Based on some sand retention test results, they concluded that the PSD from dry sieve must be considered for the sand control screen design instead of the PSD from the laser diffraction method.

The only techniques that can describe particle size using multiple values are microscopy or automated image analysis. An image analysis system could describe the non-spherical particle using the longest and shortest diameters, perimeter, projected area, or again by equivalent spherical diameter (**Figure 3-1**). When reporting a particle size distribution from image analysis systems, the equivalent spherical diameter has been the most common method that has been exercised.

### **3.2.1.3 Presentation of the PSD**

Traditionally, the results of PSD analysis are tabulated to show the mass fraction of each screen increment as a function of the mesh size of the increment. Since the particles on any screen are passed by the screen immediately ahead of it, two numbers are needed to specify the size range of an increment, one for the mesh through which the fraction passes and the other on which it is retained. Conventionally, PSDs are presented in the histogram and cumulative distribution. Cumulative distribution is commonly used in the design of sand control screens.

The cumulative particle size distribution shows what weight percent of a sample is larger than a particular particle size. The advantage of this type of display is that it allows easy fitting of discrete data and interpolation to read off particular values of the distribution. The particle size is plotted on a logarithmic scale because the logarithm of the particle sizes often comes close to being a normal or Gaussian distribution. A distribution of the logarithm of particle sizes may include many small particles but no negative size particles, which would be possible with a Gaussian distribution of particle sizes. Several quantitative parameters can be determined from a cumulative distribution. These include the median, mode, skewness, and kurtosis (Blott et al. 2001).

### ***3.2.2 Particle shape description and measurement***

For a long time, engineers have either relied on qualitative measures of shape, such as the classification of particles as angular or rounded (Powers 1953) or have compared their particles with existing charts (Krumbein and Sloss 1963) (**Figure 3-2**). With the advent of microtomography, three-dimensional mapping of sand particles became available. However, complex techniques are still required for the data analysis.

Laboratory sensors are known as size and shape analyzers, (e.g., QICPIC by Sympatec (Sympatec 2009) and Camsizer by Retsch 2005) provide PSD and some shape parameters based on dynamic image analysis. In QICPIC, two-dimensional images are captured while the particles fall and pass between a specially configured light source and a pair of imaging lenses. The advantage of the QICPIC system is that the analysis can be performed quickly. In this approach, the shapes of randomly orientated particles are captured to overcome some of the limitations of static image analysis (e.g., particles on a flat surface tend to have a preferred orientation). The drawback is that the measurements are 2D and the spatial resolution is limited.

Conventionally, particle shapes have been characterized based on the geometric dimensions of a particle, including major axis, minor axis, perimeter, and smallest circumscribing circle. With advancements in the computer technology, more sophisticated particle shape characterization approaches have emerged. **Table 3-1** shows the common shape factors for some geometrical shapes. Definitions of common shape parameters are provided herein. The QICPIC technology uses the same definitions of shape parameters, such as sphericity and convexity, as defined by Sympatec (Sympatec 2009).

### 3.2.2.1 Aspect ratio, elongation, and flatness

It is a common practice to model a particle with an ellipsoid for shape analysis (**Figure 3-1**). Aspect ratio, elongation, and flatness are the morphological parameters for comparing the particle with an ellipsoid. For spherical particles, all these properties will have a value equal to one.

Aspect ratio is commonly used to describe the relation between the minimum (thickness) and maximum (length) dimensions of the particles. Flatness is the ratio of the minimum (thickness) and the intermediate (width) dimension. The elongation is the ratio between the intermediate (width) and maximum (length) dimension. Aspect ratio, elongation, and flatness provide a good idea of the particles' shape. For an ellipsoid that has three distinct principal axis lengths, denoted as  $a$ ,  $b$  and  $c$  where  $a > b > c$ , the aspect ratio, elongation and flatness ratio are given by:

$$\textit{elongation} = \frac{b}{a} \tag{1}$$

$$\textit{flatness} = \frac{c}{b} \tag{2}$$

$$\textit{Aspect ratio} = \frac{c}{a} \tag{3}$$

### 3.2.2.2 Sphericity

Sphericity describes how close a particle resembles a sphere. In other terms, it provides a measure of compactness, as it shows the degree of similarity between a particle and a sphere (most compact possible shape). Moreover, it reflects the similarity between the particle's length, height, and width. It is defined as surface area of volume-equivalent sphere to particle surface area (Wadell 1932):

$$\varphi = \frac{\sqrt[3]{36\pi V_p^2}}{S_p} \quad (4)$$

where  $V_p$  is the volume of the particle and  $S_p$  is the surface area of the particle. In 2D image analysis, sphericity is defined and measured as the ratio of the perimeter of the circle with the same area as the 2D projected particle to the actual perimeter of the projection (Sympatec 2009). The result of the shape factors in general with 2D image analysis isn't always unique and depends on the position of the particles when they are exposed to the camera. Therefore, these analyses should be repeated for the same sample several times to ensure repeatability of the results.

A perfectly spherical particle would have a sphericity of 1, which is rather uncommon in nature. Most fluvial sand particles have sphericity numbers around 0.7. Sphericity is generally affected by elongation of the particle. Needle-like particles have a sphericity of nearly zero. However, it is rare to find natural sand with sphericity less than 0.5 (Cho et al. 2006).

### 3.2.2.3 Convexity

Convexity is largely associated with sharpness and sharp-cornered prominence of the particles. The definition of a convex shape is that a straight line joining any two points within the object also remains within the object. When this condition is not satisfied, the shape is concave. Convexity is another measure of compactness of a particle and is defined as (Fonseca 2011):

$$C_v = \frac{V_p}{V_{CH}} \quad (5)$$

where  $V_{CH}$  is the minimum convex volume containing all the points defining the particle, and  $V_p$  is the particle volume.

Convexity could also be defined for 2D projection of particles as the ratio between the actual area of the projection and minimum convex area covering all the points defining the projection (Sympatec 2009).

## 3.3. Particle shape and PSD of the oil sand in McMurray Formation

Results of the image analysis including the PSD and shape factors on samples from McMurray Formation are presented in this section. The sands were taken from core samples at the depths of

180 m to 220 m for Well A and 170 m to 190 m for Well B in Athabasca oil sands. Petrophysical log (**Figure 3-3**) indicated in-situ porosity was in 31- 35% range.

The oil sand samples were cleaned from bitumen before testing. The cleaning procedure was performed with Soxhlet extraction unit with toluene as solvent. Well log data were used to choose 23 different samples from different depths for the particle shape and size analysis. Approximately 250 gr of oil sand were used for each depth and performed image analysis on all samples to obtain the PSD and shape factors. Direct shear tests were performed on samples from a few selected depths. The testing program enabled the assessment of morphological and mechanical properties of oil sand samples. The same testing was repeated on the commercial replica to investigate the possibility of replicating the oil sands with equivalent commercial sands.

### ***3.3.1 Geological description of oil sands in McMurray Formation***

Carrigy (1966) described the lithology of Athabasca oil sands, which is a succession of depositional environments that developed because of an extensive marine transgression in early Cretaceous time. McMurray Formation consists of lower, middle and upper members.

Carrigy (1966) described the Lower McMurray Member as fluvial deposits and the Middle and Upper Members as foreset and topset beds of an ancient delta. The depositional environment resulted in a coarser sand deposition in the Lower McMurray Formation, with (1) the maximum size larger than 1 mm, (2) median particle size larger than 130  $\mu\text{m}$ , and (3) typically more than 80% larger than mesh #200 (74  $\mu\text{m}$ ). The coarser sands also have a different composition of heavy metals than those of finer sands (Carrigy, 1966). The coarser sands are mainly quartz and have up to 3.5% feldspar and up to 2.5% chert.

Fine-grained sands are most common in the Middle McMurray Formation. The median size ranges of fine-grained sands as low as 90  $\mu\text{m}$  and as high as 180  $\mu\text{m}$ . These sands consist of quartz, feldspar, and mica (Carrigy 1966). These sands are rarely cemented and are fully saturated with oil. Towards the top of Middle McMurray Formation, fine sand becomes less common and gradually replaced by beds of thick rippled sand and thin shaley silt.

The third member described by Carrigy (1966) is the Upper McMurray Formation, which consists of horizontal beds of argillaceous very fine sand and silt with moderate oil saturation. The median particle size in these facies is mostly around 120  $\mu\text{m}$ .

### ***3.3.2 Particle size distribution of oil sands in the McMurray Formation***

Before performing the PSD analysis based on image analysis, the measurements of image analysis were verified against those of sieve analysis for three samples. **Figure 3-4** shows the PSD curves from the sieve and image analysis are consistent. However, PSD results from image analysis are slightly coarser for all three cases.

Next, PSD analysis was performed for 23 cleaned oil sands from two different wells. The PSD of the oil sands is presented in **Figure 3-5** and **3-6**, which indicates moderately to very well sorted samples with uniformity coefficient smaller than 3 (**Table 3-2** and **3-3**). Most tested oil sand samples consisted of fine sand except one sample from well one and two samples from well two which were medium sand. The mean size ranged from 121.6 to 284.3  $\mu\text{m}$  for well one and 150 to 249  $\mu\text{m}$  for the second well. The uniformity coefficient for all oil sand sample tested ranged from 1.33 to 3.24.

Since the samples analyzed in this research were obtained from two wells only, the results were compared with a larger data bank in the literature for the McMurray Formation. Abram and Cain (2014) performed a detailed study of the PSD for Devon Pike 1 project and proposed four classes of oil sand (**Figure 3-7**). Class I and II described by Abram and Gain (2014) were very fine sand. Class III and IV were medium and coarse sand, respectively. The samples from both wells fit within Class II (DC-II) and Class III (DC-III) oil sands in **Figure 3-7**.

### ***3.3.3 Particle size distribution of the commercial sands and fines***

To replicate the oil sands, 11 commercially available sands and nine commercially available fines were selected for characterization. Similar tests and analysis as oil sands were performed on all commercial sands and fines. The PSD and particle shape characteristics of seven commercial sands (CS-A to CS-G) were analyzed. Commercial sands were chosen based on their availability and their close geographical location to McMurray oil sands.

Most of the commercial sands tested here were coarse to medium sand except for sample CD-C which was mainly medium- and fine-grained. The PSD of different commercial sands is shown

in **Figure 3-8**. Detailed statistical analysis of the commercial sands is summarized in **Table 3-4**. These samples are uniform sand with uniformity coefficient ranging from 1.17 to 1.75, and curvature coefficient ranging from 0.87 to 1.03. This implies that the particles are within a narrow band of sizes, which is expected as such samples are graded for commercial application. The commercial sands used in the testing program are composed of more than 98% of quartz as reported by the suppliers.

To examine the possibility of duplicating the PSD of oil sands with commercially available materials, a series of tests was performed on ten commercially available fine materials. The PSD curves for the fine samples are shown in **Figure 3-9**, which indicates the samples were mainly silt-sized. The PSD was determined using laser diffraction particle size analyzer and demineralized water (pH=7.4) as the medium.

#### ***3.3.4 Particle shape of the oil sands in McMurray Formation***

A series of image analysis was performed on all oil sand samples using QICPIC to assess the morphological properties of sand particles. The results show high sphericity for all oil sand samples (**Table 3-2** and **3-3**). The mean value of sphericity for the entire samples is ranging from 0.86 to 0.88. This implies that the samples have semi-spherical shapes. The aspect ratio for all oil sands is similarly ranging from 0.74 to 0.76. The shape factors do not show much variation with depth.

#### ***3.3.5 Particle shape of the commercial sand***

Similar image analysis was performed on all commercial sands samples using QICPIC to assess the morphological properties of commercial sand particles. The results show a wider variation in sphericity for all commercial sand samples (**Table 3-4**). The mean value of sphericity for the entire samples is ranging from 0.84 to 0.91 slightly higher than the oil sands. This implies that the samples have semi-spherical shapes. The aspect ratio for all oil sands is similarly ranging from 0.73 to 0.77.

### **3.4 Dynamic image analysis for different size groups**

Although the average values of the shape factor for two sand packs can be the same, it is still possible that the particles in different size groups can have different shapes. The shape variation in different size groups can highly affect the pore size distribution and the particle contacts. A



more elaborate characterization consisting of the shape study of the particles in different size groups for the oil sands from both wells and commercial sands is necessary. This section presents the distribution of shape factors for different size groups for the oil sands and commercial sands samples. The average values of the shape factors are usually reported as an average for all of the particles in the batch used in the image analysis test, which favors smaller particle due to a higher number of finer particles. The average values, however, do not provide information on the particle shape for different size groups of the sample. For instance, although the overall shape factors for a sand pack shows spherical particle, there may still be disagreement in the values of shape factors for certain sub-groups within the sample PSD (larger grains compare to finer particles). To overcome this problem, the shape factor distribution for different size groups was determined rather than the average of the shape characteristics for all the particles in the commercial and oil sands samples.

**Figure 3-10(a) to 3-10(c)** shows the overall shape factors for both oil sands and commercial sands. The figure indicates a close agreement between the average shape factors for the commercial sand samples and the corresponding commercial sand samples. **Figure 3-11(a) and 3-11(b)** show the sphericity change within each size group for the oil sands at different depths for Wellbore A and B, respectively. The oil sands sphericity for each size group is consistent among all samples; however, oil sand particles from Wellbore B show a slightly higher sphericity than Wellbore A. Results indicate a higher variation in the sphericity of coarser particles, which may in part be due to the smaller number of particles in coarser size groups.

**Figure 3-11(c) and 3-11(d)** show the convexity change within each size group for the oil sands samples obtained at different depths from Wellbore A and B, respectively. The figure indicates consistent values for the convexity of oil sands particles in each size group for different depth in the same wellbore. However, the convexity of oil sands particles from Wellbore A is slightly higher than the same in Wellbore B. The variation of convexity is higher for coarser size groups which may in part be attributed to the lower number of particles in the coarser size groups.

**Figure 3-11(e) and 3-11(f)** depict the aspect ratio within each size group for the oil sands samples obtained from different depths of Wellbore A and B, respectively. Results indicate consistent values for the aspect ratio for each group size at different depths in the same wellbore. However, the samples from Wellbore A show a slightly lower aspect ratio than Wellbore B.

Results also indicates a higher variation in aspect ratios for coarser size groups at a different depth, which may again, in part, be attributed to the lower number of particles in coarser size group.

### 3.5 Mineralogy testing

X-Ray diffraction (XRD) analysis of fines (<44 $\mu$ m) indicates kaolinite, illite, and smectite are the primary clay minerals in Wellbore A and B, but the clay content and composition is changing slightly with depth. The same clay composition was also used in the synthesis of commercial sands that correspond to DC-II and DC-III.

XRD analysis of the silt and sand particles indicates SiO<sub>2</sub> as the main mineral for both commercial sands and oil sands (**Table 3-5** and **Table 3-6**).

### 3.6 Surface texture of particles

This section provides only a qualitative comparison of particle surface textures due to the complexity of available methods for surface texture analysis. Scanning Electron Microscope (SEM) image of over 50 silt and sand particles (44  $\mu$ m to 850  $\mu$ m) was obtained and analyzed to assess the variations of surface texture in each size group. The sand and silt particles of desired sizes for both commercial sands and oil sands were isolated by gently sieving the bulk samples. Individual sand particles were randomly selected by using a reflected-light microscope and mounted on an aluminum stub with double-sided carbon tape for SEM analysis.

The comparison of surface texture is shown in **Figure 3-12** for samples from Wellbore A, Wellbore B, and the commercial mix. From the images, it appears that the commercial sand particles have smoother surface texture than the oil sands for very coarse, coarse and medium size. For very coarse sand from both wells, the presence of some carbonate shell among the sand particles is noted (**Figure 3-12 (b3)**). From the SEM images, it appears the particles with higher sphericity are in general smoother than particles with lower sphericity (**Figure 3-12 c(1)** vs. **c(2)**; **Figure 3-12 a(4)** vs. **a(6)**; and **Figure 3-12 a(1)** vs. **a(2)**).

Most particle sizes of all oil sands samples from both wells are either fine or very fine sand. Images indicate higher surface roughness for fine silt particles from both wells. Images indicate rougher surfaces for commercial fines than the fine particles of oil sands samples particle and growing roughness for finer particles. However, commercial fines particles, which are produced

from particle crusher, possess drastically different surface roughness's (**Figure 3-12 c(23), c(24) and c(27)** vs. **Figure 3-12 c(22), c(25), c(26) and c(28)**).

### **3.7 Conclusions**

A comprehensive characterization of the PSD and shape distribution of commercial sand samples and oil sand samples from two wells in the McMurray Formation was conducted. Results indicate a close agreement between the shape factors for all tested oil sand samples at different depths. Most of the studied oil sand samples are fine sand except one sample from Wellbore A and two samples from Wellbore B, which are medium sand. The mean sizes range from 121.6 to 284.3  $\mu\text{m}$  for all tested samples. The uniformity coefficient for all oil sand samples range from 1.33 to 2.19, except for one sample from Wellbore A with the uniformity coefficient of 3.24. This indicates that the samples are uniformly graded sands.

Particle shape characteristics of different size groups for all tested oil sand samples were also presented. Results indicate the shape factors for sands and silts for all oil sands samples are generally consistent among the samples from different depths for both wells. However, there is larger variability in the shape factors for coarser particles.

Particle shapes and size distributions were determined to assess the feasibility of using commercial sands and fines to construct representative samples with similar properties to those of oil sands. The commercial sands are ranging from fine sand to coarse sand, and the fines mainly consist of silt sizes.

SEM analysis shows random changes in the surface texture of both oil sands and commercial sands, among the particles with different sizes and even with similar sizes. Per the results of XRD analysis, the main mineralogy in the silt and sand portion of oil sands is quartz ( $\text{SiO}_2$ ). Same analysis on the commercial sands also shows the dominance of  $\text{SiO}_2$ . Clay composition of the oil sands consists mainly of kaolinite and illite.

This chapter also presented a critical review of the measurement techniques for particle shape and PSD analysis and a protocol for the particles size and shape characterization of oil sands, which could be followed as common practice for such applications as screen design and evaluation.

**Table 3-1. Examples of shape factors for known shapes**

Shape	Sphericity	Aspect ratio	Convexity
Tetrahedron	0.671	1.000	1.000
Cube	0.806	1.000	1.000
Octahedron	0.846	1.000	1.000
Dodecahedron	0.910	1.000	1.000
Icosahedron	0.939	1.000	1.000
Cone (H=1.414D)	0.794	0.707	1.000
Hemisphere	0.840	0.500	1.000
Cylinder (H=D)	0.874	1.000	1.000
Sphere	1.000	1.000	1.000

Table 3-2. PSD indices and shape factors for oil sands from different depths of McMurray Formation in Well

A

Depth (m)	D <sub>10</sub> (µm)	D <sub>50</sub> (µm)	D <sub>90</sub> (µm)	C <sub>u</sub>	C <sub>c</sub>	S <sub>50</sub>	C <sub>50</sub>	AR <sub>50</sub>
197.03	140.4	191	241.6	1.41	1.05	0.87	0.95	0.75
198.32	115.5	284.3	579.3	3.24	0.88	0.86	0.96	0.75
199.86	62.7	121.6	209.3	2.19	1.05	0.86	0.94	0.75
201.39	69.7	136.3	196.1	2.06	1.21	0.86	0.94	0.74
202.82	154.2	196	244	1.33	1.01	0.87	0.96	0.75
203.87	144.1	191.4	246.3	1.41	1.03	0.87	0.96	0.75
204.93	133.4	183.3	239.3	1.43	1.04	0.87	0.95	0.75
206.24	144.3	195.3	260.1	1.44	1.01	0.87	0.95	0.74
207.51	129.1	179.6	232.5	1.47	1.04	0.87	0.96	0.75
208.83	135.8	182	241	1.40	1.03	0.87	0.96	0.75
210.76	138.1	195.2	262.3	1.50	1.04	0.87	0.95	0.74
212.60	126.6	177.2	241.6	1.48	0.97	0.87	0.95	0.74
213.71	130.9	202.9	278.6	1.64	1.07	0.86	0.95	0.75
215.13	132.9	184.3	243.8	1.47	1.00	0.87	0.96	0.75
216.48	121.1	188.8	243.4	1.65	1.12	0.87	0.96	0.75
217.73	152	199.6	249.8	1.37	1.02	0.87	0.96	0.75
218.97	144.6	191	253	1.38	0.97	0.87	0.96	0.74

**Table 3-3. PSD indices and shape factors for oil sands from different depths of McMurray Formation in Well B**

<b>Depth (m)</b>	<b>D<sub>10</sub> (µm)</b>	<b>D<sub>50</sub> (µm)</b>	<b>D<sub>90</sub> (µm)</b>	<b>Cu</b>	<b>Cc</b>	<b>S<sub>50</sub></b>	<b>C<sub>50</sub></b>	<b>AR<sub>50</sub></b>
<b>173.47 (OS-A)</b>	169	249	339	1.56	1.05	0.87	0.96	0.74
<b>173.88</b>	159	246	332	1.67	1.07	0.88	0.96	0.75
<b>180.03</b>	82	154	210	2	1.22	0.86	0.95	0.75
<b>180.4</b>	91	150	219	1.78	1.1	0.87	0.96	0.75
<b>190.2</b>	115	170	233	1.57	1.06	0.87	0.95	0.76
<b>190.6</b>	114	175	247	1.64	1.05	0.88	0.96	0.75

**Table 3-4. PSD indices and shape factors for the commercial sands**

<b>Depth</b>	<b>D<sub>10</sub> (µm)</b>	<b>D<sub>50</sub> (µm)</b>	<b>D<sub>90</sub> (µm)</b>	<b>Cu</b>	<b>Cc</b>	<b>S<sub>50</sub></b>	<b>C<sub>50</sub></b>	<b>AR<sub>50</sub></b>
<b>CS-A</b>	695	785	936	1.17	0.98	0.91	0.97	0.76
<b>CS-B</b>	495	765	1520	1.75	0.87	0.88	0.96	0.73
<b>CS-C</b>	196	268	350	1.46	0.98	0.9	0.94	0.76
<b>CS-D</b>	346	452	552	1.37	1.03	0.91	0.96	0.77
<b>CS-E</b>	359	474	637	1.38	0.98	0.9	0.95	0.77
<b>CS-F</b>	264	361	467	1.44	1.01	0.89	0.95	0.76
<b>CS-G</b>	129	158	199	1.18	0.98	0.84	0.93	0.74

**Table 3-5. Composition of the percentage of the clays in the fines (<44µm) of the oil sands**

<b>Wellbore A</b>				
<b>Depth (m)</b>	<b>Illite (%)</b>	<b>Kaolinite (%)</b>	<b>Chlorite (%)</b>	<b>Smectite (%)</b>
<b>197.03</b>	17.60	81.20	0.10	1.10
<b>199.86</b>	22.50	76.20	0.30	1.00
<b>201.39</b>	16.90	72.50	0.60	10.00
<b>202.82</b>	22.20	77.40	0.30	0.10
<b>203.87</b>	24.60	69.80	0.10	5.50
<b>207.55</b>	18.60	80.40	0.40	0.60
<b>208.83</b>	21.20	71.30	0.70	6.80

<b>210.76</b>	19.10	74.50	0.50	5.90
<b>212.60</b>	23.80	74.30	0.20	1.70
<b>213.77</b>	28.30	64.30	0.80	6.60
<b>215.13</b>	19.80	77.50	1.30	1.40
<b>217.73</b>	31.30	65.20	0.20	3.30
<b>219.69</b>	23.20	75.20	1.00	0.60
<b>Average</b>	<b>22.24</b>	<b>73.45</b>	<b>0.50</b>	<b>3.82</b>
<b>Wellbore B</b>				
<b>190.06</b>	18.50	75.50	0.20	5.80

Table 3-6. Composition of the particle larger than 44µm in oil sands from both wells

	Depth (m)	Quartz (%)	Feldspar (%)	Chert (%)
Wellbore B	<b>190.06</b>	94.4	3.2	0.8
Wellbore A	<b>201.39</b>	93.2	2.7	0.2

Table 3-7. XRD results of the commercial sands. All values are in percentage

	CS-A	CS-B	CS-C	CS-D	CS-E	CS-F	CS-G	CS-H	CS-I	CS-J
<b>CaO</b>	0.48	1.09	1.09	0.90	0.69	0.85	1.78	1.08	0.67	0.59
<b>K<sub>2</sub>O</b>	0.99	0.68	0.68	0.76	0.88	0.71	1.08	0.69	0.86	0.47
<b>MgO</b>	0.08	0.24	0.24	0.52	0.20	0.26	0.19	0.30	0.18	0.32
<b>Na<sub>2</sub>O</b>	0.82	0.86	0.86	0.56	0.78	0.78	0.81	0.73	0.79	0.73
<b>TiO<sub>2</sub></b>	0.06	0.08	0.08	0.40	0.13	0.15	0.21	0.17	0.11	0.20
<b>Al<sub>2</sub>O<sub>3</sub></b>	4.32	3.42	4.42	1.34	3.54	3.41	5.92	12.00	9.43	1.00
<b>P<sub>2</sub>O<sub>5</sub></b>	0.03	0.08	0.08	0.08	0.05	0.06	0.10	0.07	0.05	0.07
<b>SiO<sub>2</sub></b>	92.03	92.30	92.30	94.75	92.63	92.63	88.40	83.79	86.51	95.03
<b>Fe<sub>2</sub>O<sub>3</sub></b>	0.95	0.90	0.90	0.75	0.90	0.82	0.89	1.21	1.12	0.35
<b>MnO</b>	0.01	0.02	0.02	0.00	0.01	0.01	0.01	0.02	0.01	0.01
<b>L.O.I</b>	0.24	0.54	0.54	0.34	0.32	0.40	0.57	0.45	0.32	1.40

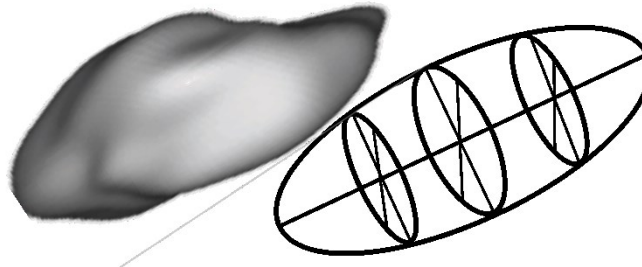


Figure 3-1. The Concept of elliptical representation of a particle

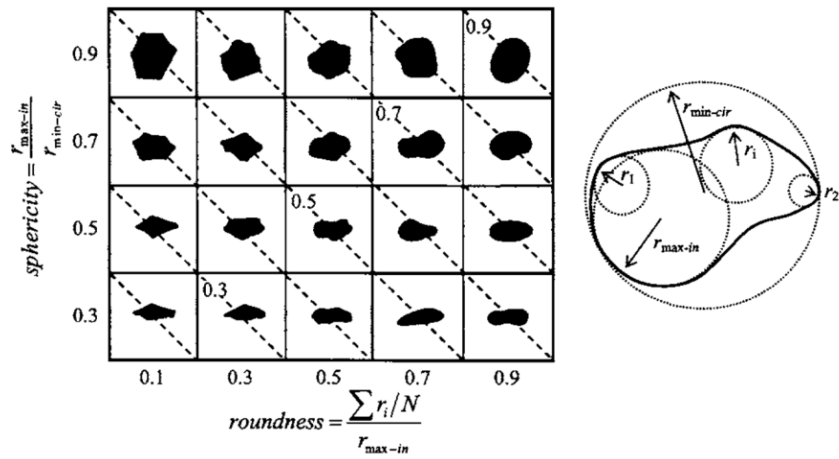


Figure 3-2. Particle shape determination (sphericity, S and roundness, R) chart, modified version from Krumbein and Sloss (1963)

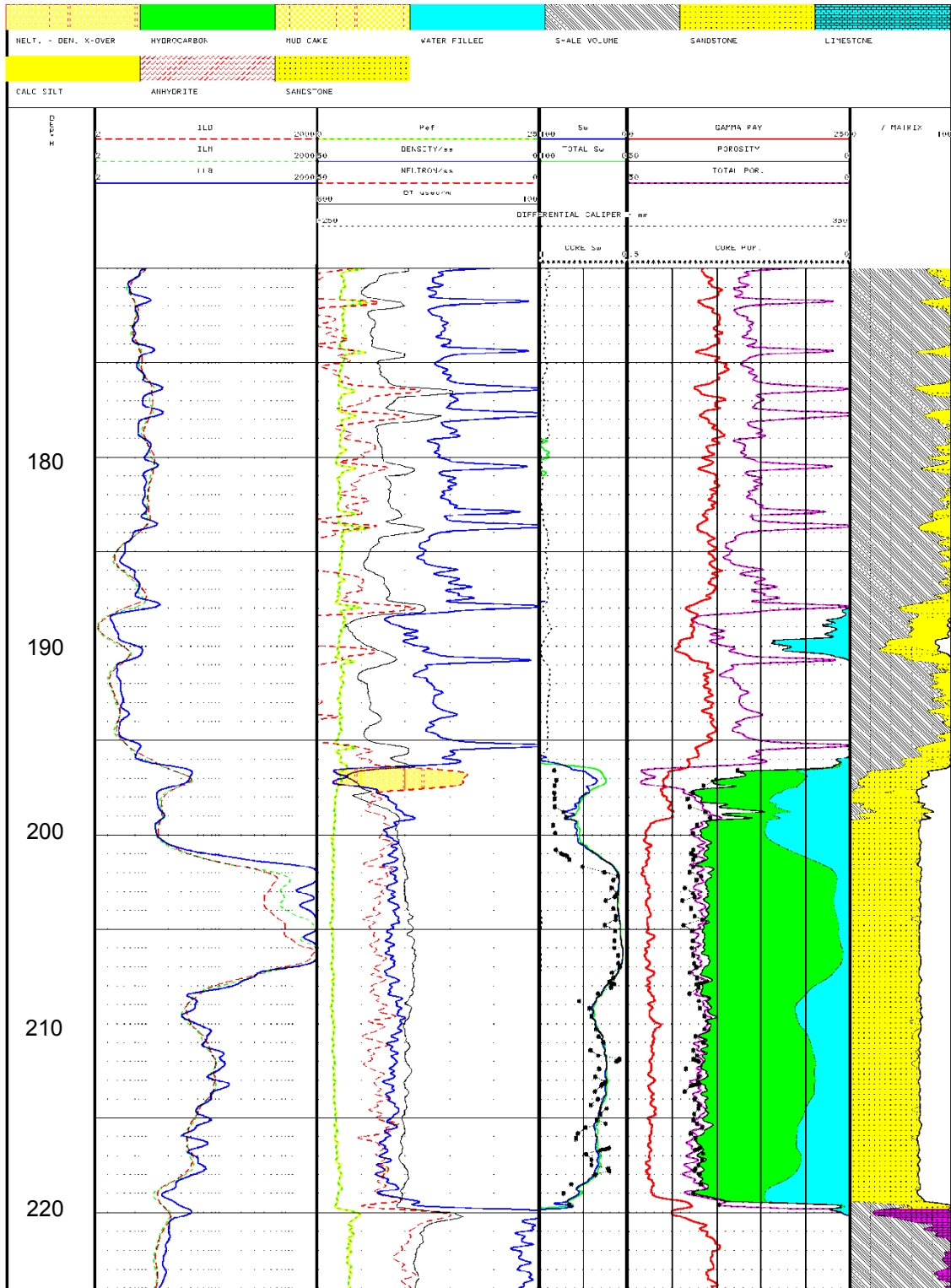


Figure 3-3. Geological log for Well A in McMurray Formation



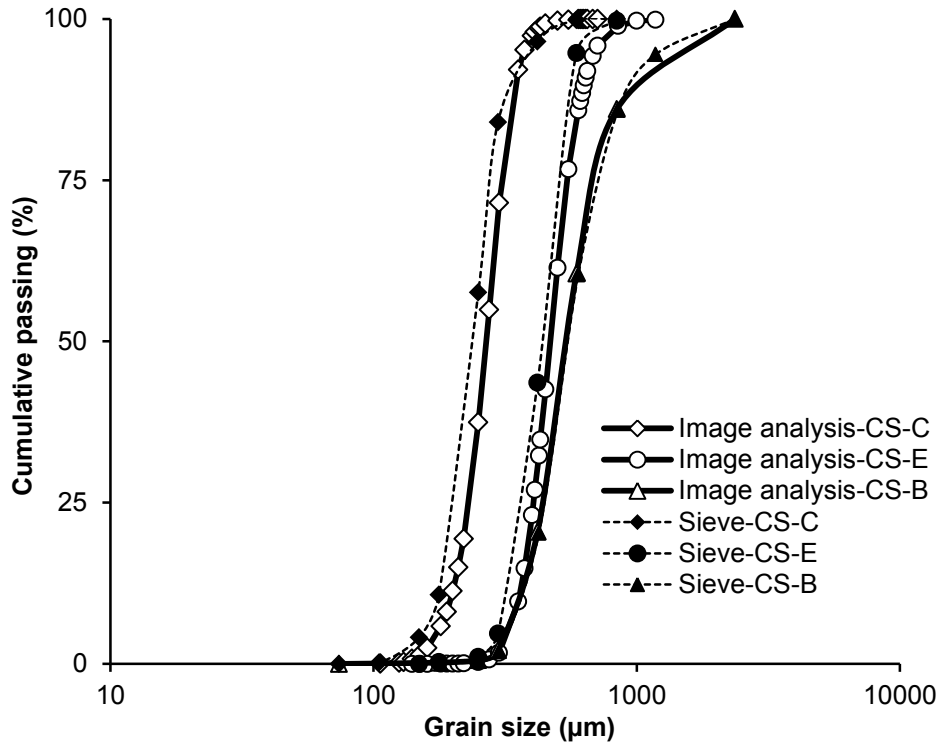


Figure 3-4. Comparison between the PSD from image analysis and dry sieve

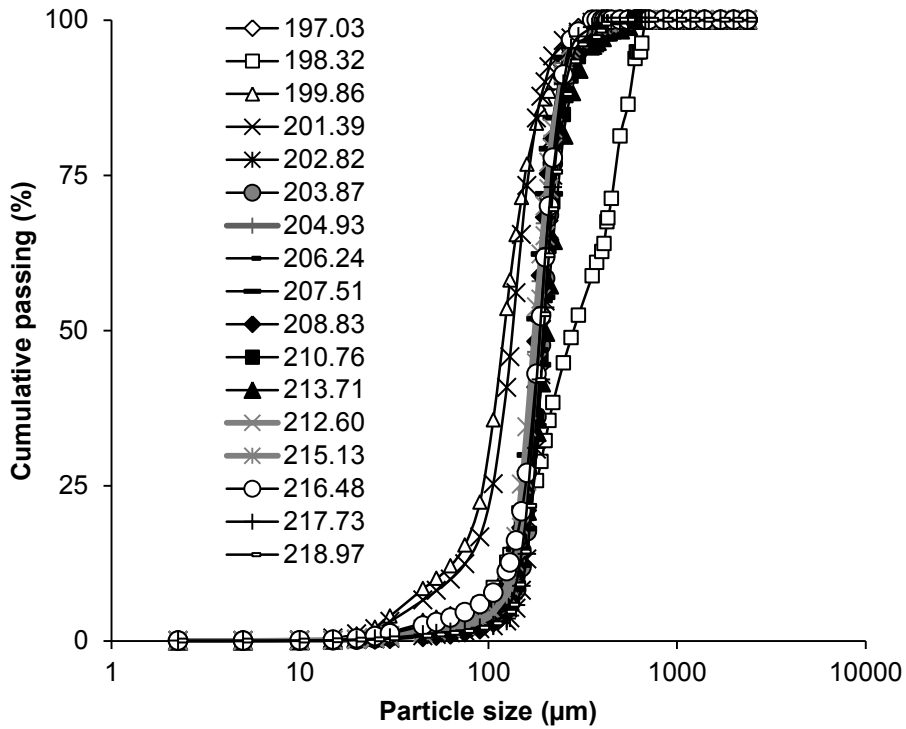


Figure 3-5. PSD for oil sand samples from different depths of McMurray Formation in Well A

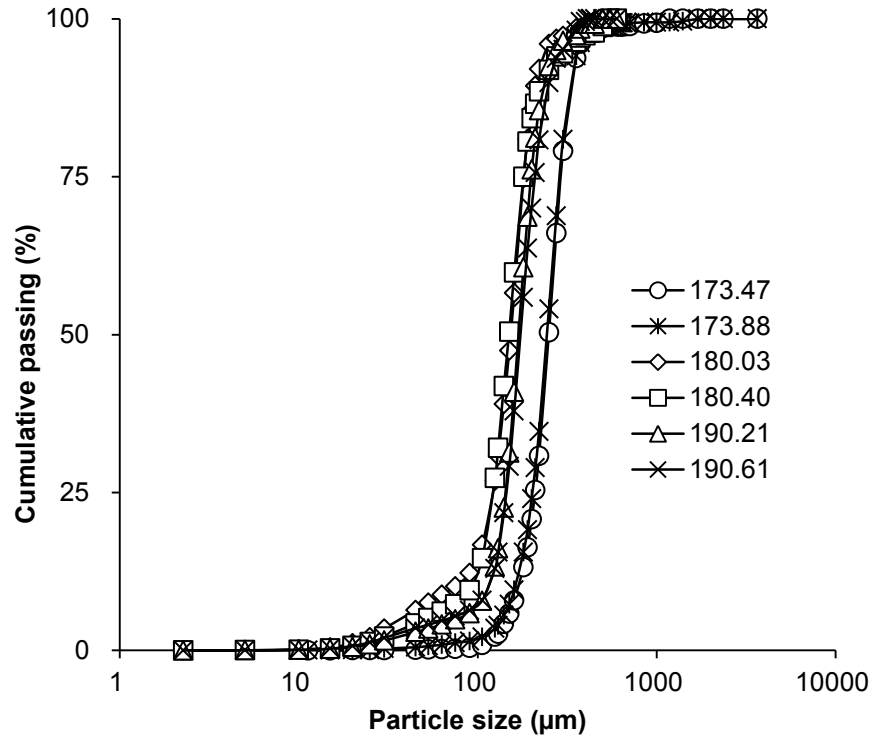


Figure 3-6. PSD for oil sand samples from different depths of McMurray Formation in Well B

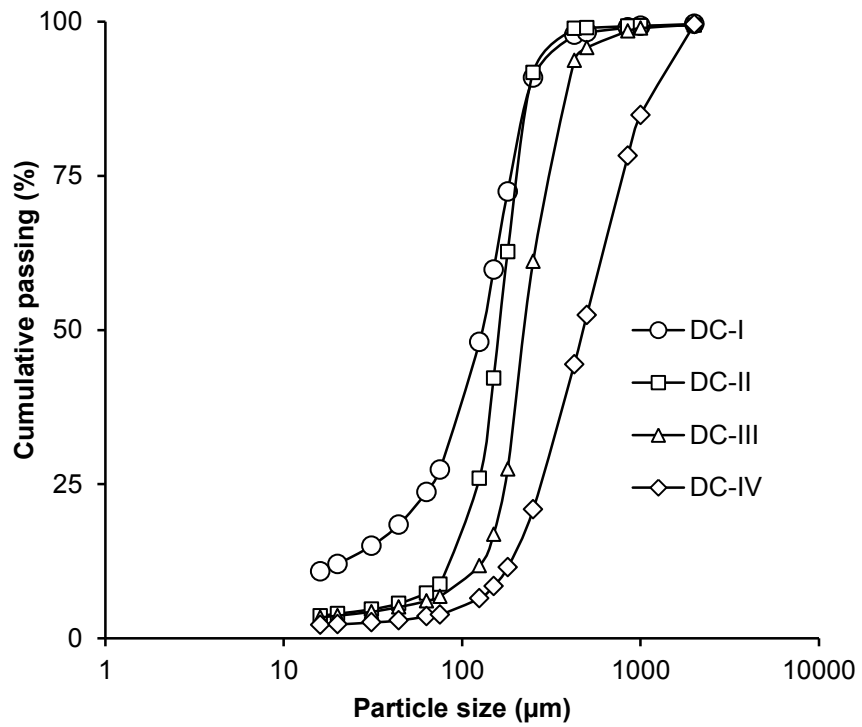


Figure 3-7. Four Representative PSDs provided by Abram and Cain (2014)

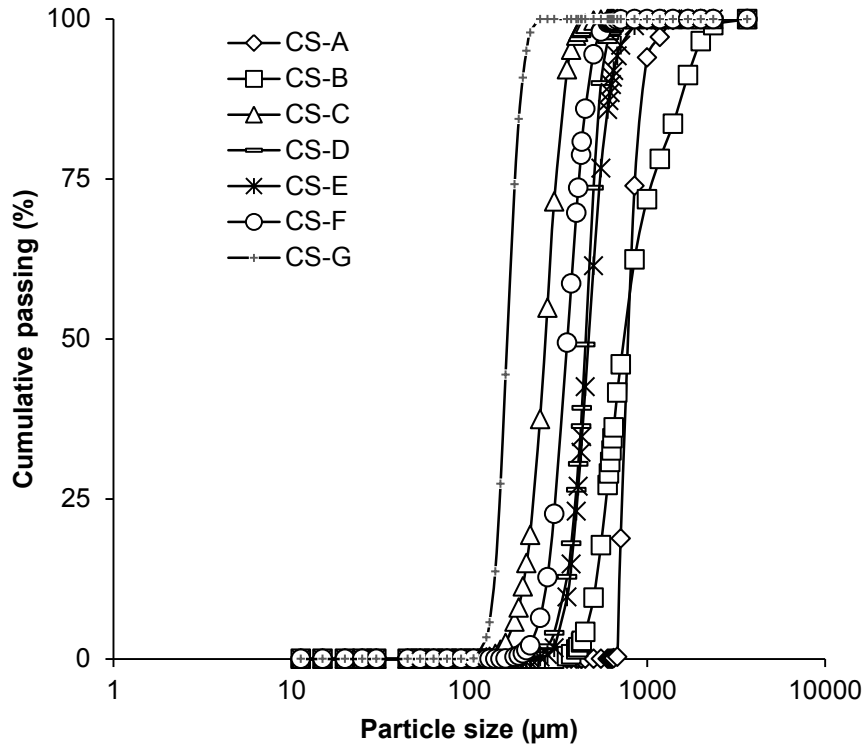


Figure 3-8. PSD for seven different available commercial sands

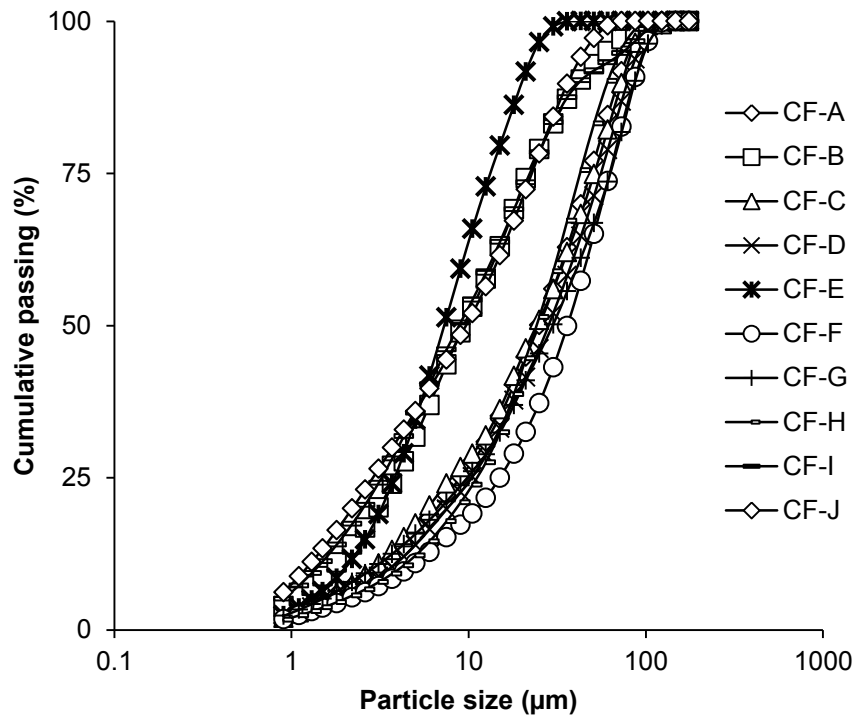
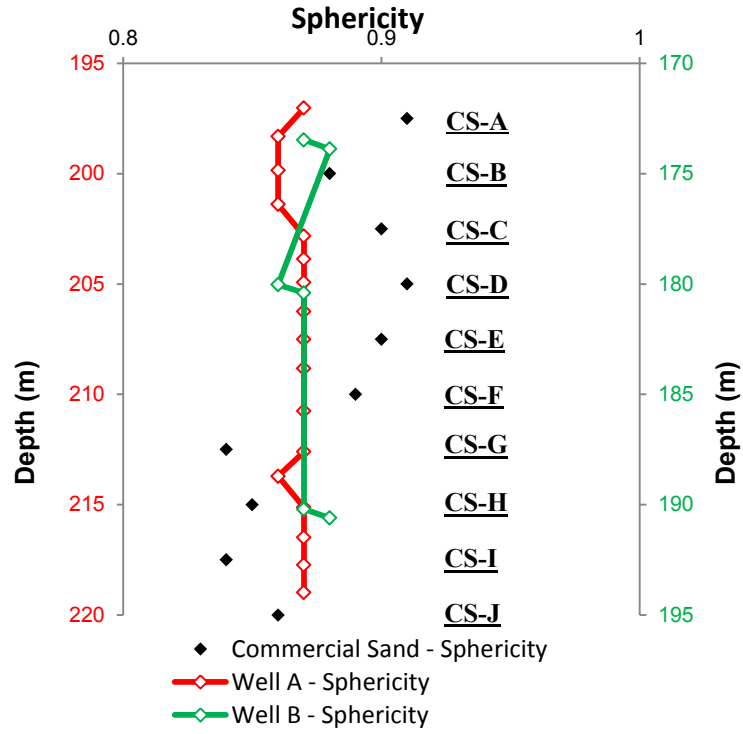
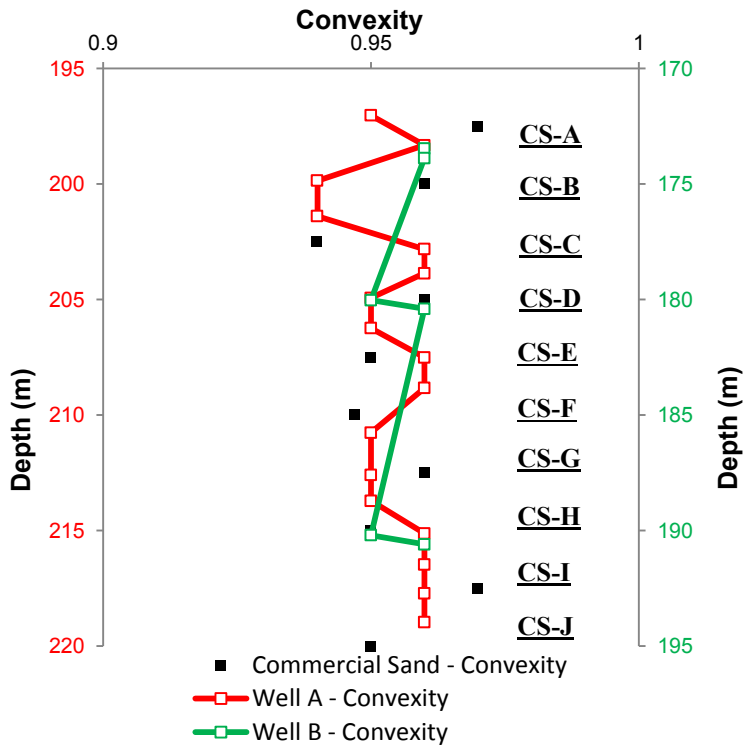


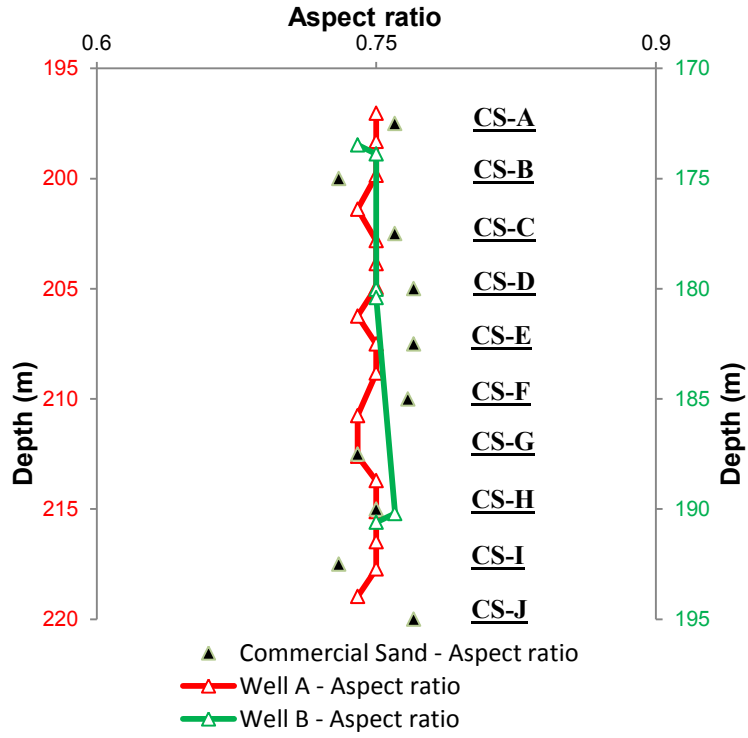
Figure 3-9. PSD for ten different available commercial fine-grained materials



(a)



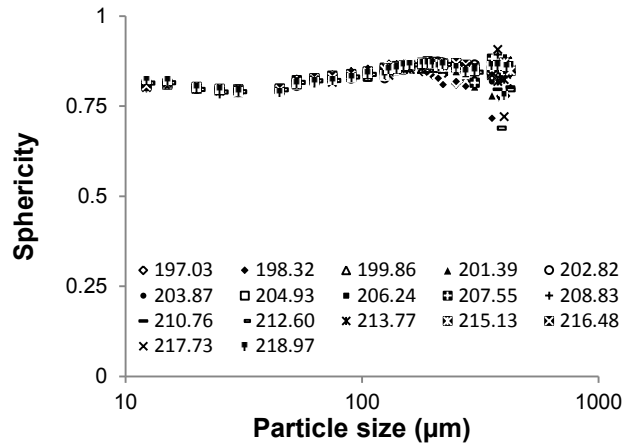
(b)



(c)

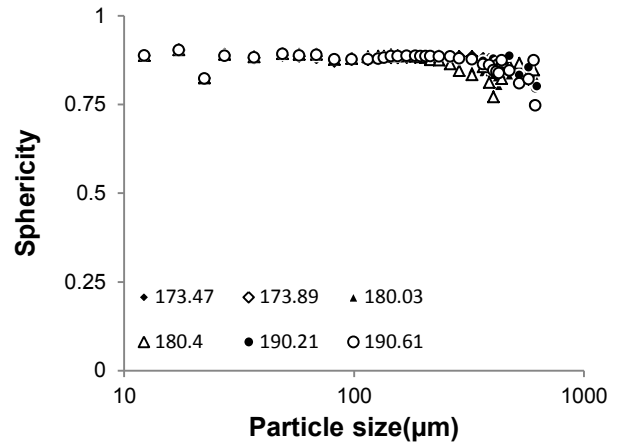
Figure 3-10. Comparison between shape factors, (a) sphericity, (b) convexity and (c) aspect ratio, for commercial sands and oil sands for Well A and B

**Wellbore A**

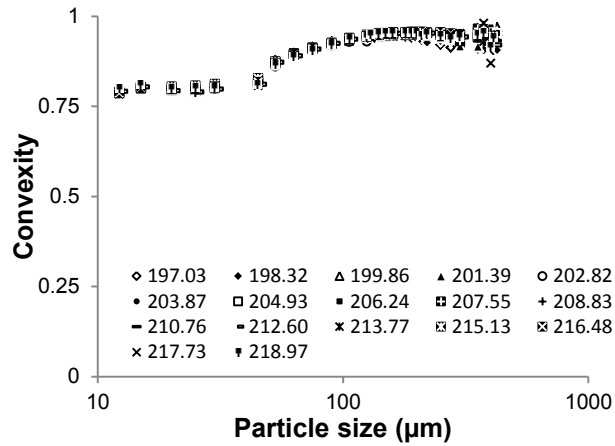


(a)

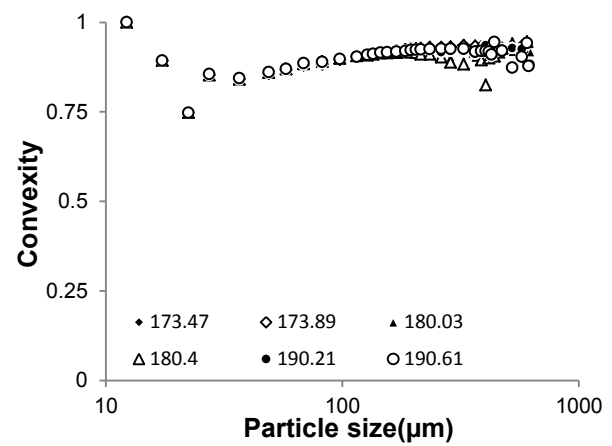
**Wellbore B**



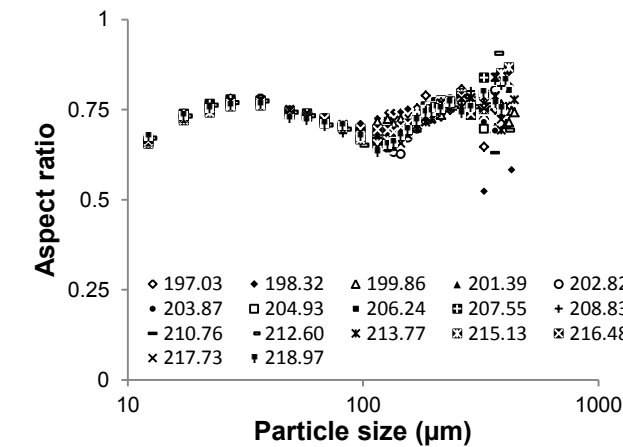
(b)



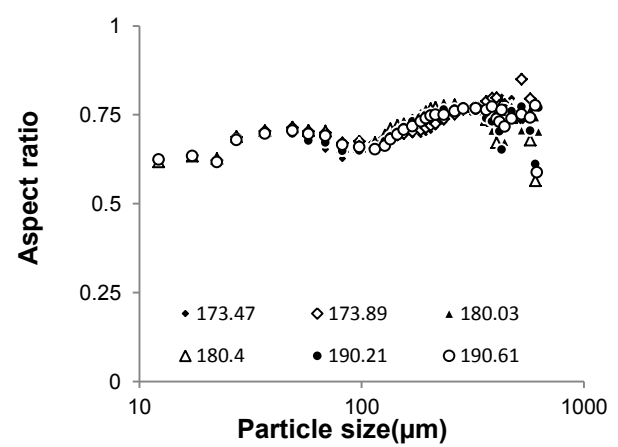
(c)



(d)

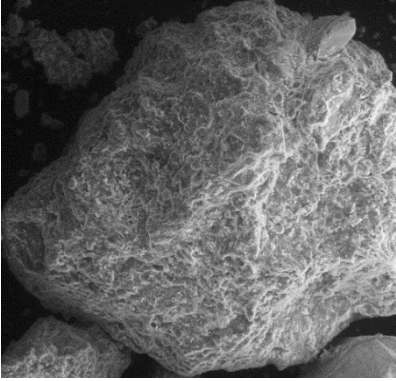
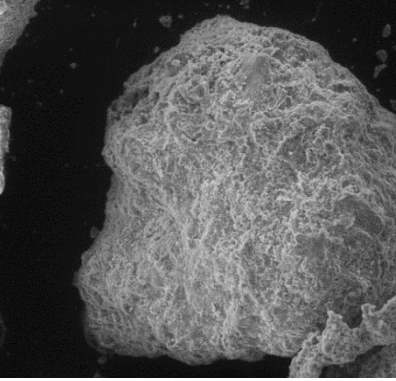
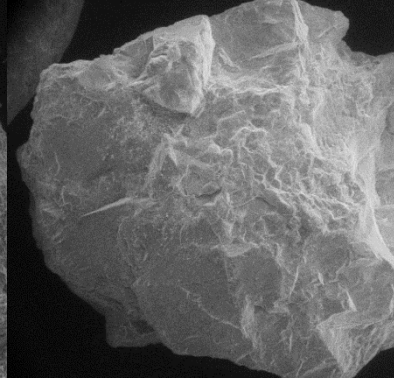
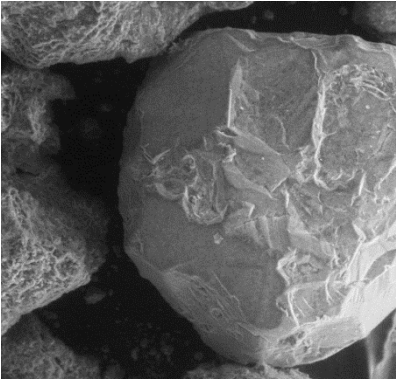
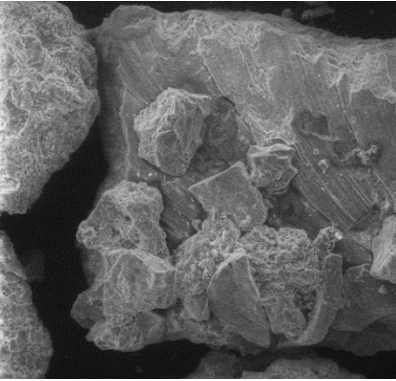
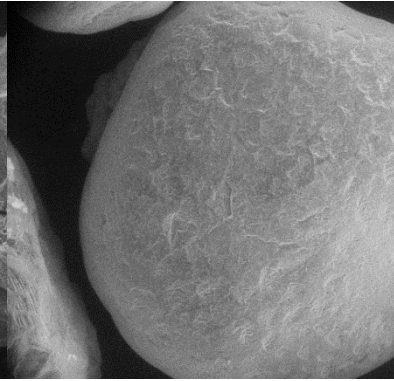
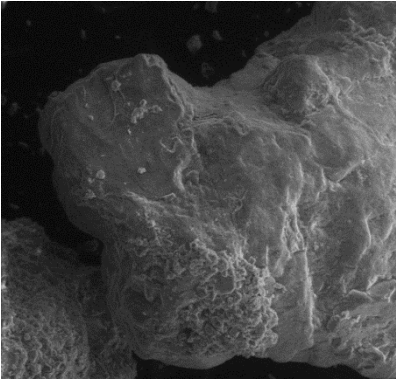
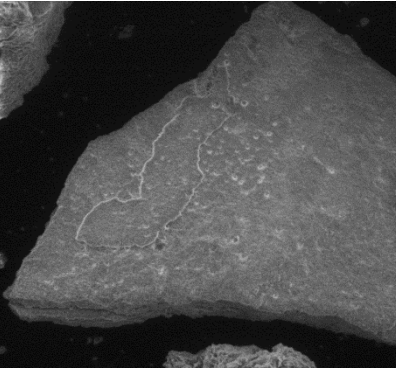
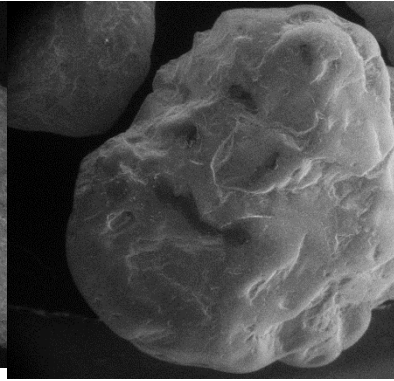


(e)

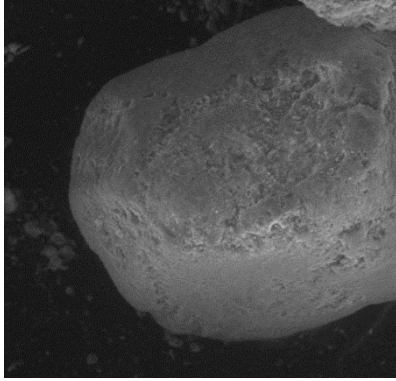


(f)

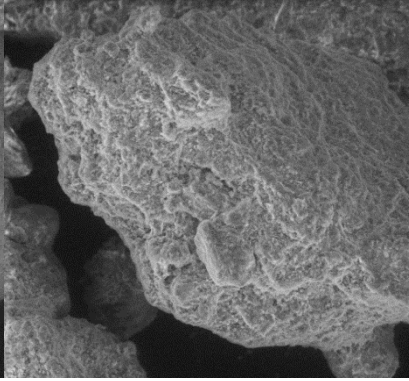
**Figure 3-11. Distribution of shape factors for different particle sizes for samples from different depths of Well A and B. Legend indicates sample depth**

	Wellbore A	Wellbore B	Commercial Sand
Very coarse sand			
	(a1)	(b1)	(c1)
			
	(a2)	(b2)	(c2)
			
	(a3)	(b3)	(c3)

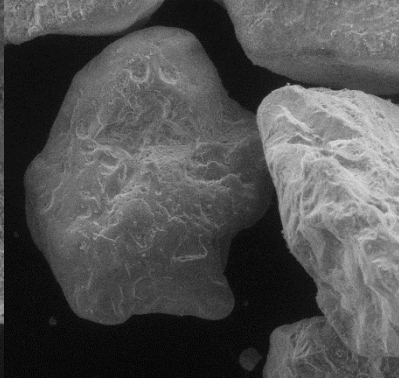
Coarse sand



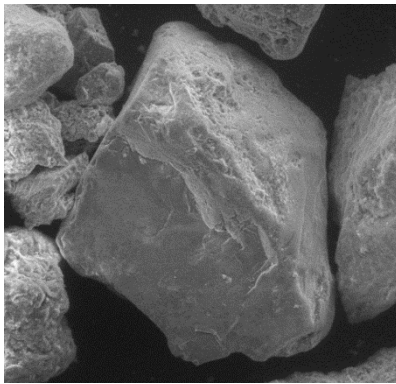
(a4)



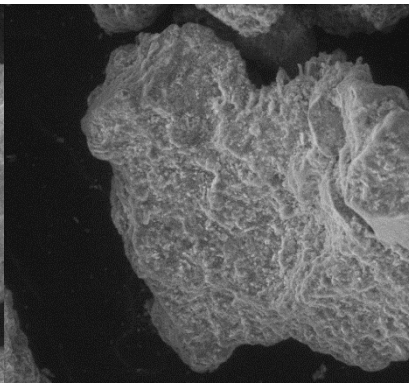
(b4)



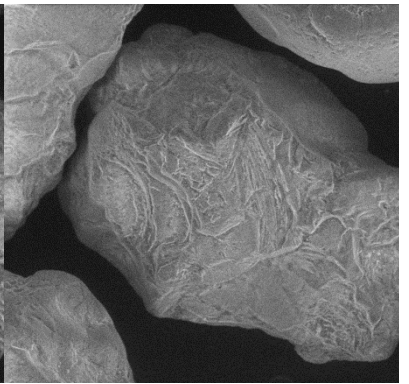
(c4)



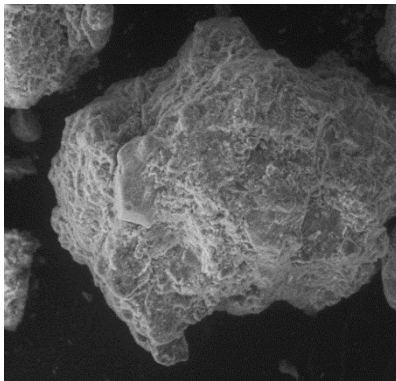
(a5)



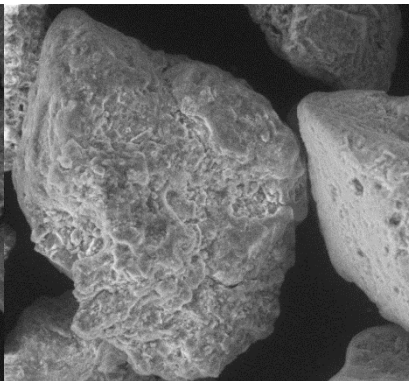
(b5)



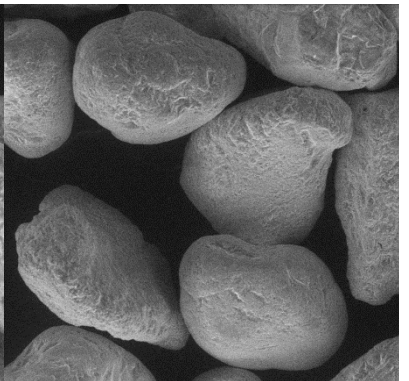
(c5)



(a6)



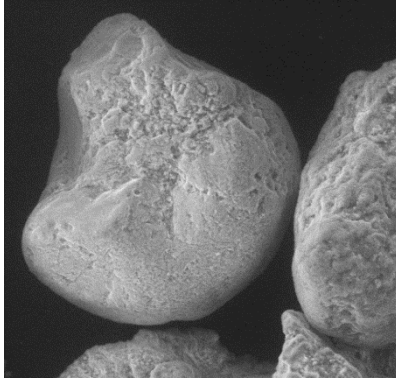
(b6)



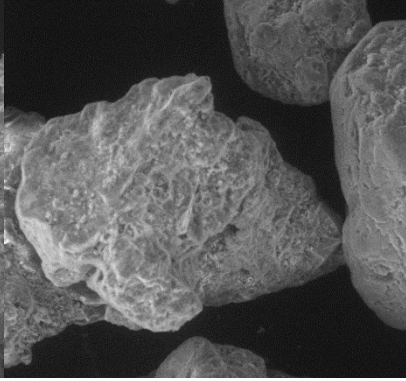
(c6)



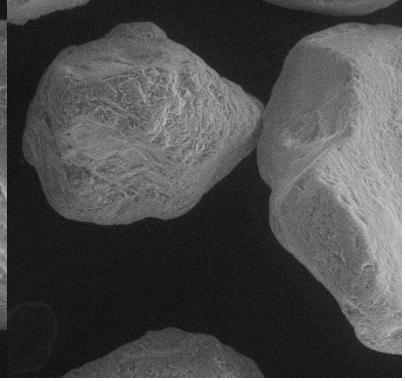
Medium sand



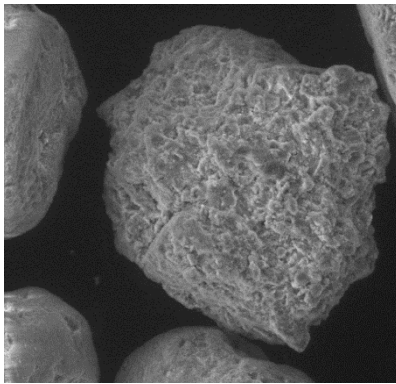
(a7)



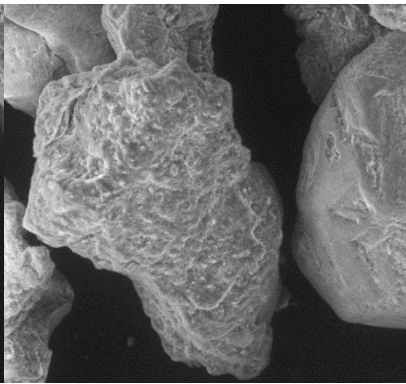
(b7)



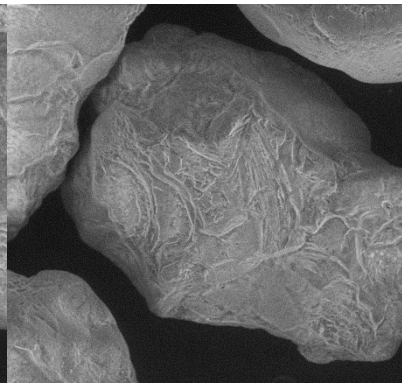
(c7)



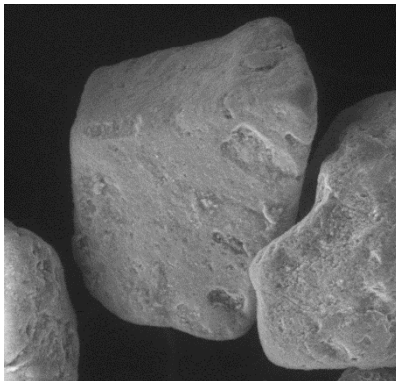
(a8)



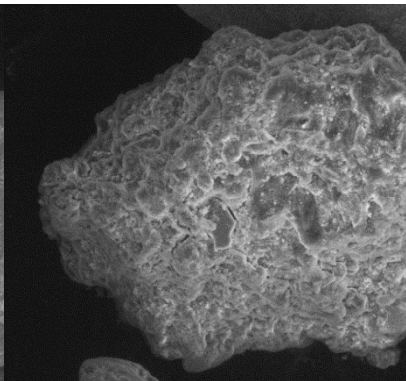
(b8)



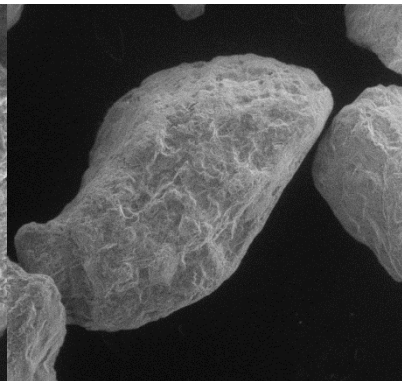
(c8)



(a9)

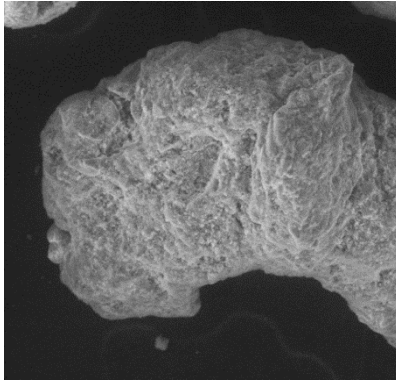


(b9)

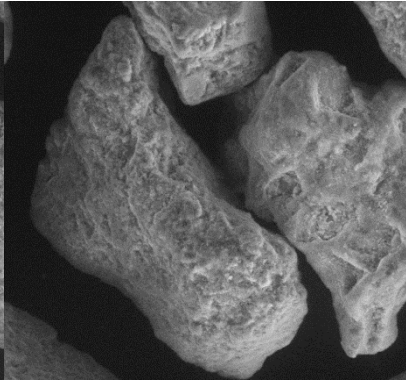


(c9)

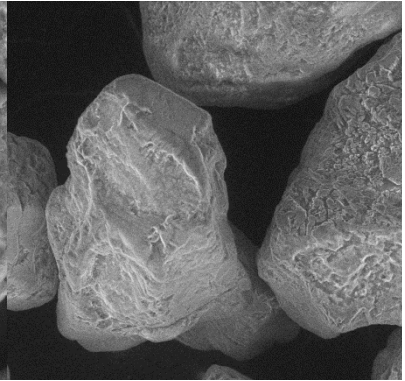
Fine sand ( $180\mu\text{m} < d < 250\mu\text{m}$ )



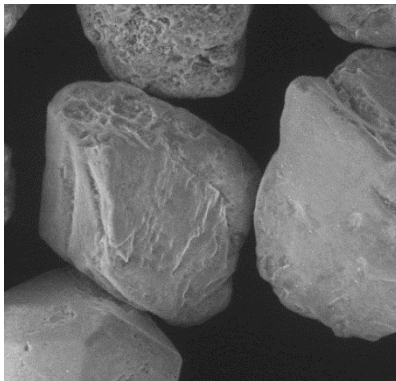
(a10)



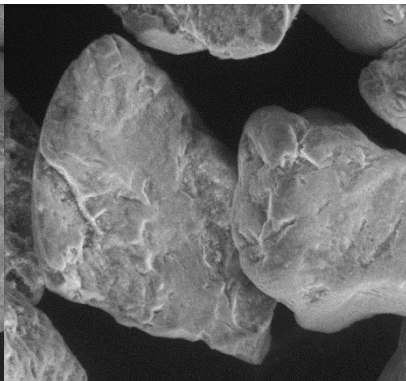
(b10)



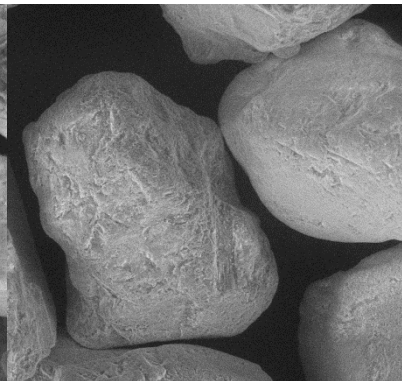
(c10)



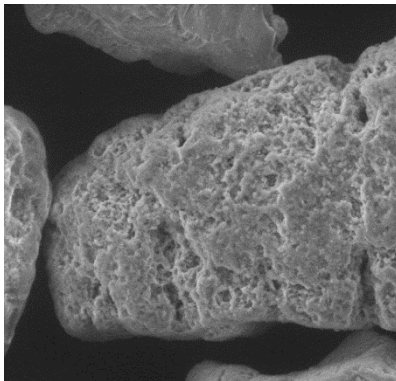
(a11)



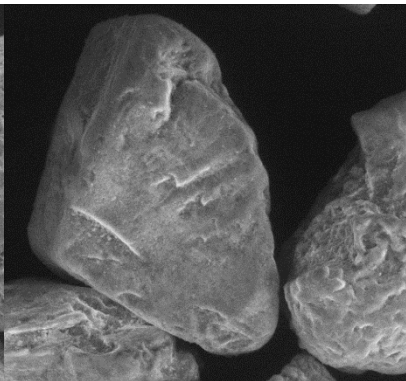
(b11)



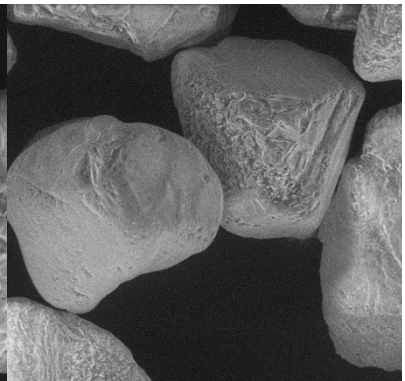
(c11)



(a12)

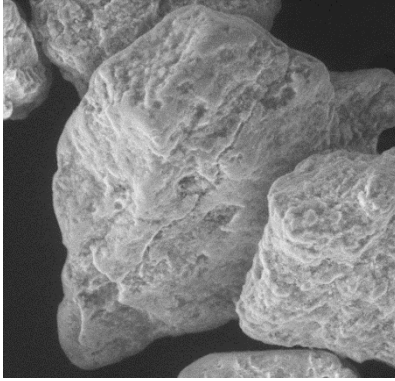


(b12)

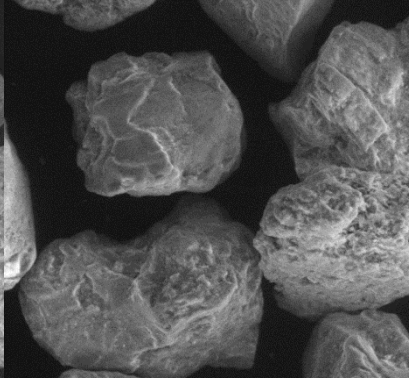


(c12)

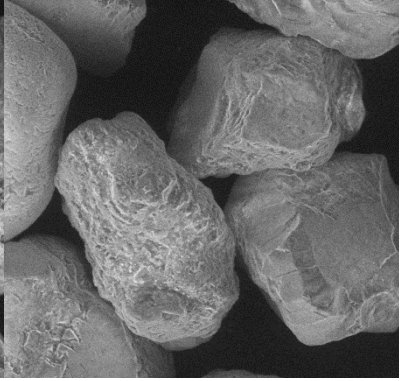
Fine sand ( $125\mu\text{m} < d < 180\mu\text{m}$ )



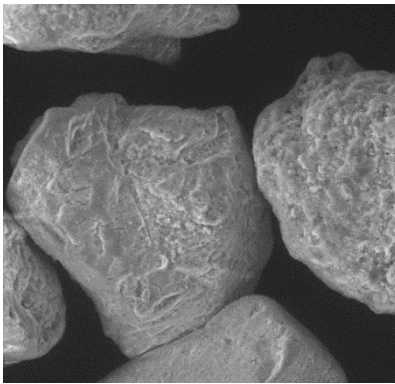
(a13)



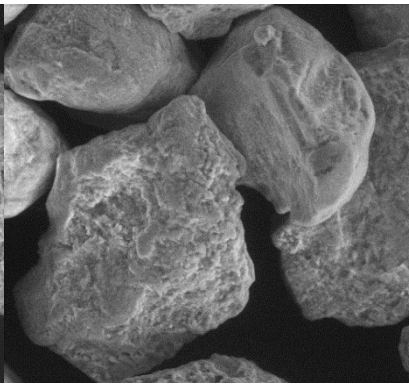
(b13)



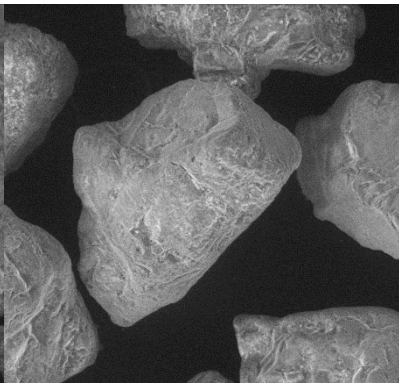
(c13)



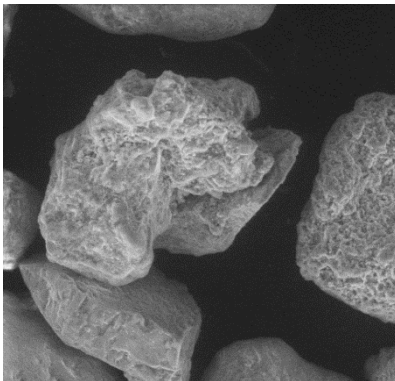
(a14)



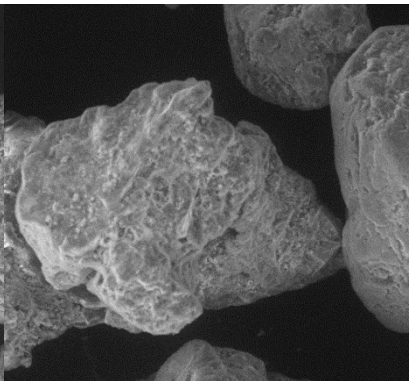
(b14)



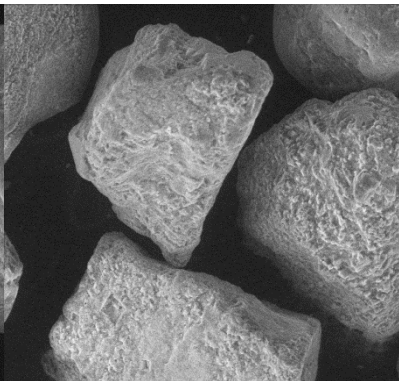
(c14)



(a15)

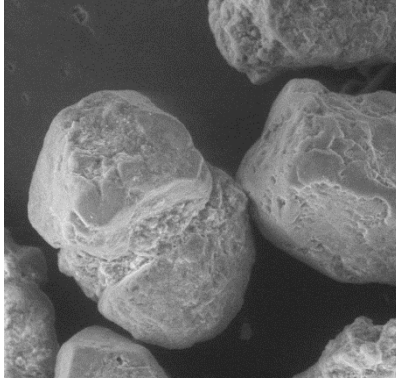


(b15)

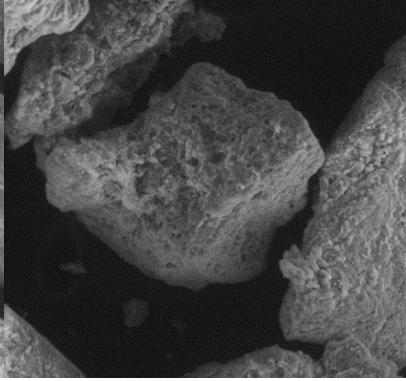


(c15)

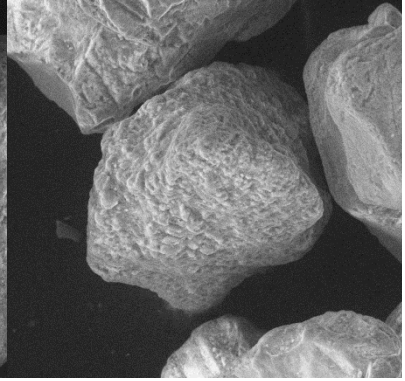
Very fine sand ( $105\mu\text{m} < d < 125\mu\text{m}$ )



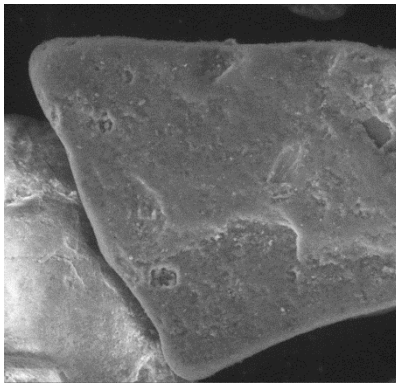
(a16)



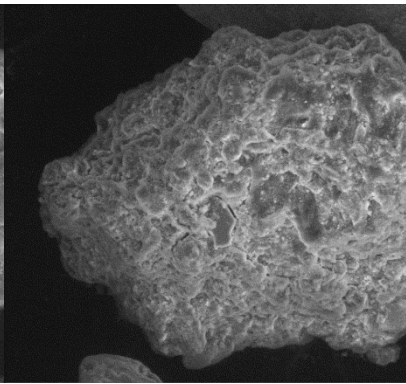
(b16)



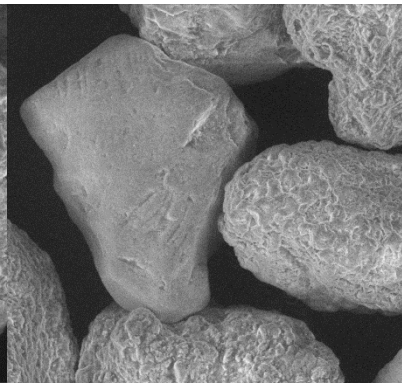
(c16)



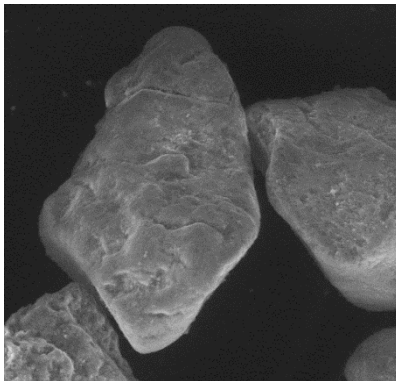
(a17)



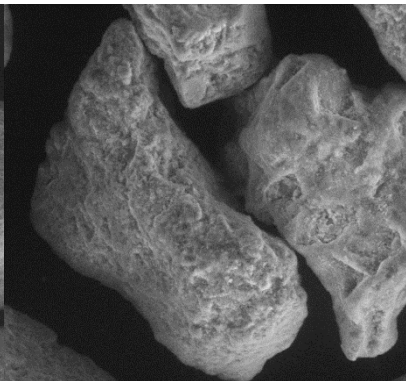
(b17)



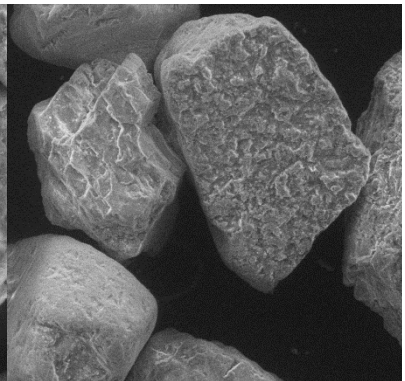
(c17)



(a18)

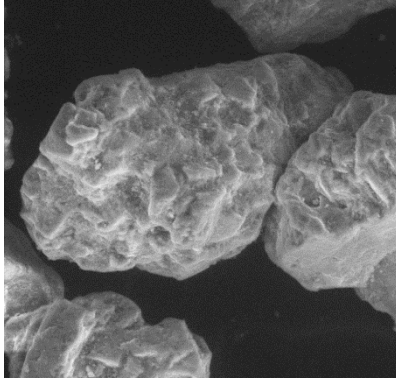


(b18)

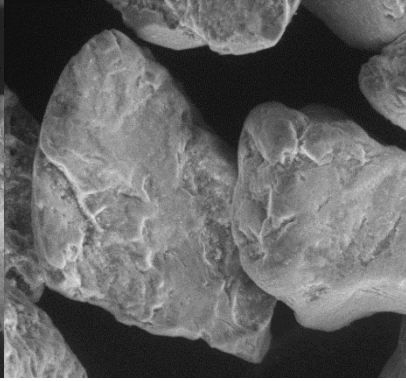


(c18)

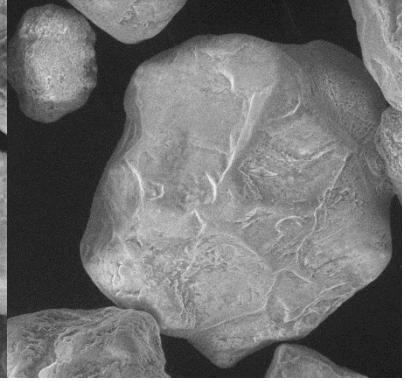
Very fine sand ( $74\mu\text{m} < d < 105\mu\text{m}$ )



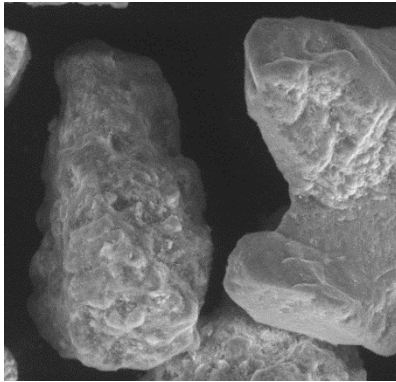
(a19)



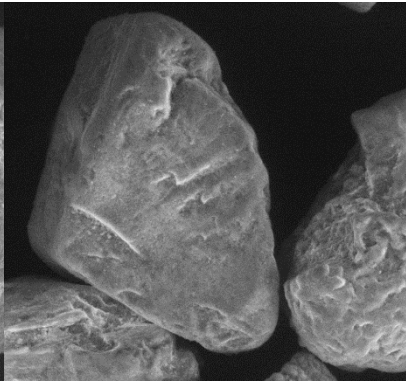
(b19)



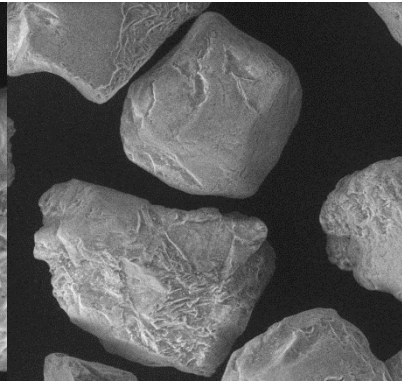
(c19)



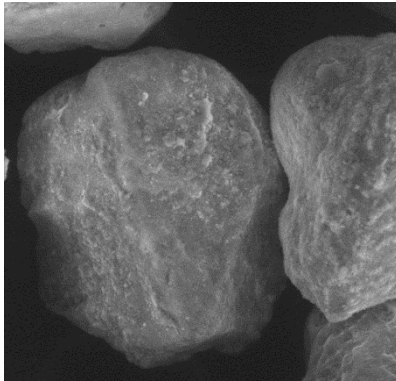
(a20)



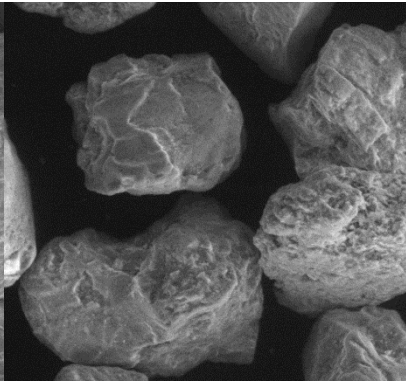
(b20)



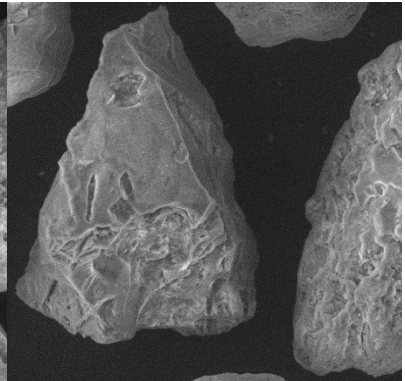
(c20)



(a21)

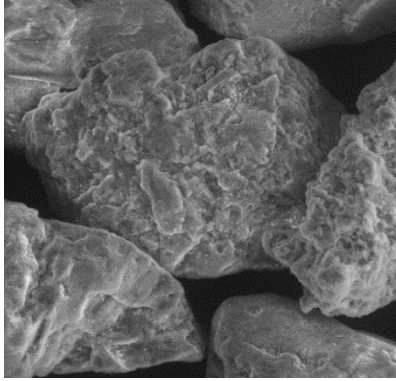


(b21)

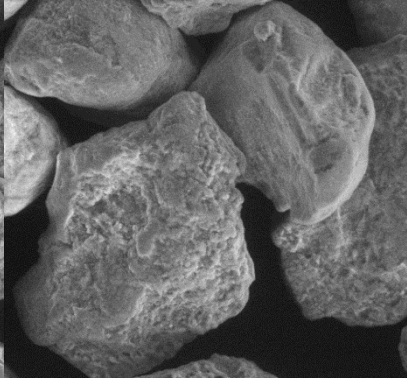


(c21)

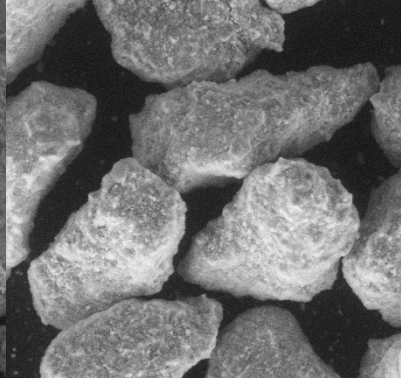
Coarse silt



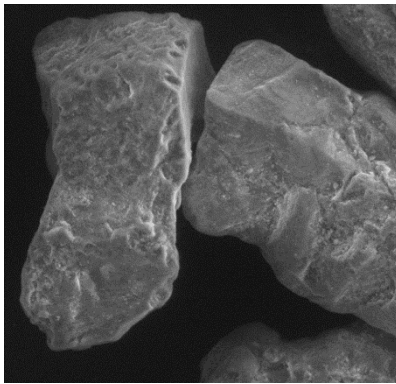
(a22)



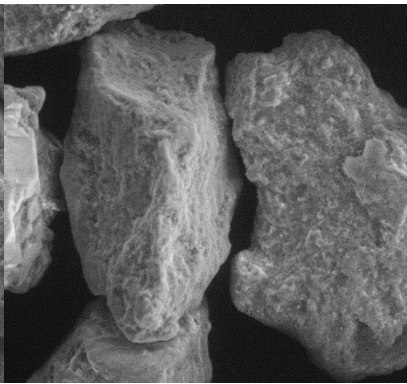
(b22)



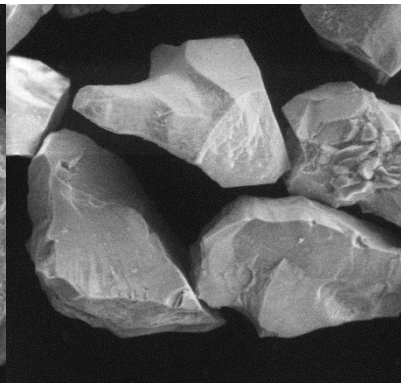
(c22)



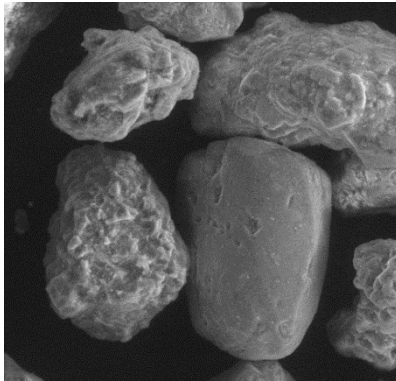
(a23)



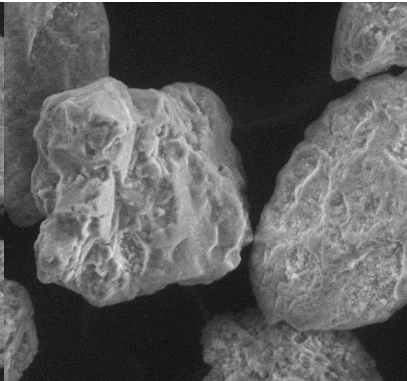
(b23)



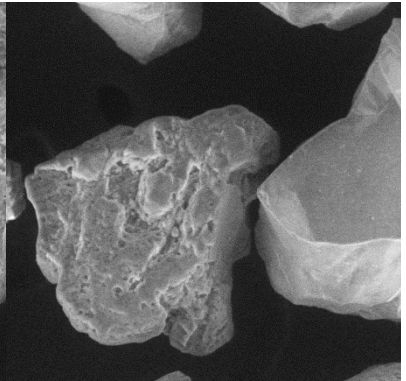
(c23)



(a24)

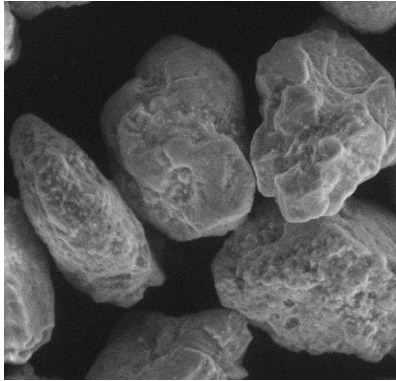


(b24)

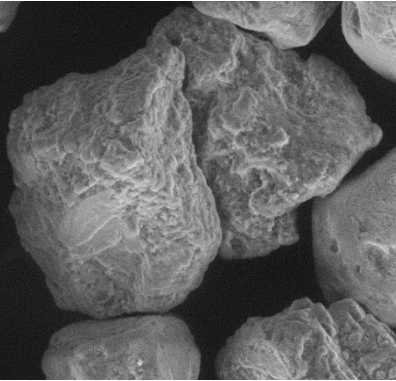


(c24)

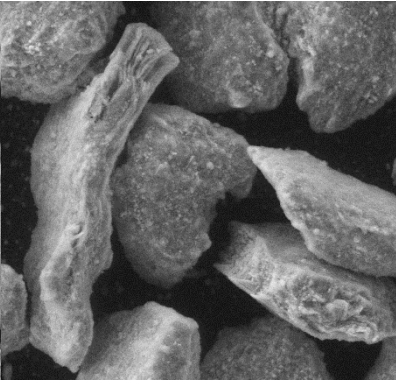
Medium silt



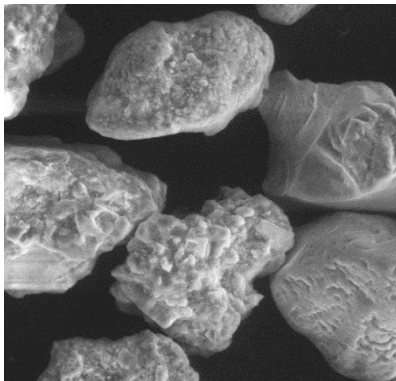
(a25)



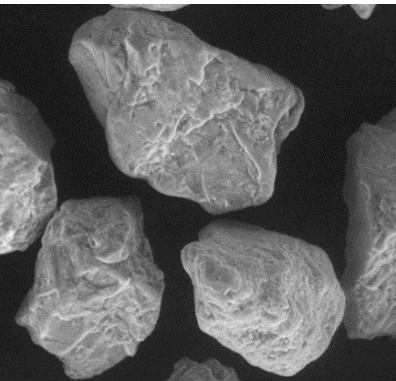
(b25)



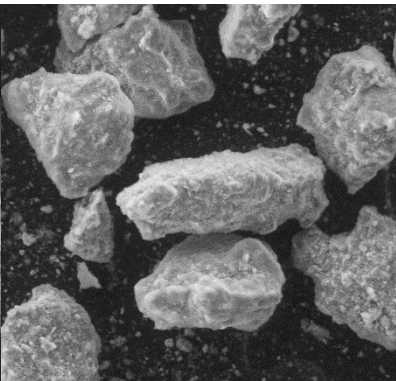
(c25)



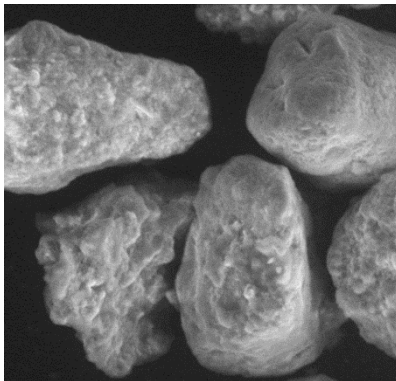
(a26)



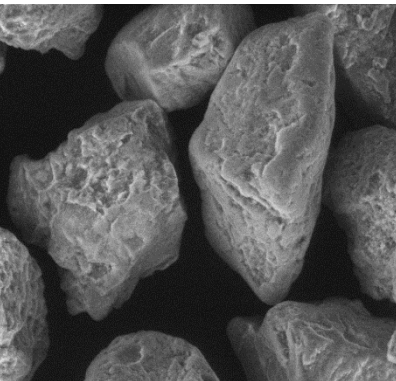
(b26)



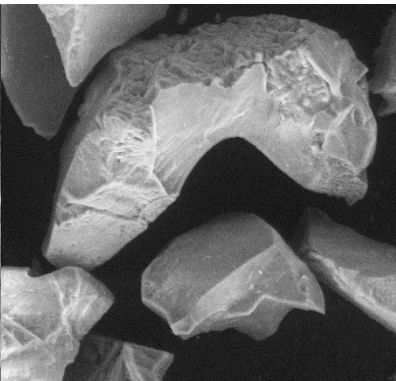
(c26)



(a27)

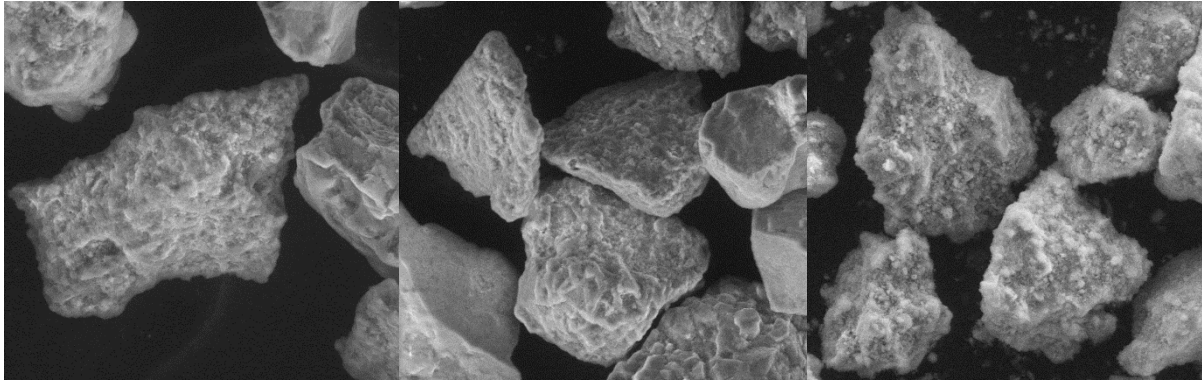


(b27)



(c27)

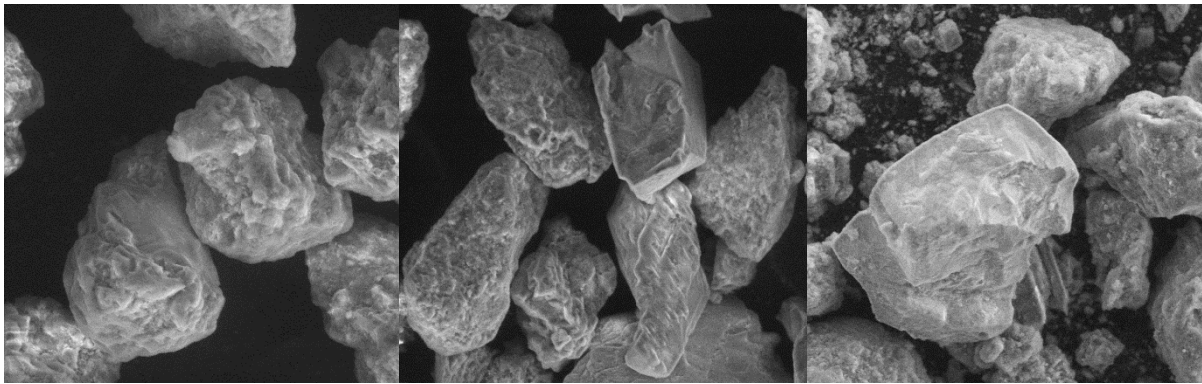
Fine silt



(a28)

(b28)

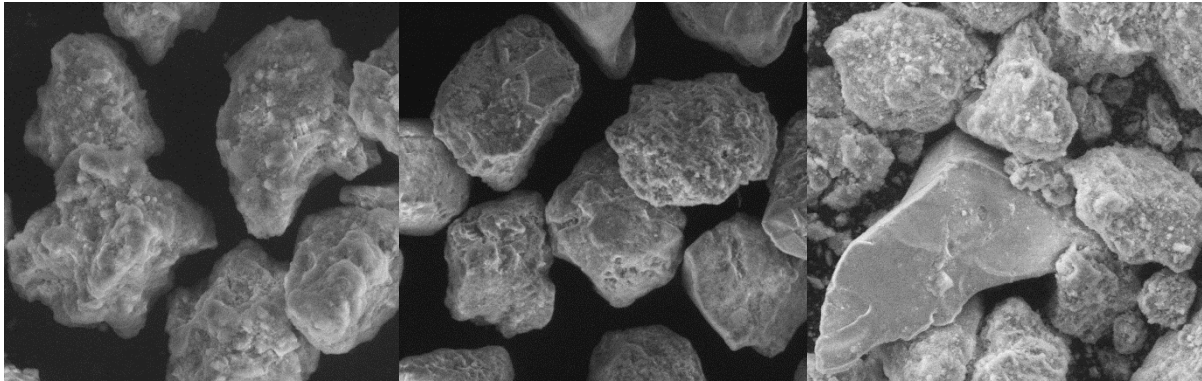
(c28)



(a29)

(b29)

(c29)



(a30)

(b30)

(c30)

Figure 3-12. SEM images from silts and sands from Well A and B and commercial sands



## **CHAPTER FOUR: INVESTIGATION INTO THE USE OF COMMERCIAL SANDS AND FINES TO REPLICATE OIL SANDS FOR LARGE-SCALE SAND CONTROL TESTING**

### **4.1 Introduction**

Sand control testing in the literature can be classified into two main groups based on the testing materials, (1) weakly consolidated sandstone, where plastic degradation results in sandstone decementation and fluid flow dislodges the degraded particles (Tronvoll et al. 1993, 1997; Nouri et al. 2005; Papamichos et al. 2008; 2010; Fattahpour et al. 2011, 2012a, 2012b; Younessi et al. 2012), and (2) unconsolidated sand, where there is no cementation, hence, sand can flow into the well along with fluid flow if there is no sand control (Markestad et al. 1996; Bennion et al. 2008; Ballard et al. 2012; Romanova et al. 2014, 2015). For both groups of testing, synthesized samples have been used, as obtaining natural core sample is difficult and costly, especially for weakly consolidated and unconsolidated formations (Younessi et al. 2012).

Several researchers attempted to replicate unconsolidated sand and weakly-consolidated sandstone with a mixture of commercial sand and fines. Younessi et al. (2012) and Fattahpour et al. (2012a, 2012b) discussed a procedure for replicating a weak sandstone by mixing a commercial sand and Portland cement. Their results showed a good agreement between the UCS of synthesized and natural samples.

In pre-pack SRT testing, there is no cementation between the particles and the only bonding agents between the particles are weak capillary forces and clay at the particle contacts. In addition to the type and geometry of the screen, results of pre-pack SRTs are mainly affected by the PSD (Markestad et al. 1996; Ballard et al. 2012; Meza et al. 2007; Bennion et al. 2008; Romanova et al. 2014), particle shapes, composition and amount of the fines (Bennion et al. 2008), ionic condition of the flowing media (Bennion et al. 2008), fluid velocity, and fluid flow phases (Bennion et al. 2008).

This chapter presents a novel procedure to duplicate oil sands by matching the oil sand's PSD, particle shape, and mineralogical compositions by mixing commercial sands and fines. Real oil sand samples and their replica are then tested to obtain their mechanical properties to gauge the success of the replication process.

## **4.2 Preparation of oil sands and commercial sand samples**

Core samples from two wells in McMurray Formation were studied in pervious chapter to quantify the particle size and shape variation. Synthetic samples were constructed using commercial sands and fines by matching the particle size and shape distributions and the fines content and composition. Direct shear testing was conducted on oil sands that were cleaned from bitumen content and the commercial replica to verify the agreement in the mechanical properties of the oil sand and the synthetic replica.

## **4.3 Replicating McMurray Formation oil sand with commercial sands and fines**

There is a growing demand for large volumes of sand for oil sand testing for a range of applications such as wellbore completion design. This demand warrants a study for the possibility of duplicating oil sand samples with artificially prepared samples from commercial sands. In-situ samples are costly and usually limited in volume. In this section, a comparison is made between the shape characteristics of oil sands from McMurray Formation with those of commercial sands. The aim is to find out if the oil sand samples and the equivalent commercial sands with similar PSD and shape parameters possess similar mechanical properties.

**Figure 4-2** through **4-5** show the PSD, convexity, sphericity and aspect ratio for an oil sample (OS-A) from Well B (sample from the depth 173.47 m) and a commercial sand (CS-C). According to **Figure 4-2**, the PSD of CS-C and OS-A sands nearly match. **Figure 4-3** through **4-5** show the close agreement between the distributions of the shape factors for both samples. The conclusion here is that CS-C can be used for constructing samples that are like OS-A oil sands in PSD and particle shapes.

The hypothesis is that synthetic sand pack sample with similar PSD, shape factors, and composition should produce sand packs with similar mechanical properties. To verify this hypothesis, a series of mechanical tests was performed to verify the agreement between the mechanical properties of the oil sand samples with those of the equivalent synthetic samples.

### ***4.3.1 PSD replication***

Chapter 3 demonstrated that the selected commercial sand yielded a similar particle shape characteristic to those of the oil sands. The next step is to replicate the PSD of the oil sands. To this end, different batches of commercial sands and fines were prepared and mixed in right

proportions. **Figure 4-6** shows the four PSD classes for Pike 1 project duplicated by mixing commercial sands.

#### ***4.3.2 Shape variation comparison***

Per **Figure 3-10**, the shape factors for both oil sands and commercial sands are in close agreement. **Figure 4-7** shows the shape factor distribution of oil sand samples with the same for the equivalent synthetic sand pack for Class II and III (depth of 217.73 m and 199.86 m of Wellbore A, respectively) oil sands proposed by Abram and Cain (2015). Although the overall shape factors of oil sands particles and their commercial replica seem to agree, slight differences are noted for some particle size groups. In general, the oil sand and equivalent commercial sand pack agree relatively well on the average particle shape and particle shape distribution.

#### ***4.3.2 Composition replication***

As indicated in Chapter 3, the XRD analysis of the silt and sand particles indicates  $\text{SiO}_2$  as the main mineral for both commercial sands and oil sands. The same clay composition (80% kaolinite and 20% illite) was also used in the synthesis of commercial sands that correspond to DC-II and DC-III.

#### ***4.2.4 Mechanical tests***

Two types of mechanical tests in direct shear test and one-dimensional consolidation test were performed on the oil sands samples and their commercial replica to compare their mechanical properties. This was an effort to verify the hypothesis that oil sands samples and commercial mixes with the same PSD and particle shapes produce comparable mechanical properties.

##### ***4.2.4.1 Direct shear tests***

Direct shear testing has been widely used to measure the angle of internal friction of granular materials such as sands. ASTM D3080 was followed for conducting the direct shear tests in this study. The PSDs of all samples from both wells are close, but not identical, to the PSD of DC-I, DC-II, and DC-III. The PSD of none of the oil sands samples matched that of the DC-IV class. Hence, oil sands samples were sieved and mixed together to produce the same PSDs as those of DC-I, DC-II, DC-III and DC-IV.

Direct shear test results for the oil sands and their corresponding replicas are shown in **Figure 4-8a and 4-8b**, respectively. Test results look not only similar between the corresponding replica

and oil sands but also very similar among all oil sands and replicas that were tested with different PSDs. Apparently, the PSD did not play the main role in the frictional behavior and the shape factors, which are shown to be very close among all the oil sands and commercial sand samples, are more important.

The cohesion, as expected, is very small for all tests due to the lack of bonding between the particles. **Table 4-1** compares the friction angle for the oil sands and the corresponding replica. Friction angles are seen to be close between the oil sands and the corresponding replicas and even among all tested samples.

#### **4.2.4.2 Uniaxial strain testing**

Uniaxial strain testing tests were performed to find how the oil sands structure and their commercial replica respond to the applied load. Due to the liner installation and collapse of the formation during the pre-heating phase, the area near the screen is a disturbed zone with a higher porosity than the porosity of the original formation. Hence, consolidation testing was performed on high-porosity (40%) saturated samples under 2 MPa normal stress. The same sand samples as those in direct shear testing were used in the consolidation tests.

The results of the uniaxial strain testing for DC-I to DC-IV are shown in **Figure 4-9(a)** through **Figure 4-9(d)**, respectively. The overall response of the oil sands and their commercial replication is similar but the commercial replicas are compacted to slightly lower porosities than the oil sands for the same normal force. This can be due to their slightly higher sphericity.

### **4.3 Conclusions**

It was shown that the commercial sand and fines can be used to replicate oil sands in term of PSD, particle shape, and composition. This investigation is meant to complete the previous chapter on the characterization of oil sands samples and commercial sand and fines to synthesize commercial replica that can be used instead of the oil sands samples for large-scale testing.

Shape analysis of the commercial sands used in this research indicates a close agreement in their distribution of shape factors with those of the oil sands. The synthetic samples also contained the same clay composition and amount compared to the corresponding oil sands.

Results of direct shear and uniaxial strain tests show a close agreement between the mechanical response of the oil sand samples with those of their replica. Results indicate that by matching the

particle shapes and size distributions, and mineralogical compositions for the oil sands and the replicated sand pack, one could expect similar mechanical responses from the oil sands and their synthetic replica.

**Table 4-1. Friction angle results for oil sands and the representative commercial replica. Sample names present depth and PSD class**

	<b>Oil sands</b>	<b>Replica</b>
<b>A197.03 – DC-I</b>	33.43	32.62
<b>A198.32 – DC-I</b>	33.39	33.01
<b>A217.73 – DC-II</b>	33.47	33.15
<b>A213.71 – DC-II</b>	33.46	33.96
<b>A216.48 – DC-II</b>	31.55	33.34
<b>A199.86 – DC-III</b>	34.06	34.21
<b>A210.76 – DC-III</b>	33.37	34.57
<b>DC-III</b>	34.16	34.16
<b>DC-IV</b>	33.72	33.96

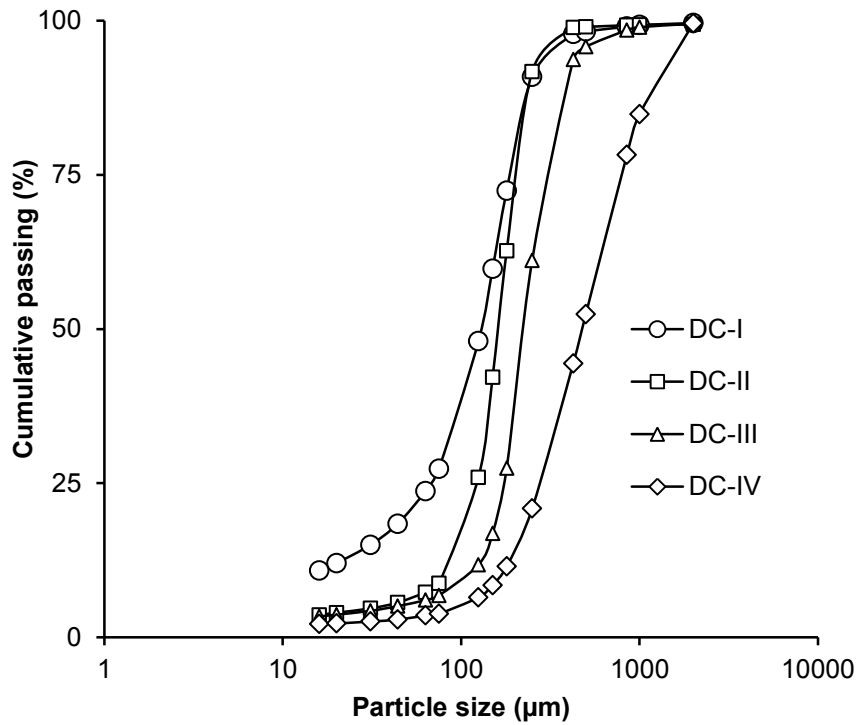


Figure 4-1. Four Representative PSD's provided by Abram and Cain (2014)

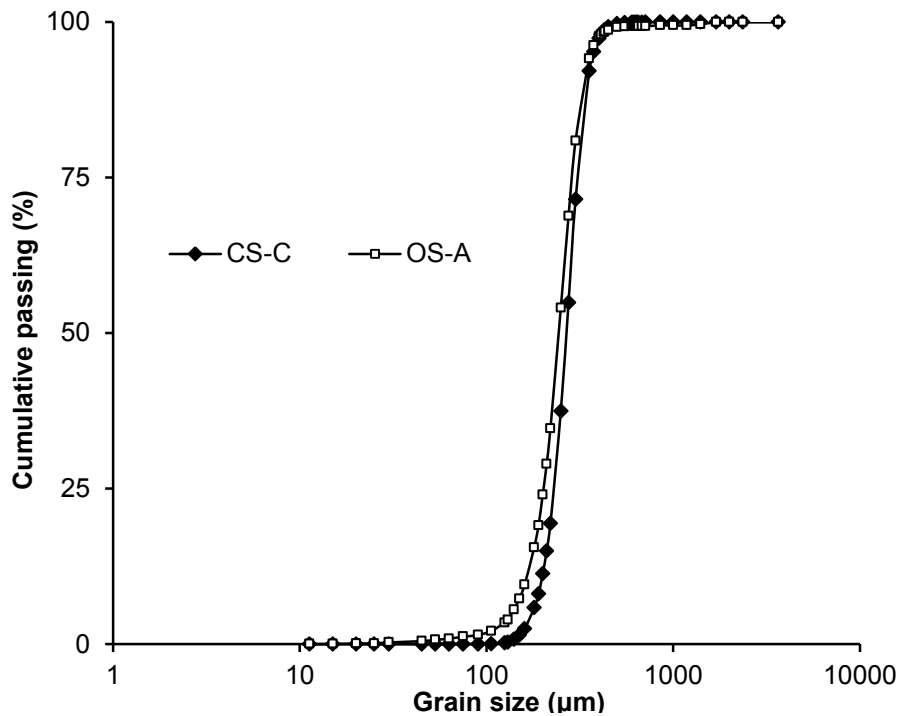


Figure 4-2. Comparison between the PSD for oil sand samples (OS-A) from depth 173.47 m in Well B and commercial sand CS-C

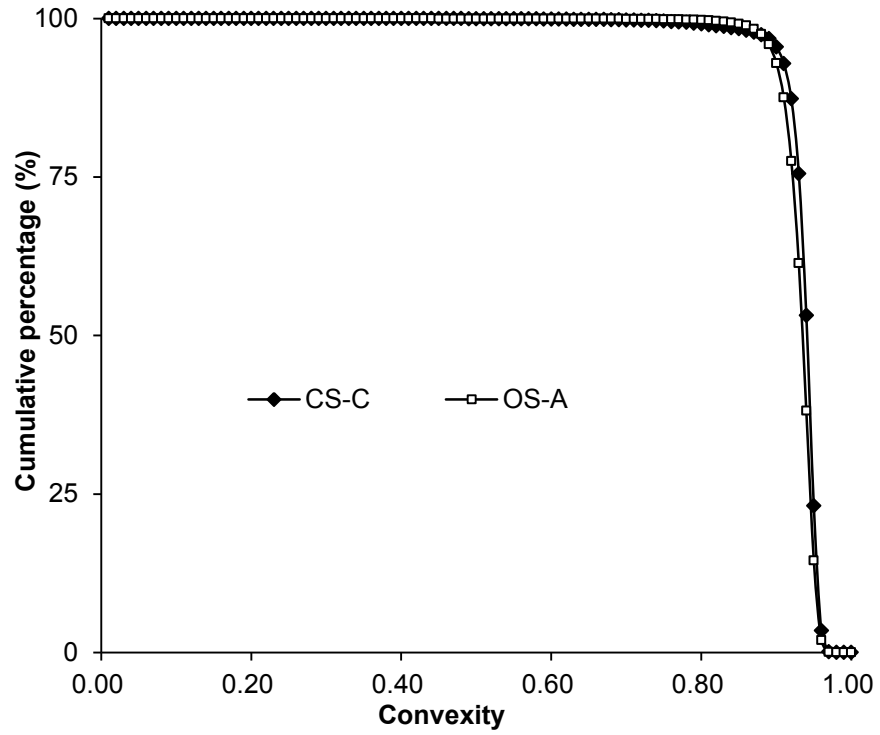


Figure 4-3. Comparison between the convexity for an oil sand sample (OS-A) from 173.47 m depth in Well B and commercial sand type C (CS-C)

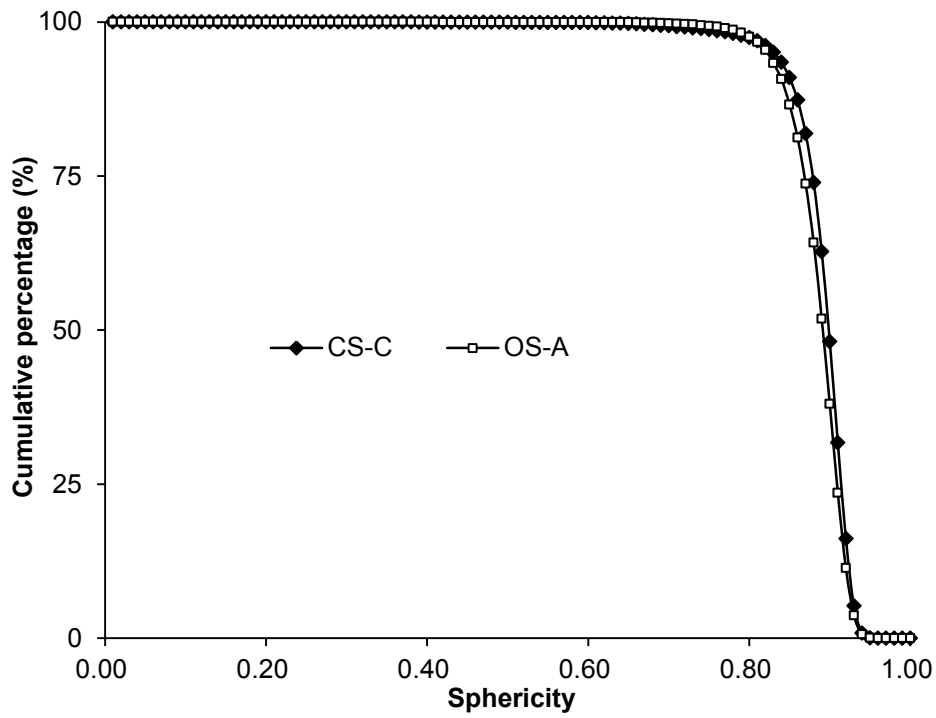
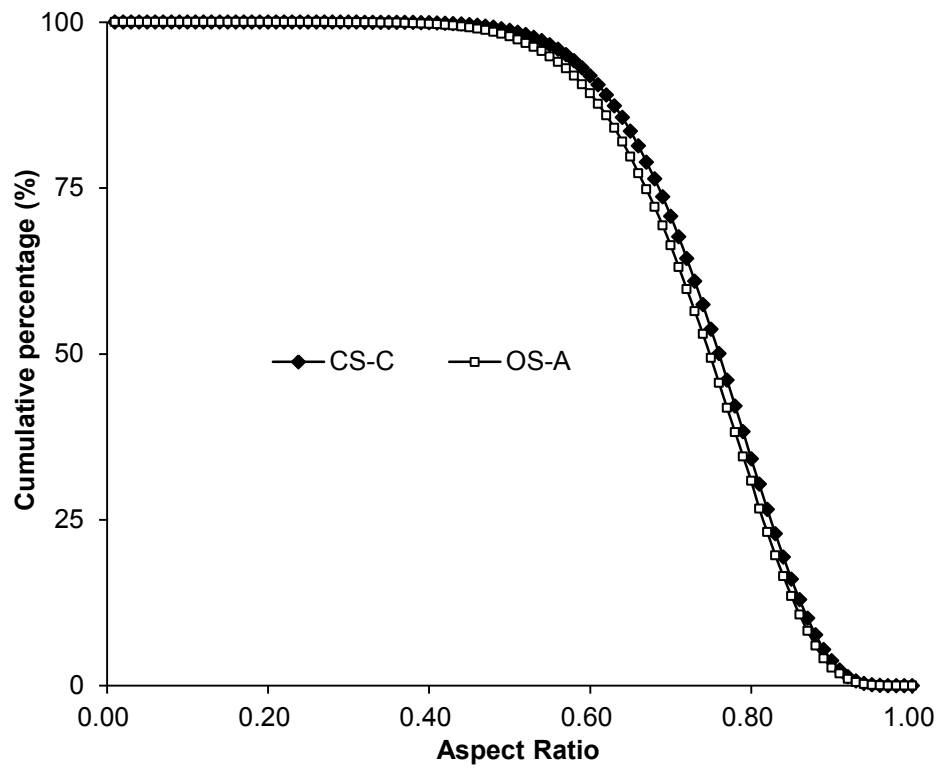


Figure 4-4. Comparison between the sphericity for oil sand sample OS-A from 173.47 m depth in Well B and commercial sand CS-C





**Figure 4-5. Comparison between the aspect ratio for oil sand sample OS-A from 173.47 m depth in Well B and commercial sand CS-C**

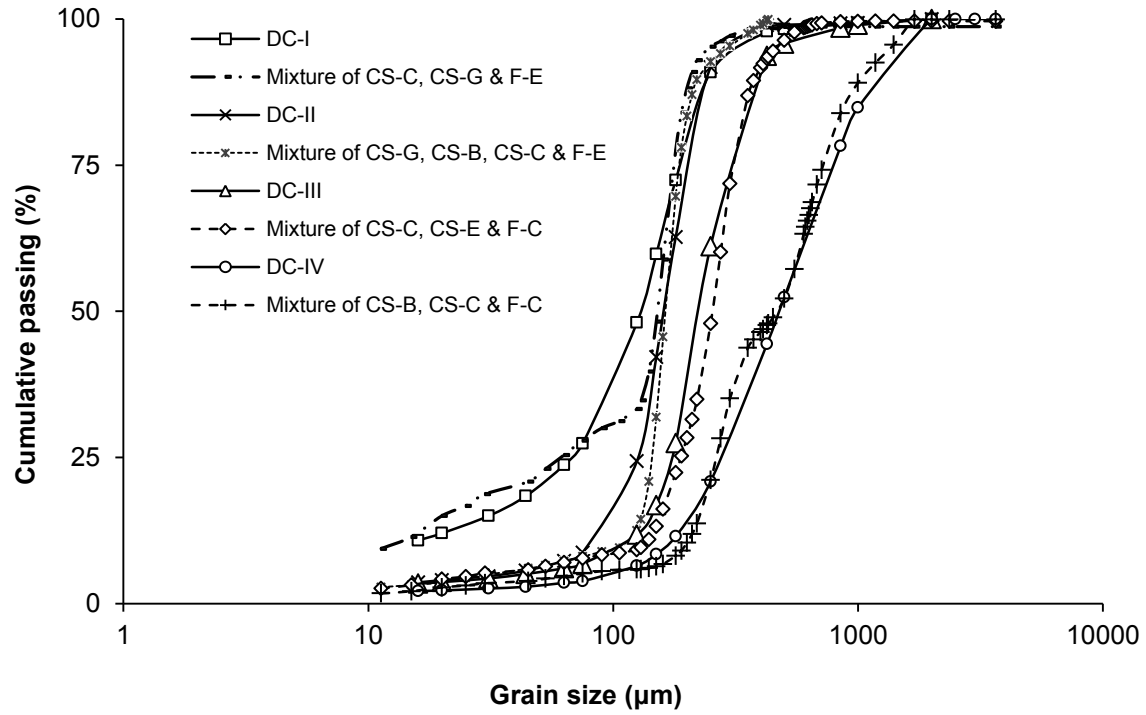
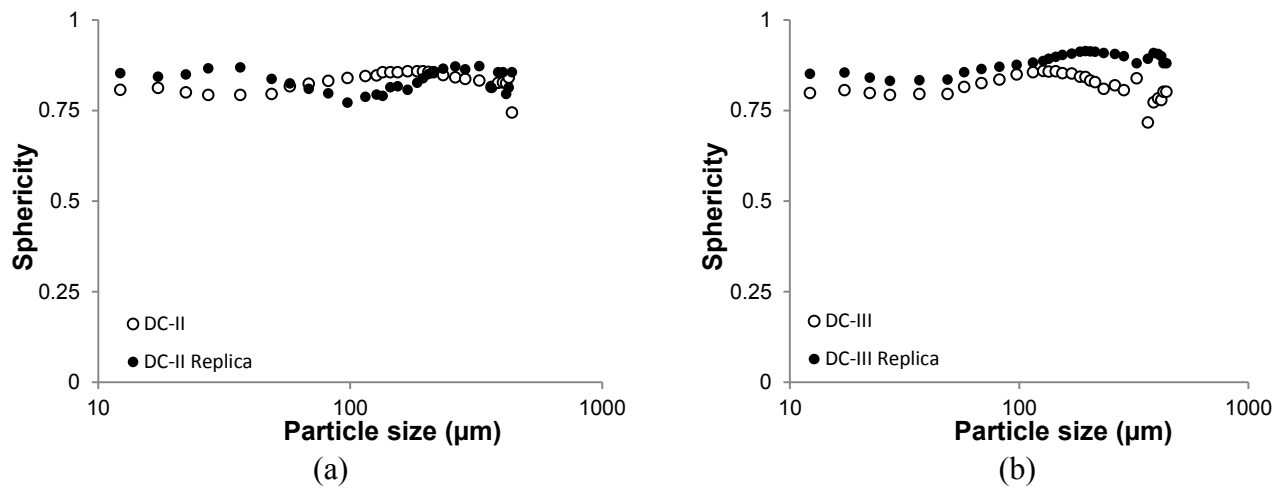


Figure 4-6. Combination of the commercial sand and fine silts to duplicate four classes of oil sands presented by Abram and Cain (2014)



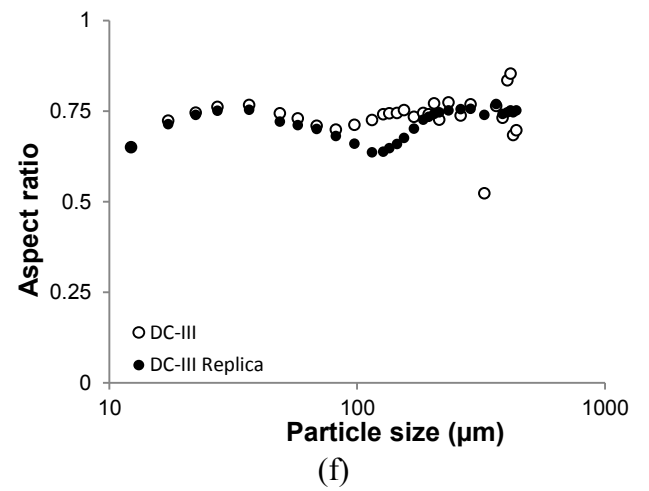
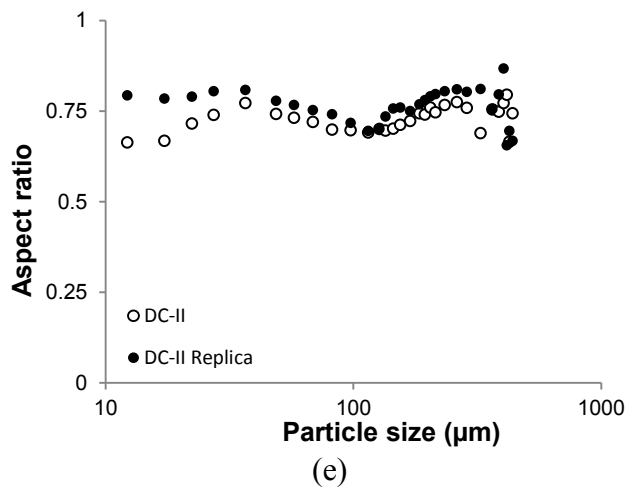
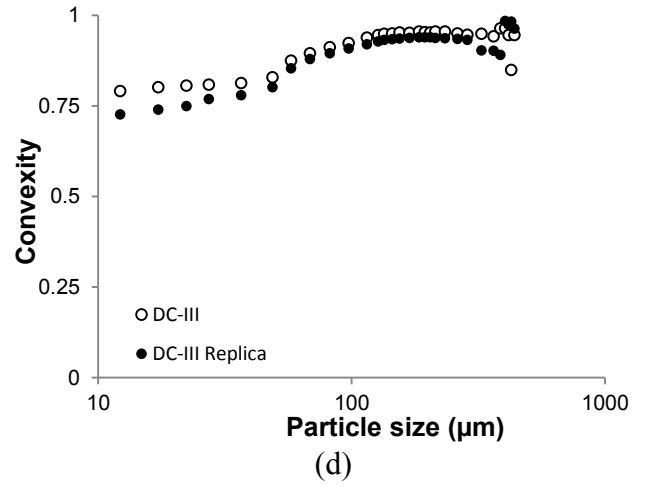
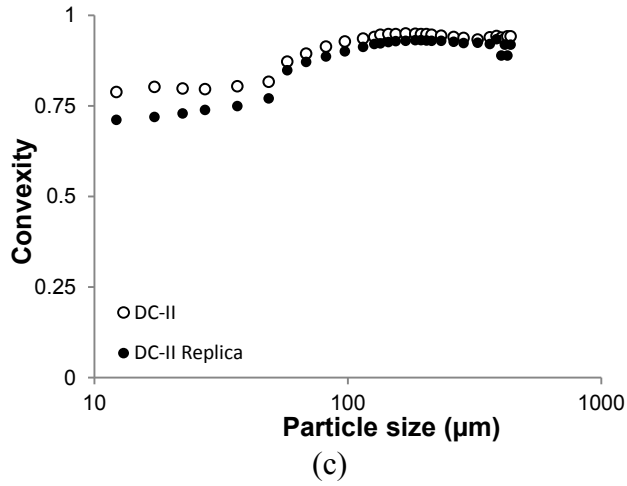
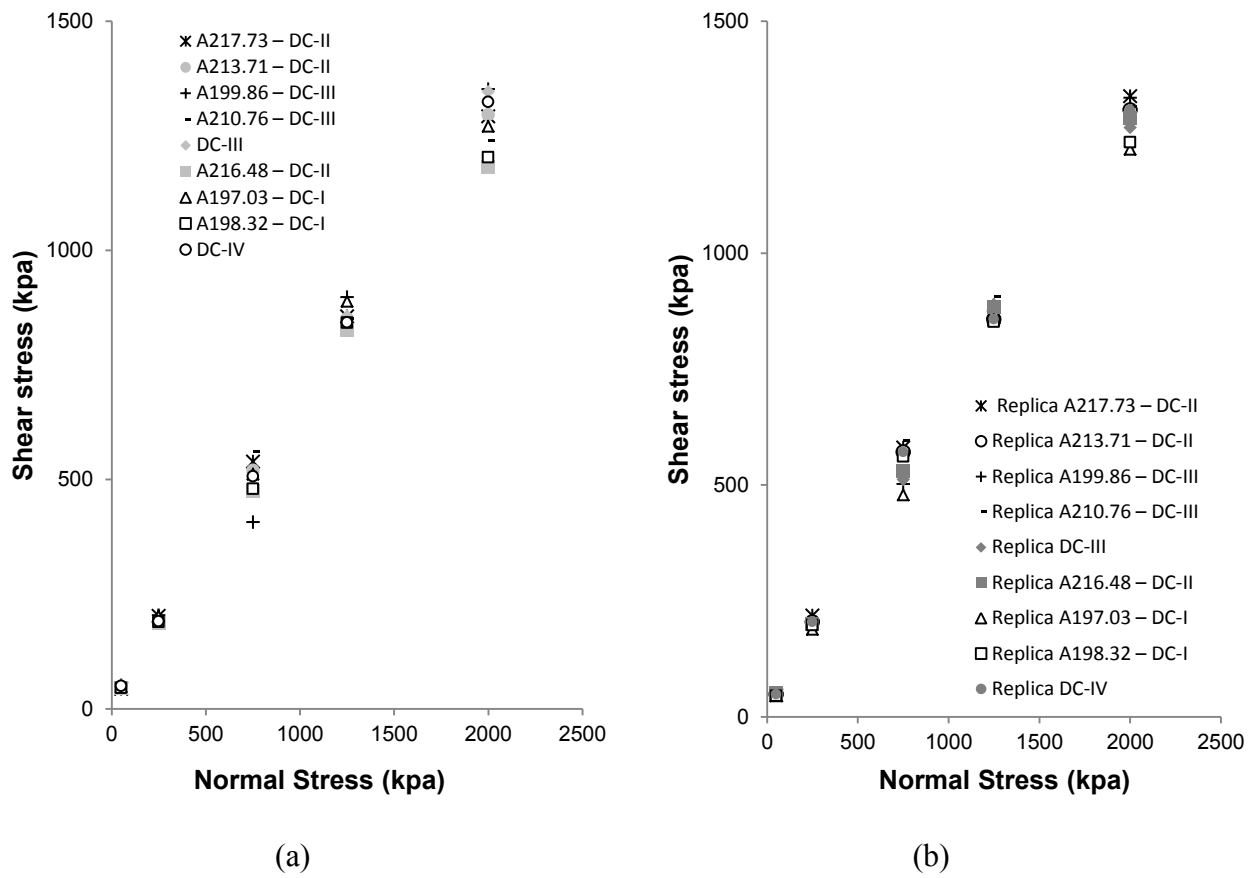


Figure 4-7. Comparison of shape factor distribution for different particle sizes for oil sands with the PSD of DC-II (a, c and e) and DC-III (b, d, and f) and the corresponding replicas



**Figure 4-8. Direct shear testing results for (a) oil sands samples from Well A and B, (b) the commercial replica**

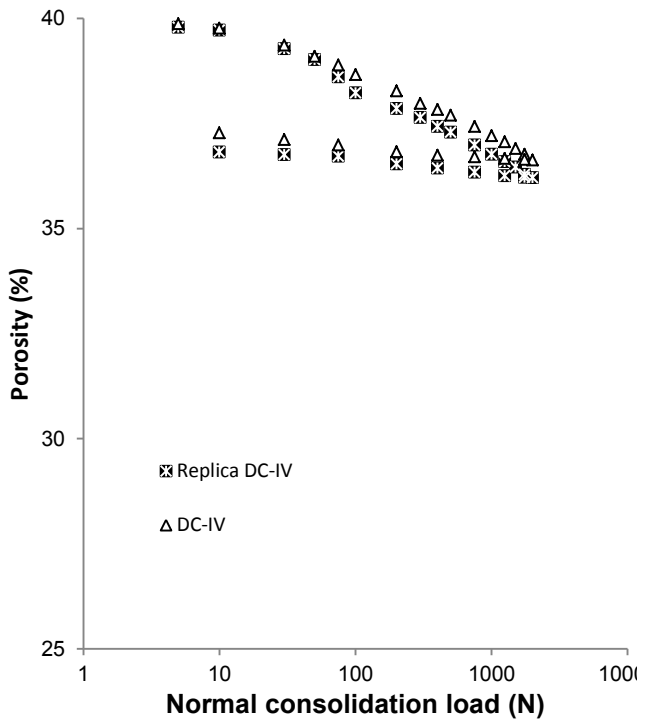
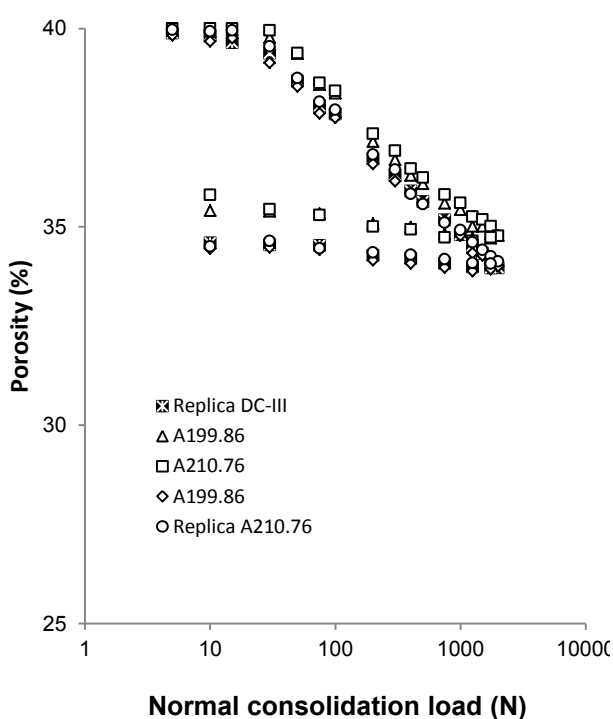
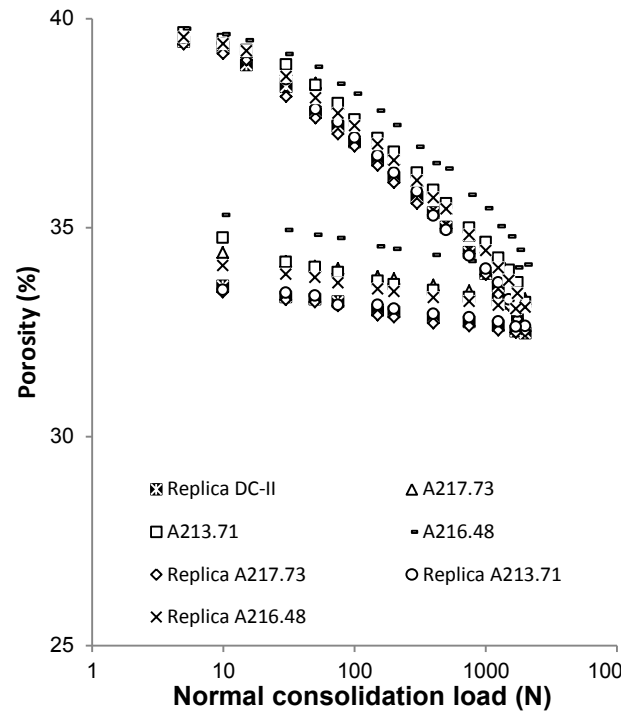
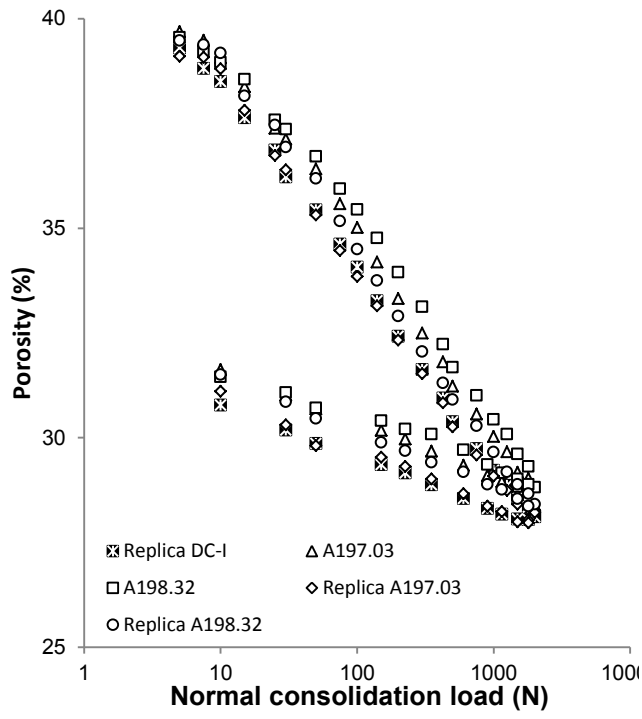


Figure 4-9. Uniaxial strain testing results for oil sands and corresponding commercial replica with the PSD of (a) DC-I, (b) DC-II, (c) DC-III, (d) DC-IV

## CHAPTER FIVE: EXPERIMENTAL SET-UP AND TESTING PROCEDURE

### 5.1 Introduction

This chapter covers the details of the pre-pack multi-slot sand retention testing (SRT) experimental facility. The facility consists of four main parts: (1) fluid injection units, (2) SRT cell, (3) measurements and data acquisition system, and (4) sand trap and back pressure unit. A series of pre-pack SRT tests was performed to establish the test procedures and understand the measurement ranges for the DC-II and DC-III PSDs.

The measurement devices were chosen to have the appropriate range and accuracies. The details of preparation, packing, and saturation of the specimens, as well as testing plans, are presented throughout this chapter. Towards the end of the chapter, the test repeatability is verified for both DC-II and DC-III. Post-mortem analysis and sample collections are presented at the end of the chapter.

### 5.2 Experimental set-up

Designs of different types of experimental setups in the literature were used to arrive at an improved apparatus for the SRT tests on unconsolidated sand pack samples. The set up consists of a cell that accommodates the sand pack sample, and the units for two-phase flow, sand measurement, and data acquisition. The coupon sits at the base of the cell on which the sand is packed. The flow is axial from the top to the base of the cell. **Figure 5-1** shows the schematic design of the SRT cell. The cell was designed to allow a 6-in.-multi-slot screen coupon (**Figure 5-1(a)**) to capture the inter-slot interaction. A series of porous disks from coarse to fine are used to ensure a uniform flow into the sample. A weight is placed over the top of the porous disks to ensure the sample would not fluidize during the saturation phase when brine is flown from the bottom of the sample to the top.

**Figure 5-2** shows a schematic view of the coupons. Multiple coupons with different slot density and slot width were used in the testing. The slot densities were chosen based on typical slot densities used in SAGD liners. The number of slots that can be cut into a pipe is limited by structural integrity requirements. Four pressure measurement ports were drilled and tapped on the coupon for pressure measurements as shown in **Figure 5-2**.

#### 5.2.1 SRT cell and accessories

The SRT cell has an inside diameter of 6.031 inches with a pressure rating of 90 psi at 100 °F. This test cell is equipped with interchangeable coupon disk at the bottom allowing to test different screen coupons. The total height of the cell is 13.5 inches. Three 1/8-inch NPT connections were carefully drilled and tapped on the side of the cell for pressure measurements. The first pressure port is located two inches above the coupon to measure the pressure drop near the screen. The pressure drop near the coupon is due to flow convergence towards the slots, pressure drop due to sand retention over the screen and possible pore plugging by fines migration over time. The next two pressure ports are placed 7.5 inches and 12.5 inches above the coupon. These two ports are designed to measure the permeability of the sample and its change due to possible fines migration.

The back-pressure unit allows the application of 1.93 psi pore pressure in the sample. This water column is also used for saturating the sample. A special design is used to ensure the produced sand is trapped in the sand measurement unit. A camera is used to track the produced sands in each step of the experiment.

### ***5.2.2 Flow injection unit***

The flow injection units consist of two solenoid diaphragm metering pump, with manual stroke control and digital pulse control, which allow controlling the rate with a high ratio of 1:33. The maximum rate for these pumps is 7.6 liters per hour (1.15 bbl/day) at 50 Psi. The two pumps allow the flow of multi-phase oil and brine injection to the sample with independent rate control. Calibration curves verified the linear variation of the flow with the change of stroke and input pulse. The outflow in each step was also measured for verification for a period of two minutes. The inlet of the pumps comes from a 120-liter reservoir. The outflow from the system is not circulated due to the fines presence in the outflow. The pH and salinity of the inflow and outflow are measured for each rate.

### ***5.2.3 Pressure and fluid flow rate measurement unit***

The design of pressure measurement unit started with a series of initial SRT tests to assess the ranges of pressure drops and the required measurement accuracies for permeability calculations. Pressure drops across the coupon for brine flow through the slots was found to be nearly zero (less than 0.01 psi), hence, can be determined by a manometer. The pressure drop in the sand pack relates to the permeability of the sand pack and evolution of the sand pack permeability for

the testing duration. Hence, the pressure measurement unit consists of three Setra differential pressure transducers (Setra 230 wet-wet differential transducer with 0.25% accuracy) and a manometer. For flow measurement, a rotameter is used and verified/calibrated by the measured volume of produced brine over two minutes.

#### ***5.2.4 Fines and sand production measurement***

The outflow line was designed to trap any size of produced sand with a camera monitoring the produced sand column. The produced sand is reported in terms of total produced sand per square foot of the screen for the test duration.

To collect a representative sample of the produced fines, a 1/8" tubing was installed right beneath the outlet of one of the slots (**Figure 5-3**). The tubing was connected to a metering needle valve to collect 100 cc outflow during each flow rate step to measure the fines concentration and PSD. The fines concentration is determined by a turbidimeter calibrated by creating solutions with known concentration of clays in demineralized water and plotting turbidity and concentrations against each other. There is a linear relationship between the turbidity measurement and fine concentration.

During each test, samples are collected from the outflow stream in certain intervals, and their turbidity is determined. The mass of eroded fines is obtained by multiplication of the total fluid injected during each step rate with the concentration of fines in the outflow.

#### ***5.2.5 Data acquisition system***

The pressure transducers and flowmeter are connected to a data acquisition device (National Instruments, Model USB-6210). The DAQ system has sixteen analog inputs, and eight differential analog inputs. Data from these devices are monitored and recorded through LabView SignalExpress software.

### **5.3 Test procedure**

Synthesized samples are constructed by mixing different proportions of commercial coarse, medium, fine, and very fine sand with silt and clay per the PSD recipe for DC-II and DC-III. The corresponding PSDs for DC-II and DC-III are shown in **Figure 4-6**.

#### ***5.3.1 Sand pack preparation***



Sample preparation starts by dry sand mixing in a large plastic container. The sand and fines proportion are mixed for about 20 minutes per the recipe presented in Chapter 4 to obtain 12 kg of the dry mixtures. 1.2 kg of water is gradually added to the dry sample, and the sand-fines-water mixture is carefully mixed by hand until it is uniform. To ensure the uniformity of the samples, three batches of the mixture were used to perform PSD measurements, which verified the uniform PSD within the mixture.

Moist tamping method like the procedure suggested by Ladd (1978) is used to prepare the sample. To ensure uniform porosity, samples are compacted in 12 equal layers (equal weight in equal volumes). Bradshaw and Baxter (2007) showed that with this technique sample with less than 1.5% variation in density can be produced.

### ***5.3.2 Sample saturation***

Due to the initial water content, samples have an initial brine saturation ( $\approx 75\%$ ). To fully saturate the sample, brine flow is established in upward direction at the slow rate of 250 cc/hr. Due to the high permeability of samples, full saturation is reached without the need of vacuuming the sample.

As the brine reaches to the top of the sample, the cell is connected to the pump, and a slow rate is applied to establish a flow from top to bottom of the sample. Then, pressure transducers are connected to the ports.

If the sample preparation and saturation are done correctly, the top and bottom portions of the sample should have the same permeability. If the bottom permeability and top permeability is more than 5% different from the average permeability obtained from previous tests, the cell is opened and the preparation and saturation procedures are repeated to obtain a uniform sample.

Brine with three different salinities (0%, 0.7%, and 1.4%) and three different pH values (6.8, 7.9, and 8.8) is used as the flowing medium in the experiments. To prepare the brine, salt is added to demineralized water and is mixed at a high-RPM mixer (1000 RPM) to obtain a uniform solution. The pH is adjusted by sodium bisulfate ( $\text{NaHSO}_4$ ) and sodium carbonate ( $\text{Na}_2\text{CO}_3$ ). Less than 10 ppm of pH booster and reducer are required to adjust the pH.

### ***5.3.3 Step-rate fluid flow injection***

A series of trial tests was performed initially to establish a standard test procedure. The goal of these initial tests is to assess the step rate tests, repeatability of the test results, and experiment

with the saturation procedure, composition of the fines particle, sample preparation, composition of injection fluid and the slot width and density.

Before carrying out the main tests, a multitude of trial tests was carried out for tuning the apparatus and calibrating the devices used for the experiments. Also, the trial testing results were used to select the initial saturation, saturation flow rate, and step rate tests.

To design the step rates, a typical SAGD production rate of 800-4000 bbl/day was considered and divided by the surface area of a SAGD well with 600-1000 m length completed with a 7-inch slotted liner. Assuming a uniform flow distribution, a liquid flux rate in the range of 0.13-1.11 bbl/day/ft<sup>2</sup> is expected. For the area of the coupons used in the testing, this variation translates to 0.03-0.27 bbl/day.

However, some slots may be plugged over time or, simply, not contribute to flow. Considering a slot plugging factor of 90%, flow rates in the range of 0.25 to 2.5 bbl/day are considered for the step rate tests as reflected in **Figure 5-5**.

Since the test were conducted at constant flow rates, pressures are measured to calculate the permeability. Flow rates are controlled through the pump stroke manual control and pulse digital control. Each test in this thesis consisted of step-rate injection at seven different flow rates each for 30 minutes (**Figure 5-5**).

#### ***5.3.4 Post-mortem analysis***

Post-mortem studies were used to characterize the slot and pore throat plugging as well as to track the fines mobilization and transport in the sample.

A 0.5-inch PVC tube is used to extract a core from the test specimen. Three core specimens are extracted and using a wet sieving method, the fines content smaller than the opening size of mesh # 325 is separated. The coarser portion is dried in an oven for 24 hrs and weighted with an accurate scale down to 0.001 gr. Furthermore, a PSD analysis is performed on the fines portion to study the size of mobilized fines. Fines concentration and PSD of samples from several elevations in the sample are determined to compare with the original PSD and fines concentration to track the mobilized fines in the sample.

#### ***5.3.5 Test assumptions and limitations***

Typical SAGD producer are producing 1500 bbl/day with typical steam oil ratio (SOR) ranging from 1.5 to 4.0. Temperatures along the horizontal well are monitored and a certain pressure

difference is targeted between the production and injector wells to ensure a minimum thickness for the liquid level (sub-cool) around the production well. The producer well has a temperature ranging from 220-350 °C depending on the reservoir depth. However, operating experiments at such high pressures and temperatures is extremely expensive, and each test will take weeks to perform. Also, operating such tests poses a great risk due to the extreme temperatures and a high potential of hot water flashing as the pressures drop.

To overcome this limitation, the experimental system was designed to assess the physical factors that affect the sand production and pore plugging at representative flow rates using realistic PSDs. The tests were designed to consider the worst-case scenario in terms of performance indicators (sand production and pore plugging) by establishing a single-phase brine flow. Single-phase flow of brine results in higher levels of fine mobilization and transport as well as a higher sand production level due to the lack of capillarity.

Typically, there is a gap between the liner and formation at the time of liner installation. During the circulation phase, the gap is expected to collapse due to the rise in temperature and melting of the bitumen. Closure of this gap creates a high-porosity zone around the liner with no stress in the collapsed region. As the SAGD chamber rises over time, the stress increases around the liner leading to the compaction of the sand around the liner. The higher stresses increase the frictional resistance among the particle, resulting in a lower produced sand. The worst-case scenario is the early stage when the effective stresses are near zero. The near-zero stress level is duplicated in the SRT testing facility described in this thesis. The flow rates, the flowing media, and the chemical and ionic strength of the flowing fluid were chosen to replicate the SAGD producer conditions.

#### **5.4 Test plan**

The pre-pack SRT tests were carried out per the plan in **Table 5-1** and **5-2**. Initial tests indicated the high sensitivity of results, particularly fines migration, to the brine pH and salinity. To assess the role of pH and salinity on the results, a series of tests was conducted at different levels of pH and salinity. Results from these tests (**Table 5-1**) are discussed in Chapter 6.

After these tests, the pH was fixed at 7.9 and salinity at 7000 ppm, which is the typical pH and salinity in produced water in SAGD. Results from these tests (**Table 5-2**) are discussed in Chapter 7 and 8.

## 5.5 SRT testing repeatability

This section examines the results of test repeatability examination. Test repeatability was examined for DC-II and DC-III samples for screen coupons with slot width of 0.014” and 0.026”, respectively, where both coupons have the same SPC of 54.

**Figure 5-5** shows the retained permeability results for the repeated tests. There is a good agreement on the value and trend of the retained permeability for the repeated tests. **Figure 5-6** shows the cumulative sand production for the repeated test. The overall produced sand and the mode of observed sand production are consistent in the repeated tests, confirming the repeatability of the test results.

**Table 5-1. Testing plan to study the role of pH and salinity on retained permeability**

	pH=6.8	pH=7.9	pH=8.8
0 ppm NaCl	DC-II, 0.014", SPC=54	DC-II, 0.014", SPC=54	DC-II, 0.014", SPC=54
7000 ppm NaCl	DC-II, 0.014", SPC=54	DC-II, 0.014", SPC=54	DC-II, 0.014", SPC=54
14000 ppm NaCl	DC-II, 0.014", SPC=54	DC-II, 0.014", SPC=54	DC-II, 0.014", SPC=54

**Table 5-2. Test matrix for the main testing program**

	SPC=30	SPC=42	SPC=54
Slot width=0.010"	DC-II & DC-III	DC-II & DC-III	DC-II & DC-III
Slot width=0.014"	DC-II & DC-III	DC-II & DC-III	DC-II & DC-III
Slot width=0.018"	DC-II & DC-III	None	DC-II & DC-III
Slot width=0.022"	None	DC-II & DC-III	DC-II & DC-III
Slot width=0.026"	DC-II & DC-III	DC-II & DC-III	DC-II & DC-III
Slot width=0.032"	DC-III	DC-III	DC-III

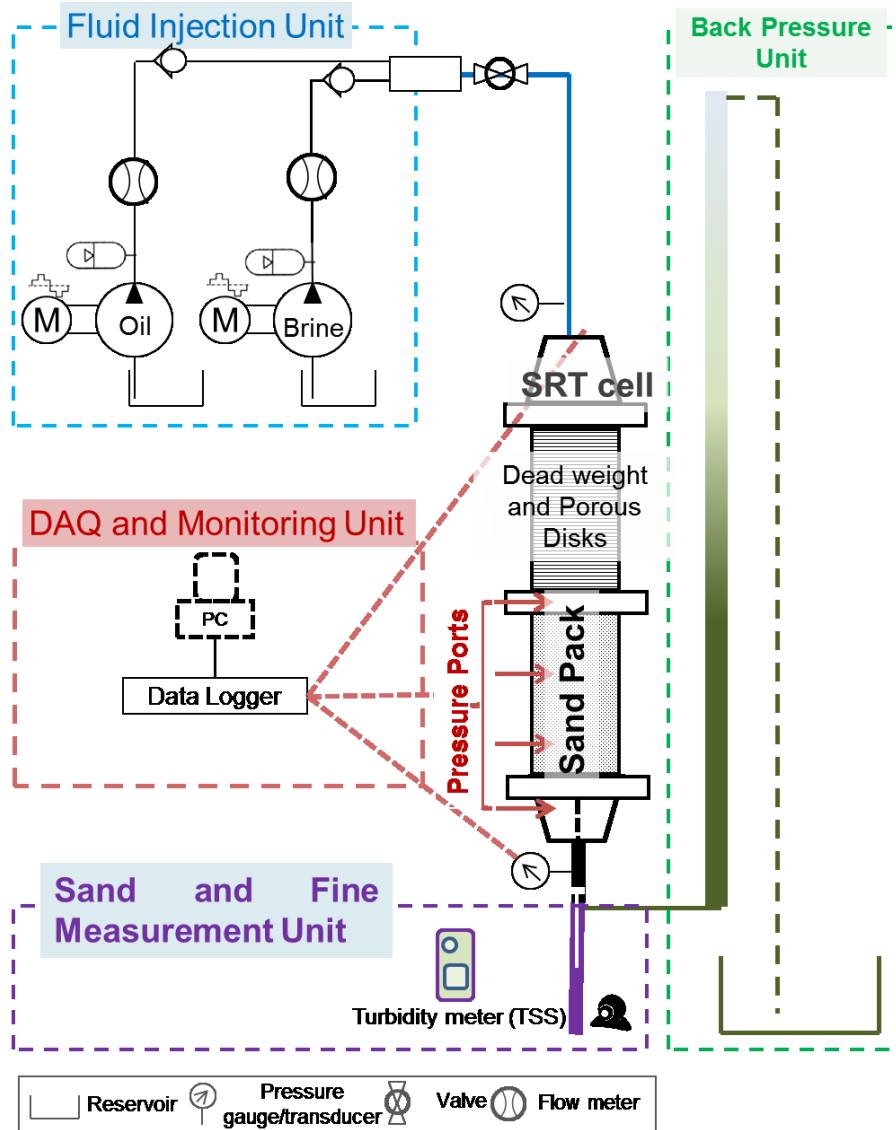


Figure 5-1. Schematic design of the SRT facility

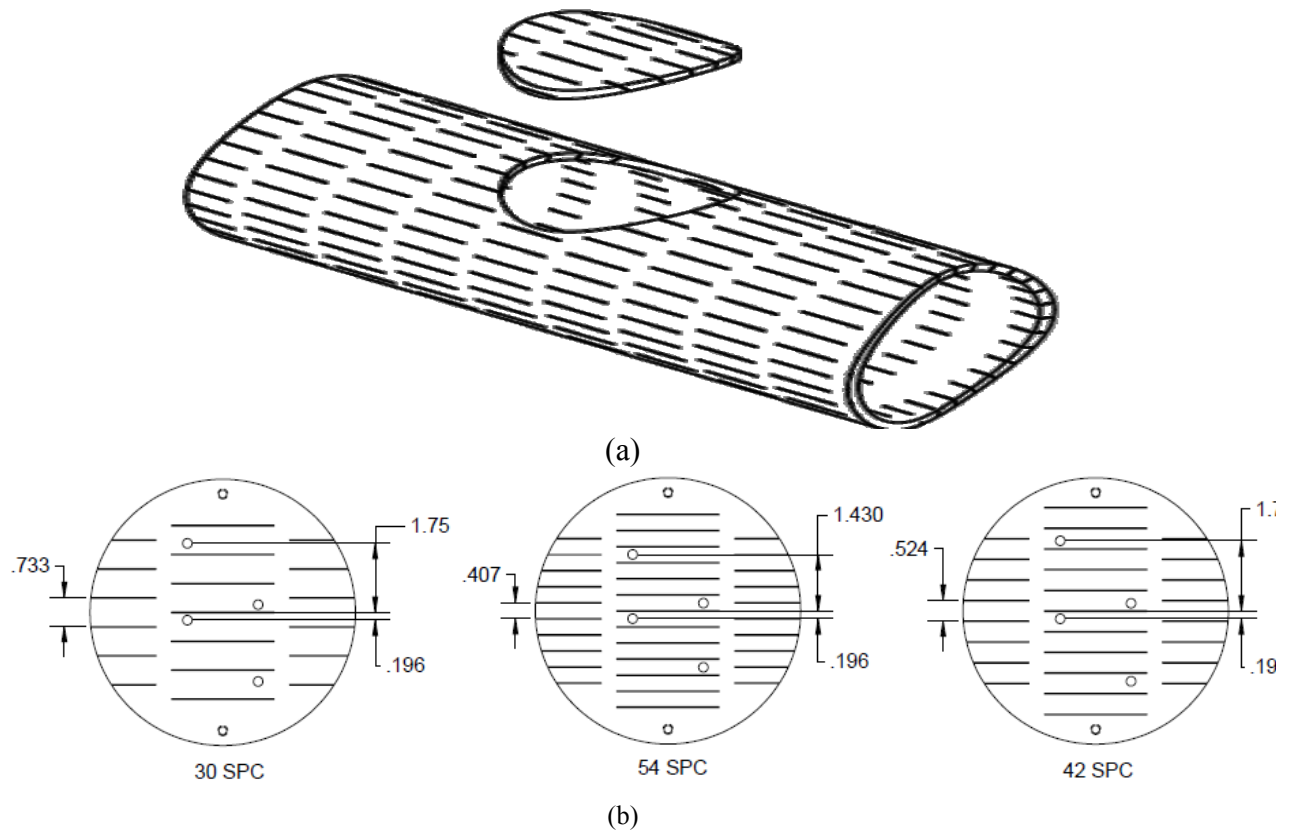
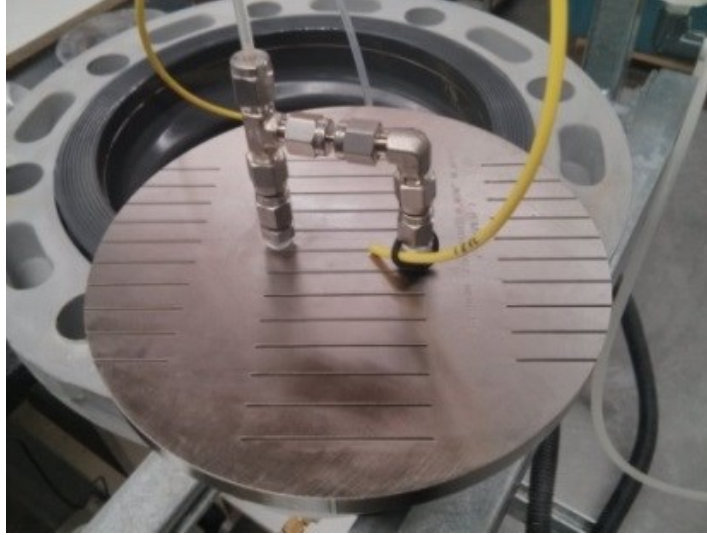


Figure 5-2. Schematic of the multi-slot coupon, (a) the multi-slot coupon as a disk cut out from a 7-inch liner, (b) slot spacing for three SPC values of 30, 42 and 54. All dimensions are in inch

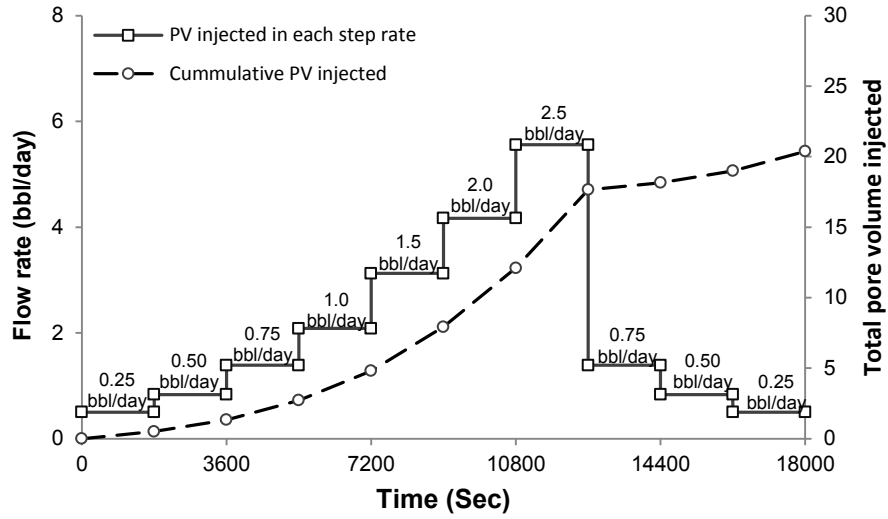


Figure 5-3. Multi-slot coupon with seamed slots

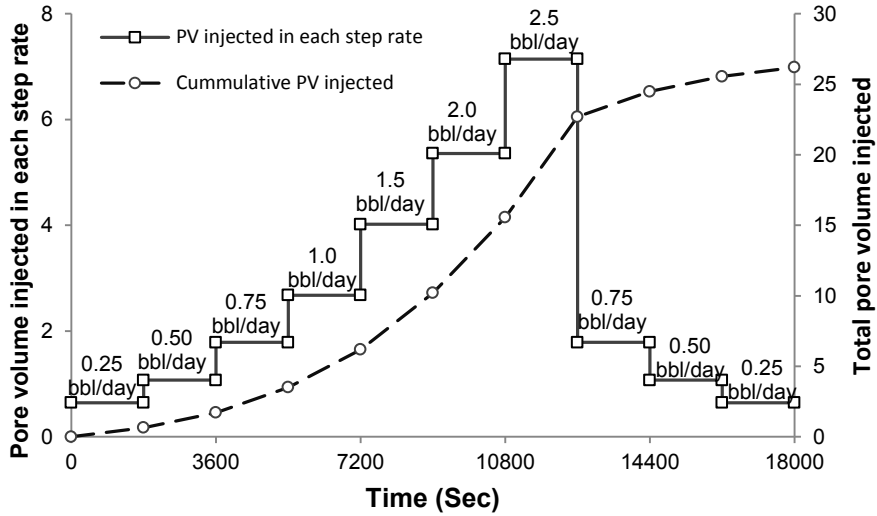


**Figure 5-4. Connections at the back of a coupon for pressure measurements; the yellow tube is to obtain samples from the outflow during the testing**





(a)



(b)

Figure 5-5. Injected PVs for step rate tests in pre-packed SRT tests on sand packs prepared by different PSDs: (a) DC-III and (b) DC-II

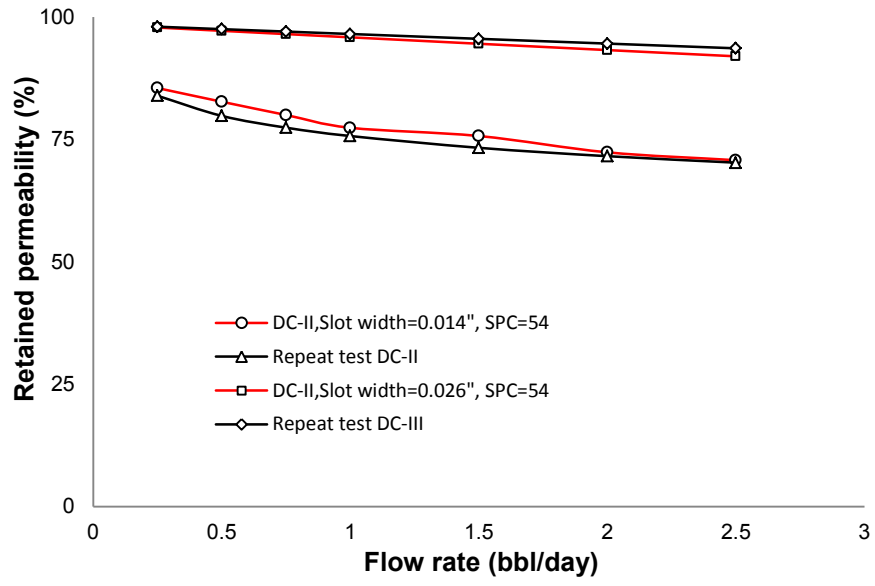


Figure 5-6. Comparison of the retained permeability for the repeated tests

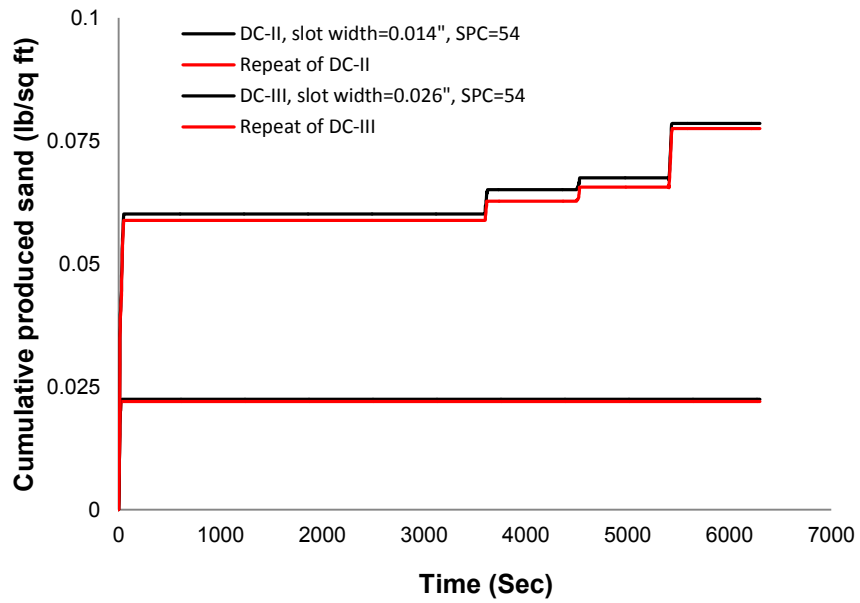


Figure 5-7. Cumulative produced sand for the repeatability tests

## **CHAPTER SIX: AN EXPERIMENTAL INVESTIGATION OF THE EFFECT OF pH AND SALINITY ON SAND CONTROL PERFORMANCE FOR HEAVY OIL THERMAL PRODUCTION**

### **6.1 Introduction**

There have been a few research works on the effect of pH and salinity on fines migration to understand the mechanisms associated with recovery improvement in low-salinity water injection operations (Tang and Morrow 1999; McGuire et al. 2005; Buckley and Morrow 2010; Sheng 2014) and formation damage due to the fines migration (Vaidya and Folger 1992; Sheng 2014). However, the pH and salinity effects have often been neglected in laboratory studies of sand control systems in the SAGD context. An exception is the work of Bennion et al. (2008) that discussed the effect of pH on pressure drop across a single-slot coupon. They found that the pressure drop is highly sensitive to the pH level of the injected water. They adjusted the pH level by adding only 1% or less HCl to the injected fluid and observed clay (kaolinite and illite) flocculation (aggregation) at low pH and deflocculation (dispersion) at high pH. They concluded that clay aggregation can result in reduced screen plugging. However, they did not study the pH effect on clay movement in the sand pack.

In SAGD, fresh steam is mixed with the formation water around the injection well. As the condensate moves toward the production well, the salinity of the condensate is elevated as it picks up the formation minerals and is mixed with the high-salinity formation water with dissolved minerals in the range of 20,000-60,000 ppm (Bhattacharjee 2011). Further, the exposure of the condensate to solution  $H_2S$ ,  $CH_4$ , and  $CO_2$  (Bhattacharjee 2011), results in a low pH value, hence a lower chance of the mobilization of formation clays in early stages around the production well. Over time, the salinity of the brine in the vicinity of the production well gradually decreases as more melted bitumen and water (formation water and condensate) are produced. Further, the pH level gradually increases as further condensate with caustic nature (Bennion et al. 2008) is injected and ion exchange happens between the adsorbed cations and  $H^+$  in solution (Mohan et al. 1993). At low salinity and high pH around the production well, the clay particles can mobilize (Khilar et al. 1990) and migrate towards the production well.

This chapter presents the results of several Sand Retention Tests (SRTs) on sand pack samples supported by multi-slot coupons and discusses permeability variations and fines migration for

brine injection with different pH and salinity values. Results show a strong relation between fines migration and retained permeability and pH and salinity.

In the experiments, NaCl was used to adjust the salinity as sodium and chlorides are observed to be the dominant ions in produced water from SAGD wells. As the worst-case scenario for clay migration, only monovalent cations were used since bivalent cations can reduce the water sensitivity and clay migration (Khilar and Fogler 1984). This study can be considered as an effort to open the discussion on the pH and salinity effect on the performance of slotted liners in SAGD wells.

## **6.2 Composition of the produced and formation water**

The knowledge of produced and formation water composition is essential before conducting a laboratory sand control or fines migration test. The interaction between the injected/produced water, formation water, clays and injected steam seems to be the main factor which controls the fines movement (Sheng 2014).

Formation water compositions for oil sands reservoirs are highly variable. Cowie (2013) mapped total dissolved solids (TDS) of 355 McMurray Formation water samples in Athabasca oil sands. His study showed that McMurray Formation waters varied from non-saline (TDS < 4,000 mg/L) to brine (TDS > 100,000 mg/L) with a regional trend of high salinity water approximately following the dissolution edge of the Prairie Evaporate Formation (red shading in the **Figure 6-1**). Cowie (2013) discussed the hydrological explanation for the observed variation in TDS in detail, which is beyond the scope of the current study. The important conclusion is that, although the SAGD projects are located mainly in similar geographical areas in Alberta, the formation water's composition changes significantly and any study of the effect of the formation water's composition must be case dependent.

Bhattacharjee (2011) characterized produced water in SAGD operations as containing dissolved solids (1,500 to 6,000 ppm TDS) and suspended solids (typically silica at 275 to 400 ppm level). Peterson (2007) concluded that produced water in northern Alberta generally has the following characteristics:

- TDS in the range of 1,500 to 5,000 mg/L
- Silica saturation up to 350 ppm

- High alkalinity and chloride (major inorganic anions)
- High sodium (major inorganic cation)
- High dissolved organic content (measured as TOC)
- Low immiscible organic content (measured as oil and grease)
- Low hardness
- Low sulfate

According to Bennion et al. (2008), the pH of produced water in SAGD wells depends on several variables such as the caustic nature of the injected steam and steam condensate and the existence of carbon dioxide and hydrogen sulfide in the reservoir. **Table 6-1** shows several examples for the composition of the produced water for SAGD projects and indicates a pH range of 7.3 - 8.8. It is likely that in some cases the produced water could become slightly acidic.

Some of above parameters (such as alkalinity of the injected steam, companion gases and additives to the injected steam) could be modified by the operator, while others relate to the original composition of the reservoir solids and fluids and cannot be changed.

### **6.3 Effect of pH and salinity on clay/fines migration**

The effects of pH and salinity on fines migration have been widely investigated to understand the mechanisms involved in low-salinity water injection (Tang and Morrow 1999; McGuire et al. 2005; Buckley and Morrow 2010; Sheng 2014) and formation damage (Vaidya and Folger 1992). The focus of this section is only on the studies related to the interaction of brine with clay particles under different pH conditions in sand and sandstone media.

The main clays in McMurray Formation are kaolinite and illite (Bennion et al. 2008). These clays can become detached during aqueous flow, especially when flowing brines become less saline in comparison with formation water (Boston et al. 1969). Mohan et al. (1993) and Mohan and Folger (1997) provided an explanation of pore blockage by clay detachment and migration. They concluded three mechanisms for permeability reduction in sandstone containing swelling (smectites and mixed layer clays) and non-swelling (kaolinites and illites) clays (**Figure 6-2**): (1) Migration: Release of clay particles from pore walls due to the change in ionic conditions which cause the pore blockage; (2) Swelling: Clay swelling blocks pore channels and reduces the

permeability. (3) Swelling-induced migration: change in the ionic condition cause swelling of the clays lining the pore walls which eventually dislodges the fines.

The first mechanism seems to apply to McMurray Formation oil sands where kaolinites and illites are the main minerals. Due to the high variation in the composition of produced water and depending on ionic concentrations, the tendency for fines migration can highly vary from one reservoir to another. For a better understanding of the fines migration, a detailed testing program is required for each particular case.

It has been shown that a Critical Salt Concentration (CSC) exists for clay particle movement in porous media (Khilar et al. 1983; Khilar and Folger 1984; Khilar et al. 1990). If the salinity of the permeating fluid falls below the CSC, the sandstone permeability is significantly reduced as a result of the detachment of clay particles from the pore walls, which block the pore throats. Khilar and Fogler (1984) found the CSC concept applies only for monovalent cations (such as  $\text{Na}^+$ ,  $\text{K}^+$  and  $\text{Li}^+$ ) and is virtually nonexistent for cations with a valence greater than one (such as  $\text{Ca}^{2+}$ ,  $\text{Mg}^{2+}$  and  $\text{Ba}^{2+}$ ). They observed that “water sensitivity” does not occur when bivalent salt solutions like  $\text{CaCl}_2$  and  $\text{MgCl}_2$  are used in the test (contrary to monovalent salts like  $\text{NaCl}$ ). Even for monovalent cations, the CSC depends on counterions. The release of clay particles is effectively prevented due to the strong ion-exchange affinity of clay for the polyvalent counterion.

In addition to salinity, pH could also affect the movement of clay particles in porous media. Mungan (1965), Simon et al. (1976), Kia et al. (1987) and Leone and Scott, (1988) concluded that permeability reduction due to the abrupt change in salinity does not occur in extremely acidic solutions (pH values below 2.6).

Different studies (Mungan 1965; Simon et al. 1976; Leone and Scott 1988; Vaidya and Folger 1992) showed that dispersion of clay particles was minimized at low pH. Variation in pH was reported to impose a great change in terms of dispersion and aggregating of the clay particles in slotted liners experiments (Bennion et al. 2008).

It has been found that during the injection of the low salinity solution, the pH of effluent increases to higher levels than the initial pH value (Vaidya and Folger 1992; Sheng 2014). The pH variation has been related to ion exchange between the adsorbed  $\text{Na}^+$  and  $\text{H}^+$  in solution which results in an increased  $\text{OH}^-$  concentration in the solution (i.e. pH increases) (Mohan et al.

1993). This increased pH is believed to amplify the release of fines and cause a drastic reduction in permeability.

In their variable pH fluid injection tests, Vaidya and Fogler (1992) reported small variations in permeability for pH values up to 9. Permeability reduction starts at pH values higher than 9. For  $\text{pH} > 11$ , they observed a rapid and drastic decrease in the permeability. Solution pH also affects the interfacial tension (IFT) (McGuire et al. 2005).

As Vaidya and Fogler (1992) discussed, in a system where exchangeable cations exist, the salinity and pH of the solution are expected to have interrelated effects. Therefore, to understand the combined effect of these two parameters, a test matrix is required in which both these parameters are varied.

#### **6.4 Testing program**

Sand retention testing (SRT) as described in Chapter 5 was used in this investigation. Brine with different pH and salinity was used to study the role of pH and salinity on the fine mobilization and transport in different flow rates. **Table 5-2** shows the test matrix consisting of three pH values (6.8, 7.9 and 8.8) and three salinity values (0, 7000, 14000 ppm NaCl solution) which were selected based on the ranges of salinity and pH for typical SAGD produced water. Brine was injected at different step rates (**Figure 5-3 (b)**) up to 15.3 times the common flow rates in SAGD operations (40 cc/hr/slot) into a sand pack with similar PSD and particle shapes to a typical oil sand from the McMurray Formation. High flow rates were tested to simulate extreme cases where local plugging of slots results in increased fluid velocity in the open slots. Each flow rate was kept constant for 30 minutes with a total of 22.7 pore volume injection. In all tests, pressure drops stabilized in less than 10 minutes.

The results of these tests are presented in this chapter to illustrate the sensitivity of screen performance indicators to fines mobilization due to the change in the ionic strength of the brine. The step rate test and the fines concentration in the outflow are used to examine the conditions required to mobilize the fines. Also, the consequence of fines mobilization and transport on the retained permeability are investigated.

#### **6.4 Results and discussions**

In this section, the term “retained permeability” is used as a primary parameter to study the impact of the pH and salinity on the results from sand retention testing. This parameter has been used before with slightly different definitions to analyze the performance of different completions/screens (Hodge et al. 2002). Retained permeability is used as an indicator of how the use of slotted liner affects the permeability of the zone near the slotted liner.

The pressure drop across the coupon was found to be less than 0.01 psi as no plugging was observed in any of the tests. Therefore, the slotted liner was not included in the definition of the retained permeability to avoid unrealistically high values.

**Figure 6-3** through **6-8** depict the retained permeability and produced fines for certain salinity and pH values, which indicate the sensitivity of the retained permeability and fines migration to salinity and pH. The flow rate in these figures is reported in terms of the equivalent field value in bbl/day/ft. An important observation is that for constant pH, the salinity, and retained permeability are directly proportional. Further, an inverse relation between salinity and the mass of produced fines is noted. **Figure 6-8** shows that for the extreme salinity of 1.4%, there is a very small change in permeability and minimal produced fines during the water injection.

**Figure 6-3** through **6-8** also indicates an inverse relation between retained permeability and pH and also a direct relation between pH and the mass of produced fines. These results on the role of pH agree with the findings reported in the literature which indicate high pH values (>9) are required to mobilize Kaolinite particles (Vaidya and Fogler 1990, 1992; Mohan et al. 1993).

**Figure 6-3** through **6-8** indicate higher rise in the pH level of the effluent for higher flow rates. The higher pH combined with the higher flow velocities elevate the fines mobility and production. Higher flow rates also increase the size (D50) of the produced fines, which is probably due to stronger drag forces.

Produced sand for all nine tests varied between 0.048 to 0.053 lb/sq ft and did not seem to be related to the pH and salinity of injected fluid. The produced sand was below 0.12-0.15 lb/sq ft, which seems to be considered as the threshold for the maximum acceptable sand production per unit surface area of the screen (Chanpura 2011).

In all tests, sanding was observed in early stages of tests at low flow rate. It seems that the slot width of the chosen coupon was appropriate in limiting the amounts of produced sand.



## 6.5 Conclusion

An experimental investigation was successfully performed to study the effect of salinity and pH on the performance of slotted liner in SAGD wells. Single-phase brine with variable salinity (0.7 to 1.4%) and pH values (6.8 to 8.8) was used in the experiments. This study considered the effect NaCl as a monovalent cation in brine, which seem to be the extreme case for clay (kaolinite and illite) production. The situation would be more complex where polyvalent counterions and swelling clays are dominant requiring a broader examination and testing.

The pH of produced water in SAGD operations is in the range of 7.3 to 8.8. However, the test matrix included a wider range of 6.8-8.8 for the pH of injected brine. The effluent pH was found to be higher (6.8-9.9) than the pH of injected brine due to the ionic exchange between the injected brine and the clay in the sand pack.

Pressure drop across the coupon was found to be negligible (less than 0.01 psi) for the range of flow rates that was tested for the single-phase brine injection as no slot plugging was observed during the tests. Therefore, the study focused more on the fines/clay migration which affects the permeability of the sand pack in the vicinity of the slotted liner.

Results show that retained permeability decreases for lower salinities while it increases for lower pH values. Retained permeability, had an inverse relation with the amount of produced fines/clays. Fines/clay production in our tests did not result in plugging due perhaps to the limited flow time for each test (5 hours) and the absence of hydrocarbon injection. In the real world, high fines production combined with other phenomena such as asphaltene and paraffin precipitation may cause severe plugging.

Unlike the fines production, sand production was not affected by the pH and salinity in our tests. Sanding was about 0.05 lb/sq ft for all the tests, which is far below the acceptable sanding threshold reported in the literature. In our test, most of the sanding occurred in early stages at low flow rates (initial sanding) and stopped at elevated rates.

**Table 6-1. Composition of produced water for different SAGD projects**

	Bhattacharjee (2011)	Hill (2012)	Hill (2012)	sand Project (2013)	Pedenaud and Michaud (2009)	Pedenaud and Michaud (2009)	Pedenaud and Michaud (2009)	Pedenaud and Michaud (2009)	Gamache et al. (2012)	Gamache et al. (2012)	Peterson (2007)	Goodman et al. (2010)
<b>Calcium (Ca) (ppm)</b>	7	4	11	NM	2.7	3.9	22	10	2	20	1-52	
<b>Magnesium (Mg) (ppm)</b>	NM	1	5	NM	6.1	0.3	11	3	1	10	1.6-14	
<b>Barium (Ba) (ppm)</b>	0.8	NM	NM	NM	0	0.2	0	NM	NM	NM	NM	
<b>Sodium (Na) (ppm)</b>	314	NM	NM	NM	2200	706	780	1310	321	1004	130-3000	
<b>Sulfate (SO<sub>4</sub>) (ppm)</b>	107	NM	NM	NM	56	1	58	NM	NM	70	NM	
<b>Chloride (Cl) (ppm)</b>	200	NM	NM	NM	1697	930	962	2060	260	1310	48-4800	
<b>Potassium (K) (ppm)</b>	NM	NM	NM	NM	NM	NM	NM	21	18	NM	14-240	
<b>Ammonia(NH<sub>3</sub>) (ppm)</b>	NM	NM	NM	NM	NM	NM	NM	NM	NM	NM	11-64	
<b>Ammonium(NH<sub>4</sub>) (ppm)</b>	NM	NM	NM	NM	NM	NM	NM	46	66	NM	NM	
<b>Bicarbonate (HCO<sub>3</sub>) (ppm)</b>	NM	NM	NM	NM	2677	332	489	493	406	429	NM	
<b>Carbonate (CO<sub>3</sub>) (ppm)</b>	NM	NM	NM	NM	108	1	0	NM	NM	2	NM	
<b>Silica (SiO<sub>2</sub>) (ppm)</b>	NM	188	261	273	260	260	250	170	255	NM	11-260	
<b>Alkalinity (as CaCO<sub>3</sub>) (ppm)</b>	NM	173	297	257	NM	NM	NM	NM	NM	NM	140-1400	
<b>Salinity (ppm)</b>	NM	NM	NM	1	NM	NM	NM	NM	NM	NM	NM	
<b>NaCl (ppm)</b>	NM	NM	NM	NM	NM	NM	NM	3400	400	NM	NM	
<b>Hardness (as CaCO<sub>3</sub>) (ppm)</b>	22	NM	NM	6	32	11	100.9	NM	NM	NM	NM	
<b>Total Solid (TS) (ppm)</b>	NM	NM	NM	NM	NM	NM	NM	5700	2800	NM	NM	
<b>Total Dissolved Solid (TDS) (ppm)</b>	1005	1290	2870	1644	6951	2370	2585	NM	NM	3040	NM	
<b>SS (Suspended Solid) (ppm)</b>	NM	NM	NM	NM	NM	NM	NM	NM	NM	<25	NM	
<b>Total Organic Carbonate (TOC) (ppm)</b>	NM	300	350	NM	NM	NM	NM	588	596	200	170-430	
<b>Oil(ppm)</b>	NM	NM	NM	82	NM	NM	NM	NM	NM	20	NM	
<b>pH</b>	8.5	NM	NM	8	7.9	8	7.7	NM	NM	7.9	7.3-8.8	
<b>Specific Gravity</b>	1.005	NM	NM	NM	NM	NM	NM	NM	NM	NM	NM	

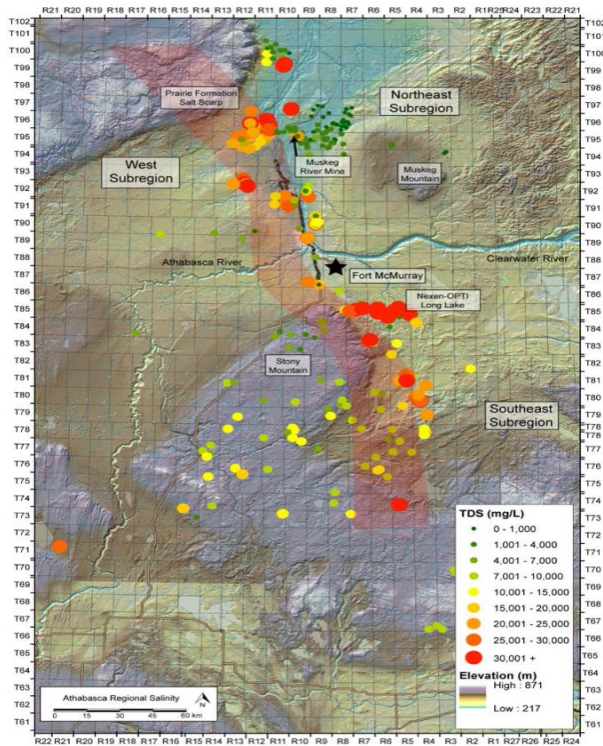


Figure 6-1. McMurray Formation water TDS in Athabasca oil sands region, overlain on ground surface elevation (Cowie, 2013)

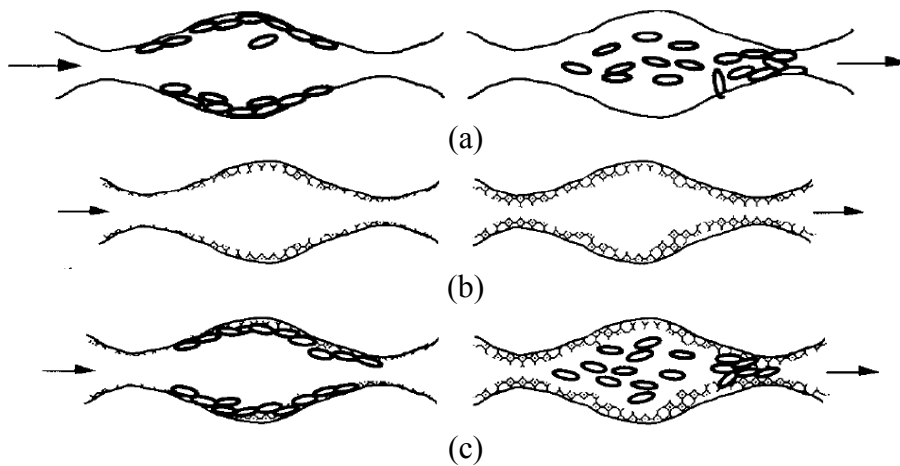
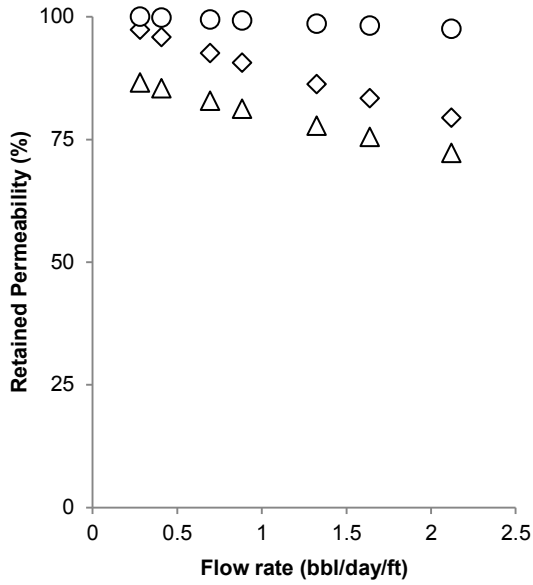


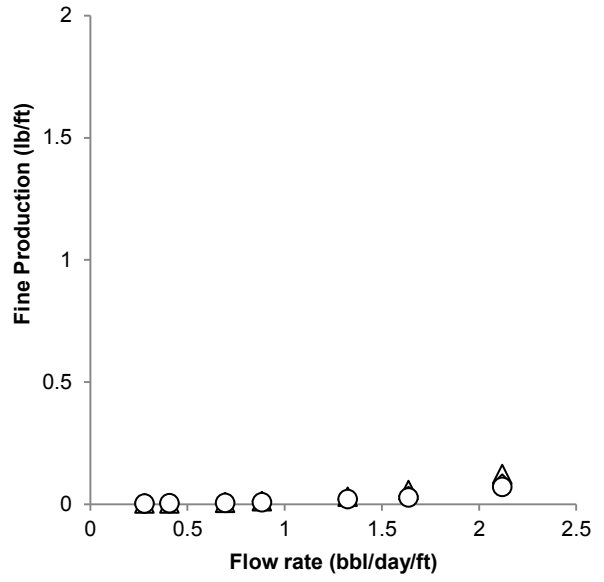
Figure 6-2. Three mechanisms for permeability reduction caused by changing the ionic condition of the environment for clay particles: (a) migration, (b) swelling, and (c) swelling-induced migration (Mohan et al. 1993)

Salinity:  $\Delta$  0%  $\diamond$  0.7%  $\circ$  1.4%

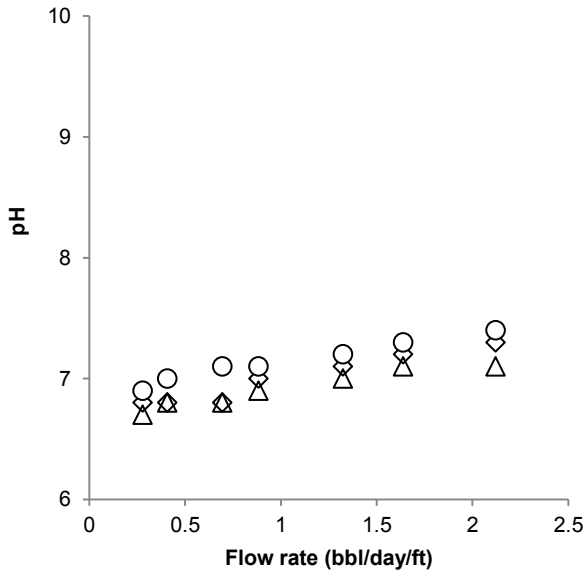
pH = 6.8



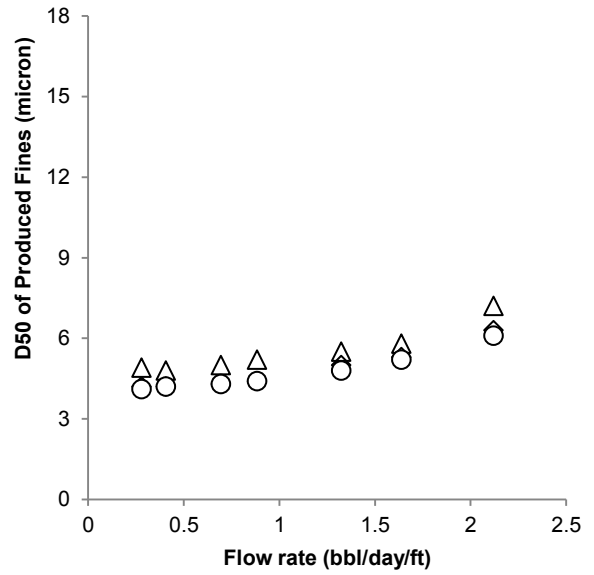
(a)



(b)



(c)



(d)

Figure 6-3. SRT results for the constant pH value of 6.8 and different salinities: (a) retained permeability, (b) fines production, (c) pH of produced fluid and (d) D50 of produced fines for different flow rates

Salinity:  $\Delta$  0%  $\diamond$  0.7%  $\circ$  1.4%

pH = 7.9

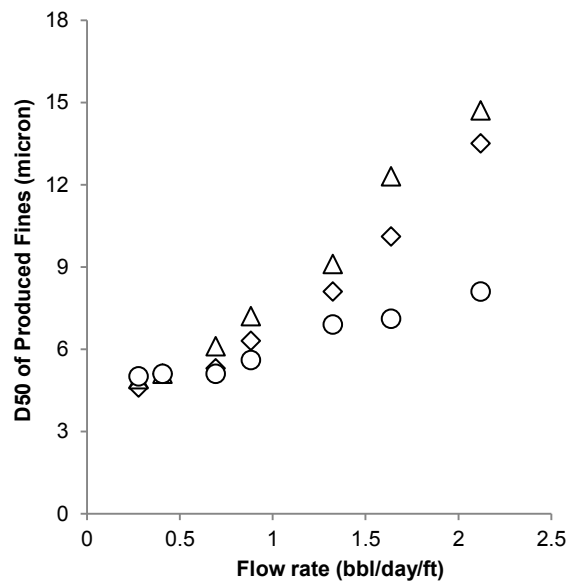
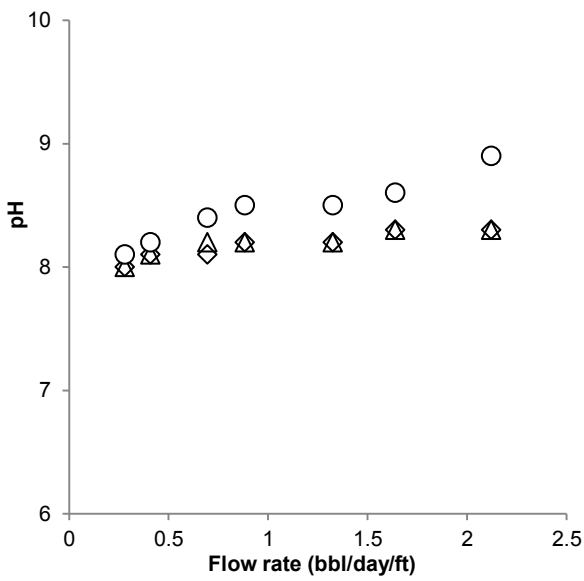
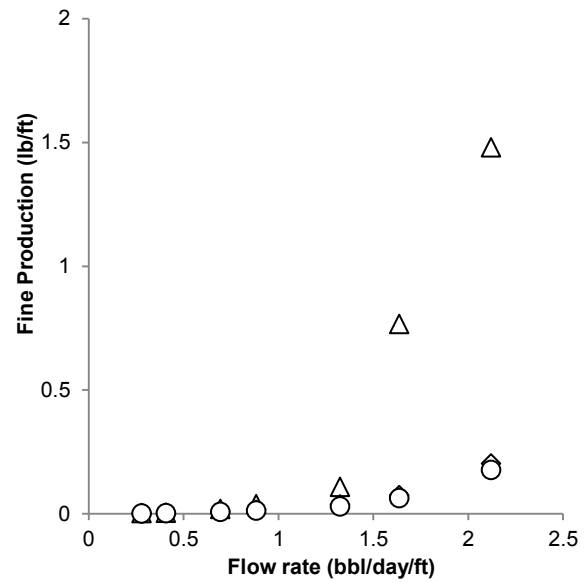
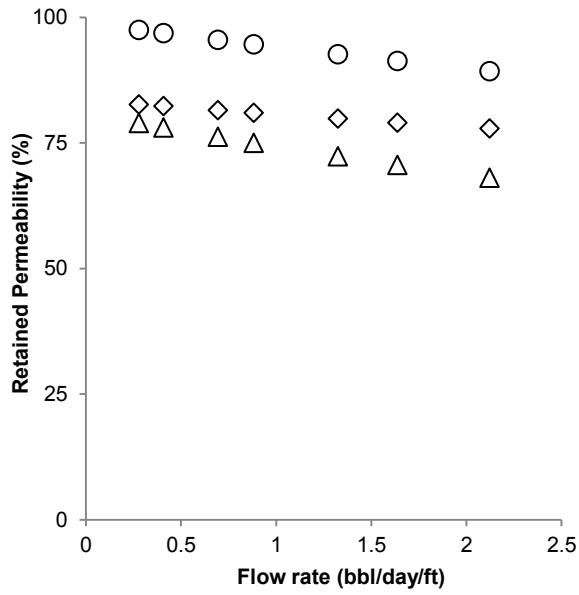
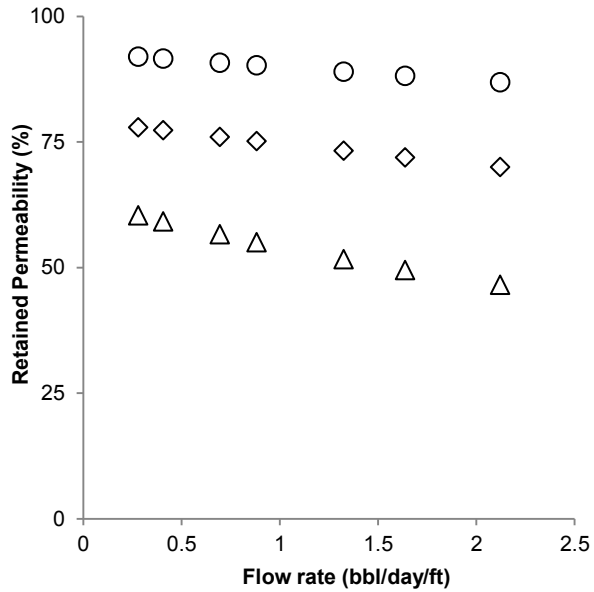


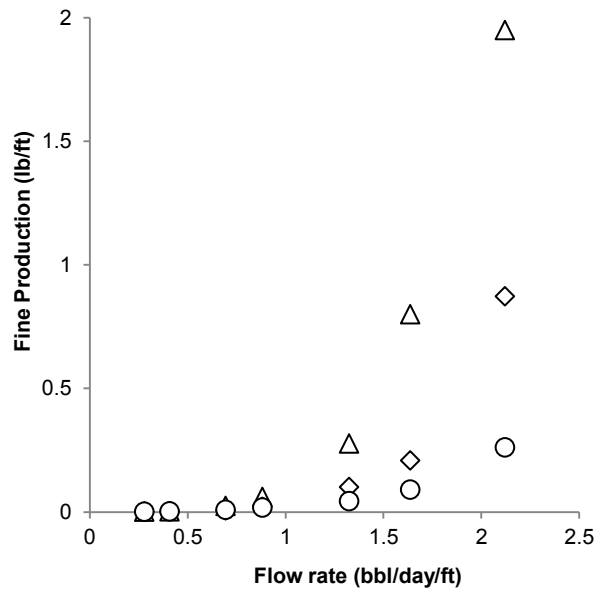
Figure 6-4. SRT results for the constant pH value of 7.9 and different salinities: (a) retained permeability, (b) fines production, (c) pH of produced fluid and (d) D50 of produced fines for different flow rates

Salinity:  $\Delta$  0%  $\diamond$  0.7%  $\circ$  1.4%

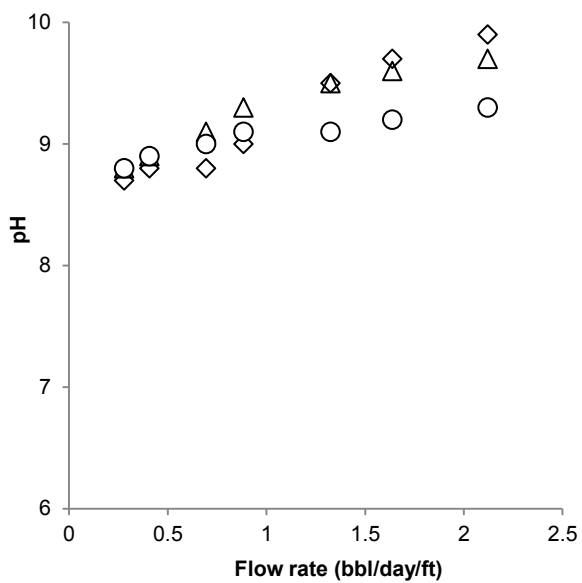
pH = 8.8



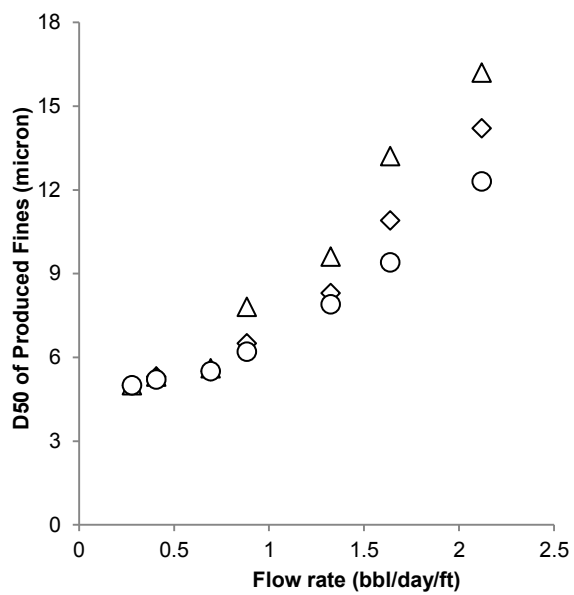
(a)



(b)



(c)

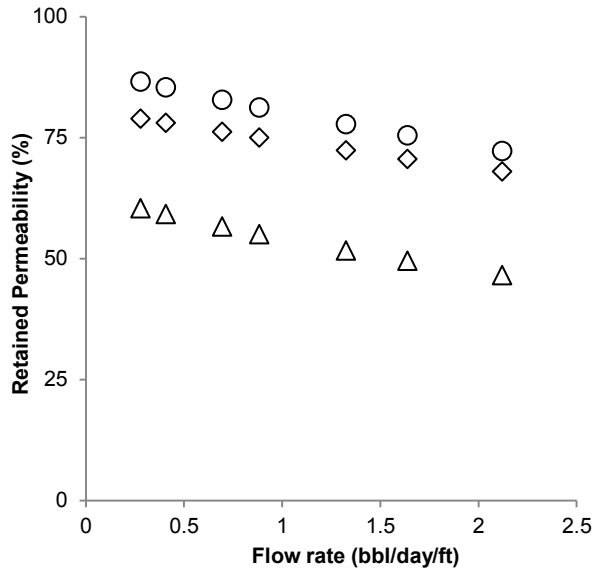


(d)

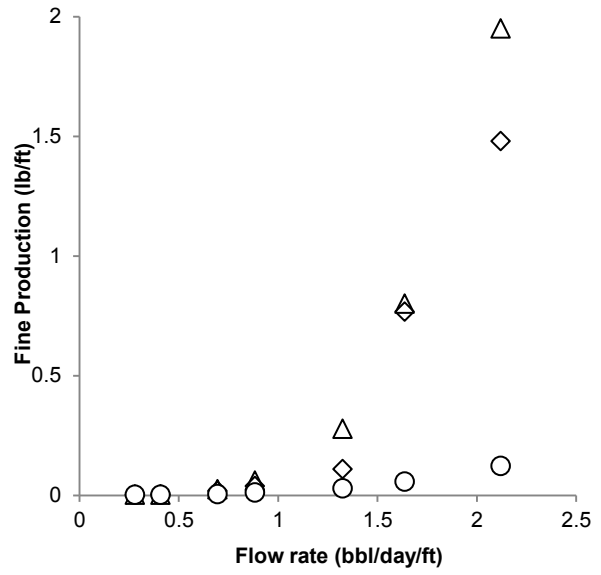
Figure 6-5. SRT results for constant pH value of 8.8 and different salinities: (a) retained permeability, (b) fines production, (c) pH of produced fluid and (d) D50 of produced fines for different flow rates

pH:  $\Delta$  8.8  $\diamond$  7.9  $\circ$  6.8

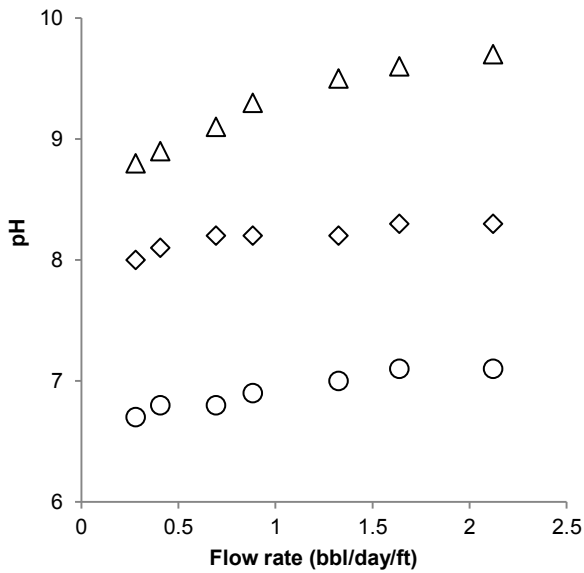
Salinity = 0%



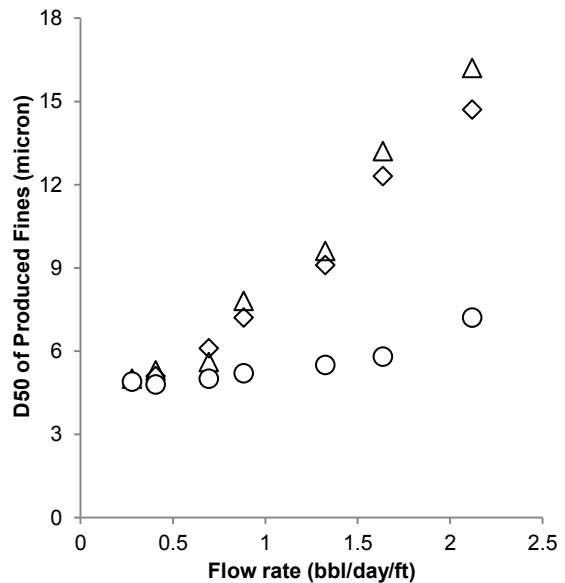
(a)



(b)



(c)

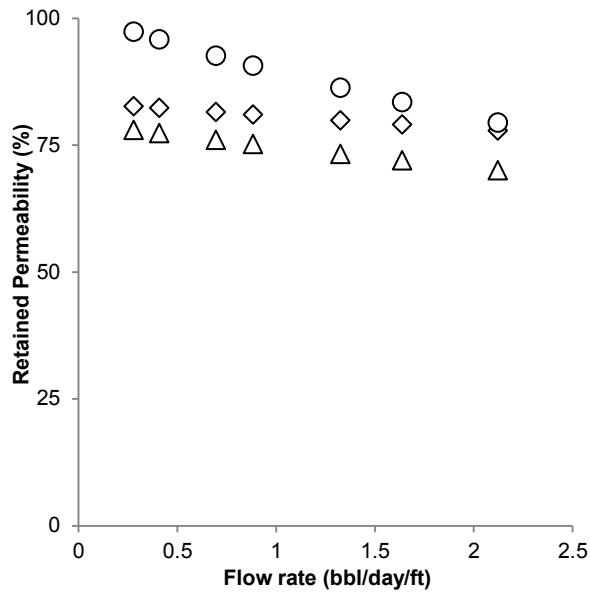


(d)

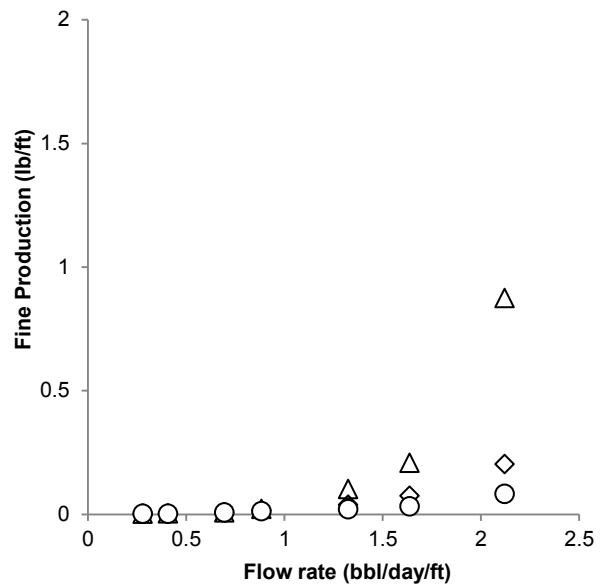
Figure 6-6. SRT results for the constant salinity of 0% and different pH values: (a) retained permeability, (b) fines production, (c) pH of produced fluid and (d) D50 of produced fines for different flow rates

pH:  $\Delta$  8.8  $\diamond$  7.9  $\circ$  6.8

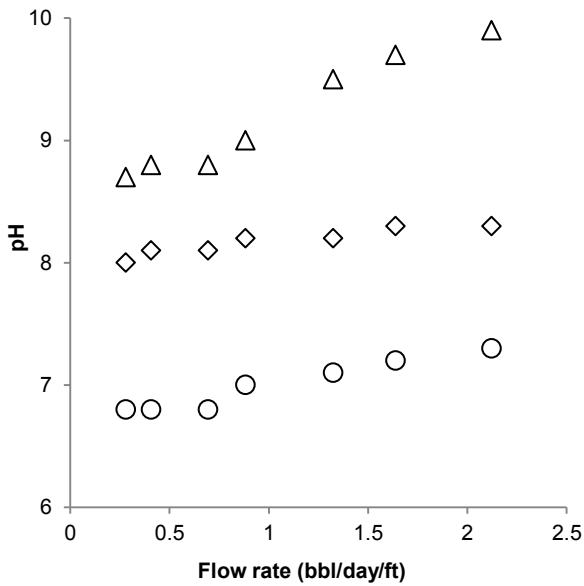
Salinity = 0.7%



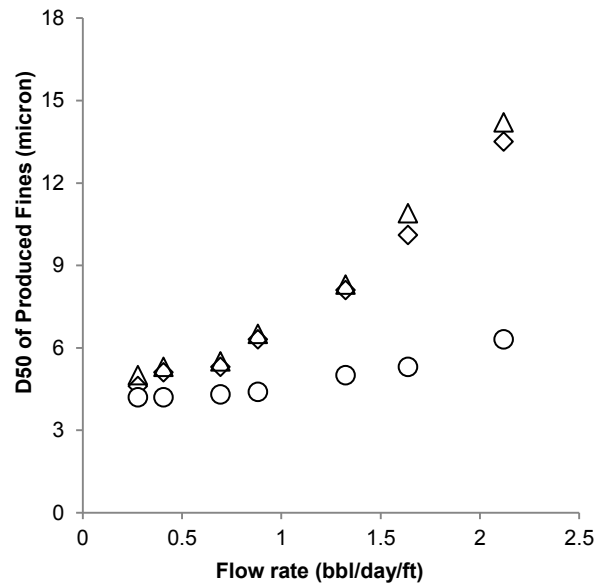
(a)



(b)



(c)



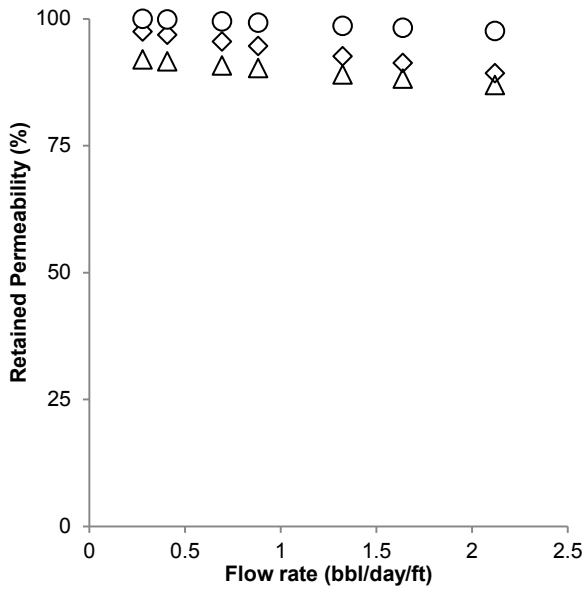
(d)

Figure 6-7. SRT results for the constant salinity of 0.7% and different pH values: (a) retained permeability, (b) fines production, (c) pH of produced fluid and (d) D50 of produced fines for different flow rates

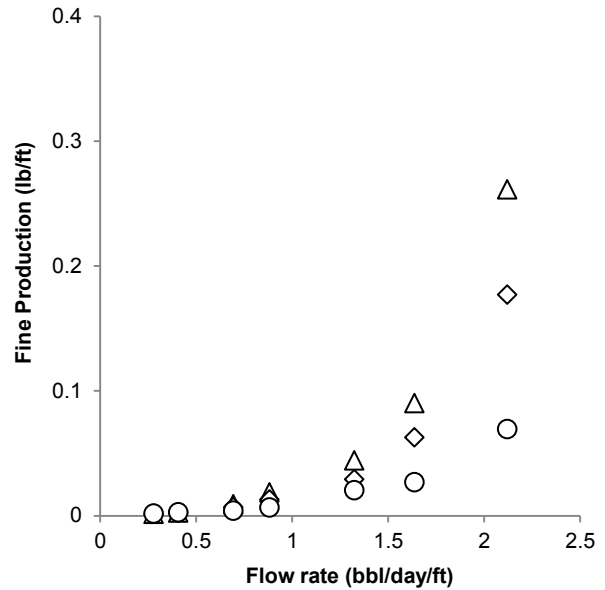


pH:  $\Delta$  8.8  $\diamond$  7.9  $\circ$  6.8

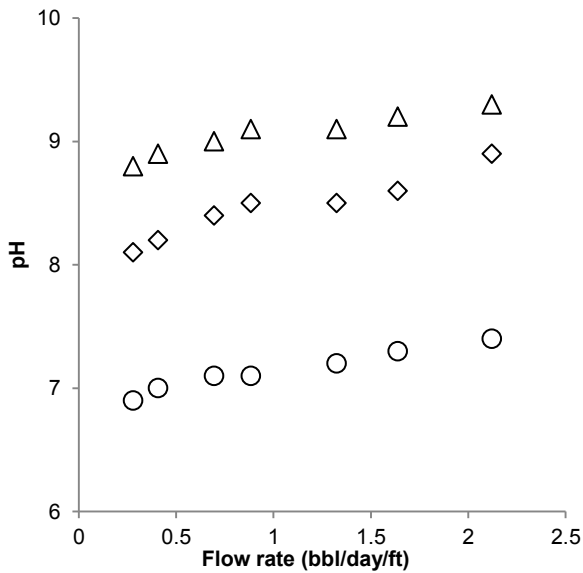
Salinity = 1.4%



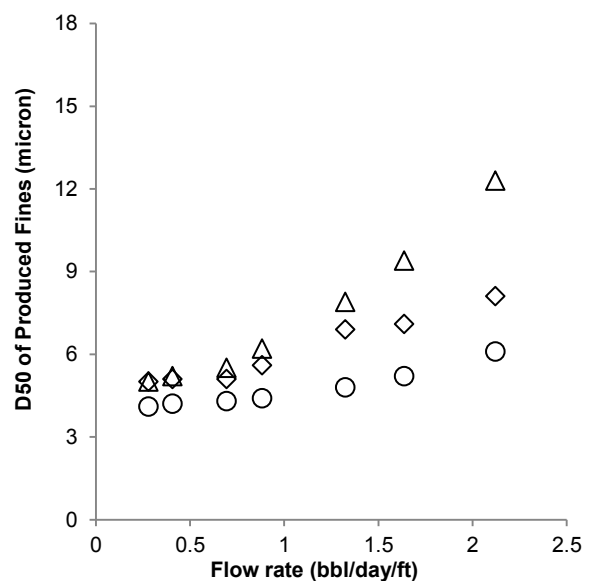
(a)



(b)



(c)



(d)

Figure 6-8. SRT results for the constant salinity of 1.4% and different pH values: (a) retained permeability, (b) fines production, (c) pH of produced fluid and (d) D50 of produced fines for different flow rates

## CHAPTER SEVEN: EFFECT OF SLOT WIDTH AND DENSITY ON FINES MIGRATION AND PRODUCTION IN SAGD OPERATIONS

### 7.1 Introduction

Slotted liners and Wire-wrapped Screens (WWSs) are widely used as a Sand Control Device (SCD) for SAGD operations. These devices are designed to (1) control the sand flow into the horizontal well, (2) discharge the mobilized fines ( $<44\ \mu\text{m}$ ), and (3) provide the required path for fluid flow (hot bitumen and water).

In many cases, although SCDs successfully halt the production of sand, they are not successful in preventing severe plugging and the ensuing increase in the pressure drop between the injector and producer wells (Williamson et al. 2016). This high pressure drop can be due to the plugging of the pore in the near screen area and/or screen plugging. The screen plugging can be compounded with liner corrosion, chemical scaling, fines migration, steam breakthrough, water breakthrough, asphaltene precipitation, silica scaling and clay scaling (Schulien et al. 1997; Bennion et al. 2008; Goodman et al. 2010; Romanova and Ma 2013; Fermaniuk et al. 2015). To understand how fines migration affects the screen performance, one needs to understand the fines mobilization, transport, and capture.

De Zwart (2007) identified two conditions for fines mobilization in porous media: (1) presence of the fines which is determined by the lithological conditions, and (2) certain chemical and hydrodynamic local conditions, which let the particles enter and remain in suspension. In addition to the presence of the existing fines due to the lithological condition, further fines could be generated via in-situ precipitation of supersaturated mineral phases (De Zwart 2007) and thermal mineral diagenesis (Williamson et al. 2016).

Certain chemical and physical conditions influence the mobilization and transport of the fines (Valdes 2002; De Zwart 2007). For large particles ( $>10\ \mu\text{m}$ ), hydraulic drag forces are the dominant particle removal mechanism. For smaller particles ( $<1\ \mu\text{m}$ ), electro-kinetic forces are the dominant forces (De Zwart 2007). Particles between 1 and 10  $\mu\text{m}$  are subjected to different forces controlling their mobilization and transport.

The transport of fines relates to the pore throat size distribution within the sand, fluid chemistry, distribution of the fines in the pore structure, and hydrodynamic conditions (De Zwart 2007).

The mobilized fines can be transported by the fluid flow through the pore space leading to the entrapment and clogging by hydrodynamic bridging, sedimentation, and interception (Valdes 2002).

The average pore diameter, pore throat size, ratio of the pore body to the pore-throat size and the ratio of pore throat size to mobilized fines size are of significant importance in fines transport and entrapment. There are several experimental/ analytical methods (Kovacs 1981; Pittman 1992, 2001; Uno et al. 1998; Nabawy et al. 2009; Blunt et al. 2013; Mukunoki et al. 2016) and heuristic rule of thumbs (Coberly 1937; Harris and Odom 1982) to predict the average pore/pore throat size based on PSD, permeability and porosity. Using these correlations, bridging theory and the impairment rule, one could get an estimate of the size of the particles which could plug the pores. Experimental work (Barkman and Davidson 1972; Abrams 1977; Van Oort et al. 1993) concluded that:

1. Particles equal or larger than one-third of the average pore throat size, bridge at the entrance of pore throat.
2. Particles smaller than one-third but larger than one-seventh of the average pore throat size deposit in the pore and cause the reduction in effective pore/pore throat size.
3. In slow flow rates, where the gravitational force is considerable for the small particle compared to the drag force, particles smaller than one-seventh but larger than one-fourteenth of the average pore size deposit in the pore and cause the reduction in effective pore/pore throat size.
4. Particles that are smaller than one-fourteenth of the pore throat size pass through the pores with minor or no impairments.

The fines concentration and distribution in the flow stream are controlled by the velocity (hydrodynamic forces/drag forces) and the direction of the flow (De Zwart 2007). Field observations by Prins (2003) also indicated the dependency of pore plugging in near wellbore region to fluid velocities. In the near wellbore region, due to the flow convergence, fluid velocity is high and the streamline is changed due to the convergence of flow toward the screen. The effect of this acceleration of the flow towards the screen and change in the flow path is more

significant in higher flow rate. Kaiser et al. (2000) concluded that the convergence and drag forces in the vicinity of slotted liners are related to the flow rate, size, and spacing of the slots.

Regarding the effect of the slot size and density on local fluid velocity close to the screen and fines migration, one would expect that the slot size and density selection could affect to the plugging tendency of the screen. Flow performance of the screen could be reduced due to the fines capture and precipitation in pore/pore throats or within the slots.

In this study, we use the pre-packed Sand Retention Test (SRT) facility to investigate the effect of slot width and slot density on the produced fines concentration and size. Also, we studied the changes in fines concentration above the screen via the post-mortem analysis.

## **7.2 Testing program**

Different multi-slot coupons with slot densities of 30, 42 and 54 slots per column (SPC) and slot widths ranging from 0.010” to 0.032” were used in the test matrix. Slot widths cover the lower and upper bound slot widths obtained by using existing design criteria for two representative PSDs in the McMurray Formation in Alberta.

The brine used in the testing was synthesized by dissolving NaCl, which is a monovalent salt, in distilled water. The use of NaCl seems to result in brine with the most adverse effect due to its ability to interact with kaolinite and illite, resulting in their mobilization. All tests were performed at a constant pH and salinity level (pH=7.9; Salinity= 0.7%).

Brine was injected at different rates up to more than 10 times the typical flow rates in SAGD operations (40 ml/hr/slot) into a sand pack with similar PSD and particle shapes to a typical oil sand from the McMurray Formation (medium-size sand DC-III, and fine sand DC-II).

High flow rates were tested to simulate extreme cases where local plugging of slots results in increased fluid velocities in the open slots. The total pore volume injected during each test was constant for each PSD.

**Table 5-2** shows the test matrix used in this study and the result are shown to address the effect of slot width, slot density and flow rate on the fines mobilization and entrapment above the screen for each PSD.

## **7.3 Results and discussions**

Pressure measurements indicate negligible pressure drops across the coupon (less than 0.01 psi) for the duration of testing. Post-test inspections indicate no plugging or scaling in the slots, which is consistent with the low pressure drops. Therefore, this section focuses on the changes in the concentration of fines (<44 $\mu$ m) close to the slotted liner coupons, and the concentration and size of the produced fines.

Results indicate that slot width and slot density influence the fines migration. **Figure 7-1** and **7-5** show the fines concentration above the screen for DC-III and DC-II, respectively. A lower porosity and permeability for DC-II compared to DC-III suggests a smaller average pore size for DC-II (see **Table 7-1**), hence, a higher potential to pore plugging by fines for DC-II compared to DC-III. For the same fluid flow rate, the pore-scale flow velocities (real velocities) in DC-II are higher than the same for DC-III. Higher real velocities facilitate the fines migration.

**Figure 7-1(a)** and **7-5(a)** show the fines concentration above the screen versus slot density for different slot widths. The figures indicate lower fines concentration above the screen for higher slot densities at a constant slot width. The figures also show drastically lower fines concentration above the screen for wider slots. The comparison of **Figure 7-1(a)** and **7-5(a)** indicates higher fines accumulation (plugging) near the coupon for the finer-grained DC-II compared to DC-III.

**Figure 7-1(b)** and **7-5(b)** show the near-screen fines concentration versus slot width for different slot densities for DC-II and DC-III, respectively. The figures indicate a decreasing trend in the near-screen fines concentration for higher slot widths. It is interesting to note that the fines content for wider slots approaches the original fines concentration in the sand pack. This suggests the benefit of using the widest slot size that can still keep the sanding within tolerance in reducing the plugging potential.

**Figure 7-2(a)** and **7-6(a)** show the cumulative fines production at the end of the tests versus slot density. Results show higher cumulative fines production for wider slots. Massive solid production (fines and sands) are expected if the slot width exceeds a certain threshold. Cumulative fines production decreases for higher slot densities, which can be attributed to the lower real flow velocity for the same flow rate.

**Figure 7-2(b)** and **7-6(b)** show the cumulative fines production at the end of the test versus slot width. The figures show higher cumulative fines production for larger slot widths at a constant

slot density. Further, the cumulative fines production shows a decreasing trend for higher slot densities at a constant slot width.

**Figure 7-3(a)-7-3(c)** and **7-7(a)-7-7(c)** show the fines production for the same fluid flow rate and the same slot density but different slot widths. For lower flow rates, results indicate only slightly higher fines production for higher flow rates. Increasing the flow rate beyond a certain level, however, results in a drastically higher fines production. The figures also indicate higher fines production for wider slots for a given slot density. Based on these results, one can expect plugging of slots may increase the flow rates in adjacent open slots, which, in turn, may lead to higher fines production and fines movements toward that open slots.

**Figure 7-3(d)** and **7-7(d)** show higher produced fines for lower slot densities. The reason is the lower OFA for the lower density, resulting in higher flow velocities at the constant flow rate, hence, stronger drag forces.

**Figure 7-4(a)-7-4(c)** and **7-8(a)-7-8(c)** show the median size of produced fines versus the fluid flow rate for different slot widths at a constant slot density. The figures indicate larger median size (D50) for the produced fines at higher flow rates. In particular, increasing the flow rates beyond a certain threshold results in a more drastic increase of the D50, especially, for larger slot widths.

**Figure 7-4(d)** and **7-8(d)** show the median size of the produced fines versus flow rate for different tested coupons. As expected, stronger drag forces near the screen increase the median size of the produced fines. Therefore, for a constant slot width, D50 shows a decrease for higher slot densities at a constant flow rate, because of the lower flow velocities and weaker drag forces. The effect of slot density appears to be stronger for larger slot widths.

Results in **Figure 7-4(a)** to **7-4(c)** and **7-8(a)** to **7-8(c)** indicate smaller-size produced fines and low fines concentrations for typical SAGD production rates ( $\approx 1.0$  bbl/day/ft). The figures also indicate the high sensitivity of the fines size and concentrations to the flow rate. This may explain field observations which indicate extreme plugging when using aggressive flow rates (Williamson et al., 2016). As some slots are plugged, the flow from open slots increases, resulting in higher fines concentration and coarser produced fines. The increase in the size of the mobilized fines facilitates the formation of a bridge at the pore channels, hence, increases the plugging potential (De Zwart 2007).

**Figures 7-9** shows the retained permeability for constant slot density for DC-II. **Figure 7-9(a)** through **7-9(c)** and **Figure 7-10(a)** through **7-10(c)** show the retained permeability change with slot width for the slot density of 30, 42 and 54 SPC and the PSD of DC-II and DC-III, respectively.

For DC-II at low slot density (**Figure 7-9(a)**), where flow convergence effect and pressure gradients are higher, more fines are mobilized than can be produced, leading to a drop in the retained permeability at higher flow rates. This drop is more pronounced for 0.010” slot size, where retained permeability falls below 50% for high flow rates (**Figure 7-9(a)**). However, for the coarser sand (DC-III) with lower fines content, the reduction in retained permeability is lower (**Figure 7-10(a)**) than finer sand with higher fines content (DC-II).

As the slot density increases, the drop in retained permeability for narrower slot sizes reduces. However, the retained permeability still falls below the 50% limit for the slot size of 0.010” and the slot density of 54 SPC for DC-II. Due to the larger pore sizes for DC-III, the pore plugging potential is lower in comparison to DC-II. However, a similar trend is observed at low slot densities for DC-III (**Figure 7-10**). For DC-III, the drop in retained permeability for larger flow rates is slightly less than the drop observed in DC-II. Similar to the DC-II, the drop in retained permeability is more pronounced for narrower slots. Yet, for none of the slot sizes the retained permeability dropped below 50%. Using wider slots helps achieve higher retained permeabilities for both PSDs.

**Figure 7-11** and **7-12** show the retained permeability for a constant slot width for DC-II and DC-III, respectively. A higher slot density at a constant slot width results in a slightly higher retained permeability for all flow rates. An increase in the slot width and slot density reduces the fines accumulation near the slotted liner due to the lower real velocities near the slots. A comparison between **Figure 7-11** and **7-12** indicates a higher impact for the slot width at a constant slot density on the retained permeability compared to the effect of slot density at a constant slot width.

#### **7.4 Conclusion**

This chapter presents the results of pre-packed SRT testing to study the role of slot width and slot density on fines production and accumulation above the screen.

The pressure drop across the slotted liner coupon was found to be negligible (less than 0.01 psi) for the range of flow rates that was used for the single-phase brine injection as no slot plugging was observed during the tests. Therefore, the study focused on the fines/clay migration, which affects the permeability of the filtrate near the liner coupon.

Results indicate a drastic increase of fines concentration above the screen for narrow slots, which can lead to pore plugging, hence, low wellbore productivity. In the contrary, the increase of fines concentration above the coupon after injecting brine with the total volume of over 20 times the pore volume is still negligible for wider slots.

It is evident that the fluid flow rate plays a critical role in mobilizing and transporting the fines. However, the role of slot width and density seems to also be crucial. The concentration and size of produced fines are highly affected by the slot size and density. The slot width highly affects the concentration and size of the produced fines. As the slot width increases, the size and concentration of the produced fines increases and the concentration of the fines above the slotted liner reduces. As the slot density increases, the concentration and size of the produced fines decrease. The increase in the slot density also reduces the concentration of the fines above the screen. This implies that for a given sand, increasing the slot width and slot density reduces the plugging tendency of the screen due to the fines migration.

Flow rate has also an adverse effect on retained permeability. Results also show that the slot density and size have a combined effect on retained permeability. Higher slot size and higher slot density result in the highest retained permeability for the same flow rate. Analyses also show that changes in slot width for the same slot density has a larger effect on retained permeability in comparison with changing the slot density for the sane slot width.



**Table 7-1. Average pore throat size calculated using different methods**

PSD	Porosity (%)	Permeability (md)	Average Pore size ( $\mu\text{m}$ )				Average pore size ( $\mu\text{m}$ )	$1/3$ rule	$1/7$ rule	$1/14$ rule	Critical Plugging range
			Harris and Odom (1982)	Uno et al. (1998)	Pittman (1992)	Nabawy et al. (2009)					
DC-II	30.8	3600	60.0	39.3	41.7	49.8	47.7	16.8	7.2	3.6	$\approx 3.6-16.8$
DC-III	39.6	4650	68.2	46.1	46.9	56.3	54.4	19.0	8.2	4.1	$\approx 4.1-19$

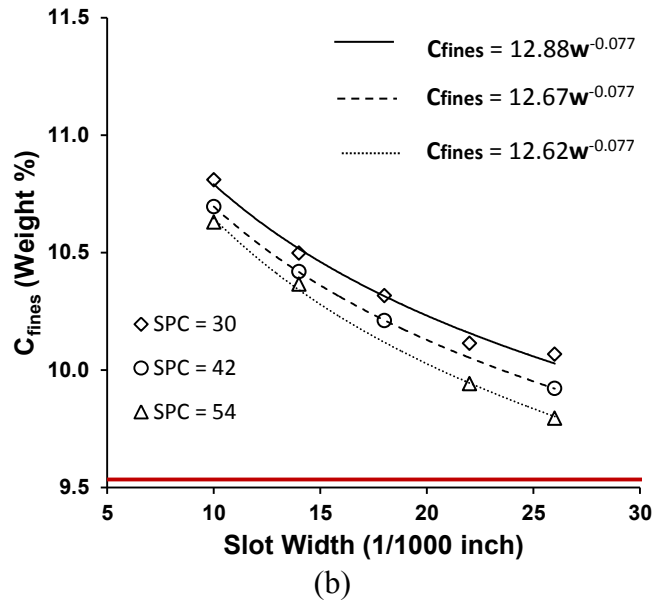
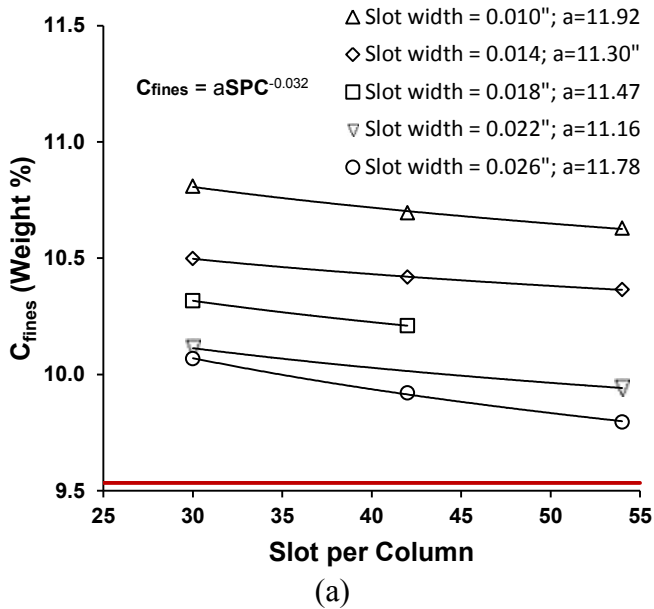


Figure 7-1. For DC-II (a) effect of slot density on the concentration of fines near the screen, (b) effect of slot width on the concentration of fines near the screen

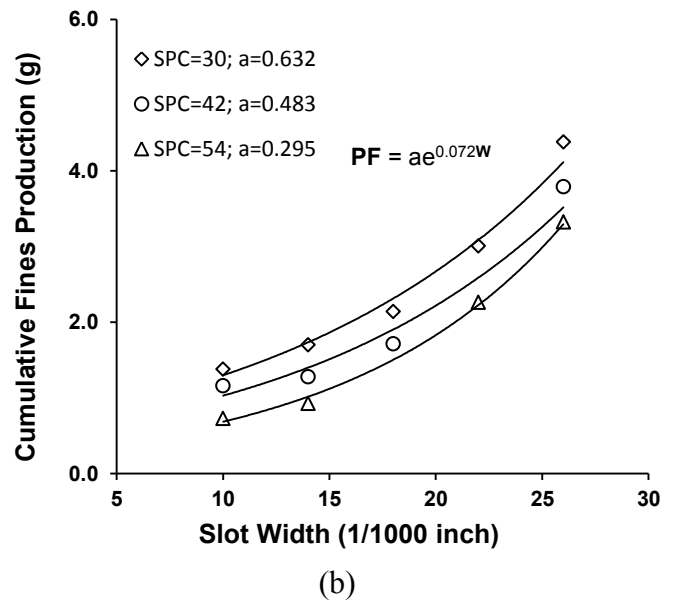
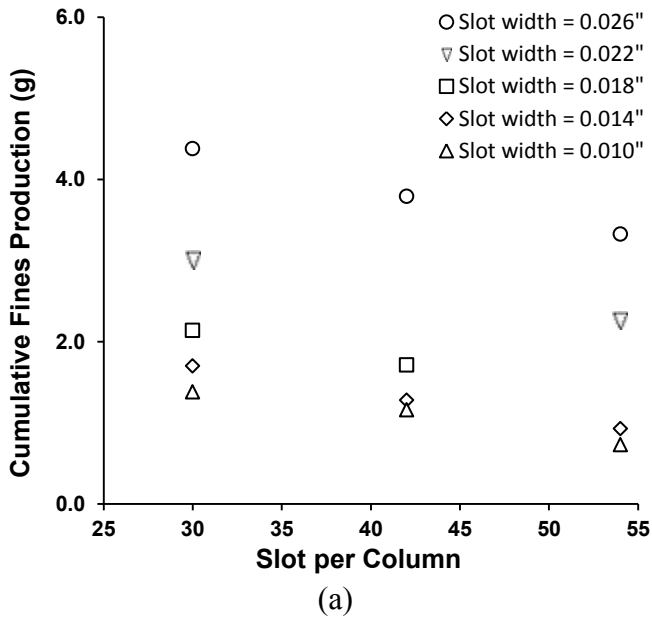


Figure 7-2. For DC-II: (a) effect of slot density on cumulative fines production, (b) effect of slot size on cumulative fines production

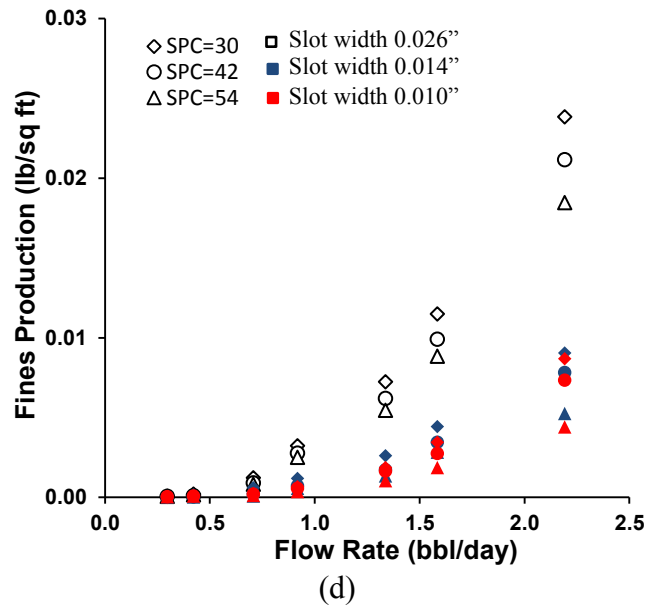
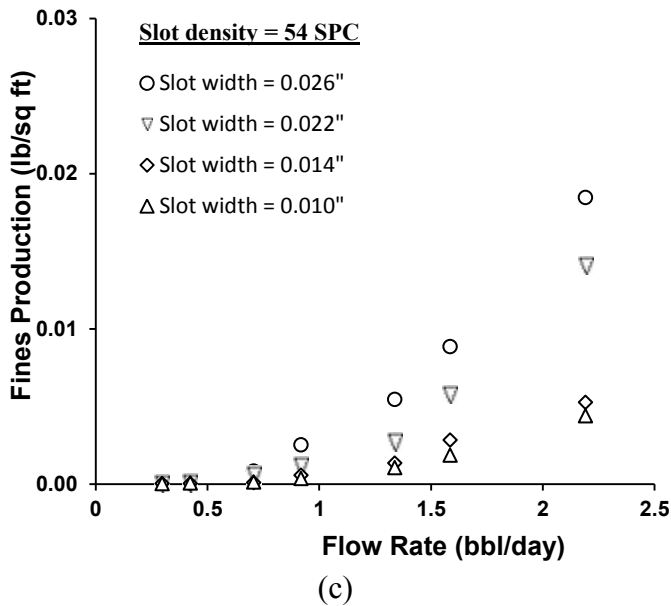
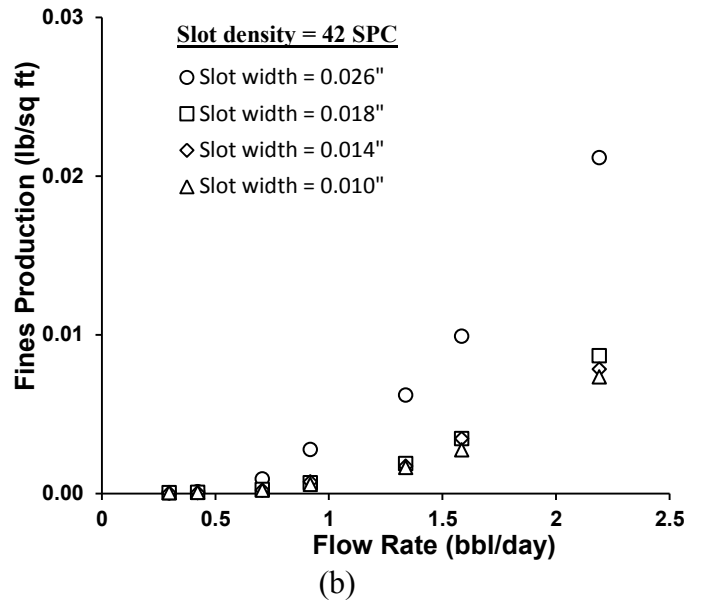
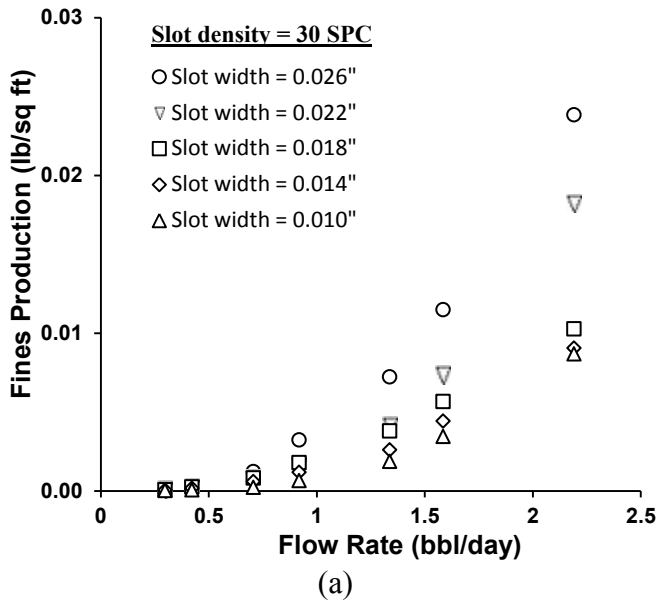


Figure 7-3. For DC-II: (a) effect of slot size on fines production for different flow rates at SPC=30, (b) effect of slot size on fines production for different flow rates at SPC=42, (c) effect of slot size on fines production for different flow rates at SPC=54, (d) fines production for different flow rates and different slot densities and widths

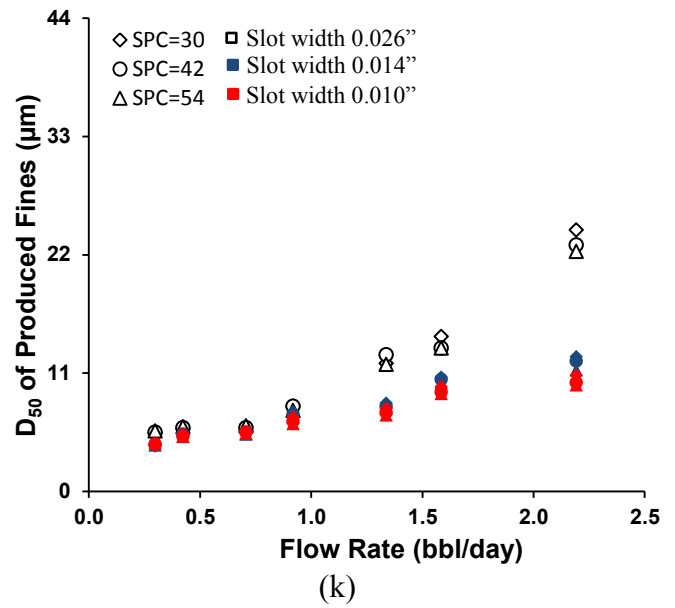
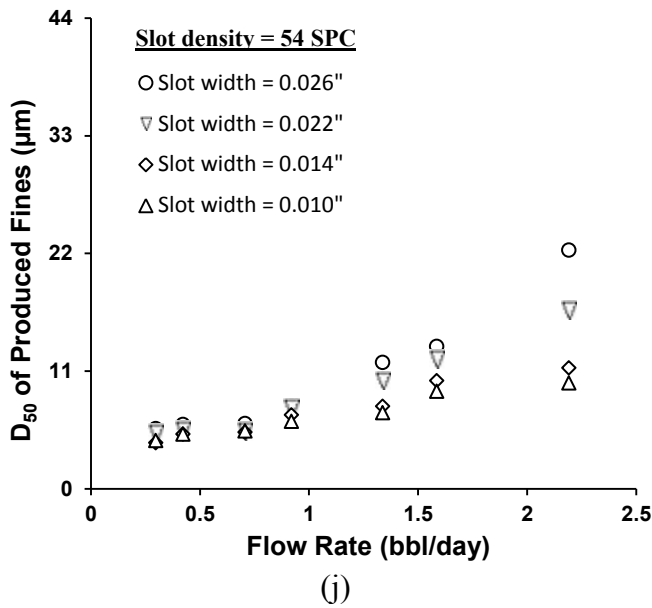
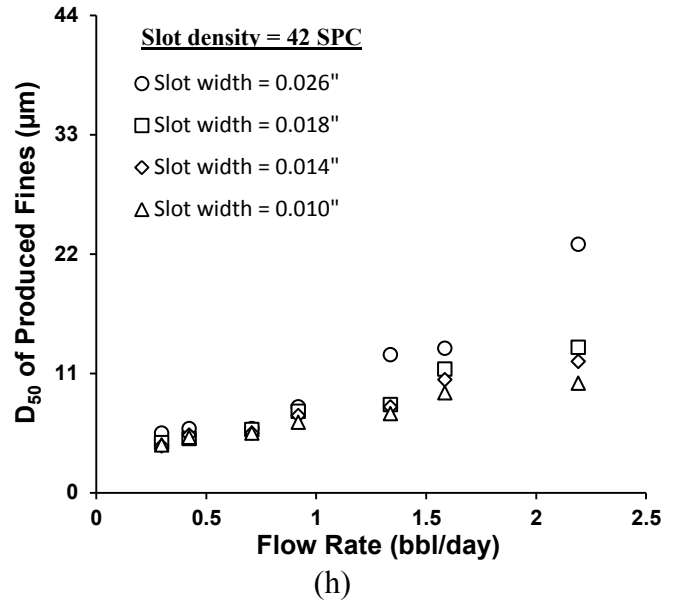
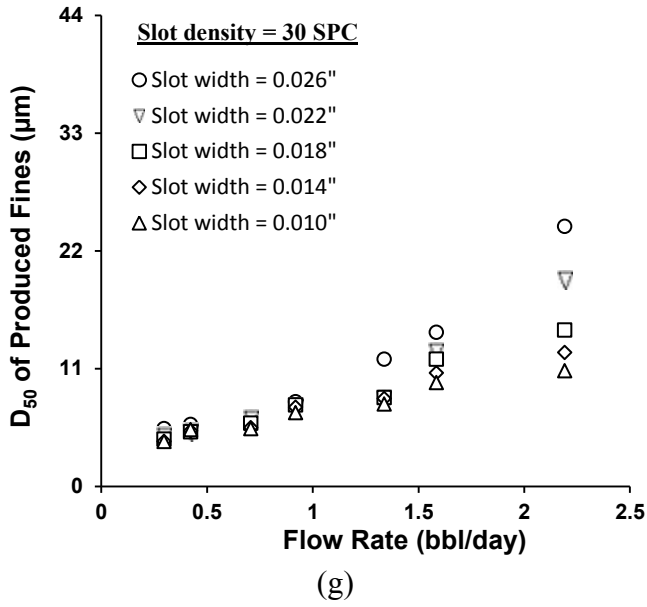


Figure 7-4. For DC-II: (a) D50 of produced fines for different flow rates at SPC=30 and different slot widths, (b) D50 of produced fines for different flow rates at SPC=42 and different slot width, (c) D50 of produced fines for different flow rates at SPC=54 and different slot width, (d) D50 of produced fines for different flow rates and different slot densities and widths

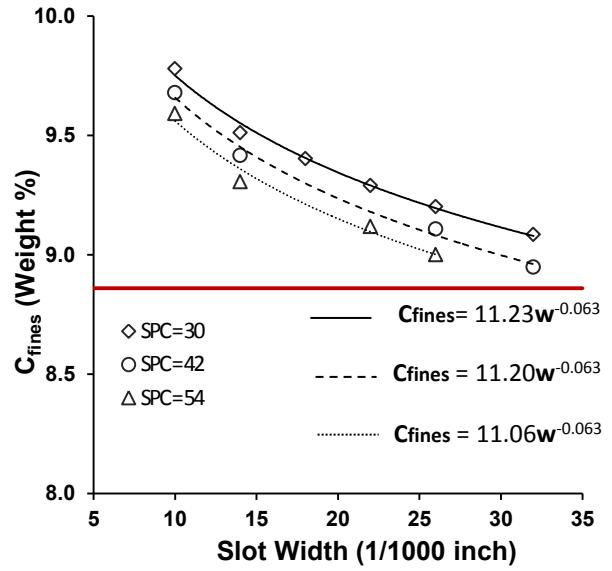
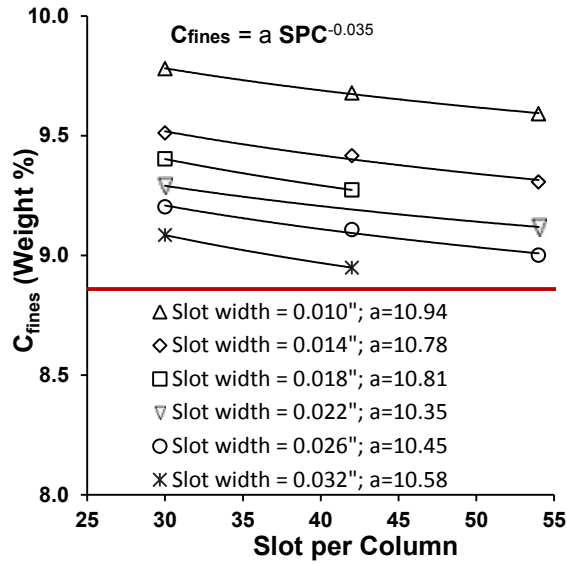


Figure 7-5. For DC-III: (a) effect of slot density on the concentration of fines near the screen, (b) effect of slot width on the concentration of fines near the screen

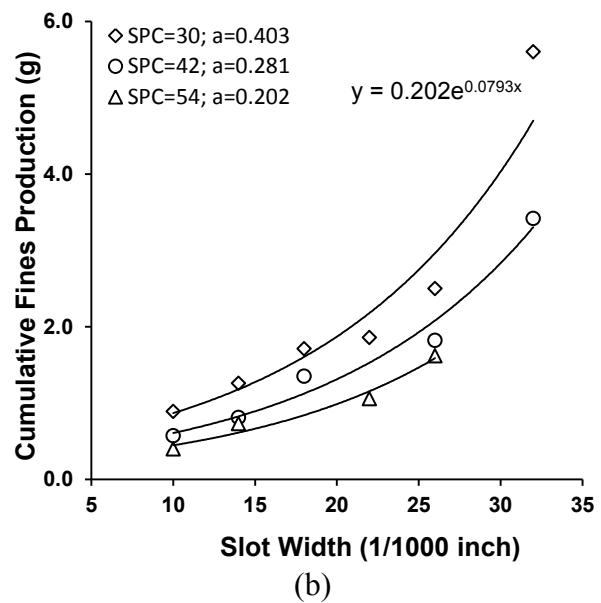
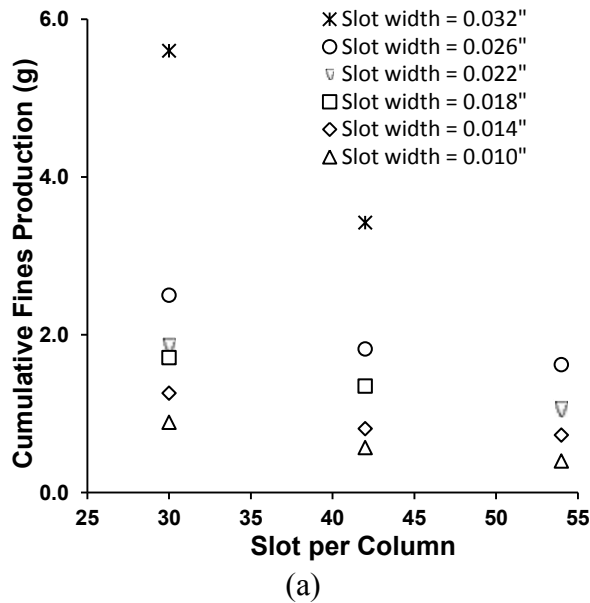


Figure 7-6. For DC-III: (a) effect of slot density on cumulative fines production, (b) effect of slot size on cumulative fines production

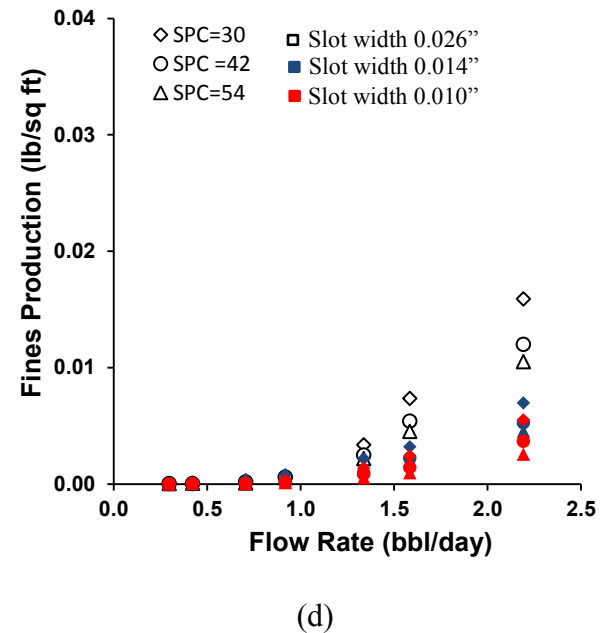
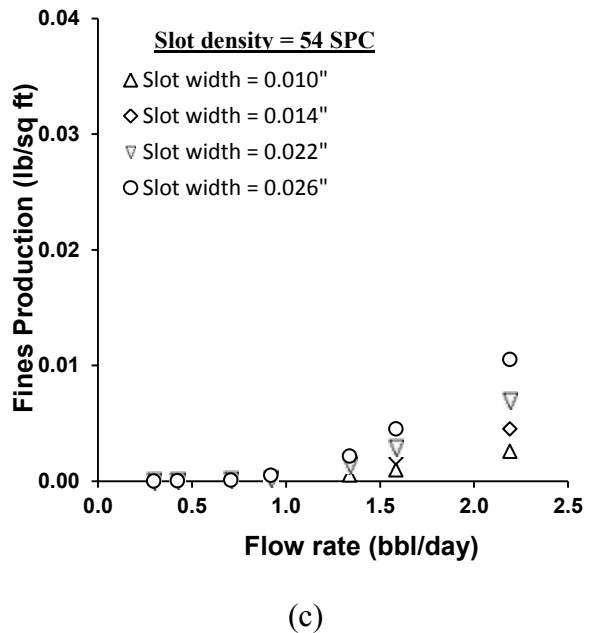
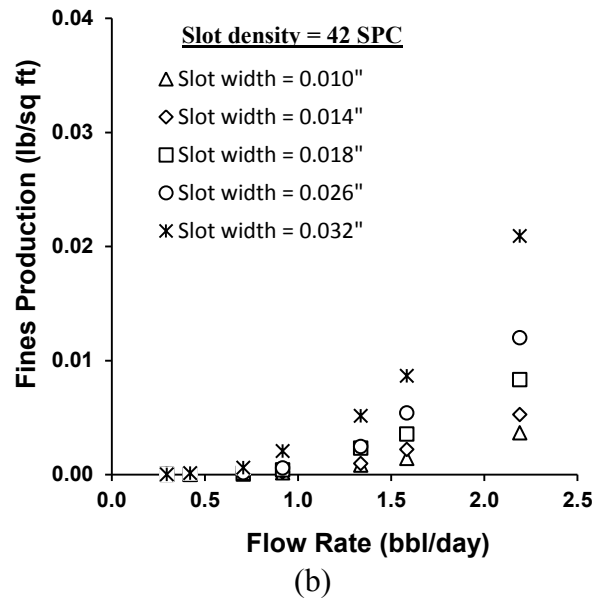
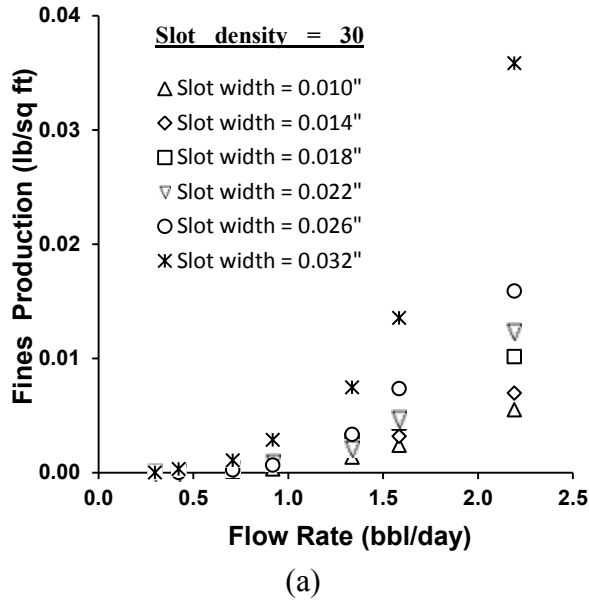


Figure 7-7. For DC-III: (a) effect of slot size on fines production for different flow rates at SPC=30, (b) effect of slot size on fines production for different flow rates at SPC=42, (c) effect of slot size on fines production for different flow rates at SPC=54, and (d) fines production for different flow rates and different slot densities and widths

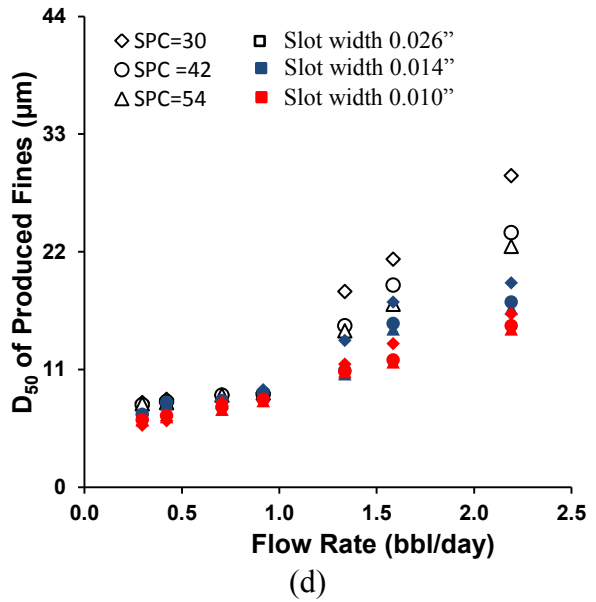
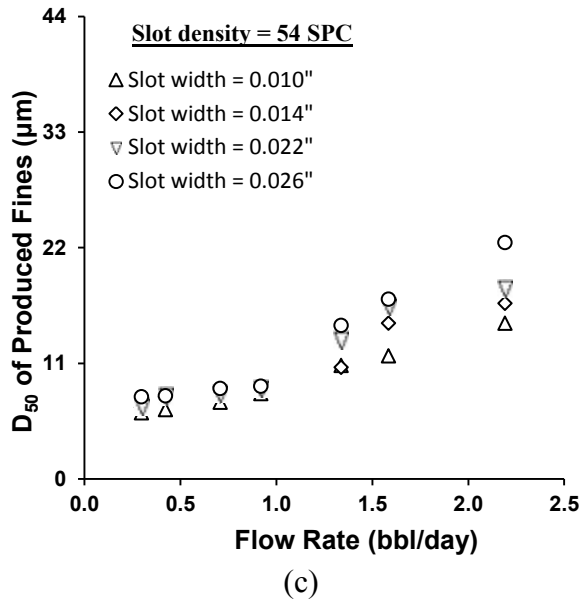
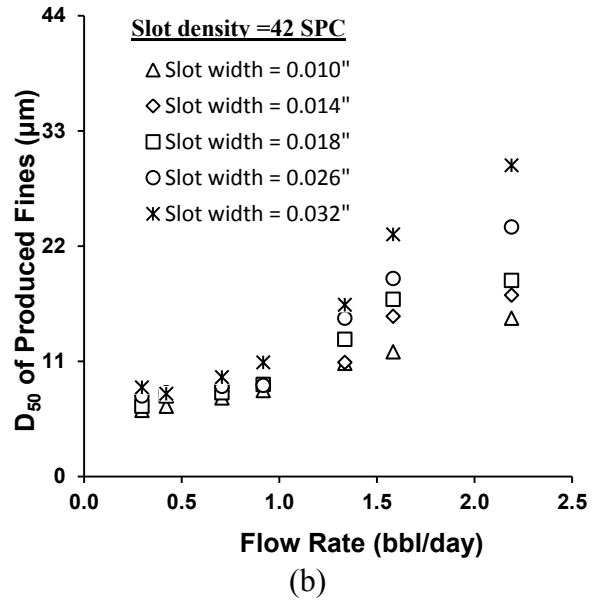
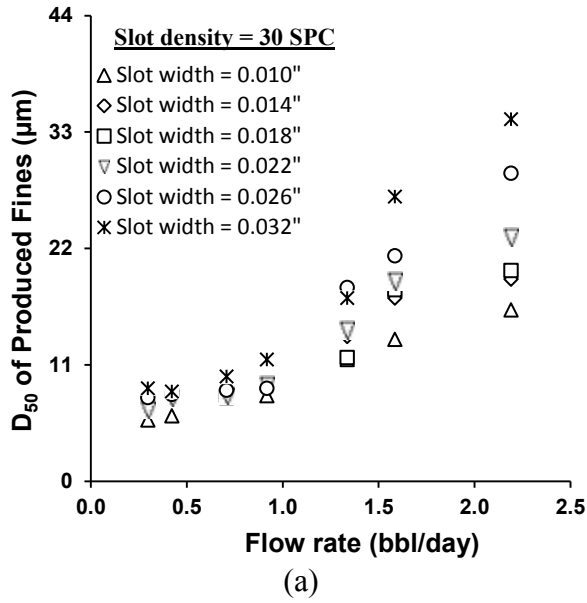
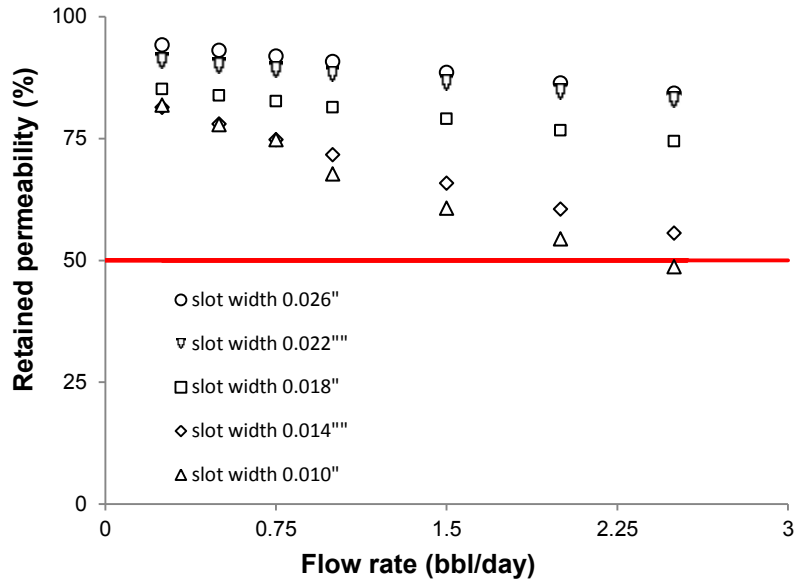
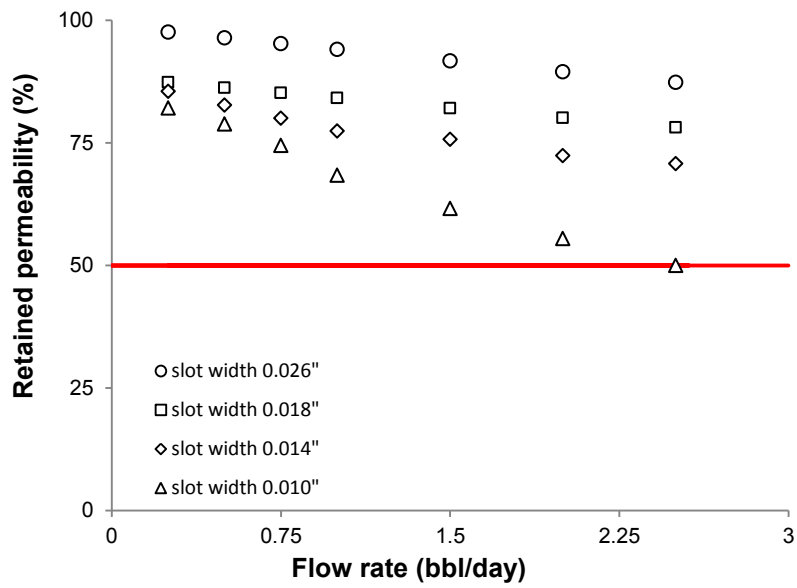


Figure 7-8. For DC-III: (a) D<sub>50</sub> of produced fines for different flow rates at SPC=30 for different slot widths, (b) D<sub>50</sub> of produced fines for different flow rates at SPC=42 for different slot widths, (c) D<sub>50</sub> of produced fines for different flow rates at SPC=54 for different slot widths, (d) D<sub>50</sub> of produced fines for different flow rates and different slot densities and widths

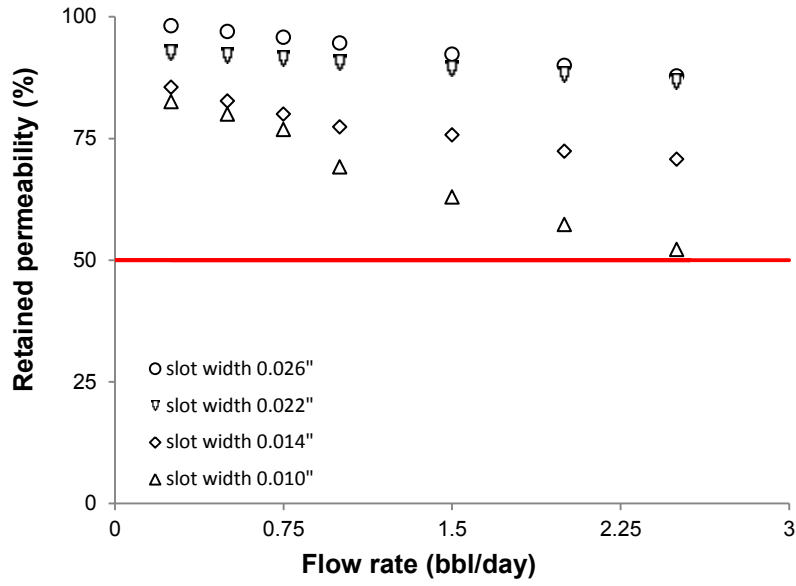


(a) Slot density: 30 SPC



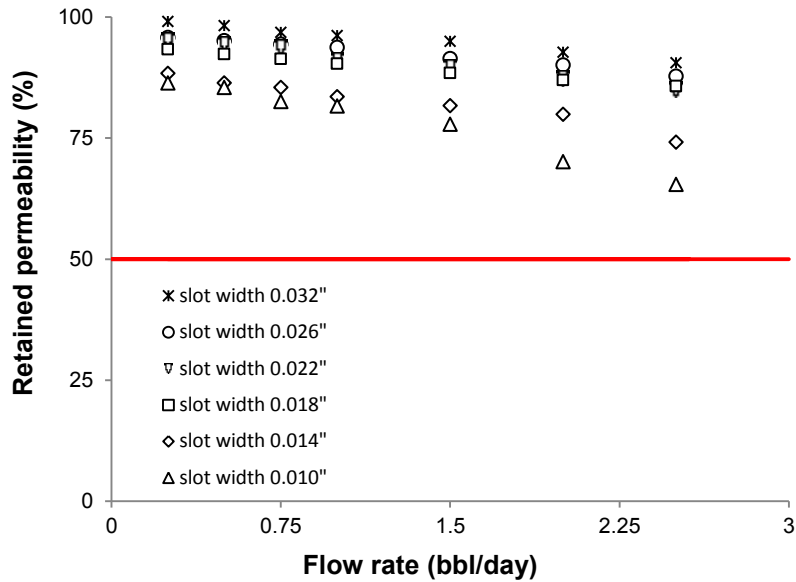
(c) Slot density: 42 SPC



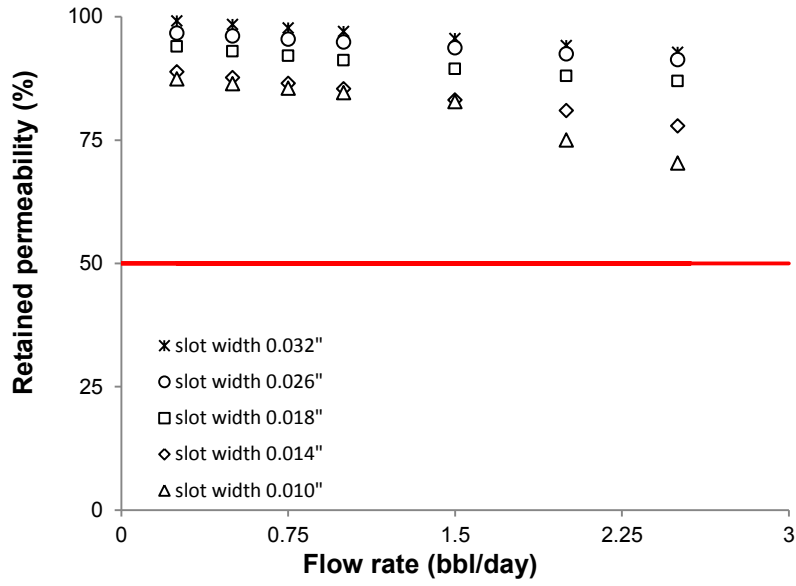


(e) Slot density: 54 SPC

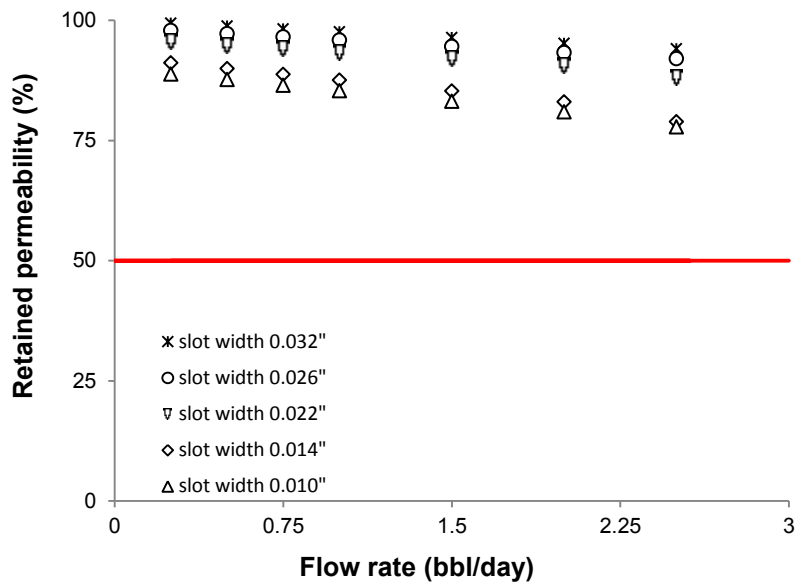
Figure 7-9. Retained permeability of sand packs versus flow rate for DC-II (a) for different slot widths and SPC=30, (c) for different slot widths and SPC=42, (e) for different slot widths and SPC=54; solid red line shows the suggested threshold for an acceptable retained permeability for SRT



(b) Slot density: 30 SPC

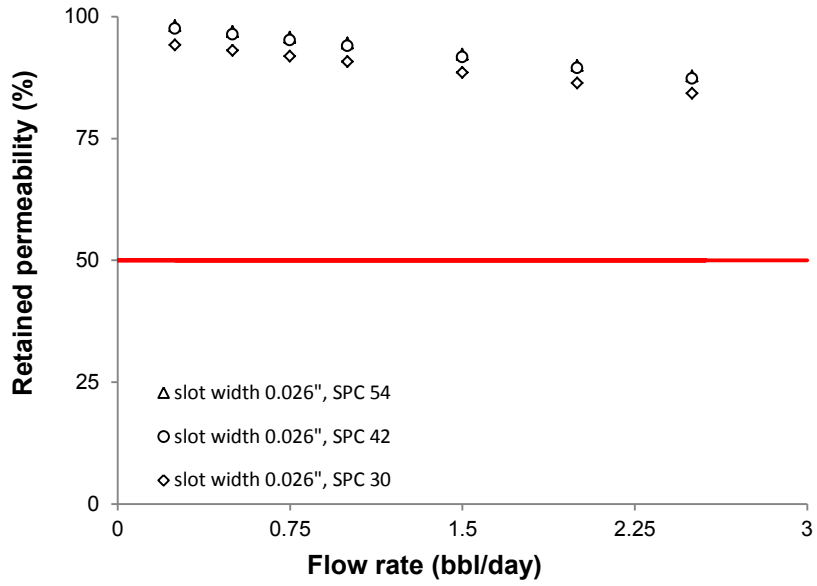


(b) Slot density: 42 SPC

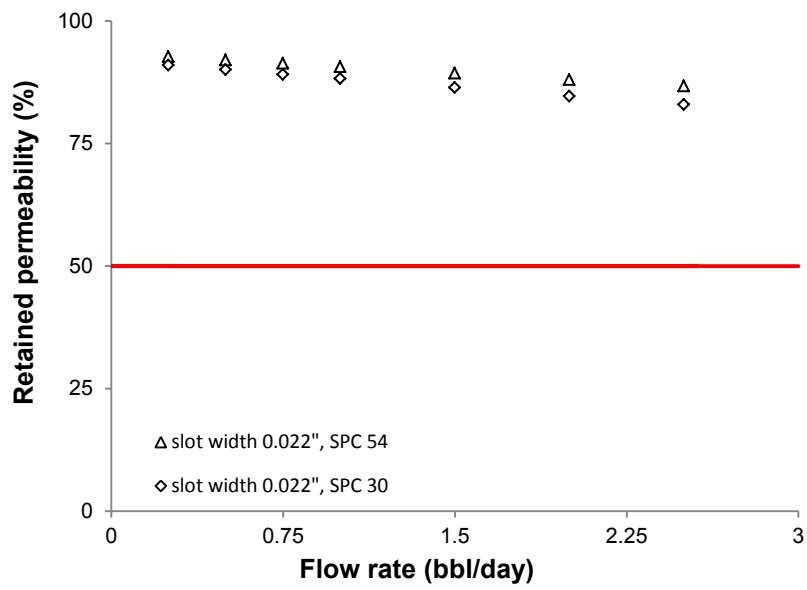


(c) Slot density: 54 SPC

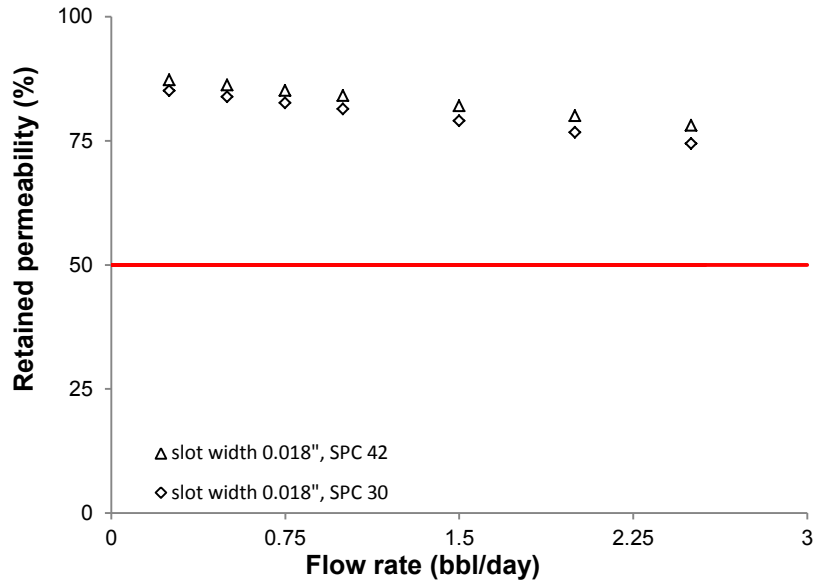
**Figure 7-10. Retained permeability of sand packs versus flow rate for DC-III (a) for different slot widths and SPC=30, (b) for different slot widths and SPC=42, (c) for different slot widths and SPE= 54; solid red line shows the suggested threshold for an acceptable retained permeability for SRT**



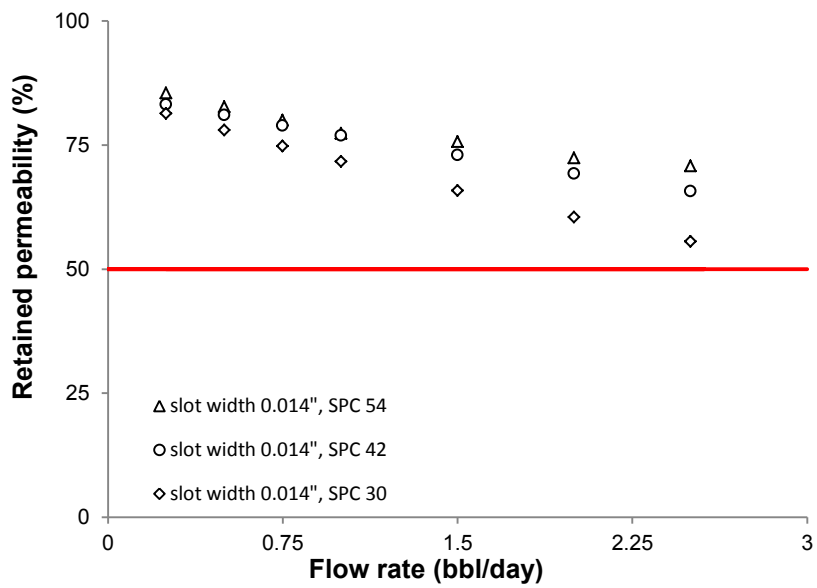
(a) Slot width: 0.026"



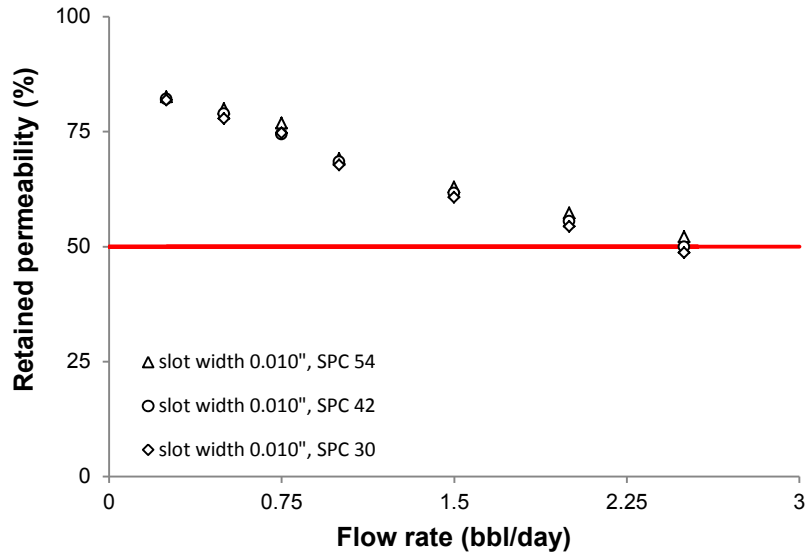
(b) Slot width: 0.022"



(c) Slot width: 0.018"

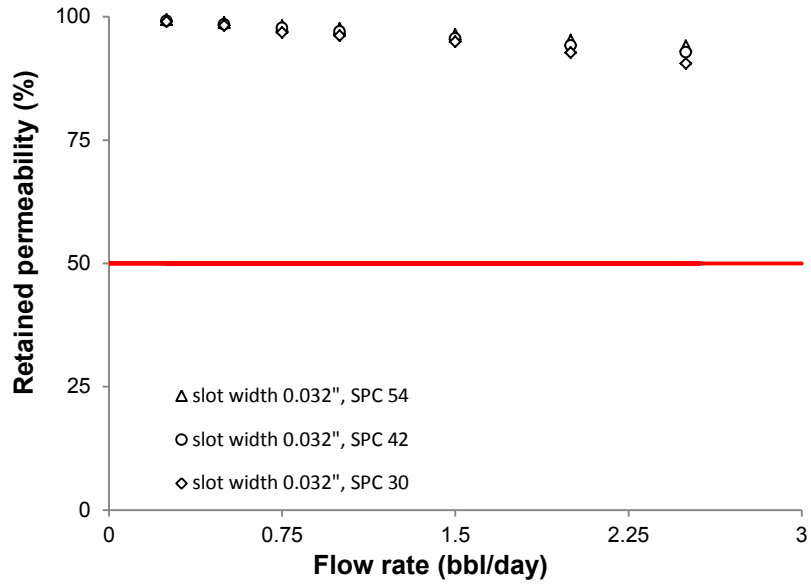


(d) DC-II – Slot width: 0.014"

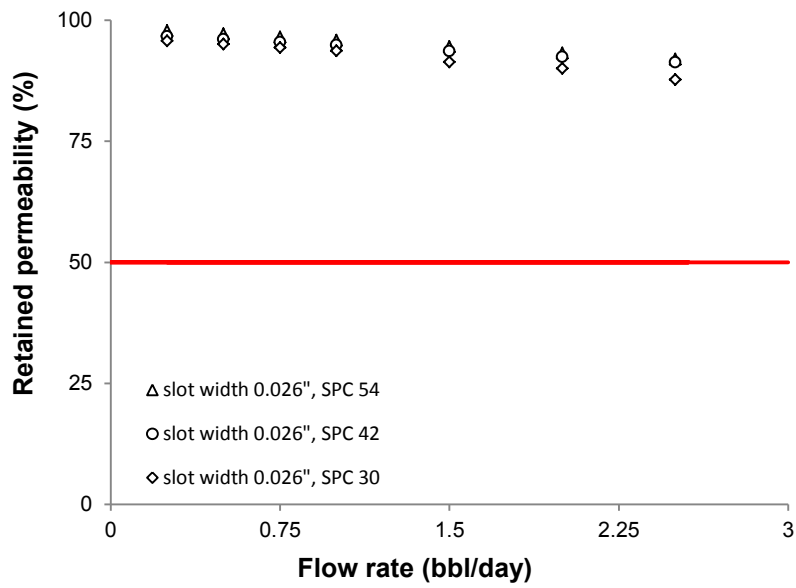


(e) DC-II – Slot width: 0.010"

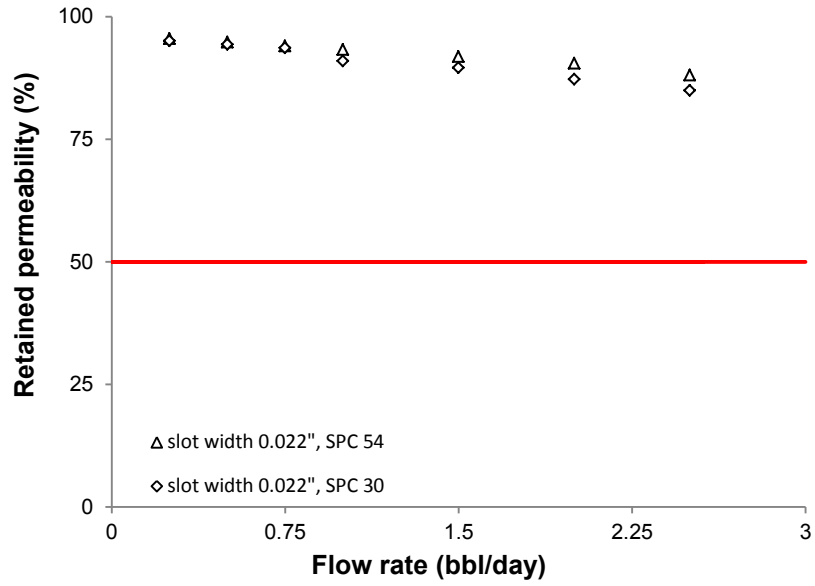
Figure 7-11. Retained permeability versus flow rate for DC-II (a) slot width of 0.026", (b) slot width of 0.022", (c) slot width of 0.018", (d) slot width of 0.014", (e) slot width of 0.010"; Solid red line shows the suggested threshold for an acceptable retained permeability for SRT



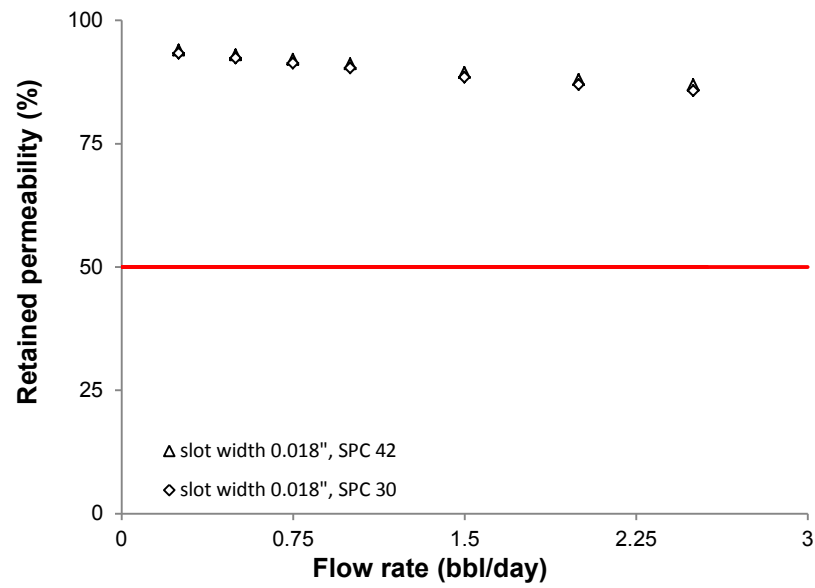
(a) Slot width: 0.032"



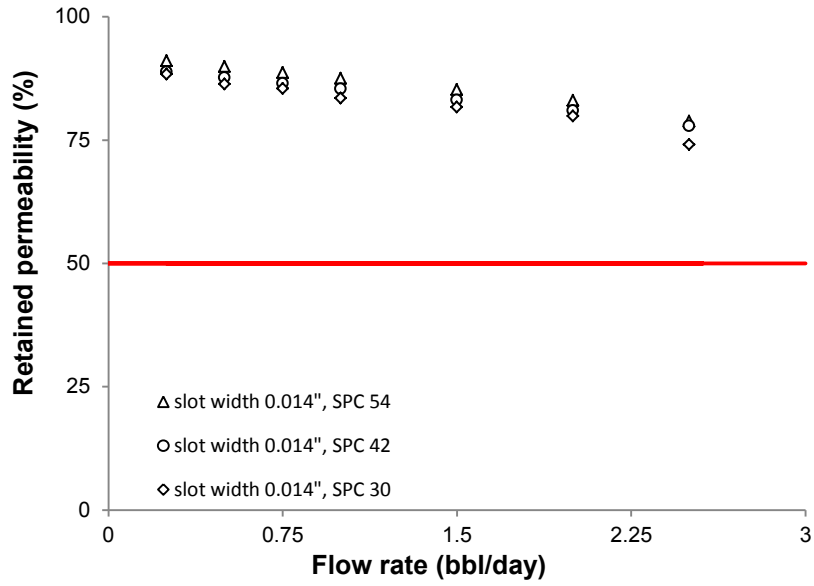
(b) Slot width: 0.026"



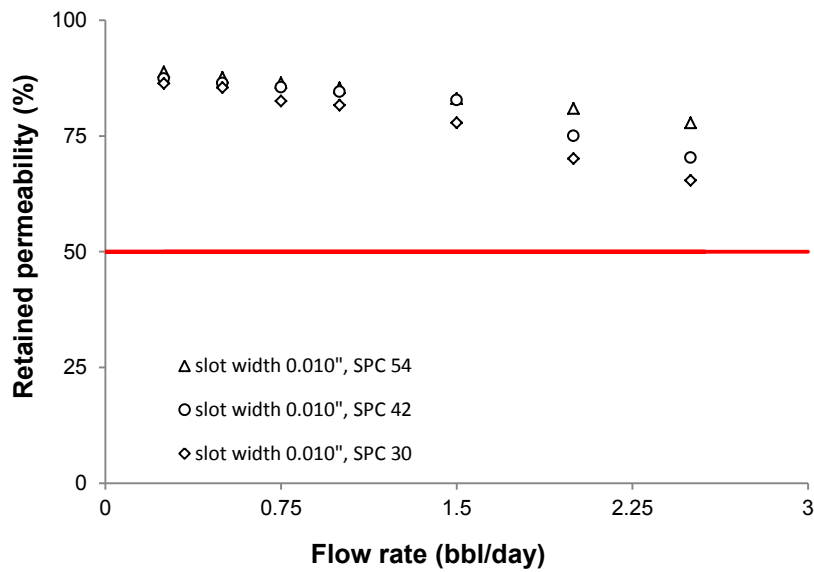
(c) Slot width: 0.022"



(d) Slot width: 0.018"



(e) Slot width: 0.014"



(f) Slot width: 0.010"

Figure 7-12. Retained permeability versus flow rate for DC-III (a) slot width of 0.032", (b) slot width of 0.026", (c) slot width of 0.022", (d) slot width of 0.018", (e) slot width of 0.014", (f) slot width of 0.010"; Solid red line shows the suggested threshold for an acceptable retained permeability for SRT



## CHAPTER EIGHT: EFFECT OF SLOT WIDTH AND DENSITY ON SAND PRODUCTION IN SAGD OPERATIONS

### 8.1 Introduction

Slotted liners have been used in oil and gas production and water wells since the early 1900's (Kobbe 1917; Alcorn and Teague 1937; Dean 1938; Chenault 1938). The main advantage of slotted liner over other standalone completions such as wire-wrapped screens and premium screens is the low cost (Petrowiki 2013). However, slotted liners have proven to be less effective in more challenging formations with higher fines content and more reactive clays such as smectite and illite (Romanova and Ma 2013).

Slotted liners work based on size exclusion and bridging to stop the sand inflow into the wellbore. Particle bridging is described as the physical mechanism for the case that many particles attempt to simultaneously flow through an opening (Vitthal and Sharma 1999); particle bridges form as the formation collapses around the slotted liner (Mahmoudi et al. 2016a). Stable bridge formation depends on the ratio between slot size and sand particle size and shape, porosity (Valdes 2002), and the flow velocity (Krueger et al. 1967; Muecke 1979).

Kaiser et al. (2000) suggested that sand control, inflow resistance, and cost are the main criteria for the design of sand screens for SAGD wells. Later, the design workflow evolved to also include plugging tendency, which can be evaluated through laboratory testing (Bennion et al. 2008; Romanova et al. 2014; Mahmoudi et al. 2016c). Screen opening is usually considered as the main sand control parameter (Coberly 1937; Markestad et al. 1996; Meza-Diaz et al. 2003; Ballard and Bear 2006; Bennion et al. 2008; Chanpura et al. 2011a, 2011b, 2012b), while Open to Flow Area (OFA) (dictated by both screen opening size and slot density) is used as a flow performance indicator (Tang et al. 2000; Kaiser et al. 2000; Furui et al. 2007). Screen aperture selection for sand control applications has been studied extensively through laboratory studies (e.g. Coberly 1937; Suman et al. 1985; Markestad et al. 1996; Ballard et al. 1999; Meza-Diaz et al. 2002, 2003; Ballard and Beare 2003, 2006, 2012; Bennion et al. 2008; Chanpura et al. 2011a, 2011b, 2012b) and numerical simulations (e.g. Mondal et al. 2011, 2012; Chanpura et al. 2012a).

Conventionally, the upper bound for slot aperture is designed to limit the potential for sand production and the lower bound is specified with respect to the plugging potential (Markestad et al. 1996). The slot aperture is designed to keep the amount of produced sand below an acceptable

level. The criteria for slot aperture design relate to one or more points on the Particle Size Distribution (PSD) curve. Different authors have proposed values in the range of 0.12-0.15 lb/ft<sup>2</sup> for cumulative transient sand production over the life of the well (Chanpura et al. 2011a). 50 g/bbl of continuous sanding is considered acceptable in thermal projects based on artificial lift requirements (Devere-Bennett 2015). Veeken et al. (1991) suggest a range of 0.95-95.38 g/bbl for conventional oil producers and 453.6 g/MMscf for gas producers in vertical wells. Screen designers for SAGD projects tend to opt for the lower bounds of design criteria to minimize sanding. This conservative approach can result in the selection of narrow slots with a significant plugging tendency (Romanova and Ma 2013) for both the pore structure behind the slots and the open space in the slots (Bennion et al. 2008).

The amount of produced sand is a function of slot aperture, slot profile, OFA, flow rate, formation PSD, and fluid-formation interactions. Despite the complexity of the phenomena, current screen design approaches are simply based on defining a safe sanding window for the different sand facies within the reservoir and the selection of an aperture size within the safe sand window (Markestad et al. 1996; Fermaniuk 2013). Slot density is typically recommended based on the expected flow rate from the well. This approach neglects the dependence of produced sand on both slot width and slot density. Further, great weight is given to the sanding potential, while downplaying the effect of slot width on the plugging tendency. Per Chapter 7, both slot size and density affect the plugging potential of the near-screen zone.

Some designers verify their design by performing evaluation tests based on the protocol proposed by Bennion et al. (2008). However, the proposed testing method neglects the interaction of the slot size and density on sanding and flow performance of the screen as it only uses single-slot coupons. In addition, the reported tests commonly use extremely high flow rates compared to typical SAGD flow rates, which leads to biased results that are in favor of screens with higher OFA, such as wire-wrapped and premium screens. To address this problem, a new Sand Retention Testing (SRT) facility was built in this research, which accommodates multi-slot coupons to capture the interaction of different slots as well as the influence of both slot aperture and density on the performance of the screen.

The main objective of this chapter is to understand the role of slot width and slot density on sand production from slotted liners. The model outlined by Fermaniuk (2013) is used as a guide and

example for the industrial approach. Details of the design criteria proposed by Fermaniuk (2013) are presented in Appendix A.

## 8.2 Testing program

Sand retention testing (SRT) as described in Chapter 5 was used in this investigation. Brine with pH of 7.9 and salinity of 7000 ppm was injected in step rates (**Figure 5-3**) to study the role of slot width and slot density on sand production. **Table 5-3** shows the test matrix. High flow rates were used to simulate extreme cases where local plugging of slots results in increased fluid velocity in the open slots. Each flow rate was kept constant for 30 minutes with a total of 22.7 pore volume fluid injection. In all tests, pressure drops stabilized in less than 10 minutes. The mass, PSD, and shape of produced sand is presented in this chapter to examine the factors that govern sand production in slotted liners.

## 8.3 Results and Discussion

**Figure 8-1** and **8-2** show the cumulative produced sand for different flow rates for DC-II and DC-III, respectively. The sand production in the tests could be categorized in three modes.

Mode-I is the initial sanding or sand occurrence at start-up. This is related to an initial sand occurrence which happens at the start of the test with minimum flow rate. Some sand particles fall in the slots or outlet during the compaction and some loose sands are washed away at low flow rates before stable bridges form. The quantity of this initial produced sand is dependent on both slot density and slot width (**Figure 8-1** and **8-2**).

Mode-I is dominant for the slot aperture sizes of 0.010”-0.014” for DC-II and (**Figure 8-1**), and 0.010”-0.018” for DC-III (**Figure 8-2**). In other words, after the initial sand production, no further sanding is observed, even for the highest flow rates tested during this investigation.

Mod-II is the flow rate dependent transient sand production which is observed for certain flow rates in some cases. In this mode, for any increase in flow rate, some sand is produced but the rate of sanding declines over time at constant flow rate and becomes nil until the flow rate is increased again. At constant step flow rate increases, the higher the flow rate, the higher the cumulative sanding for the duration of that step rate.

Episodes of transient sanding are usually observed after each incremental increase in the flow rate. Mode-II was observed in tests with slot sizes of equal and larger than 0.018” and 0.022” for

DC-II and DC-III, respectively. This mode can be explained by the dependency of the bridge stability on pressure gradient. As the flow rate increases the pressure gradient at the bridge face and seepage drag forces exceed the resisting frictional forces, the bridge is destabilized leading to the formation of larger stable bridge. The formation of these more stable bridges prevents further sanding at the constant flow rate.

Mode-III is the continuous sanding which happens with a combination of high flow rates and wide slot sizes. This mode is observed only for slot widths close to and greater than the upper bound of the slot width, proposed by the industrial design criteria, and high flow rates. This continuous sanding can be explained by high drag force due to the extreme flow rates, which doesn't allow stable bridges to be formed.

The three modes are identified by different colors in **Figure 8-1** and **8-2**. The existing 0.12-0.15 lb/ft<sup>2</sup> limit for SRT is also annotated in the graph. These figures show how changing the slot width, slot density, and flow rate result in different cumulative sand production and different sanding modes. Note, the data points in the figures for continuous sanding mode are subjected to the duration of the constant flow rate steps. The longer the constant flow rate steps, the larger the cumulative sanding due to the continuous mode of sanding.

This graphical presentation of the sanding amount and sanding mode could be used as a novel improvement to current slotted liner design approach which relies merely on experience to select a slot width for sand control in the widely subjective safe slot opening window (Chapter 10). This new approach includes the concept of the sanding mode and flow rate into sand control design.

**Figure 8-3** relates the elevated flow rates to the level of slot plugging for different slot densities. It can be seen that flow rates beyond 1.5 bbl/day are only relevant in the case of extreme slot plugging (beyond 90%). This could be also explained as 90% loss in OFA due to plugging.

Testing results indicate that slot width and slot density both influence the sand production. **Figure 8-4(a)** and **8-5(a)** indicate an exponential increase in cumulative sanding, at the end of the test, with the increase of the slot width for both PSDs. **Figure 8-4(b)** and **8-5(b)** illustrate the influence of slot density on the cumulative sanding amount at the end of the testing. Increasing the number of slots in each column, for same slot width, reduces the pressure gradient and flow velocity for each slot, which in turn reduces the sand production.

The highest produced sand belongs to the largest slot aperture and lowest slot density due to the pressure gradient dependency of sand production. Higher slot densities reduce the amount of flow rate per slot, hence, the flow velocity and pressure gradient behind each slot. **Figure 8-4(a)** and **8-5(a)** also compare the cumulative sanding at the end of the test for the slots designed based on the upper and lower bounds of the design criteria discussed in Appendix A. As discussed before, there is a possibility for continuous sanding usually for highest flow rates and slot width at the upper bound of the slot criteria and beyond that, continuous sanding occurs. This will cause the violation of the existing criteria for cumulative sanding for SRT.

**Figure 8-4(b)** and **8-5(b)** show the cumulative produced sand at the end of the test, for each slot width at different slot densities. For lower slot width, where the sand production is not flow rate (or pressure gradient) dependent (Mode-I), the produced sand for the same slot size are slightly increased by increasing the slot density, perhaps because with Mod-I sanding we mainly see loose sands or fines dropped or forced in the slots during the compaction and initial minimal flow rate through slots as produced sand.

Hence, the greater the number of slots, the more the washed-out particles are observed. For larger slot width, transient sanding is observed (Mode-II) and the produced sand is affected by the slot density. In Mode-II sanding, lower drag forces, hence, smaller amounts of sand production result for the same slot width (0.022" for DC-II and 0.026" for DC-III) but higher slot density. Mode III sanding is observed for wider slot aperture (0.026" for DC-II and 0.032" for DC-III) with continuous sanding. Therefore, as slot density increases, initially the produced sand decreases due to the dominance of the drag force reduction but as the number of the slots increases further, the produced sand starts to increase again.

As the number of slots increases, two competing factors affect the sanding. Increasing the slot density reduces the pressure gradient which helps reduce the amount of sand that is produced from each slot until stable bridges form. On the other hand, increasing the number of slots should increase the total produced sand as the produced sand is the summation of the sand produced from the total number of slots. For the largest slots (0.026" for DC-II in **Figure 8-4(b)** and 0.032" for DC-III in **Figure 8-4(b)**), eventually increasing the number of slots overweighs the benefit of lower pressure gradients.

To better understand the role of slot size and slot density on produced sand, we analyzed the PSD and shape of the produced sand. **Figure 8-6** through **8-9** show the PSD of the produced sand. **Figure 8-6** and **8-7** compare the size distribution of the produced sands for each slot width with the slot size (solid line) and one-third of the slot size (dash line). It is commonly believed that the Natural Bridge Tendency (NBT) decreases as one-third of the slot size reaches or exceeds the D50 of the produced sand (Fermaniuk 2013).

This 1/3 rule could be approximately considered as a threshold for Mode-III or continuous sanding for our tests. For both DC-II and DC-III, the cases where Mode-III sanding was observed (0.026” for DC-II and 0.032” for DC-III), one-third of slot size exceeds the D50 of the produced sand.

Another interesting result is the similarity of the PSD of produced sand regardless of the slot density (**Figure 8-6** and **8-7**). However, produced sands from narrower slots are slightly finer in comparison to wider slots (**Figure 8-8** and **8-9**). For all tests, the produced sand is slightly finer in comparison to the PSD of the sand pack (**Figure 8-8** and **8-9**).

**Figure 8-10** through **8-15** show the shape characteristics of the produced sands. Details about the measurement technique and definition of the shape factors could be found in Chapter 3. **Figure 8-10** and **8-11** show the distribution of sphericity for the produced sand for different slot widths at a constant slot density. For all tests, the sphericity of the produced sand is slightly higher than the sphericity of the sand-pack. This is more pronounced for smaller slot sizes and DC-III in comparison to DC-II.

**Figure 8-12** and **8-13** show the distribution of the convexity for the produced sand for different slot widths at a constant slot density. Similar to sphericity, the convexity of the produced sand is slightly higher than the convexity of the sand pack. This is more pronounced for smaller slot sizes.

**Figure 8-14** and **8-15** show the distribution of the aspect ratio for the produced sand for different slot widths at a constant slot density. The aspect ratio of the produced sand is slightly higher than the aspect ratio of the sand pack. However, the difference between the aspect ratios of the produced sand and sand pack is not as significant as the same difference for convexity and sphericity.

A comparison between the convexity, sphericity, and aspect ratio of the produced sands and the sand pack shows that particles with higher sphericity, and convexity are more prone to production. In addition, results indicate that the aspect ratio is not as important as the other two shape factors. These observations are in agreement with similar observations from Valdes (2002), which found the bridge of spherical particles to be less stable than the bridge formed by particle with lower sphericity.

### **8.3 Conclusion**

This chapter presents the results of pre-packed SRTs to investigate the role of slot width and slot density on the produced sand. The SRTs aim at validating the current industrial slotted liner design in terms of sand control.

Different multi-slot coupons with slot densities of 30, 42 and 54 SPC and slot widths ranging from 0.010” to 0.032” were used in the test matrix. Slot densities are calculated based on a 7” liner. Tested slot widths cover the lower and upper bound for slot widths obtained by using the existing design criteria for two representative PSDs in the McMurray Formation in Alberta.

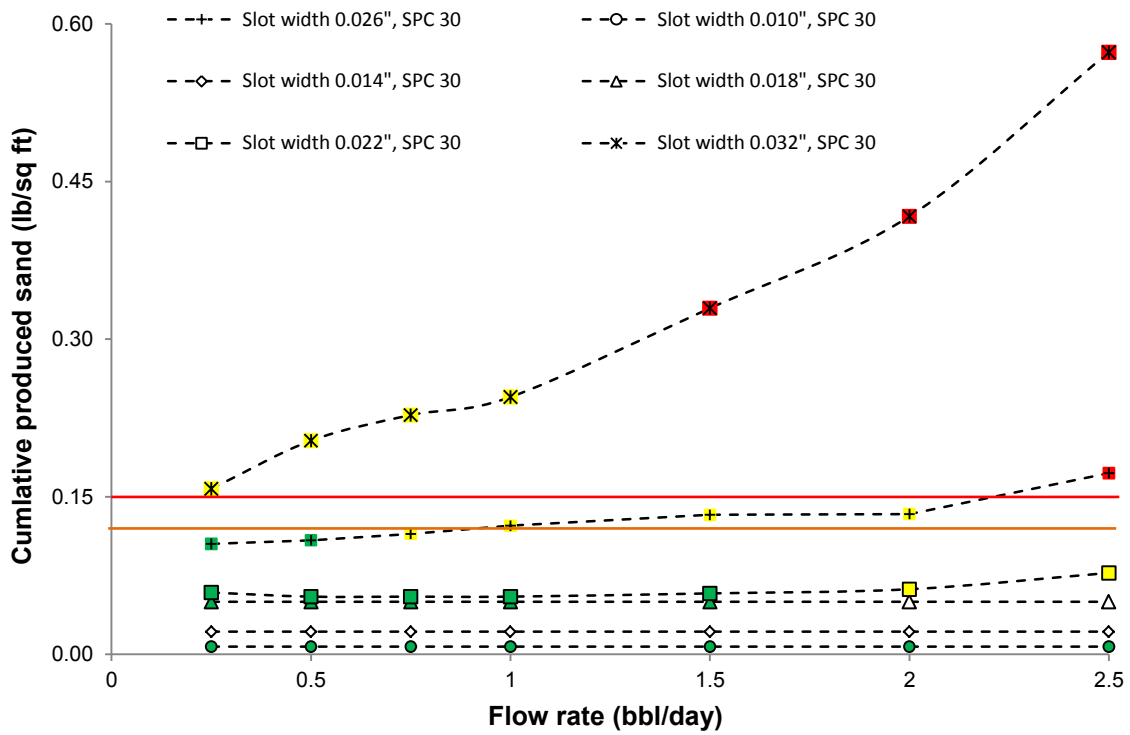
Brine was injected at different rates up to 10 times the typical flow rates in SAGD (40 ml/hr/slot) into a sand pack with similar PSD and particle shapes to a typical oil sand from the McMurray Formation (medium size sand in DC-III, and fine sand in DC-II). High flow rates are injected to simulate extreme cases, where local plugging of slots results in increased fluid velocities in the open slots. Injected brine is prepared with 7.9 pH and 0.7% salinity. The use of monovalent salt (NaCl) seems to be the worst case for mobilization of kaolinite and illite.

Pressure drop across the multi-slot coupon is found to be negligible (less than 0.01 psi) for the range of the injected flow rates and single-phase brine injection as no slot plugging was observed during the tests.

It is evident that the fluid flow rate plays a critical role in forming and destructing the sand bridge. Further, the produced sands from different coupons with different slot widths and density have a similar PSD and are finer than the original sand pack. Further, produced particles are more spherical than the sand pack. This means rounder particles are more prone to production.

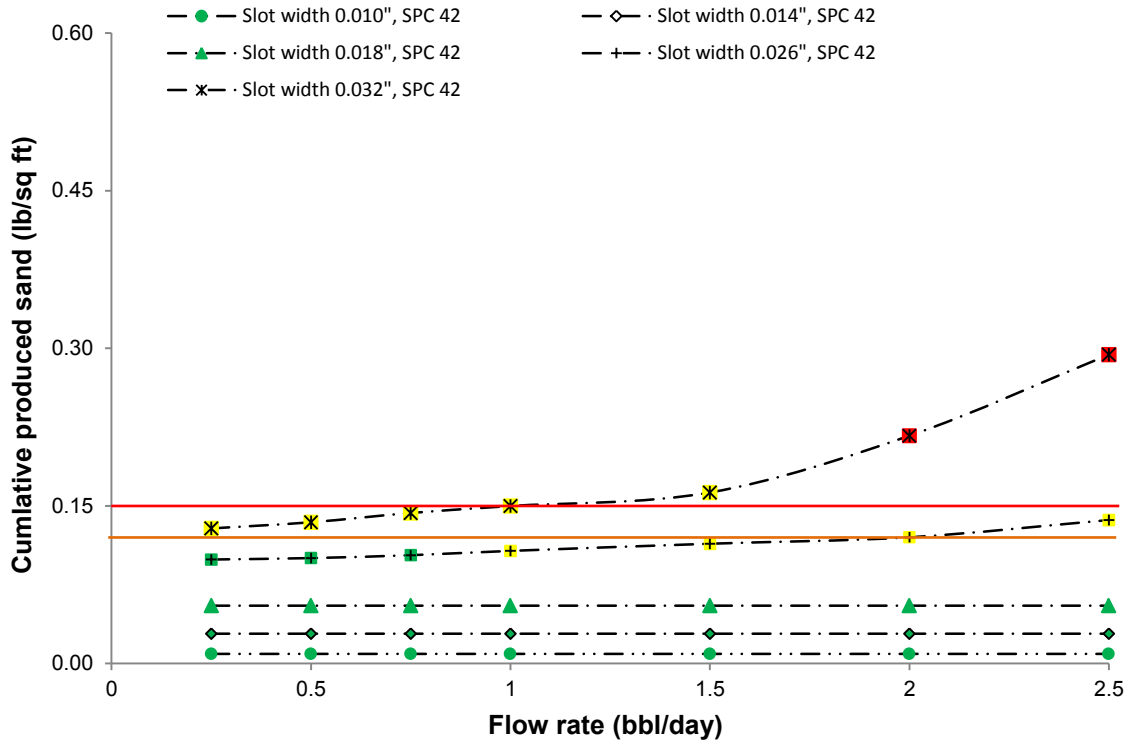
The most significant finding of this chapter is the observed modes of sand production. This chapter classifies sand production into three modes. In Mode-I (initial sanding), there is an initial

sand occurrence, but the sanding ceases and does not reoccur regardless of the level of flow rates. In Mode-II (flow rate-dependent transient sanding), there is an initial spurt sanding after the increase of flow rate beyond a certain flow rate and sanding rate reduces gradually to zero at the constant rate. Mode-III relates to continuous sanding as the flow rate exceeds a certain threshold.

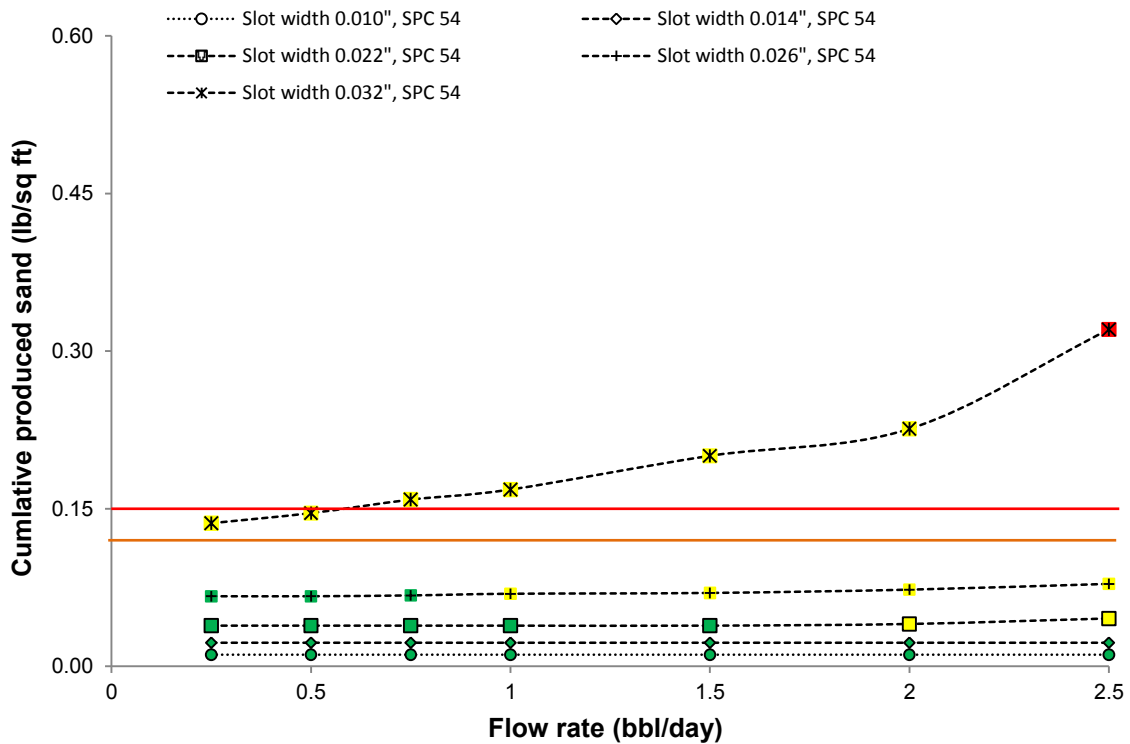


(a)



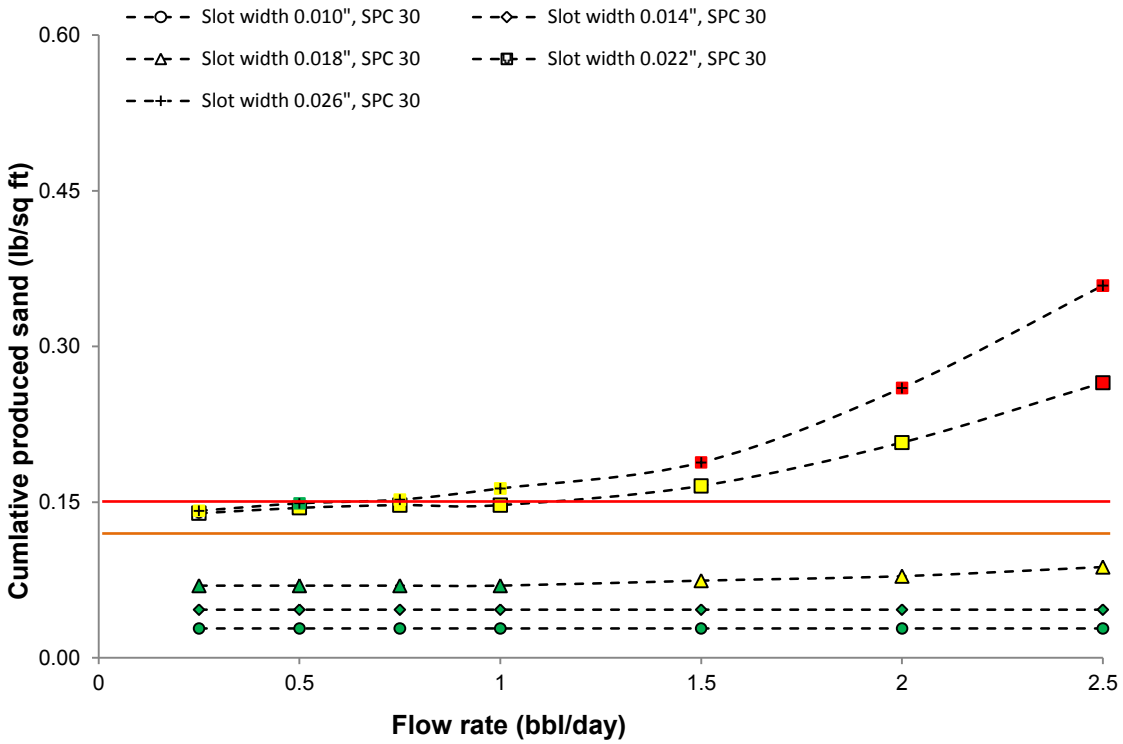


(b)

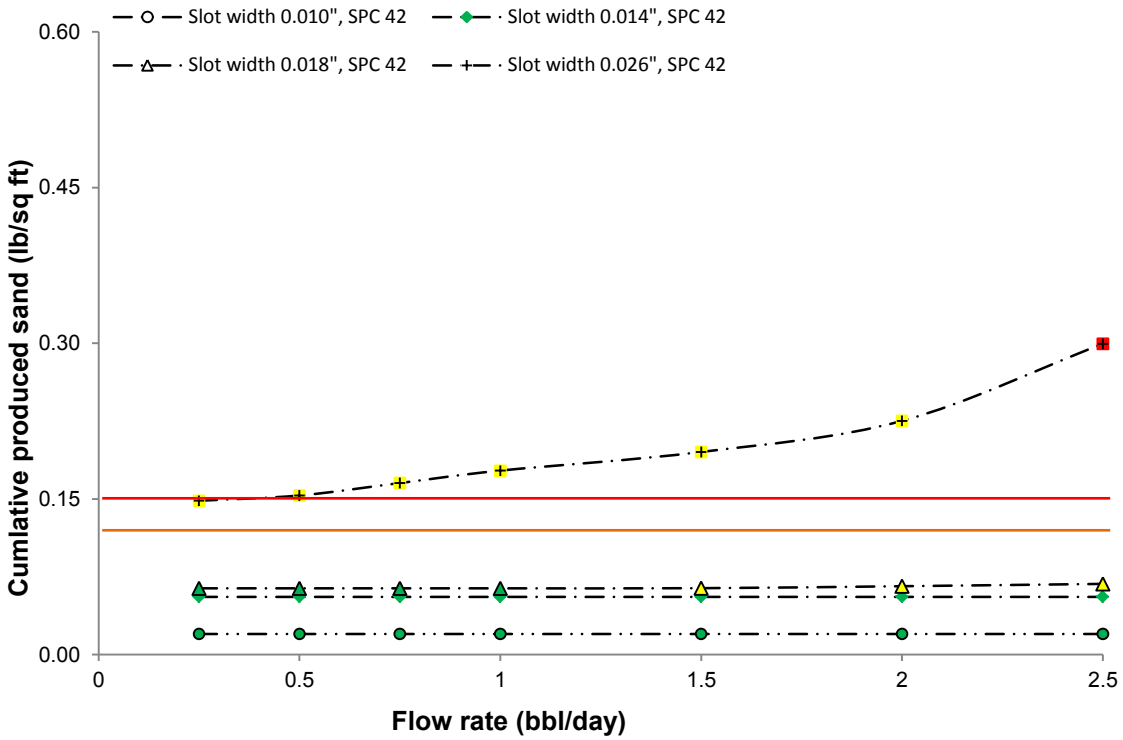


(c)

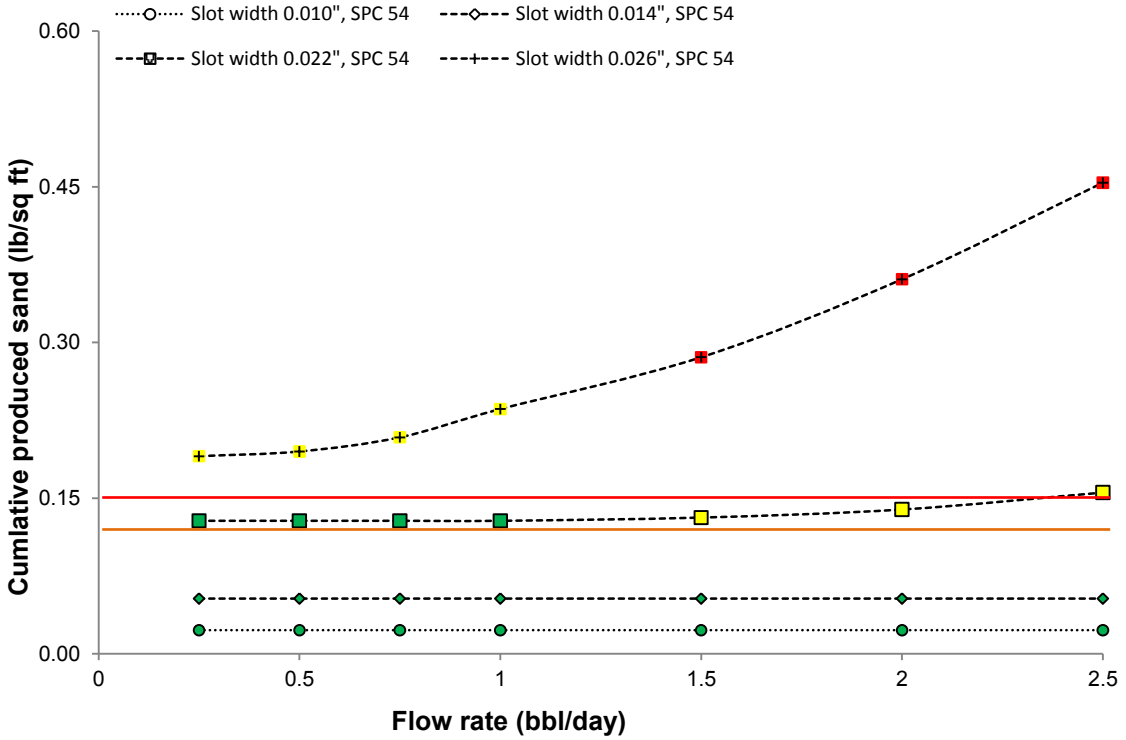
Figure 8-1. Cumulative sand production for different flow rate steps for DC-III. Green, yellow and red colors relate to Mode I, Mode II and Mode III, respectively, (a) SPC=30, (b) SPC=42, (c) SPC=54



(a)



(b)



(c)

Figure 8-2. Cumulative sand production for different flow rate steps for DC-II. Green, yellow and red colors relate to Mode I, Mode II and Mode III, respectively, (a) SPC=30, (b) SPC=42, (c) SPC=54

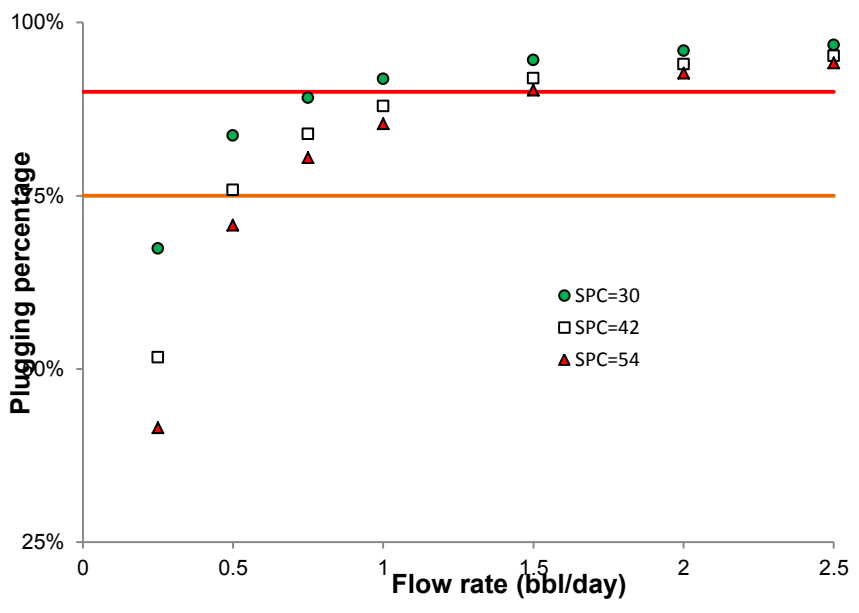
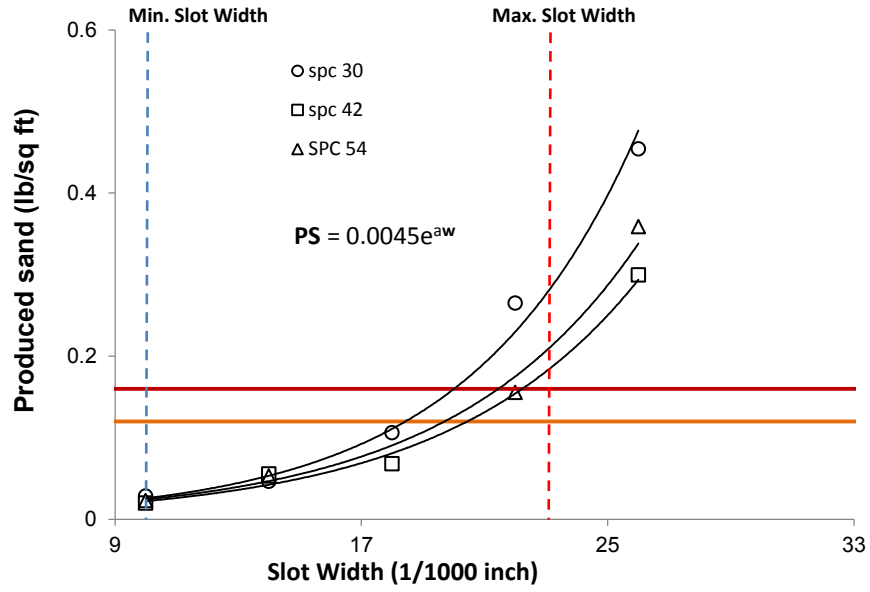
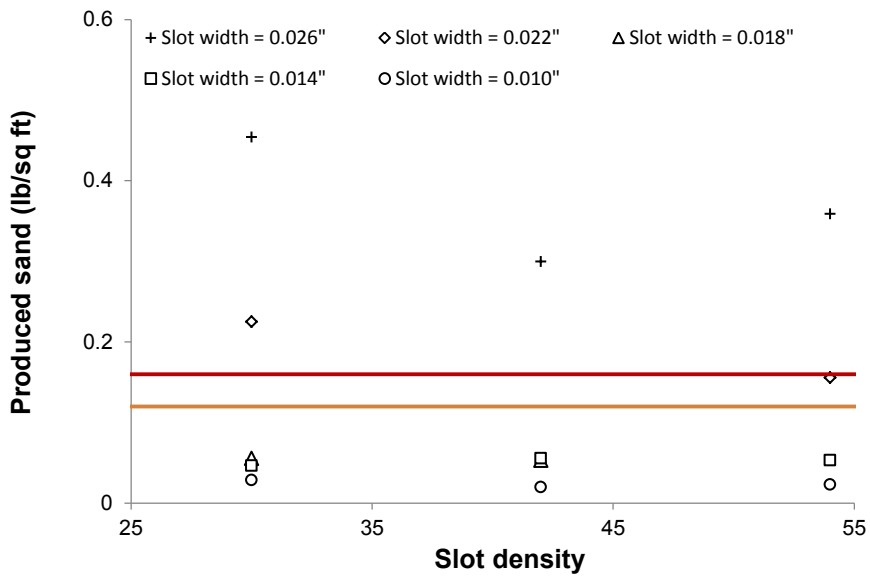


Figure 8-3. Equivalent plugging for different flow rates calculated based on the flow rate of 40 ml/hr/slot for no plugging cases

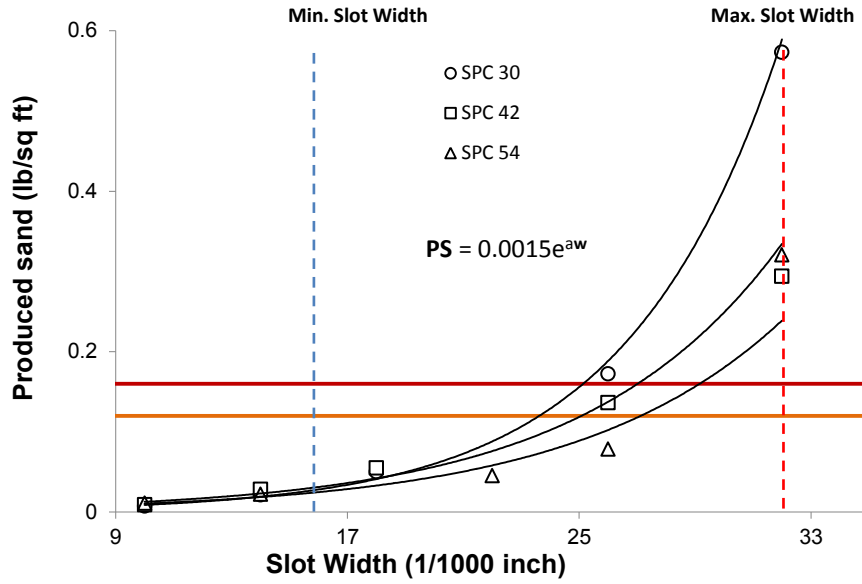


(a)

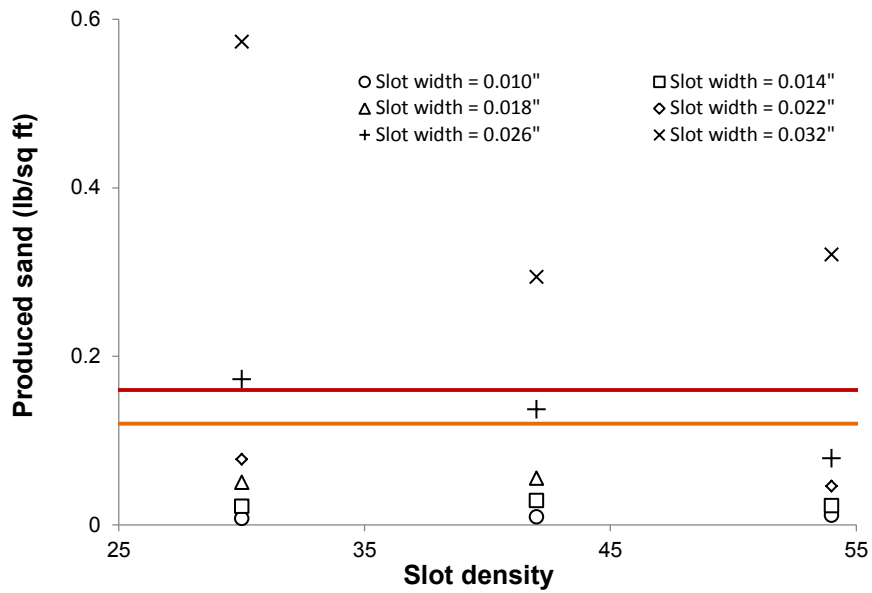


(b)

Figure 8-4. Produced sand for DC-II (a) produced sand for different slot widths at a constant slot density, (b) produced sand at a constant slot width for different slot densities; solid lines are the upper limit for the acceptable sand production of 0.15 lb/sq ft and 0.12 lb/sq ft

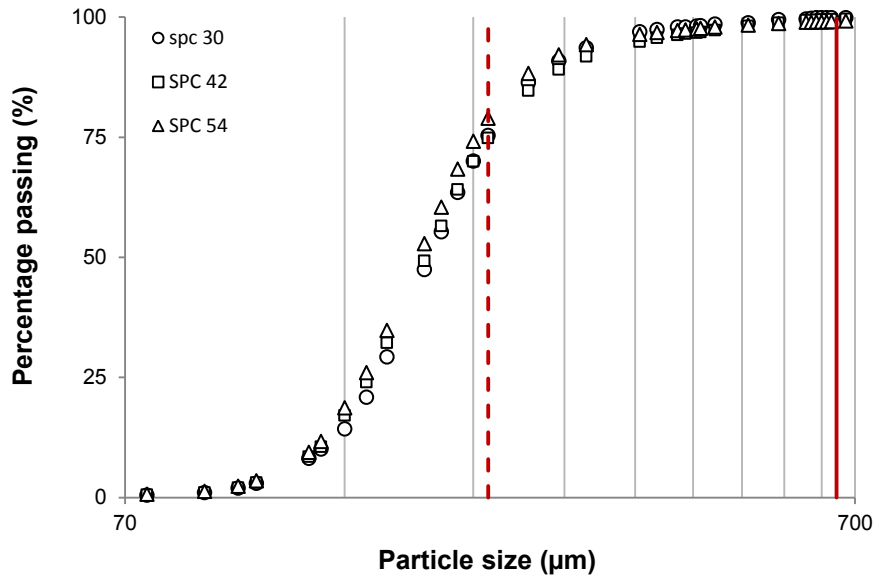


(a)

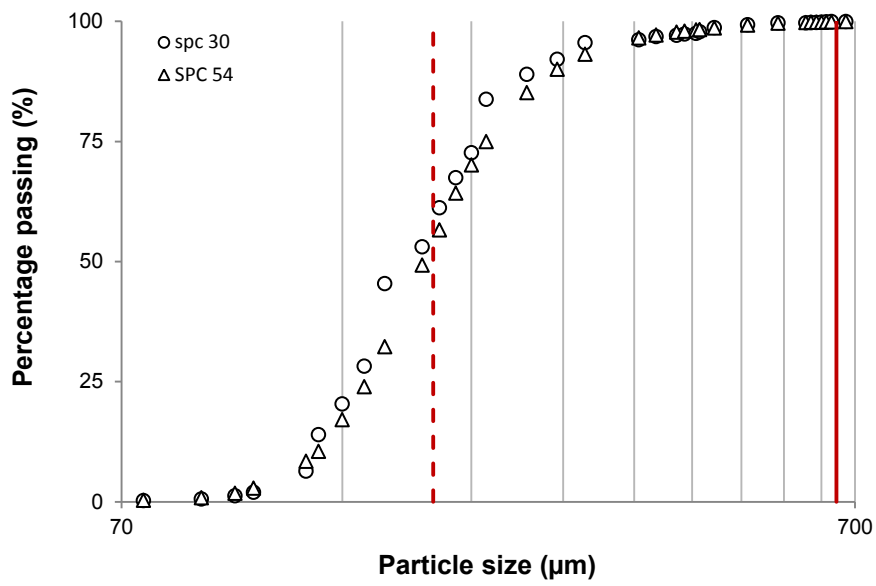


(b)

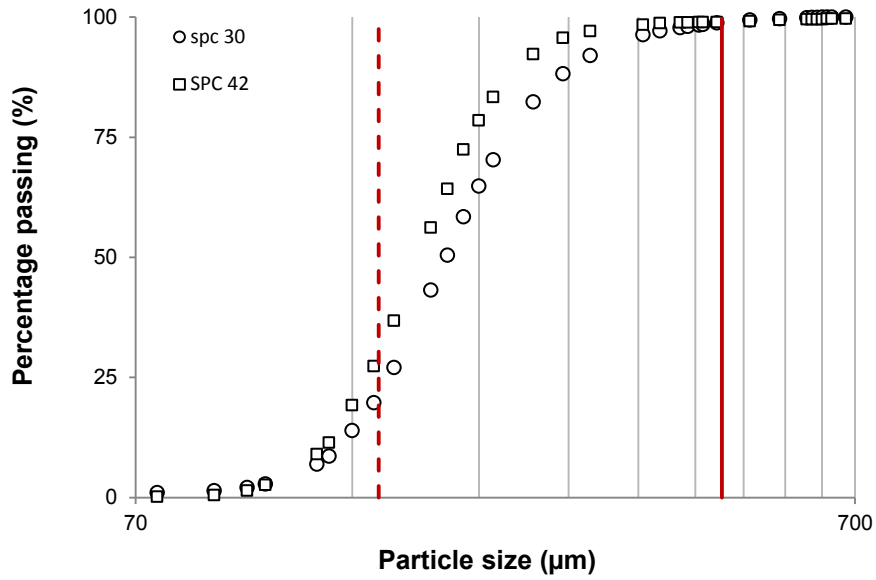
Figure 8-5. Produced sand for DC-III (a) produced sand for different slot widths at a constant slot density, (b) produced sand at a constant slot width for different slot densities; the solid lines show the upper limit for acceptable sand production of 0.15 lb/sq ft and 0.12 lb/sq ft



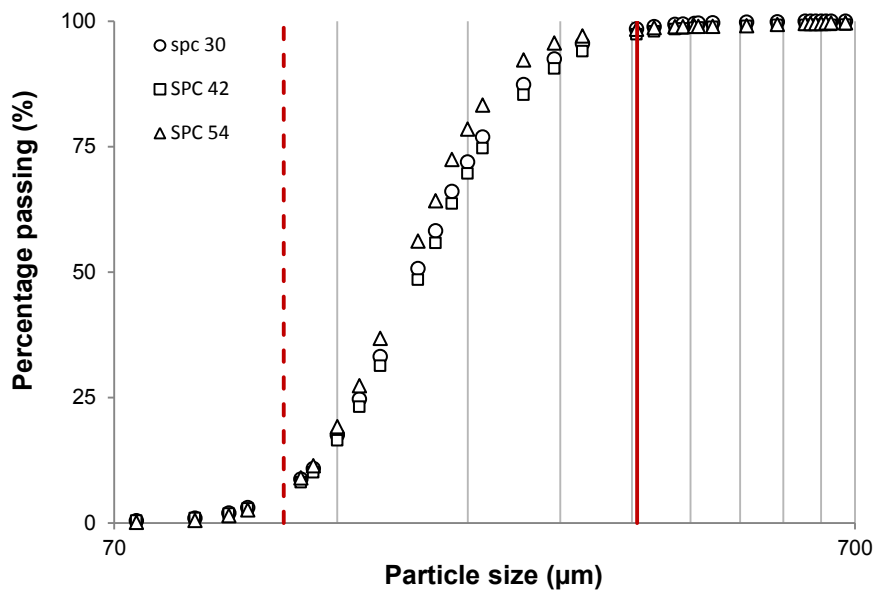
(a) Slot width: 0.026"



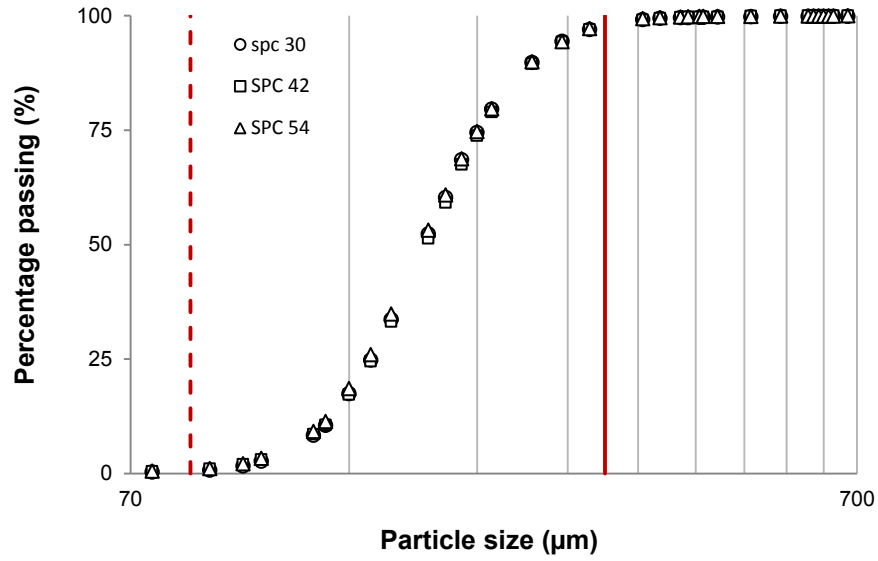
(b) Slot width: 0.022"



(c) Slot width: 0.018"



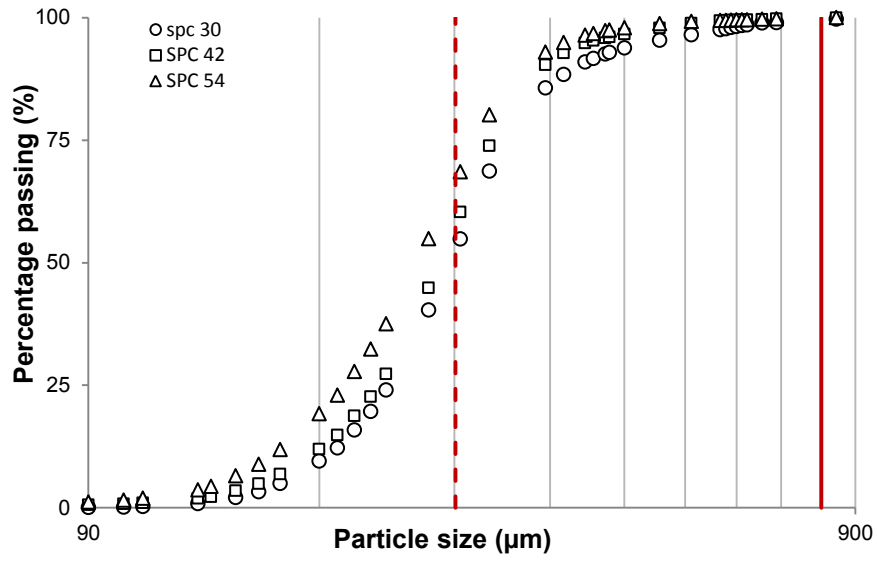
(d) Slot width: 0.014"



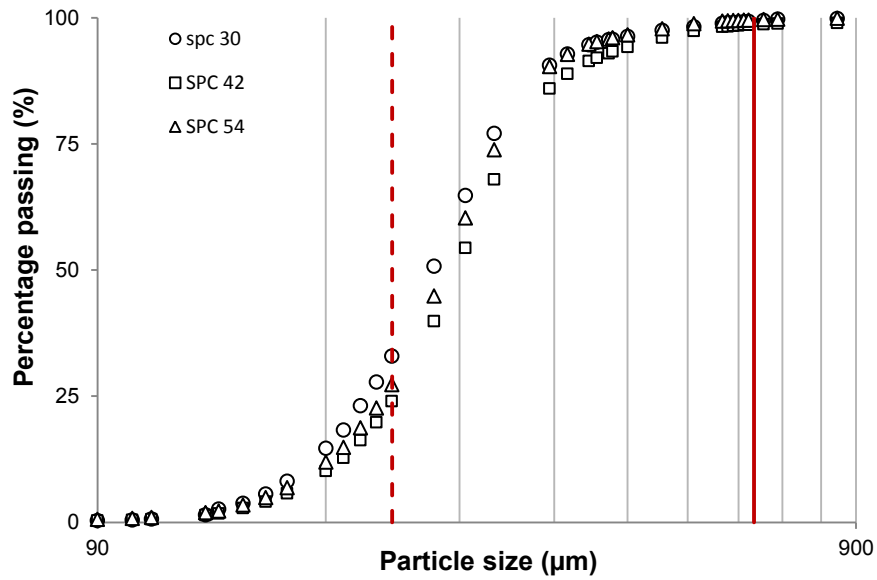
(e) Slot width: 0.010"

Figure 8-6. Comparison between the produced sand size and the slot width for DC-II; solid red line shows the slot width; dashed red line shows the 1/3 size of the slot width. (a) slot size=0.026", (b) slot size=0.022", (c) slot size=0.018", (d) slot size=0.014", (e) slot size=0.010"

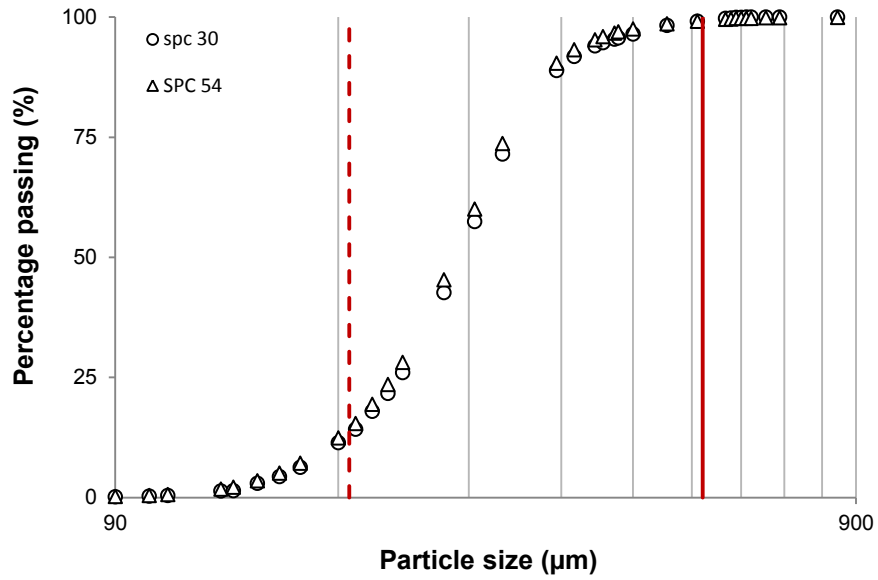




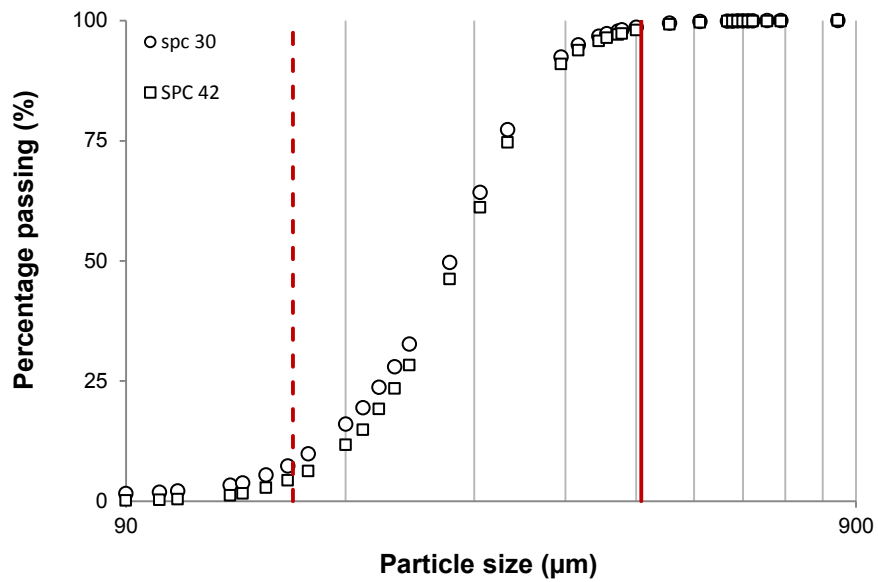
(a) Slot width: 0.032"



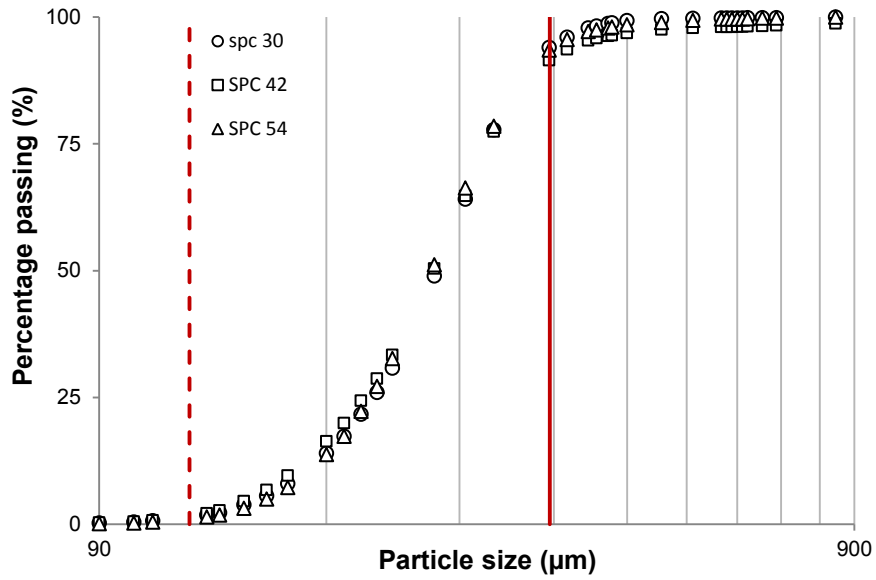
(b) Slot width: 0.026"



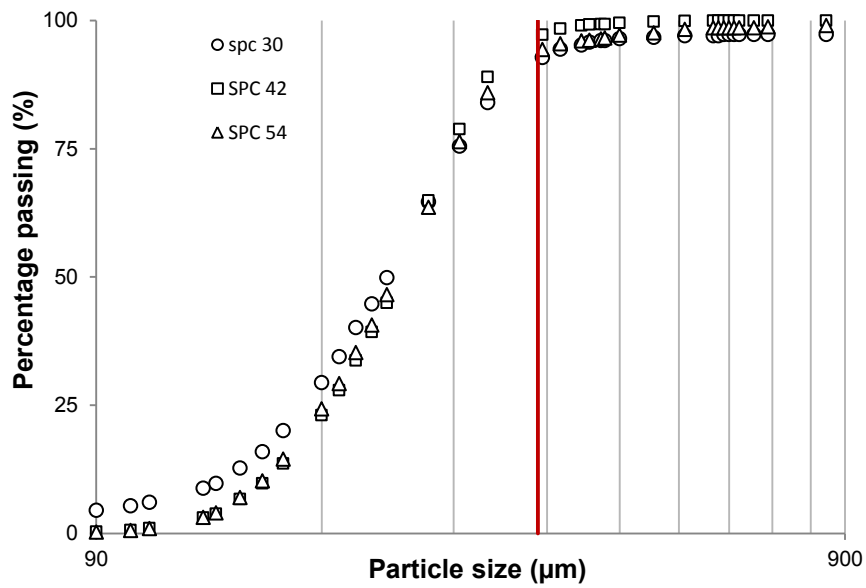
(c) Slot width: 0.022"



(d) Slot width: 0.018"

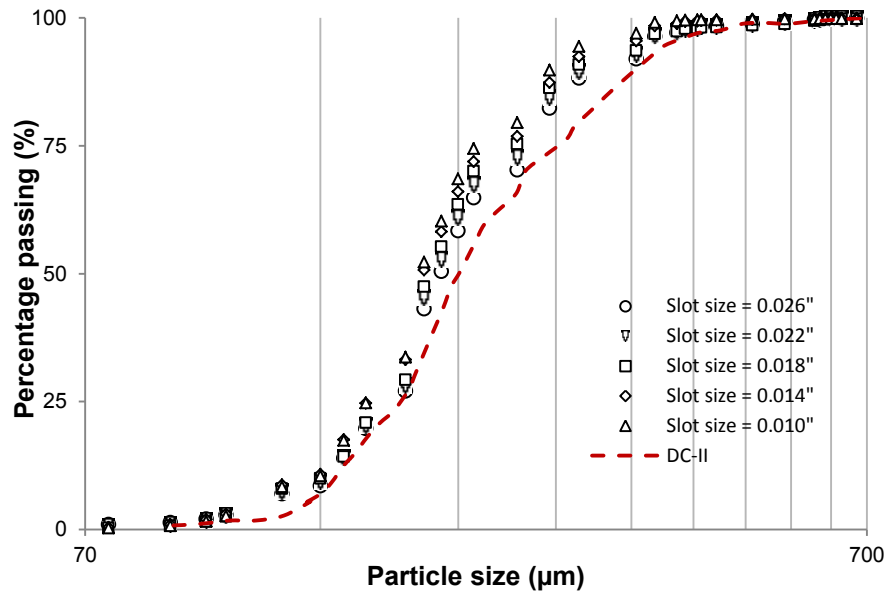


(e) Slot width: 0.014"

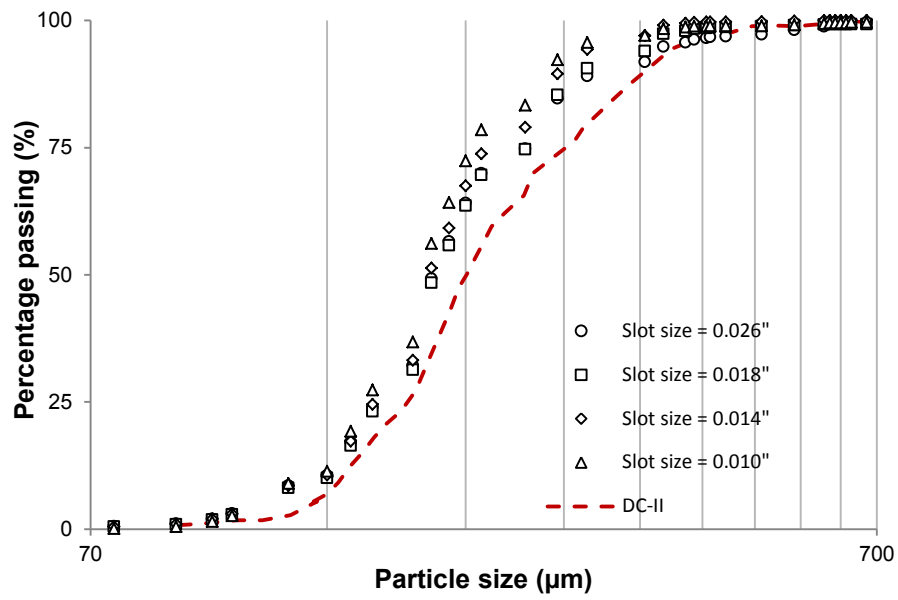


(f) Slot width: 0.010"

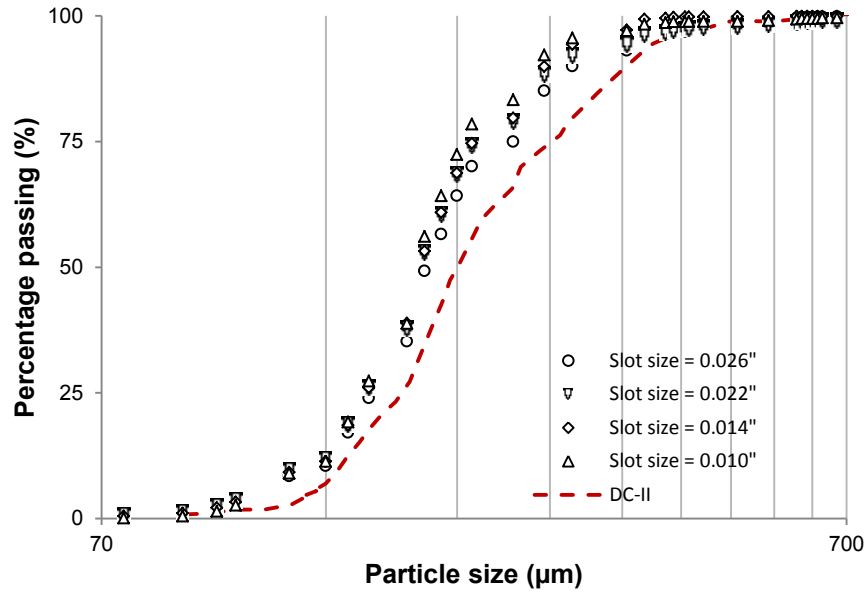
Figure 8-7. Comparison between the produced sand size and the slot width for DC-III; solid red line shows the slot width; dashed red line shows the 1/3 of the slot width. (a) slot size=0.032", (b) slot size=0.026", (c) slot size=0.022", (d) slot size=0.018", (e) slot size=0.014", (f) slot size=0.010"



(a) Slot density: 30 SPC

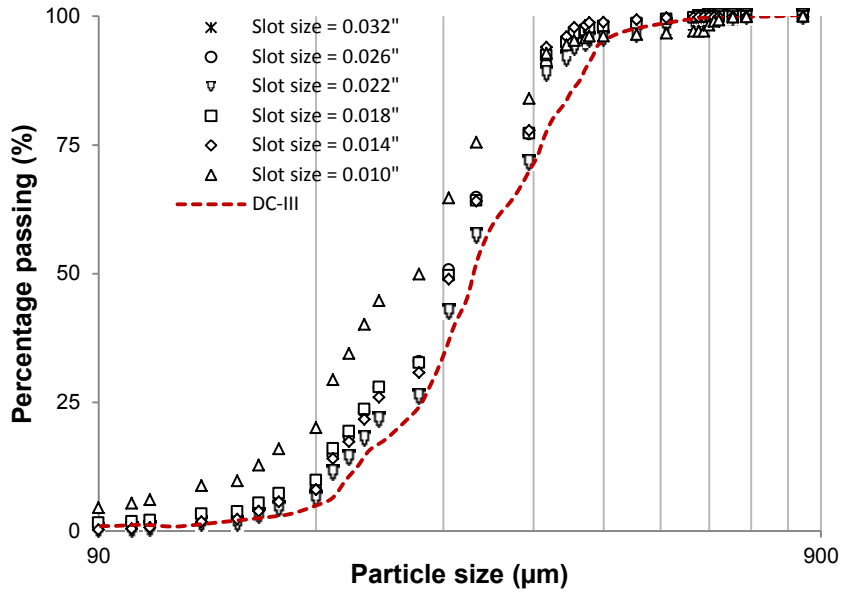


(b) Slot density: 42 SPC

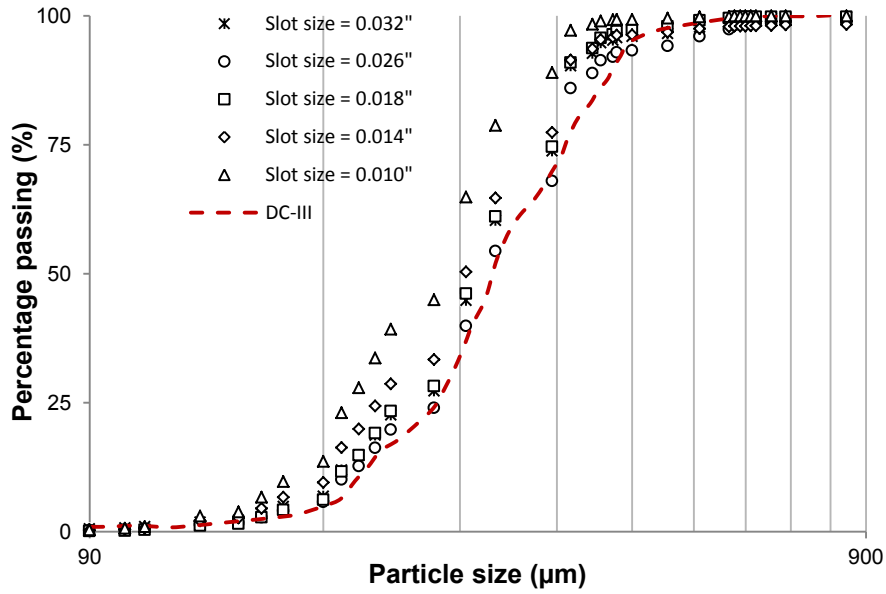


(c) Slot density: 54 SPC

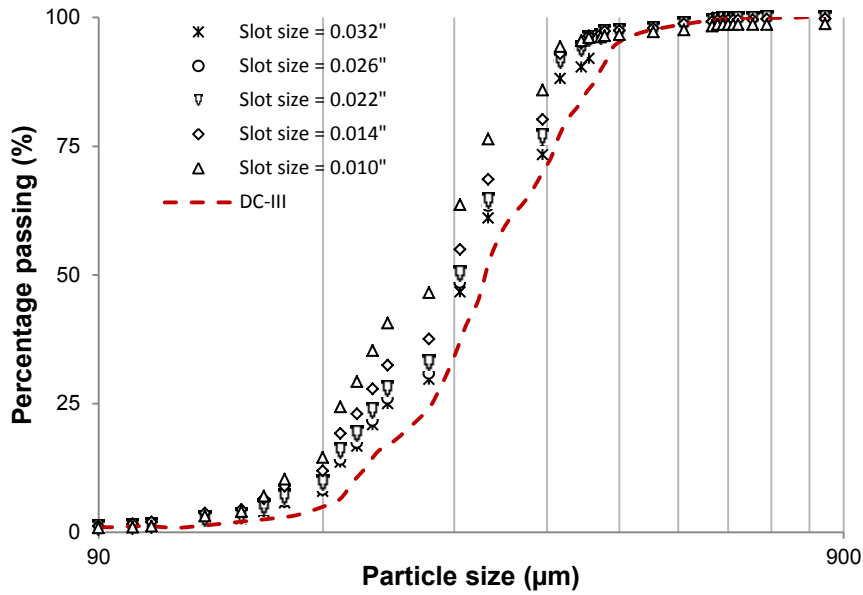
Figure 8-8. Comparison of the produced sand size distribution for different slot sizes for the coarser portion of sand pack PSD ( $>44\mu\text{m}$ ) for DC-II; dashed line shows the sand pack PSD, (a) SPC=30, (b) SPC=42, (c) SPC=54



(a) Slot density: 30 SPC

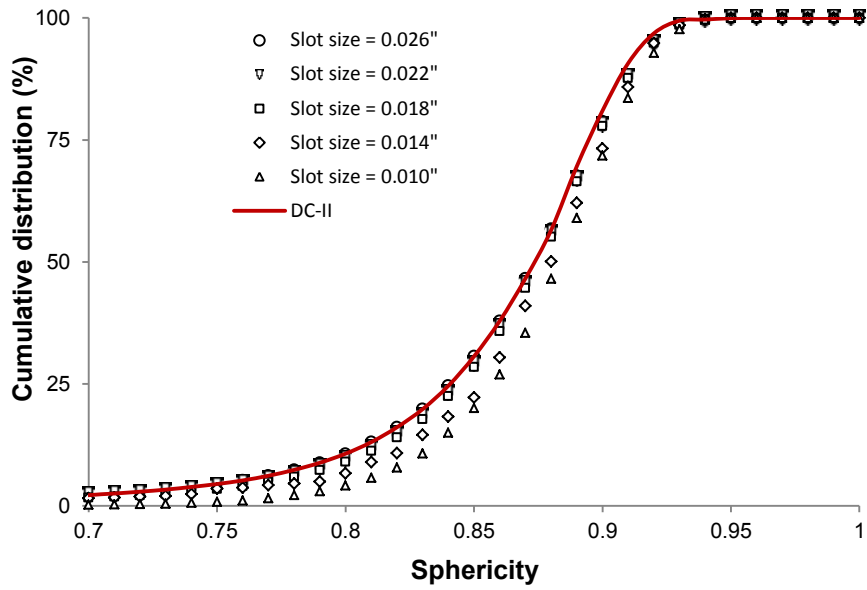


(b) Slot density: 42 SPC

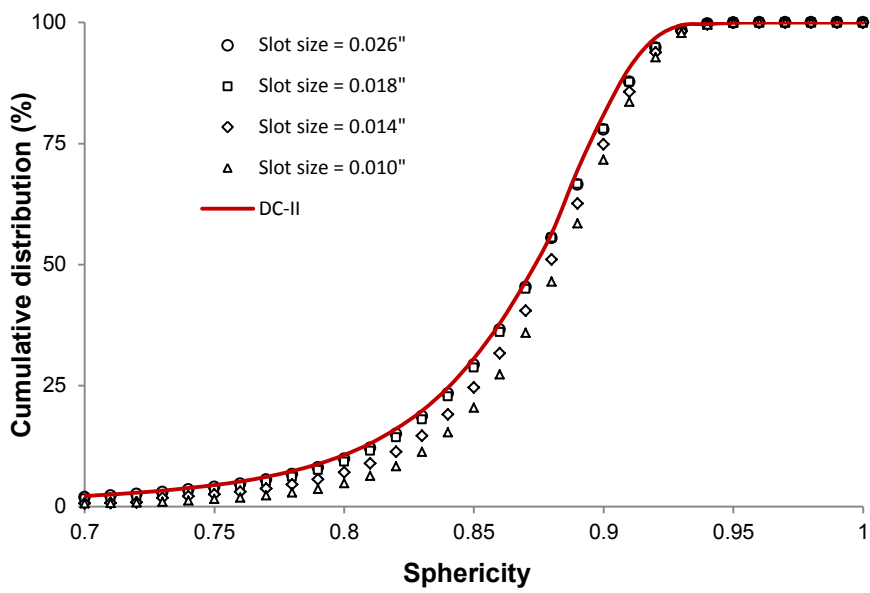


(c) Slot density: 54 SPC

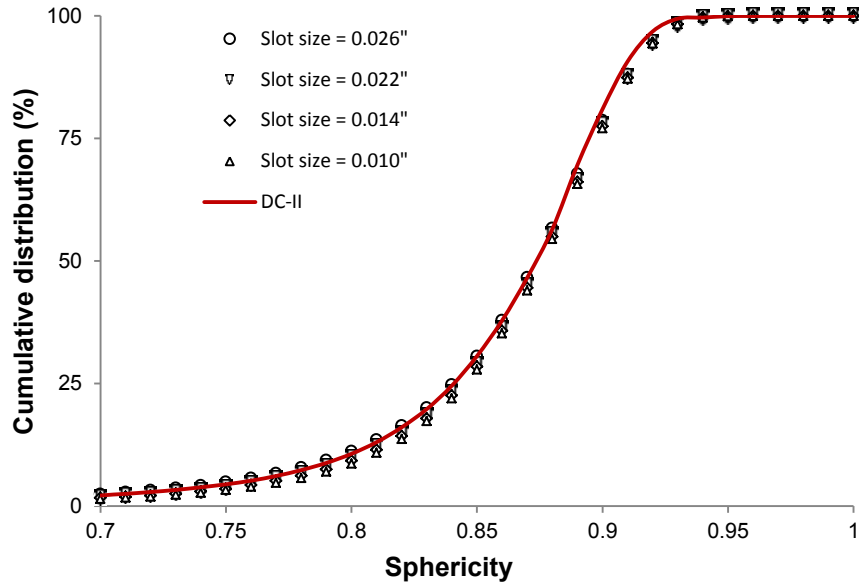
Figure 8-9. Comparison of the produced sand size distribution for different slot sizes for the coarser portion of sand pack PSD ( $>44\mu\text{m}$ ) for DC-III; dashed line shows the sand pack PSD, (a) SPC=30, (b) SPC=42, (c) SPC=54



(a) Slot density: 30 SPC

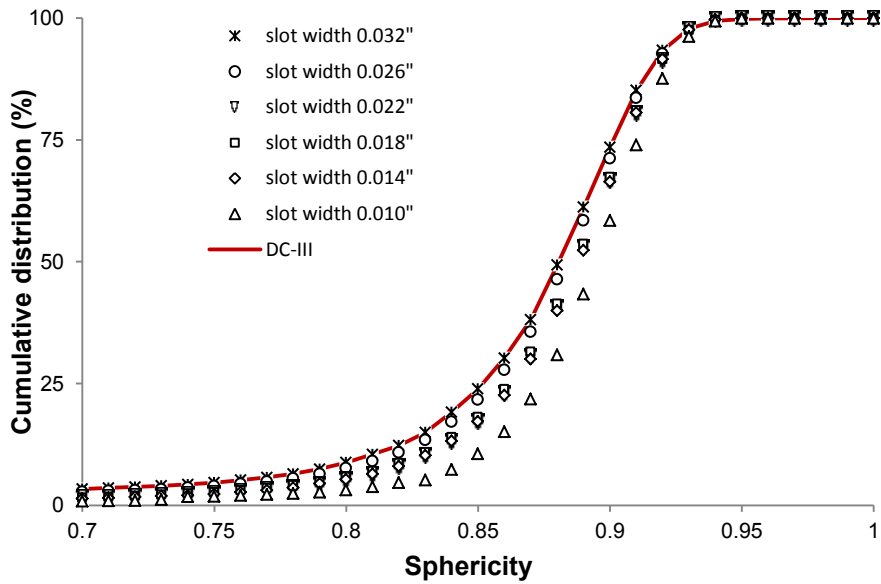


(b) Slot density: 42 SPC



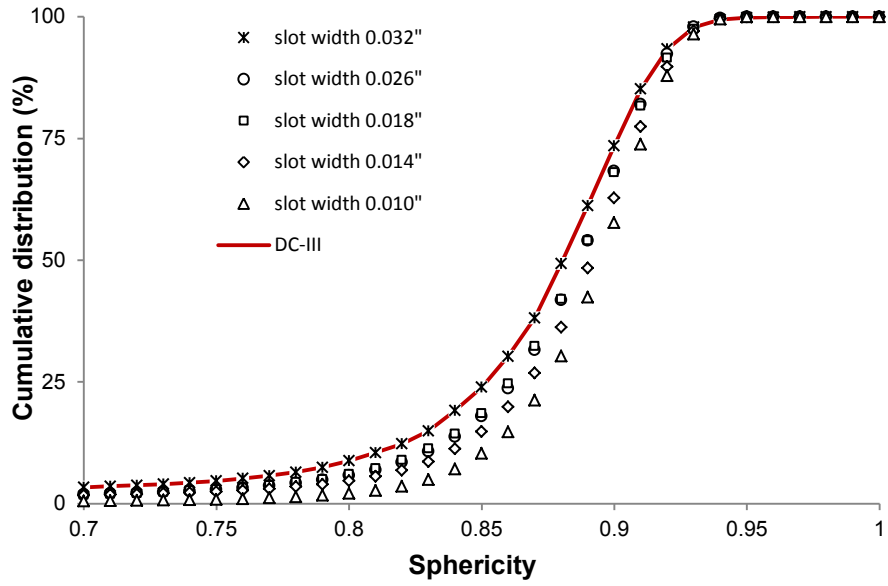
(c) Slot density: 54 SPC

Figure 8-10. Sphericity distribution of the produced sand in comparison with the sphericity distribution of the sand pack for DC-II; solid red lines show the sphericity distribution of the sand pack. (a) SPC=30, (b) SPC=42, (c) SPC=54

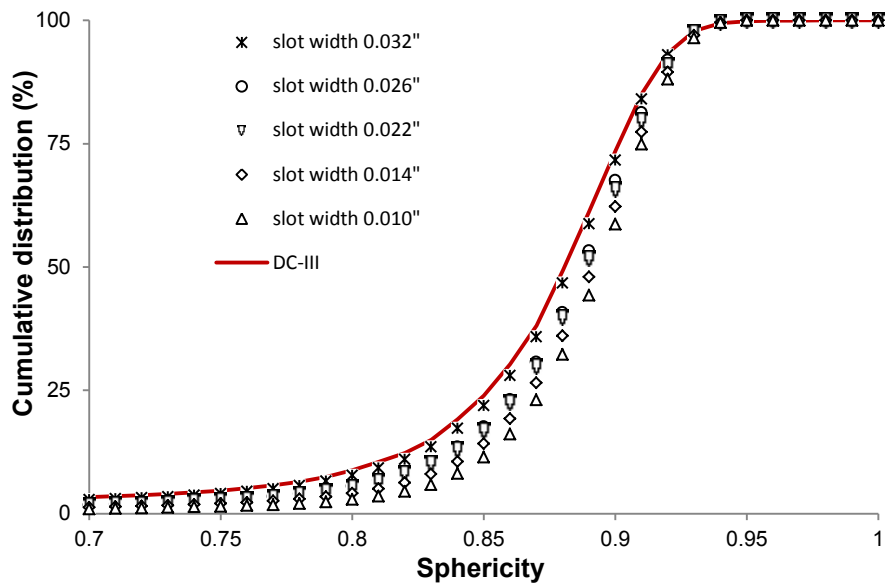


(a) Slot density: 30 SPC



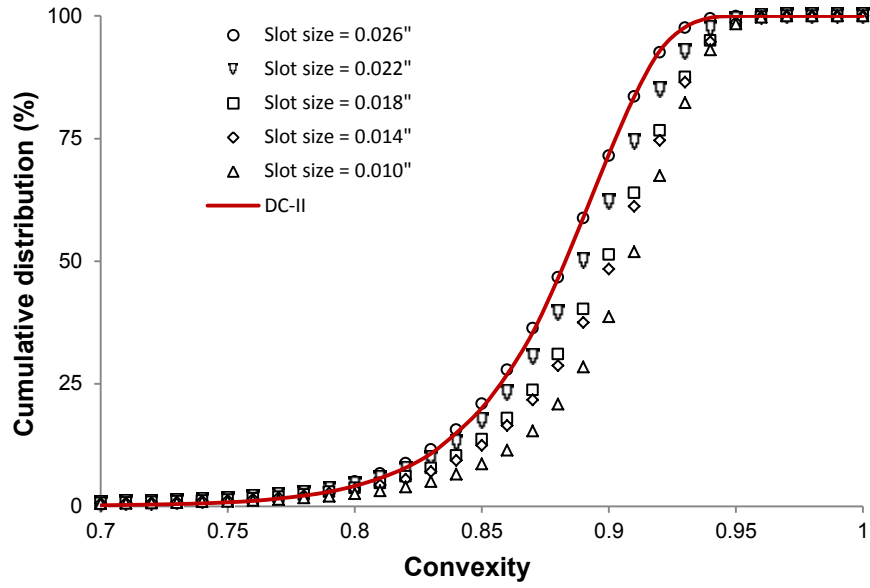


(b) Slot density: 42 SPC

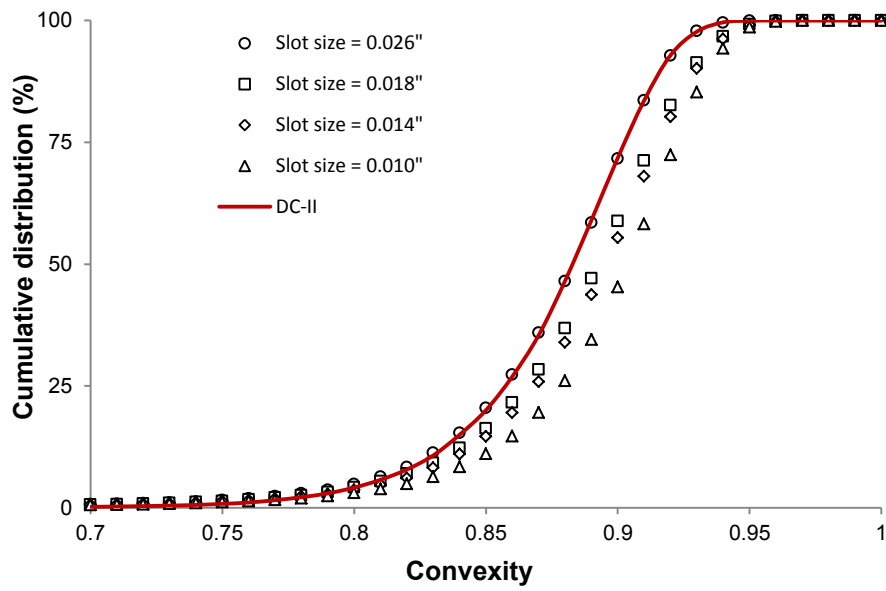


(c) Slot density: 54 SPC

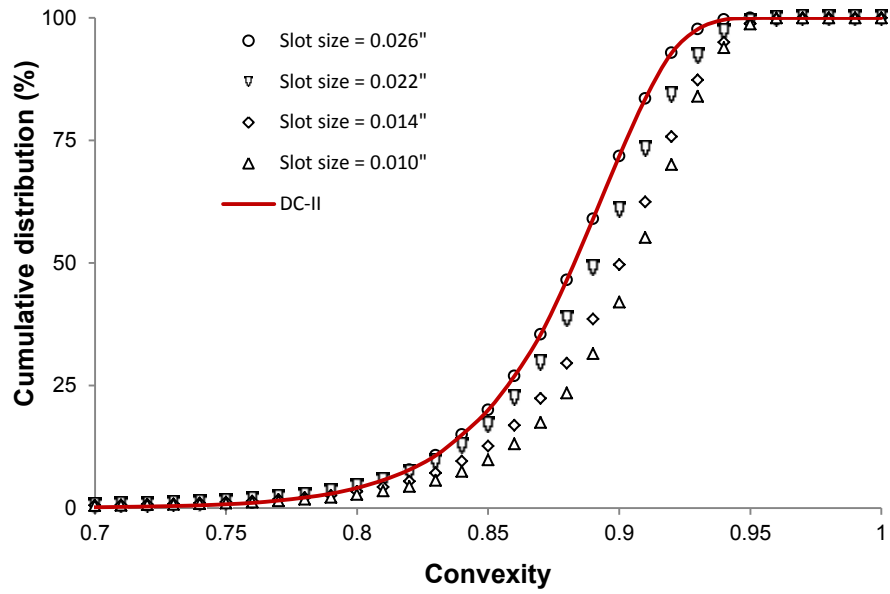
Figure 8-11. Sphericity distribution of the produced sand in comparison with the sphericity distribution of the sand pack for DC-III; solid red lines show the sphericity distribution of the sand pack. (a) SPC=30, (b) SPC=42, (c) SPC=54



(a) Slot density: 30 SPC

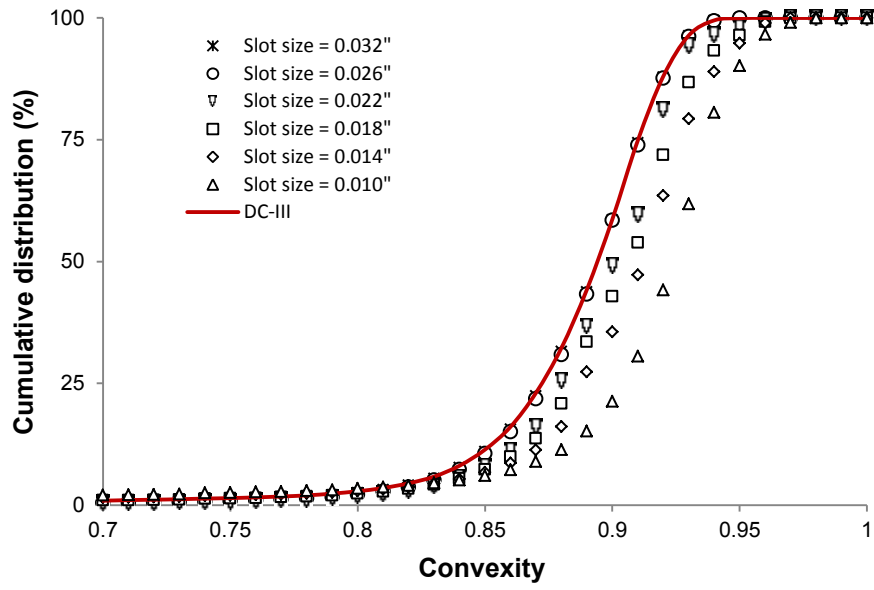


(b) Slot density: 42 SPC

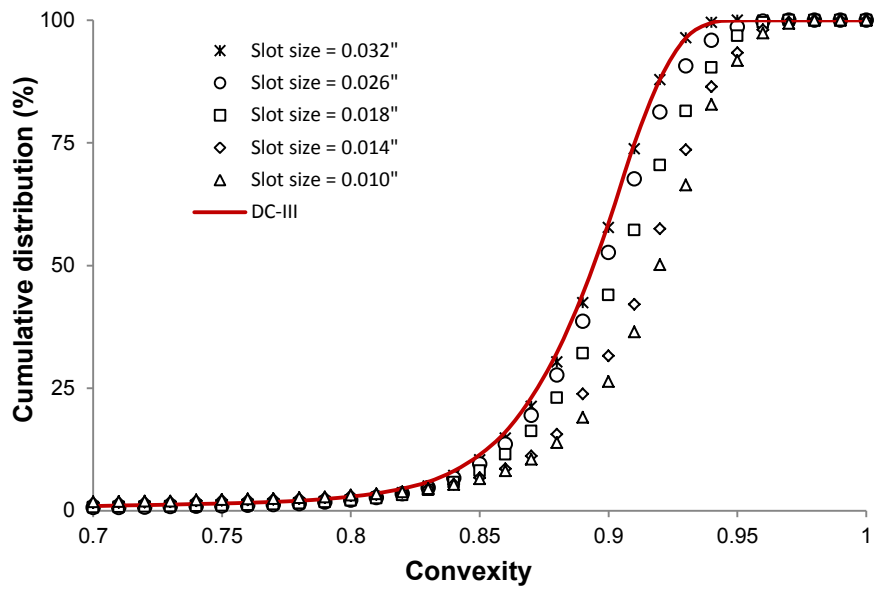


(c) Slot density: 54 SPC

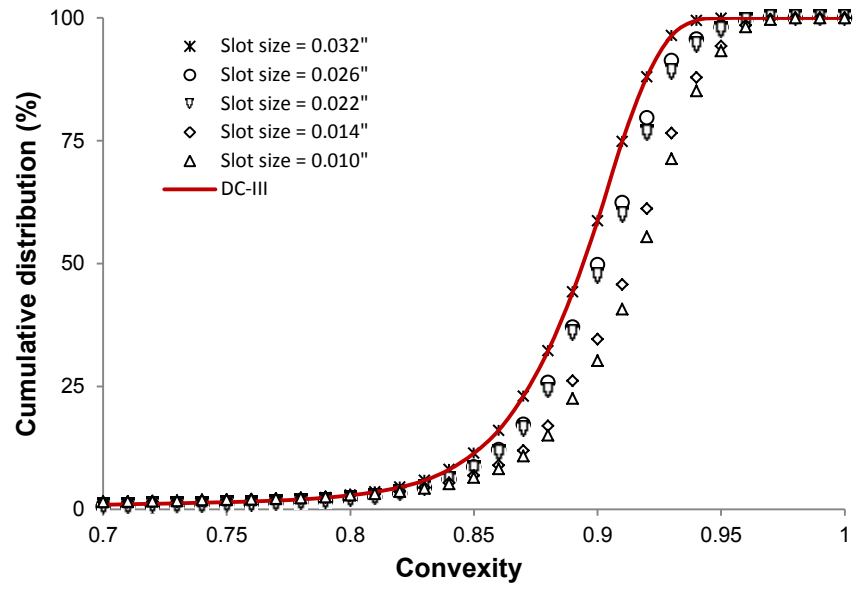
Figure 8-12. Convexity distribution of the produced sand in comparison with the convexity of the sand pack for DC-II; solid red lines show the convexity distribution of the sand pack. (a) SPC=30, (b) SPC=42, (c) SPC=54



(a) Slot density: 30 SPC

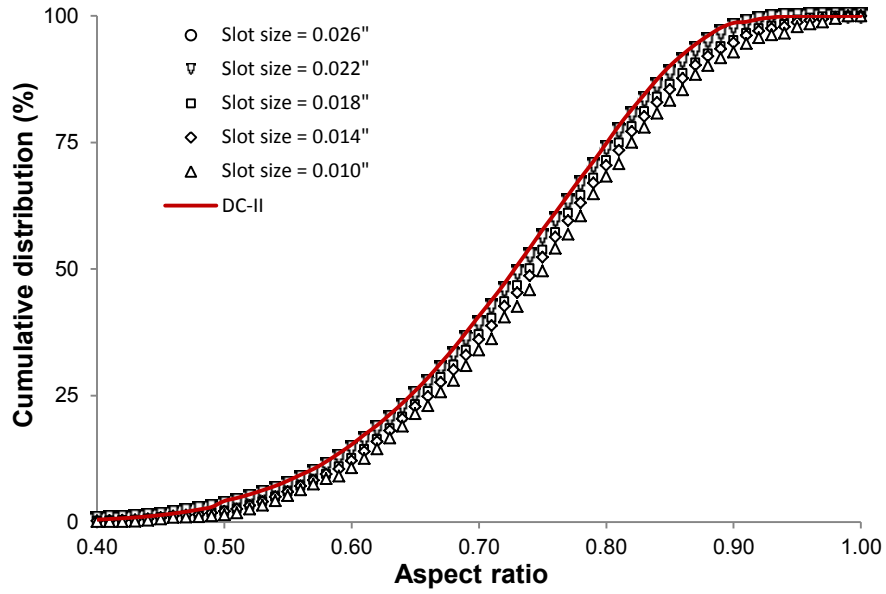


(b) Slot density: 42 SPC

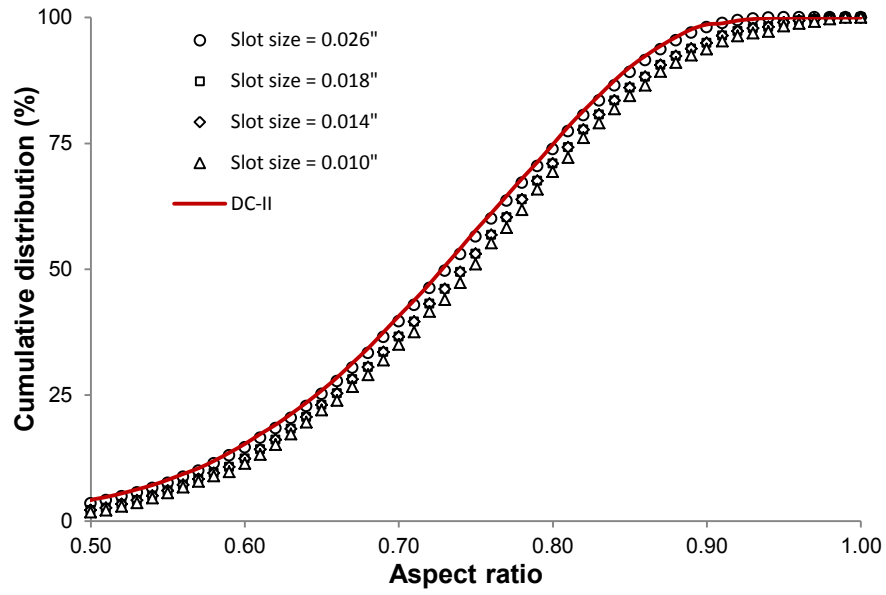


(c) Slot density: 54 SPC

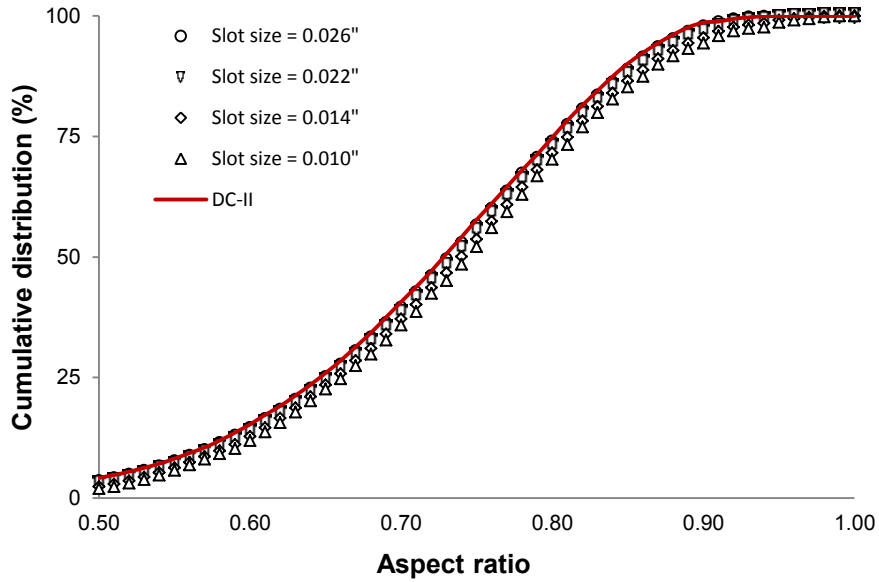
Figure 8-13. Convexity distribution of the produced sand in comparison with the convexity of the sand pack for DC-III; solid red lines show the convexity distribution of the sand pack. (a)SPC=30, (b) SPC=42, (c) SPC=54



(a) Slot density: 30 SPC

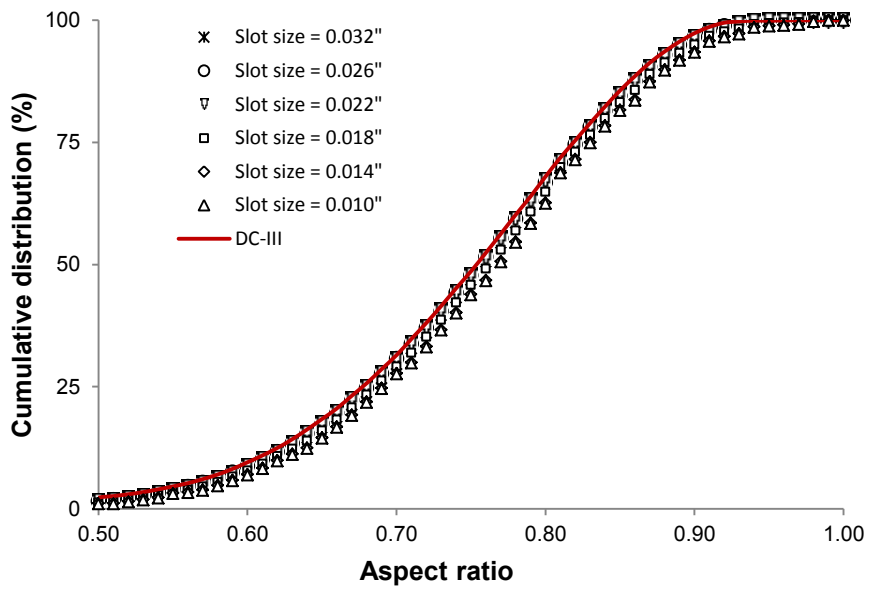


(b) DC-II – Slot density: 42 SPC

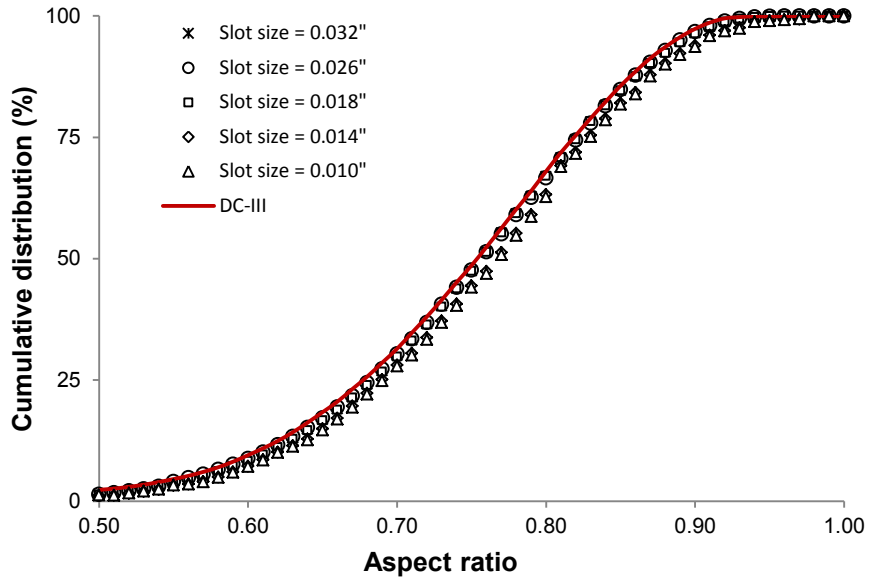


(c) Slot density: 54 SPC

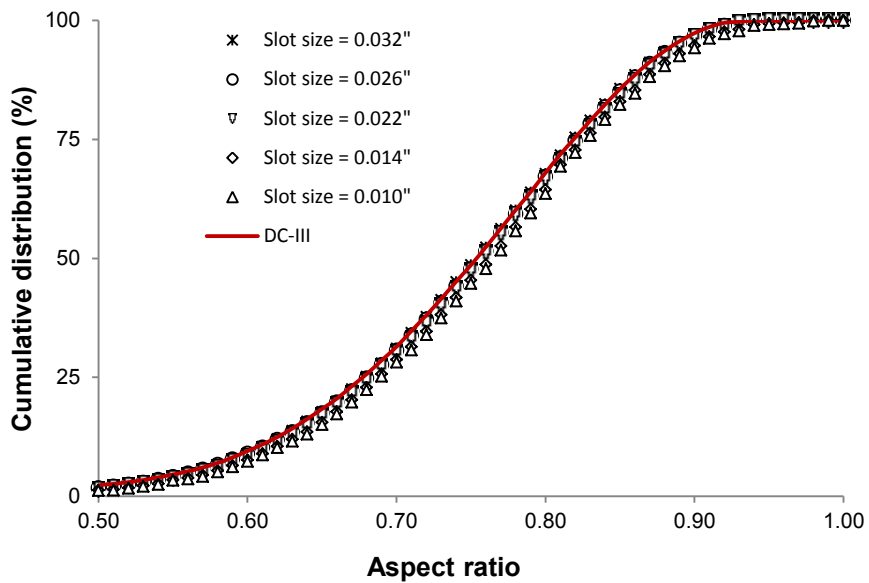
Figure 8-14. Aspect ratio distribution of the produced sand in comparison with the aspect ratio of the sand pack for DC-II; solid red lines show the aspect ratio distribution of the sand pack. (a) SPC=30, (b) SPC=42, (c) SPC=54



(a) Slot density: 30 SPC



(b) Slot density: 42 SPC



(c) Slot density: 54 SPC

Figure 8-15. Aspect ratio distribution of the produced sand in comparison with the aspect ratio of the sand pack for DC-III; solid red lines show the aspect ratio distribution of the sand pack. (a) SPC=30, (b) SPC=42, (c) SPC=54



## **CHAPTER NINE: NEW CRITERIA FOR SLOTTED LINER DESIGN FOR HEAVY OIL THERMAL PRODUCTION**

This chapter combines the Sand Retention Testing (SRT) results in term of flow performance and sand production performance to formulate a set of design criteria for slotted liners. The proposed criteria specify the slot density and width with the aim of keeping the produced sand within an acceptable limit while sustaining the wellbore productivity by minimizing pore plugging in the zone adjacent the liner.

Current design criteria are only based on the formation PSD. The testing in this research takes the operational parameters (e.g. pH and salinity of injection fluids, production rate, and production ramp-up rate) into account in the screen performance evaluation. Further, existing design criteria specify only the slot width and the design criteria are independent of the slot density. The proposed design criteria use the slot density as a design parameter. Additionally, existing design criteria are assumed to work for different sand types, regardless of the sand sizes, the shape of the PSD curve, and the amounts of fines. The proposed design criteria are, however, PSD specific. It is assumed that Alberta oil sands can be categorized in a few PSD classes, such as those (DC-I through DC-IV) proposed by Abram and Cain (2014). Hence, the first stage of the design is to find the best match PSD group and use the design criteria specified for that specific group. This chapter presents design criteria for two PSD classes (DC-II and DC-III) out of four proposed by Abram and Cain (2014). It remains for the future work to complete the design criteria for the remaining PSD categories.

In proposing the design criteria, this chapter uses the sanding and plugging (in terms of retained permeability) data presented in Chapter 7 and 8.

### **9.1 New design criteria for slotted liners**

The new design criterion for slotted liners is based on defining a safe slot window with respect to both sand production and flow performances. The criteria are developed based on a series of SRT experiments by using two common particle size distributions (PSDs) in the McMurray Formation. The testing program uses slotted liner coupons with different slot widths and slot densities. A novel Traffic Light System (TLS) is used to determine if the specified design is acceptable or unacceptable with respect to sanding and flow performance indicators.

### ***9.1.1 Traffic light design approach***

The slot width selection based on existing design criteria consists of specifying a slot window for an acceptable sanding and flow performance (Markestad et al. 1996). Existing design criteria, however, do not take into account wellbore operational parameters and slot density. Further, they existing criteria are assumed to work for different PSDs regardless of the PSD characteristics such as the PSD shape, fines content, and particle sizes. Additionally, existing criteria do not provide any information on the severity of sanding and plugging for the specific design. The proposed sanding criteria in this research uses a Traffic Light System approach by using the familiar traffic light color coding with the red, yellow, and green colors indicating unacceptable, caution, and acceptable, respectively. The proposed criteria accounts for the PSD, slot density, and the level of flow rate per slot. It also provides some information on the expected performance of a specific design in terms of sanding and plugging.

### ***9.1.2 Acceptable sanding limits***

An acceptable sanding level is highly dependent on the wellbore trajectory (horizontal, slant, and vertical), sand transportability in the produced fluids, artificial lift requirements, susceptibility of wellbore and surface installations (such as tubing, choke, fittings) to erosion, and surface separator capacity, among others.

In low-rate long horizontal wells, such as SAGD wells, the potential of sand transport in the horizontal well is low, hence, sand the produced sand accumulates in the horizontal well, and reduces wellbore productivity. The general rule of thumb is that the sand production should be limited to less than 1% of the liner volume. **Figure 9-1** shows a typical completion design for a SAGD producer well. Most SAGD wells use a 7-inch or 8 5/8-inch liner with production tubing size ranging from 2 7/8 inch to 4 1/2 inch. The 1% limit for these typical liner sizes result in an approximately  $0.15 \text{ lb/ft}^2$  sanding, which is the cumulative sand produced over the entire SAGD well life cycle per unit area of the outer surface of the liner. Usually, the limit of  $0.12\text{-}0.15 \text{ lb/ft}^2$  is adopted for the maximum acceptable sand production (Chanpura et al. 2011; Hodge et al. 2002). In the proposed TLS, the green color for sanding is dedicated to cumulative sand production below  $0.15 \text{ lb/ft}^2$  for Mode-I sanding and  $0.12 \text{ lb/ft}^2$  for Mode II sanding. The yellow color in the TLS for sanding is defined as sand production between  $0.12$  to  $0.15 \text{ lb/ft}^2$  for Mode II sanding. The yellow color represents higher risk as more plugging and

higher production rate can potentially lead to excessive sanding and potential need for wellbore intervention to clean out the wellbore from sand. However, the transient nature of sanding in Mode-II sanding ensures the sanding will eventually stop as new stable bridges form; hence, the total amount of produced sand will be limited.

The red light is defined as sand production in excess of  $0.15 \text{ lb/ft}^2$  for Mode II or Mode III sand production. The red light represents the case with excessive risk as more plugging than expected or higher production rates can result in excessive sanding which can potentially lead to complete fill up of the liner by sand, and damage to the artificial lift system (e.g. downhole pump). **Table 9-1** summarizes the TLS color coding with respect to sanding for defining the slot window.

### ***9.1.3 Flow performance and plugging tendency***

The installation of a sand control liner in a wellbore causes an additional pressure drop (hence increases skin) and changes the flow geometry, and velocities near the wellbore. Further, the near screen pore space and permeability are different than those of the formation. In general, the additional pressure drop in the near-wellbore zone consists of two terms: a flow-dependent term and a constant (flow independent) term (Furui 2007). The flow-dependent term is due to the flow convergence that changes the flow velocity and geometry near the wellbore. The flow-independent term is related to the pore space alteration, sand retention on the screen, and the pressure drop within the screen (open slots versus partially plugged).

In typical SAGD production rates, the pressure drop in open slots is negligible (less than 0.01 psi). However, the amount of pressure drop increases significantly as the slots are gradually plugged. The higher pressure drop is due to higher velocities in the convergence zone, larger convergence zone, and higher pressure drops inside the slots.

Two terms have been used in the past to characterize plugging: retained permeability and screen permeability (Markestad et al. 1996; Ballard et al. 1999). Screen permeability is an equivalent permeability for the near screen zone including the screen. Screen permeability is smaller than the formation permeability due to the additional pressure drop across the screen and the plugging of the pore space in the porous medium adjacent the screen. Retained permeability is defined as the ratio of the screen permeability to the original formation permeability. An ideal screen is defined as the screen with screen permeability equal to the original permeability of the formation

(i.e. retained permeability of one) which means little effect of the screen on wellbore productivity. In the past SRT tests, a retained permeability of 0.5 (i.e. 50%) has been considered as an acceptable limit (Markestad et al. 1996).

#### ***9.1.4 Design and SRT testing assumptions***

It is important to note that SRT tests are not designed to be fully representative of the field conditions (Ballard 2011). The primary reason behind SRT testing is to produce repeatable results to assess different screen specifications (i.e. slot width, slot density, slot pattern, etc.), and different types of screen (i.e. wire-wrapped screen and slotted liner) for a particular application. SRT tests are designed to help engineers make decisions with limited information. While they form a good starting point, the guidelines developed based on the SRT tests, commonly tend to be conservative (Ballard 2011).

Engineers tend to consider the worst-case scenario in their design process. One of the most important and challenging missions in well completion design is to maximize production where the redundancy, robustness, and resilience of the completion design plays an important role in such circumstances. However, such an approach is conservative and leads to increased completion cost.

Design complexity and uncertainty and the interrelationship between different design components in relation to the overall screen performance require a shift from the worst-case scenario approach toward the so-called “design optimization under uncertainty”. In the latter, the design under uncertainty is examined by understanding how the uncertainty affects the optimal design (Bernardo et al. 2000). In this context, a slot size window is defined that considers two performance indicators that are used to decide on a design specification (slot width, and density) or to select among different sand screens. Such approach can be combined with completion costs (screen cost, ICD/OCD cost, instrumentation cost, etc.) in the selection of the best overall completion design.

The TLS approach is used to design the slotted liner based on the result of SRT testing on two PSD categories for the McMurray Formation. It is important to note the proposed criteria in this work should be used as the first-pass design. In any new design work for a particular field, a detailed characterization and SRT testing of the formation sand is required to further refine the design and select the best specification.

The SRT test can also be used to rank different screens based on performance indicators discussed earlier. Testing conditions are designed to mimic the worst-case scenario for sand production (low stress, single phase flow, hence, zero capillary pressure) and plugging (higher fines mobilization and plugging in brine flow), and is not the exact condition of the SAGD operation (temperature, flow rate, flowing fluid composition, etc.).

It is important to note the difference in the time scale of the testing versus the full life cycle of a SAGD well during which phenomena such as corrosion and scaling may develop and play important role in the plugging tendency of the screen.

#### ***9.1.5 New criteria for slotted liner design***

This section describes how the traffic light approach is used along with the acceptable sand production and flow performance (**Table 9-1**) to arrive at the new design criteria for slotted liners. The design criteria are still based on certain points on the oil sand PSD (D-values). Two most common points for the design of screens are the median size (D<sub>50</sub>) and upper 10% in the coarser portion of the PSD (D<sub>10</sub>).

To determine the safe slot window, a linear representation of the PSD is used as the x axis (**Figure 9-2(a)** for DC-II and **Figure 9-2(b)** for DC-III) and is annotated in terms of D values. **Table 9-2** summarizes the DC-II and DC-III representation based on the D values. Slot sizes used in the testing program were varied from 1.5 D<sub>50</sub> to 3.5 D<sub>50</sub> as shown in dashed lines in **Figure 9-2(a)** and **9-2(b)**.

**Figure 9-3(a)** through **9-3(c)** show the proposed design criteria for slot width design for a low slot density (number of slots per column, SPC=30) for DC-II. **Figure 9-3(a)** shows the sanding performance, while **Figure 9-3(b)** illustrates the flow performance, and **Figure 9-3(c)** shows the overall slot window for SPC=30. Similarly, the sanding performance for two more SPC values is presented in **Figure 9-4(a)** and **9-5(a)** for DC-II, and **Figure 9-6(a)** and **9-8(a)** for DC-III. The corresponding flow performance is also shown in **Figure 9-4(b)** and **9-5(b)** for DC-II and **Figure 9-6(b)** and **9-8(b)** for DC-III. Overall slot window for these two SPC values are presented in **Figure 9-4(c)** and **9-5(c)** for DC-II and **Figure 9-6(c)** and **9-8(c)** for DC-III.

It is evident from the overall slot window for the two PSDs that increasing the slot density leads to a wider safe slot window. This indicates a deficiency in the current testing protocols that are based solely on single-slot testing to select the appropriate slot width.

### ***9.1.6 Incorporation of flow rate in the design criteria***

Typical flow rates in SAGD production wells is around 1,000-2,000 bbl/day, which translates to less than 0.25 bbl/day in the SRT testing which uses 6.75-inch diameter liner coupons assuming all slots are open. However, (1) some slots may plug over time, resulting in higher flow rates into open slots; (2) production from the entire well length may not be uniform rendering higher flow rates in some slots and less in others; and (3) aggressive production ramp-ups have been exercised in some SAGD wells following a period of wellbore intervention resulting on higher than typical pressure gradients over a finite period of time. Hence, use of higher flow rates than typical should be exercised in SRT testing.

Testing results in Chapter 7 showed that flow velocity (hence the flow rate) must exceed a critical level for fines migration and production to take place. In the SRT tests performed in this study, the critical flow rate is ranging from 0.8-1.0 bbl/day. Hence, flow rates below 0.8 bbl/day (corresponding to a field level of about 15,500 bbl/day) are considered as moderate. In Chapter 8, Mode III sanding was observed to occur at flow rates above 1.5 bb/day (corresponding to a field level of about 29,000 bbl/day). Hence, flow rates beyond 1.5 bbl/day are considered as excessive. The flow rates between 0.8 bb/day to 1.5 bbl/day are defined as moderate rate.

**Figure 9-9** through **9-17** show the slot width window for three flow rate ranges for DC-II and different values of SPC. It is evident the slot window shrinks for higher flow rates per slot as the flow rate per slot reduces by increasing the SPC.







Similarly, slot size windows for the three flow scenarios for DC-III are presented in **Figure 9-18** through **9-26** for different SPCs. It is evident from the results that the slot window shrinks at higher flow rates due to the stronger fines migration (hence more plugging) and more sanding (due to stronger seepage forces). However, these effects are PSD-dependent, requiring nine design criteria for three flow rate and three slot density cases for each PSD.

## **9.2 Conclusion**

This chapter presented a graphical set of new design criteria for the slot width and density for slotted liners by combining the effect of sand PSD, slot density, slot width, flow rate, and sanding mode. The criteria were developed by using the results of SRT testing on two types of sand materials. The upper bound of the design criteria is governed by sand production while the lower bound is dictated by the flow performance of the liner. Testing results indicate wider slot window for higher slot densities. Further, the slot window are shown to be highly sensitive to wellbore operational parameters, which are reflected in terms of flow rate per coupon area. It is found that the slot window shrinks for high production rates per slot. Although typical flow rates per slot are relatively low in SAGD, it is recommended to use higher flow rates in the design to account for such factors as slot plugging, non-uniform production along the well which leads to the contribution of limited number of slots in the total production, and aggressive production practices following a period of well intervention period.

The proposed criteria should be further refined by including a larger number of sand types in the testing.

**Table 9-1. TLS color code definition for sand production and flow performance**

Sand production performance	
	Mode-III or more than 0.15 $lb/ft^2$
	Mode-II and sand production between 0.12-0.15 $lb/ft^2$
	Mode-I and less than 0.15 $lb/ft^2$ or Mode-II sand production with less than 0.12
Flow performance	
	Retained permeability less than 50%
	Retained permeability between 50-70%
	Retained permeability higher than 70%

**Table 9-2. PSD representation of DC-II and DC-III based on D-values**

	DC-II	DC-III
D1 ( $\mu\text{m}$ )	317	425
D5 ( $\mu\text{m}$ )	278	401
D10 ( $\mu\text{m}$ )	240	380
D30 ( $\mu\text{m}$ )	194	343
D50 ( $\mu\text{m}$ )	165	230
D70 ( $\mu\text{m}$ )	118	175
D90 ( $\mu\text{m}$ )	80	110
UC	2.3	2.3



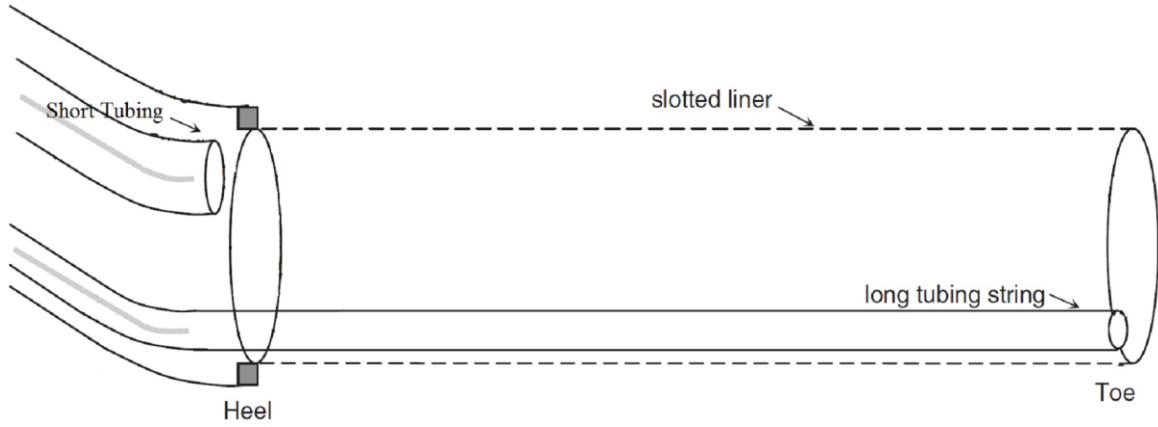


Figure 9-1. Schematic design of a typical SAGD producer well completion with dual tubing string completion

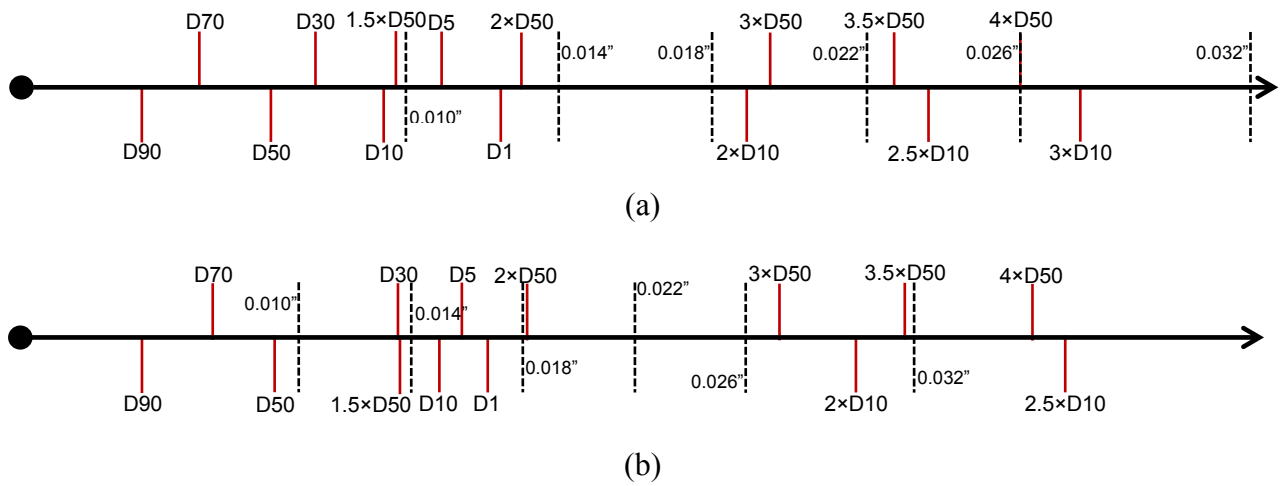
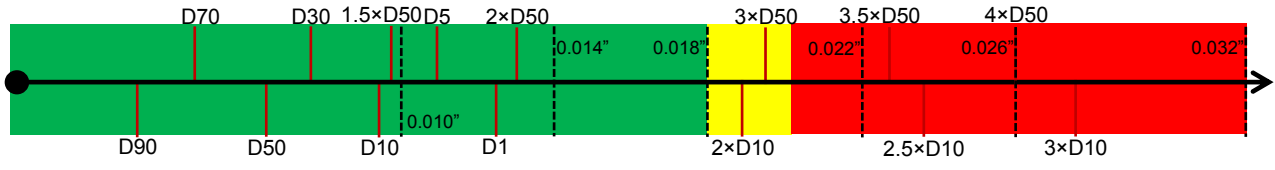
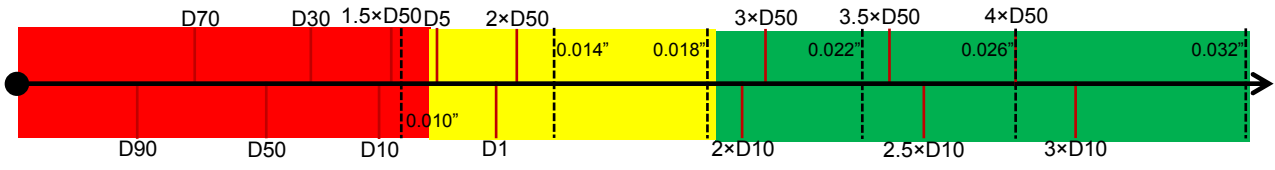


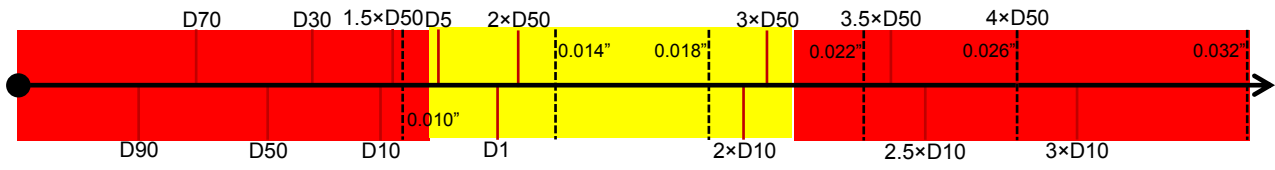
Figure 9-2. Linear x-axis representation of the PSD and slot sizes in tested coupons, (a) DC-II (b) DC-III



(a)

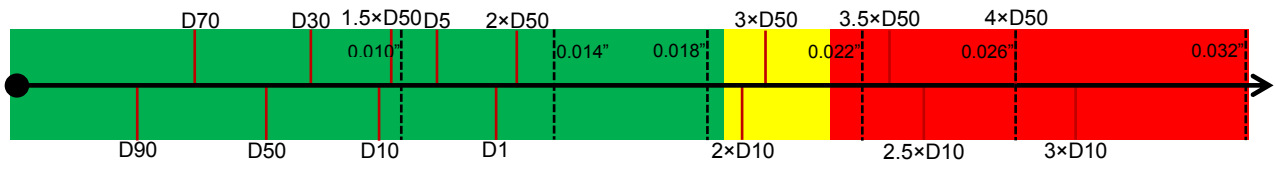


(b)

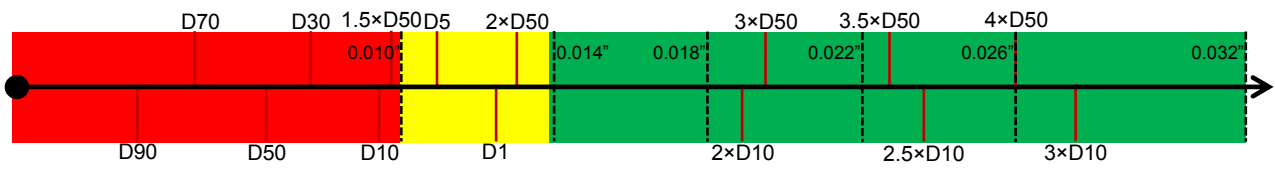


(c)

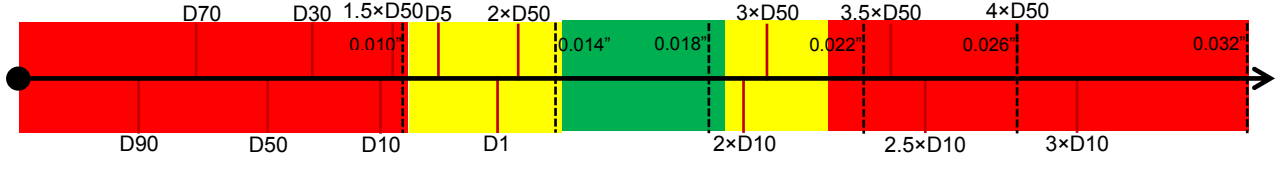
Figure 9-3. Slot window for DC-II for SPC=30, (a) sanding performance, (b) flow performance, (c) overall design window



(a)

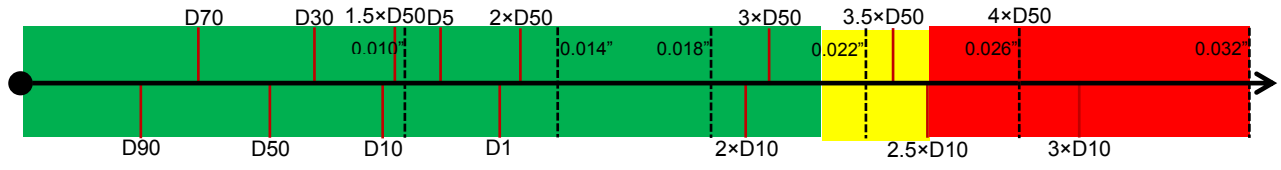


(b)

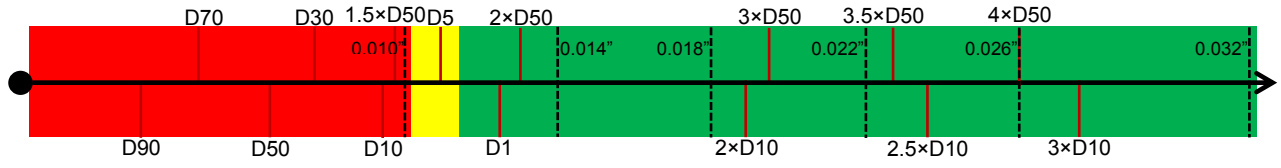


(c)

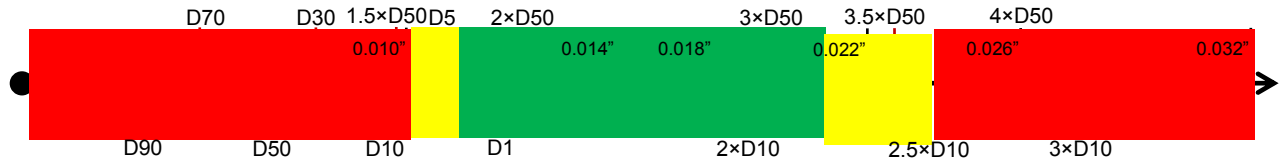
Figure 9-4. Slot window for DC-II for SPC=42, (a) sanding performance, (b) flow performance, (c) overall design window



(a)

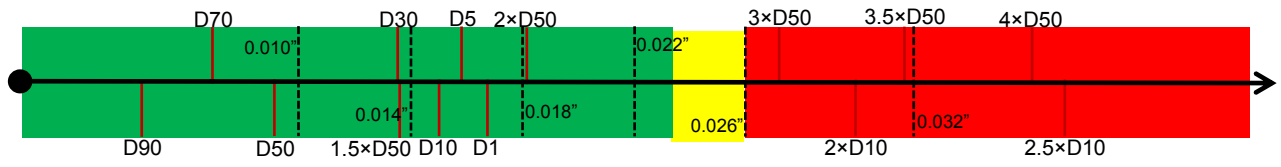


(b)

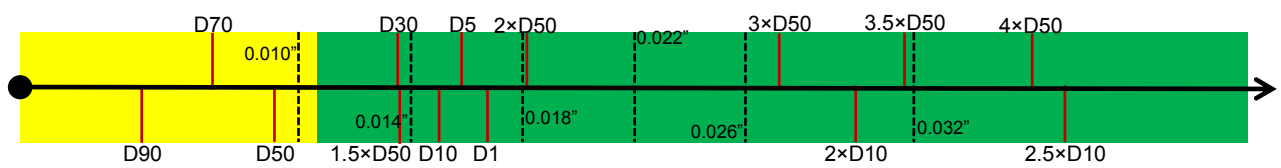


(c)

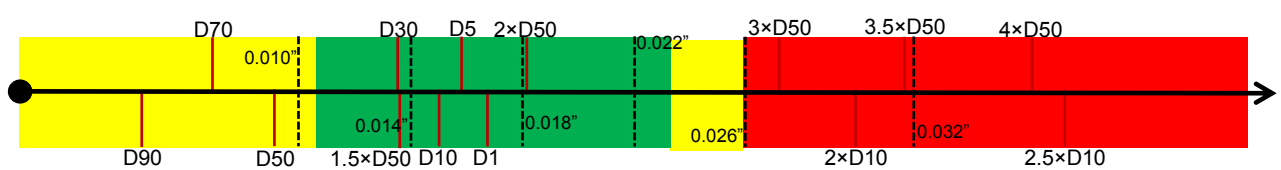
Figure 9-5. Slot window for DC-II for the SPC=54, (a) sanding performance, (b) flow performance, (c) overall design window



(a)

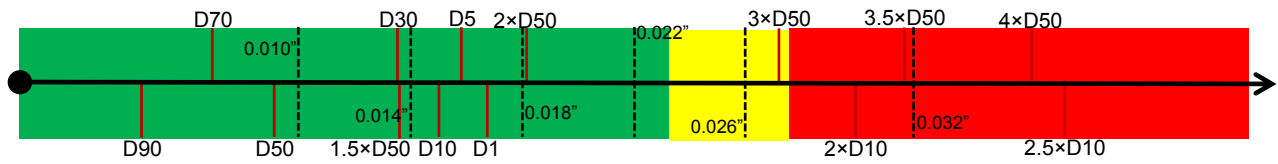


(b)

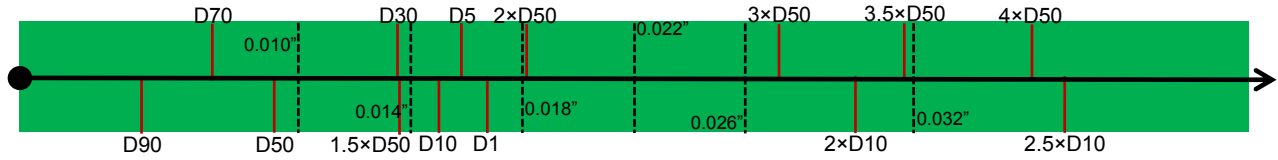


(c)

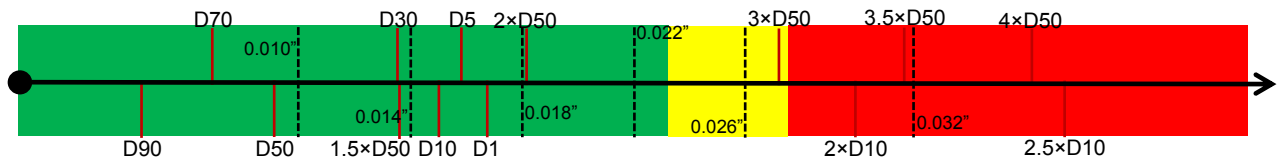
Figure 9-6. Slot window for DC-III for SPC=30, (a) sanding performance, (b) flow performance, (c) overall design window



(a)

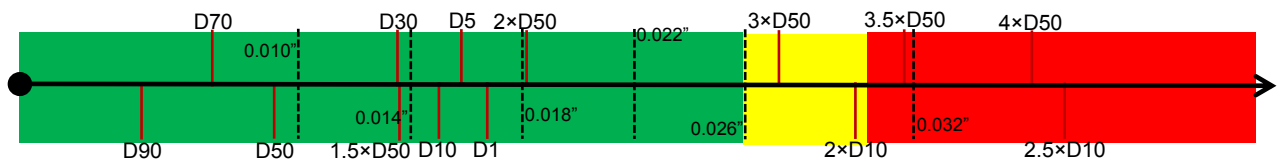


(b)

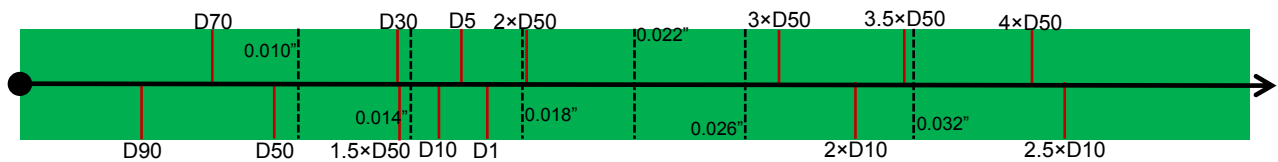


(c)

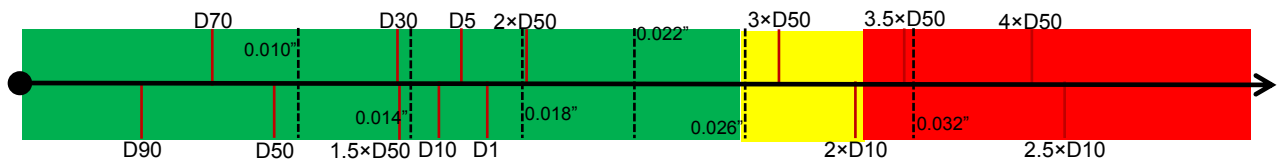
Figure 9-7. Slot window for DC-III for SPC=42, (a) sanding performance, (b) flow performance, (c) overall design window



(a)

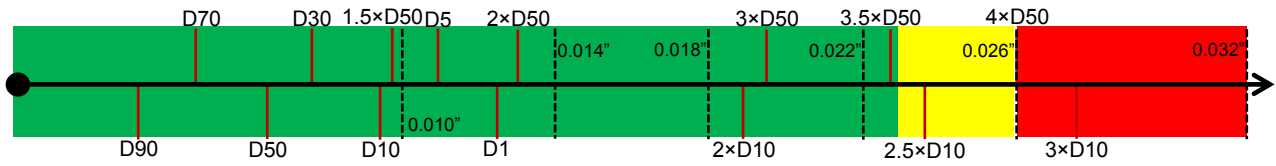


(b)

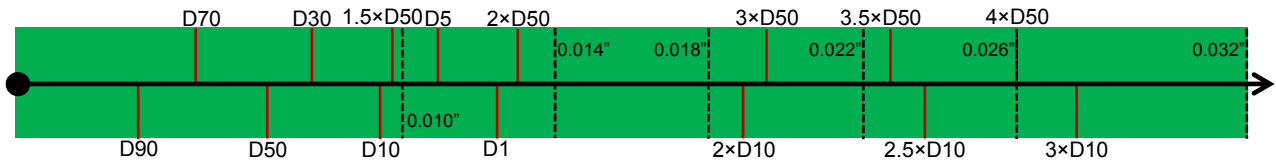


(c)

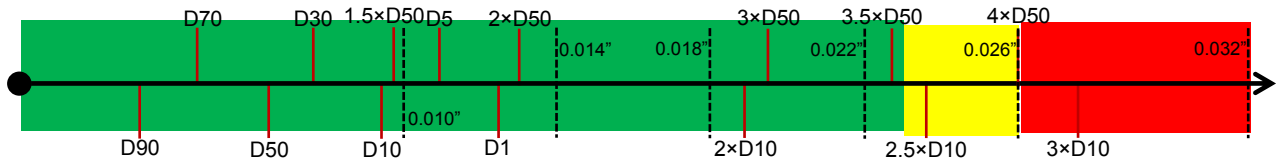
Figure 9-8. Slot window for DC-III for SPC=54, (a) sanding performance, (b) flow performance, (c) overall design window



(a)

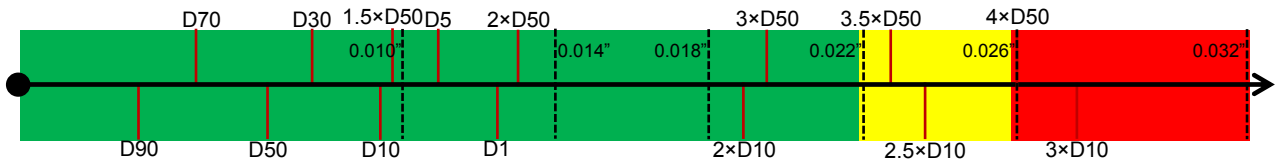


(b)

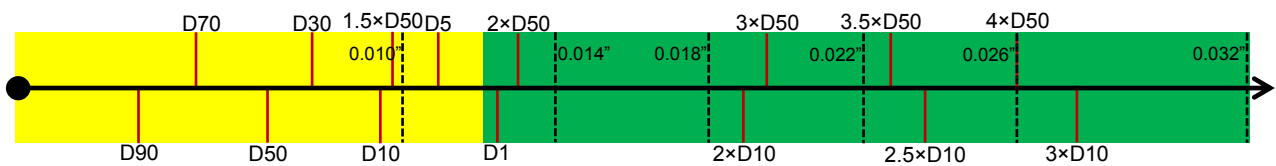


(c)

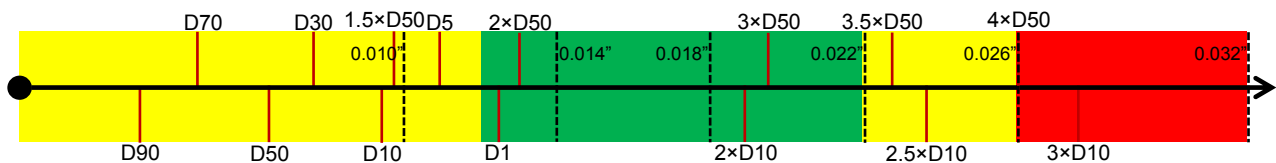
Figure 9-9. Slot window for DC-II and SPC=30 for low flow rate ( $<0.8$  bbl/day), (a) sanding performance, (b) flow performance, (c) overall design window



(a)

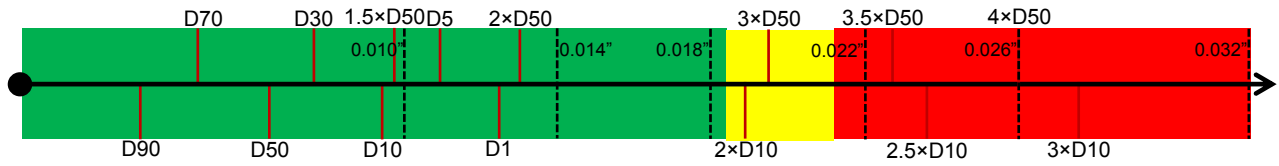


(b)

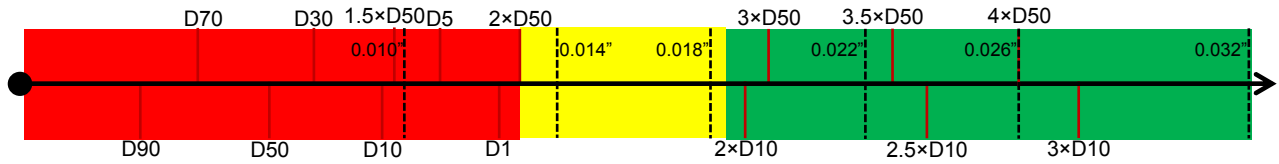


(c)

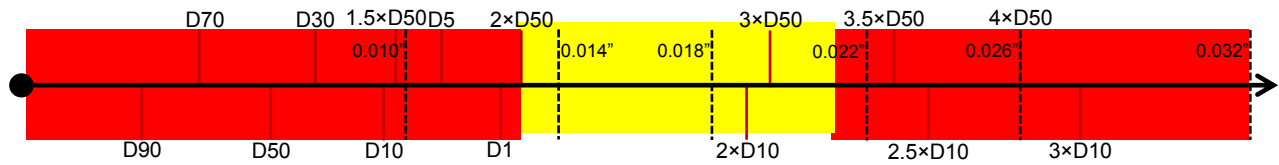
Figure 9-10. Slot window for DC-II and SPC=30 for moderate flow rate ( $0.8$  bbl/day  $< Q < 1.5$  bbl/day), (a) sanding performance, (b) flow performance, (c) overall design window



(a)

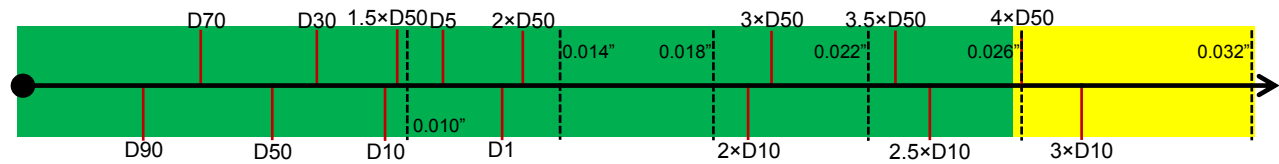


(b)

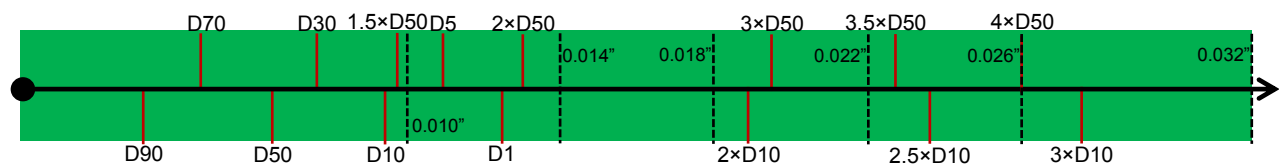


(c)

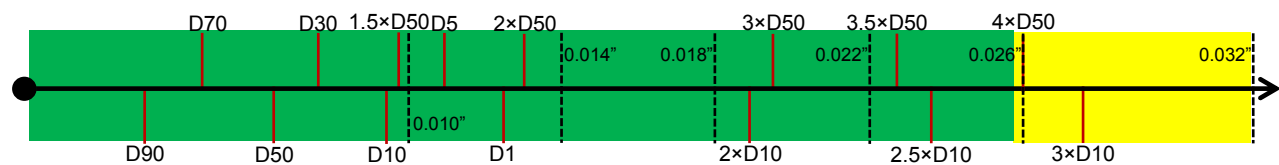
Figure 9-11. Slot window for DC-II and SPC=30 for aggressive flow rate (>1.5 bbl/day), (a) sanding performance, (b) flow performance, (c) overall design window



(a)

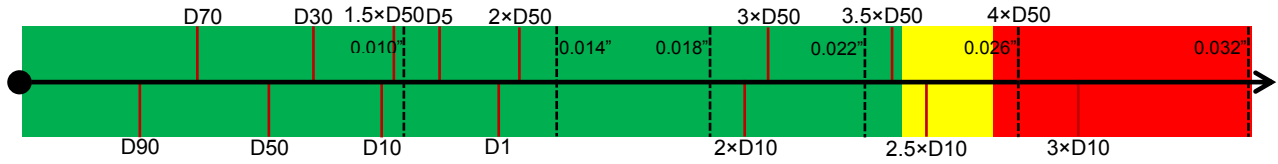


(b)

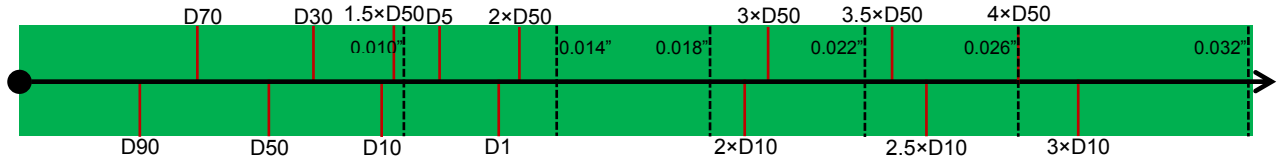


(c)

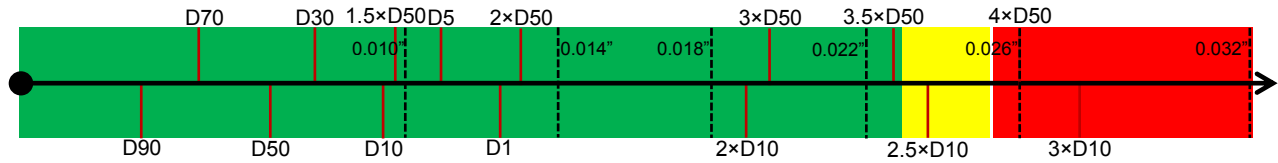
Figure 9-12. Slot window for DC-II and SPC= 42 for low flow rate (<0.8 bbl/day), (a) sanding performance, (b) flow performance, (c) overall design window



(a)

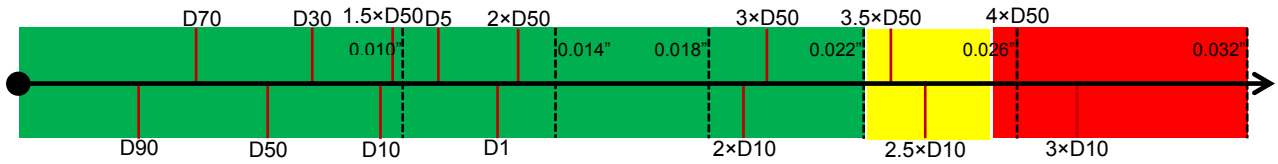


(b)

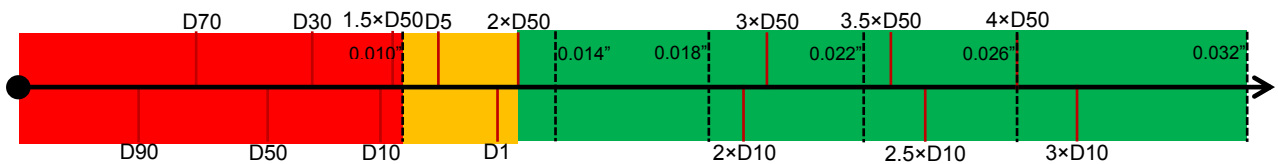


(c)

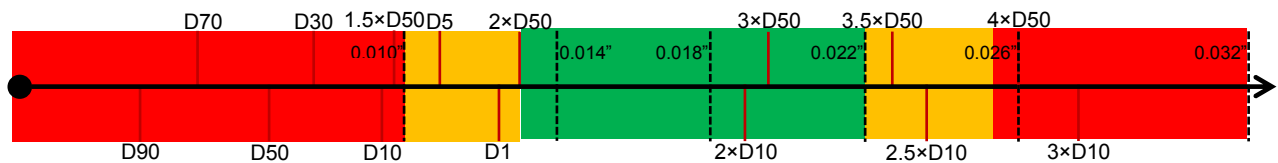
Figure 9-13. Slot window for DC-II and SPC= 42 for moderate flow rate ( $0.8 \text{ bbl/day} < Q < 1.5 \text{ bbl/day}$ ), (a) sanding performance, (b) flow performance, (c) overall design window



(a)

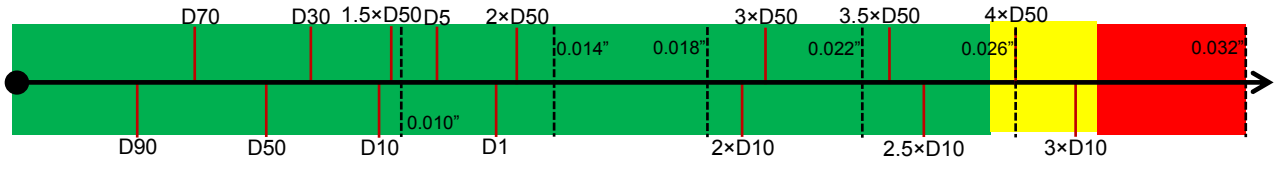


(b)

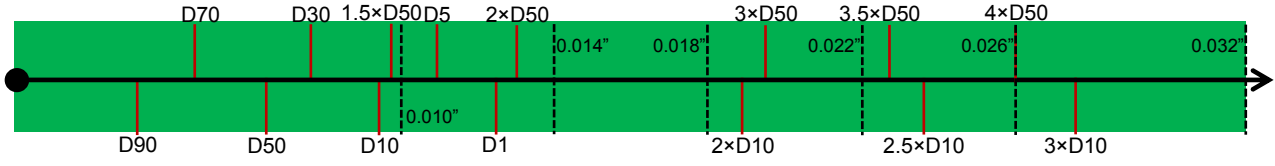


(c)

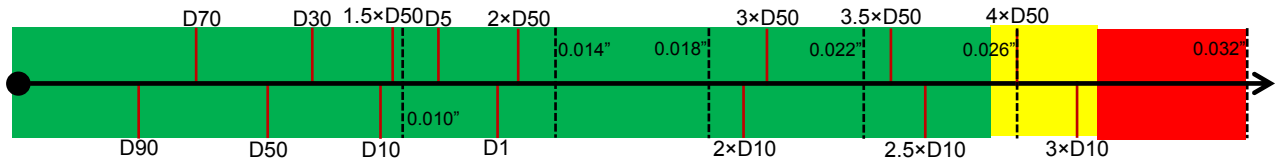
Figure 9-14. Slot window for DC-II and SPC= 42 for aggressive flow rate ( $> 1.5 \text{ bbl/day}$ ), (a) sanding performance, (b) flow performance, (c) overall design window



(a)

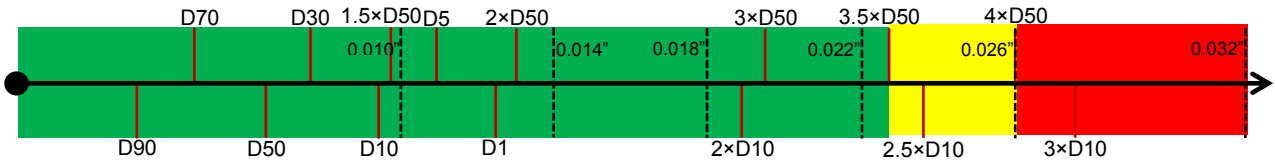


(b)

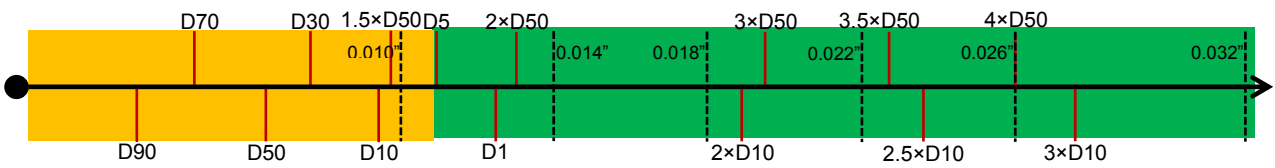


(c)

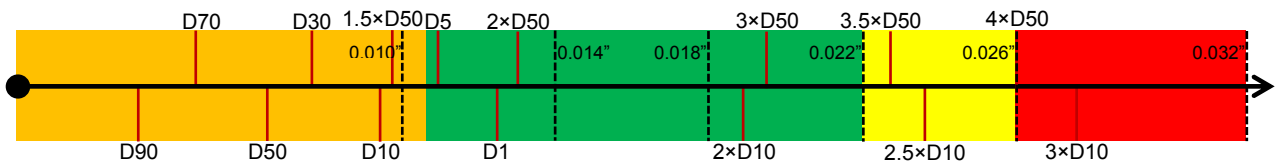
Figure 9-15. Slot window for DC-II and SPC= 54 for low flow rate (<0.8 bbl/day), (a) sanding performance, (b) flow performance, (c) overall design window



(a)



(b)



(c)

Figure 9-16. Slot window for DC-II and SPC= 54 for moderate flow rate (0.8 bbl/day<Q<1.5 bbl/day), (a) sanding performance, (b) flow performance, (c) overall design window



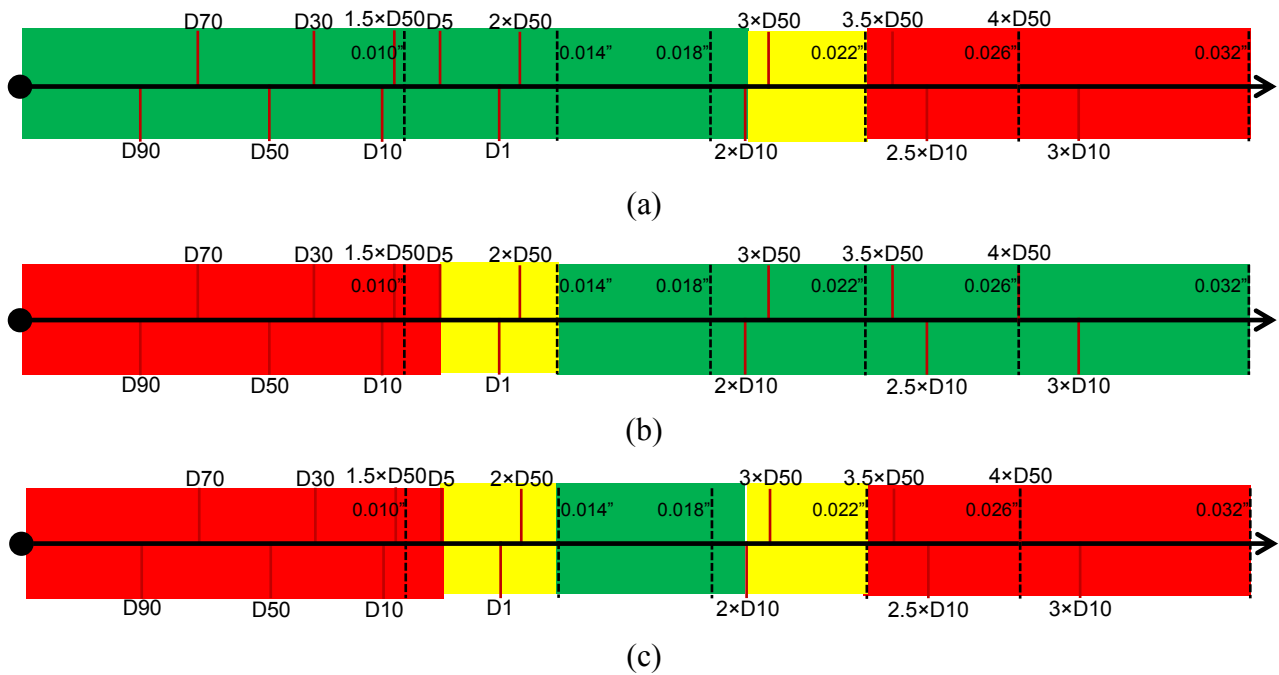


Figure 9-17. Slot window for DC-II and SPC= 54 for aggressive flow rate (>1.5 bbl/day), (a) sanding performance, (b) flow performance, (c) overall design window

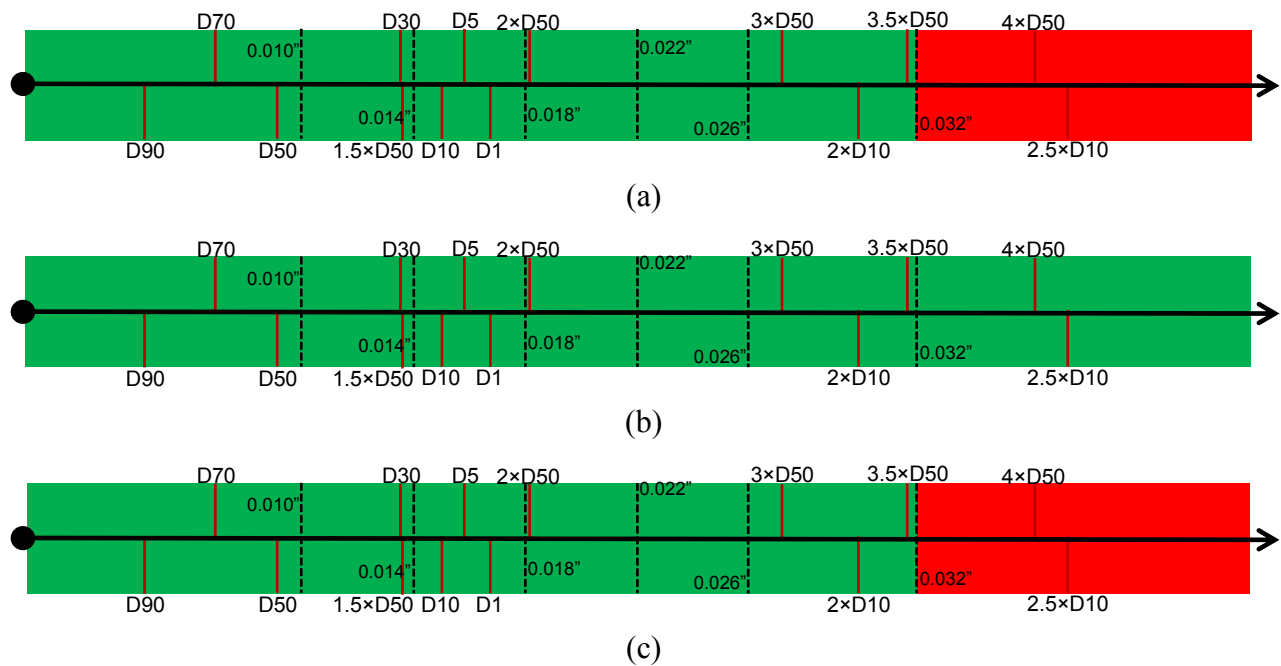


Figure 9-18. Slot window for DC-III and SPC=30 for low flow rate (<0.8 bbl/day), (a) sanding performance, (b) flow performance, (c) overall design window

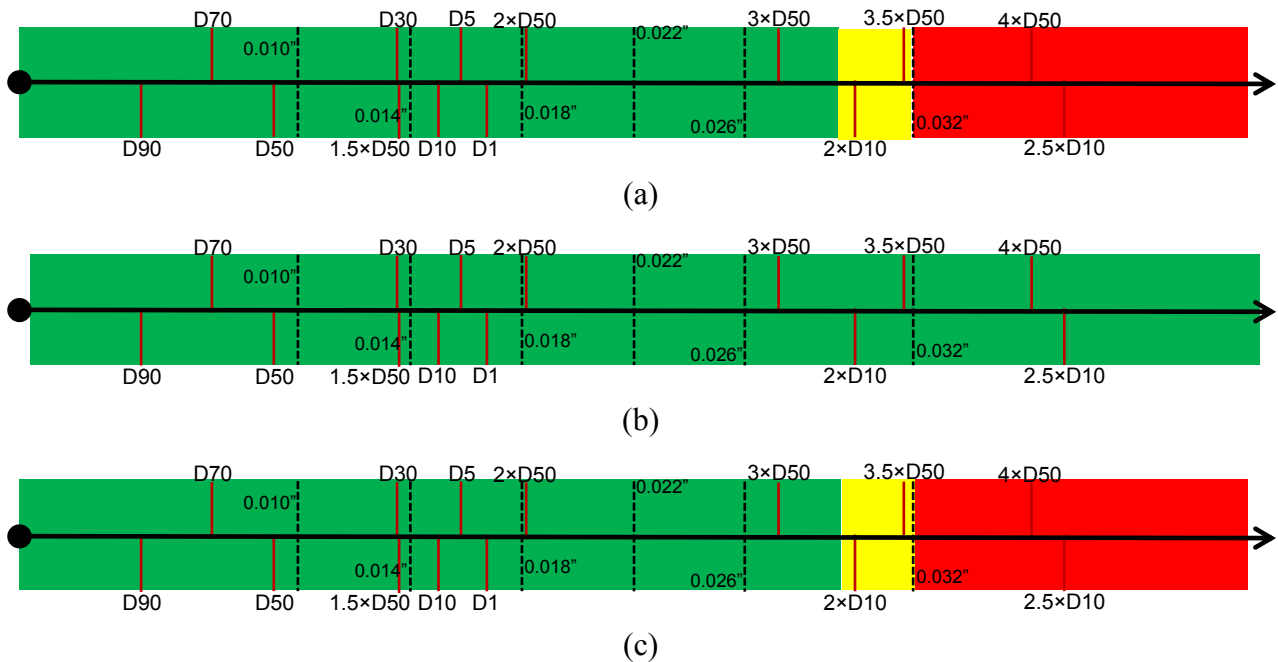


Figure 9-19. Slot window for DC-III and SPC=30 for moderate flow rate ( $0.8 \text{ bbl/day} < Q < 1.5 \text{ bbl/day}$ ), (a) sanding performance, (b) flow performance, (c) overall design window

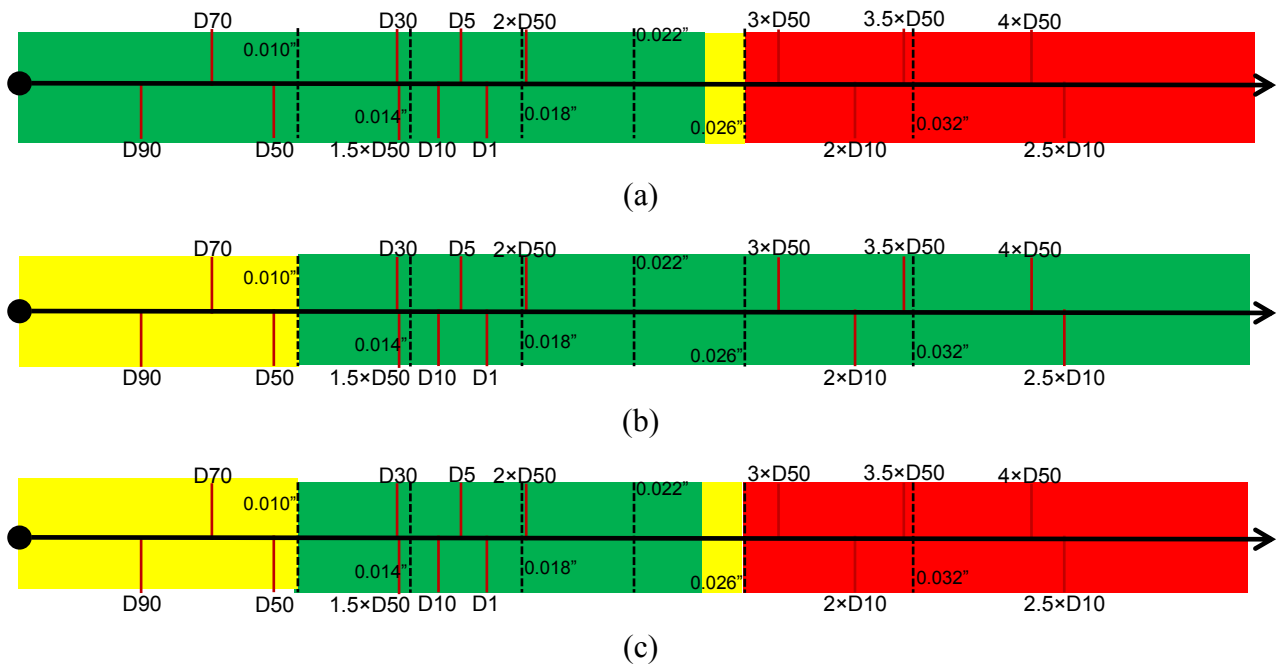


Figure 9-20. Slot window for DC-III and SPC=30 for aggressive flow rate ( $> 1.5 \text{ bbl/day}$ ), (a) sanding performance, (b) flow performance, (c) overall design window

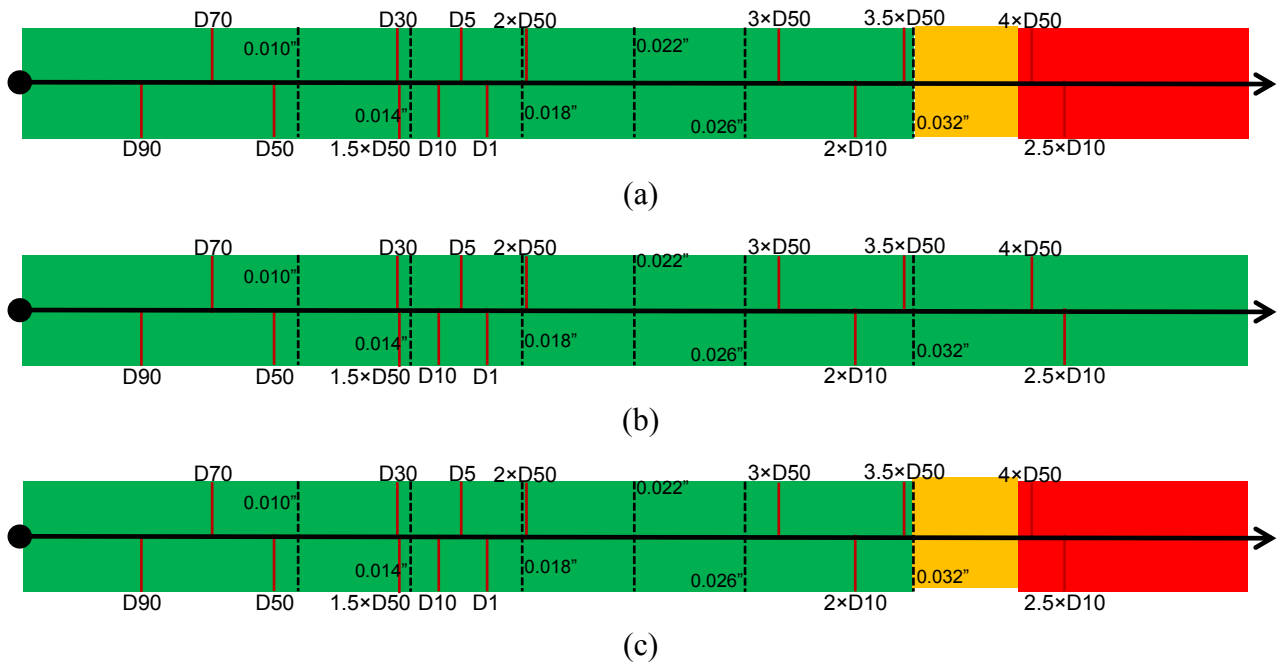


Figure 9-21. Slot window for DC-III and SPC=42 for low flow rate (<math><0.8 \text{ bbl/day}</math>), (a) sanding performance, (b) flow performance, (c) the overall design window

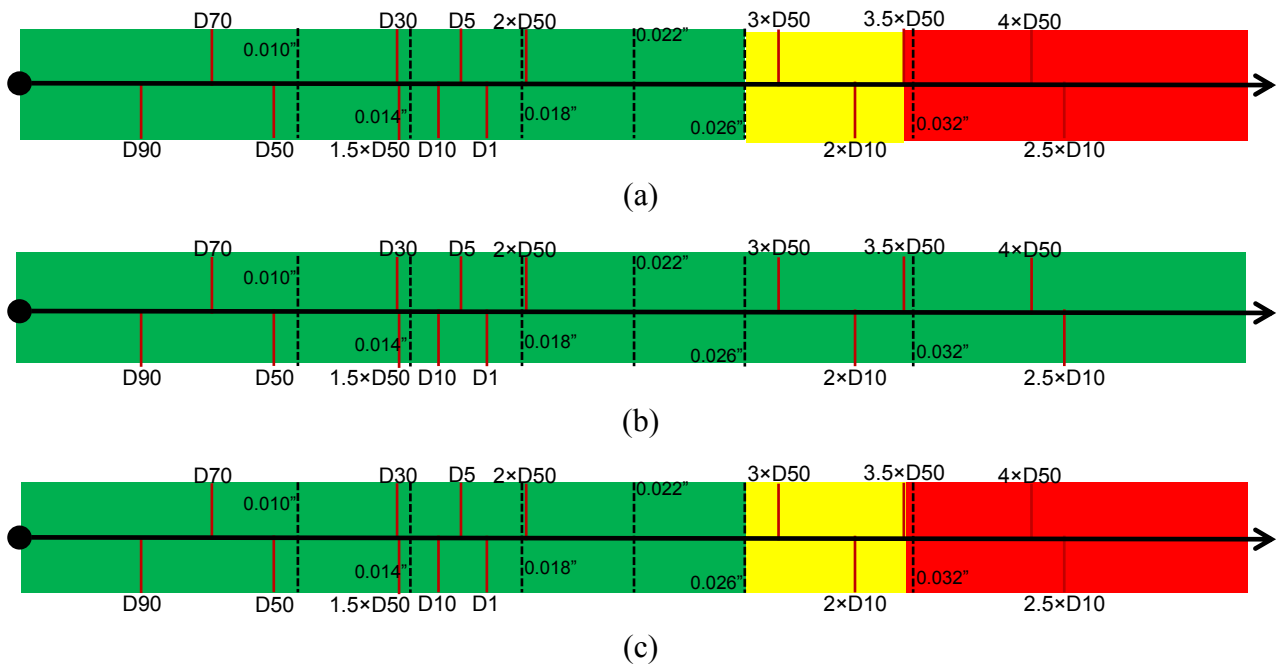


Figure 9-22. Slot window for DC-III and SPC=42 for moderate flow rate (<math>0.8 \text{ bbl/day} < Q < 1.5 \text{ bbl/day}</math>), (a) sanding performance, (b) flow performance, (c) overall design window

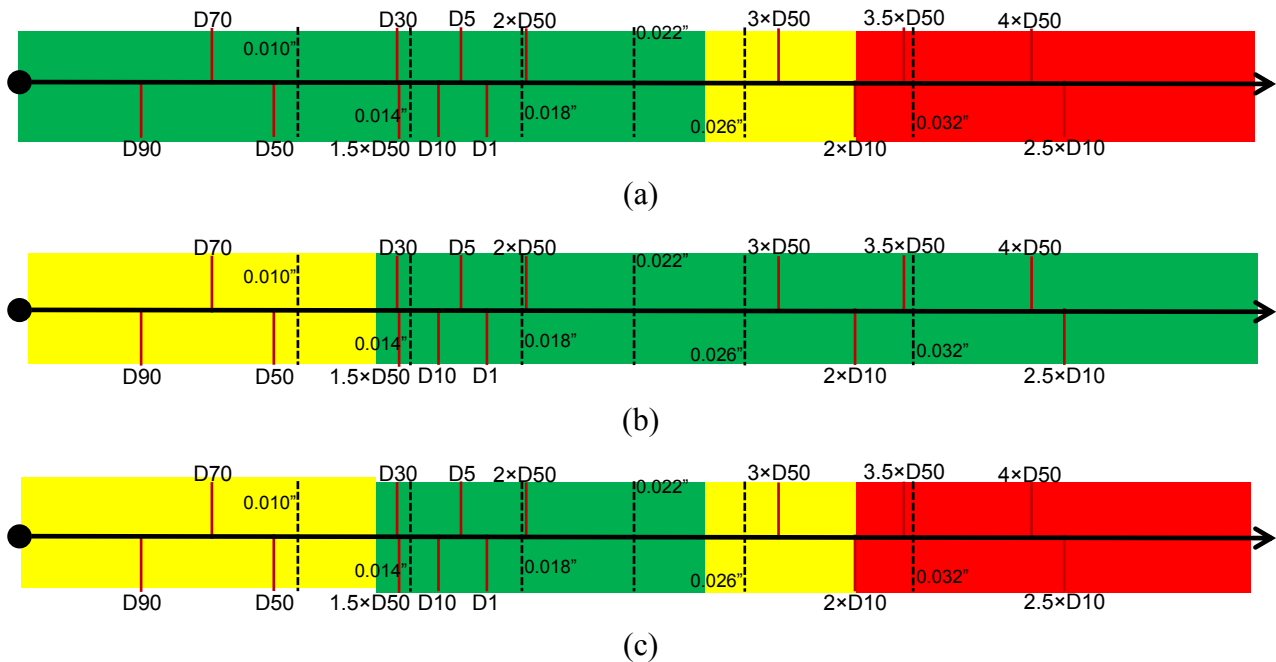


Figure 9-23. Slot window for DC-III and SPC=42 for aggressive flow rate (>1.5 bbl/day), (a) sanding performance, (b) flow performance, (c) overall design window

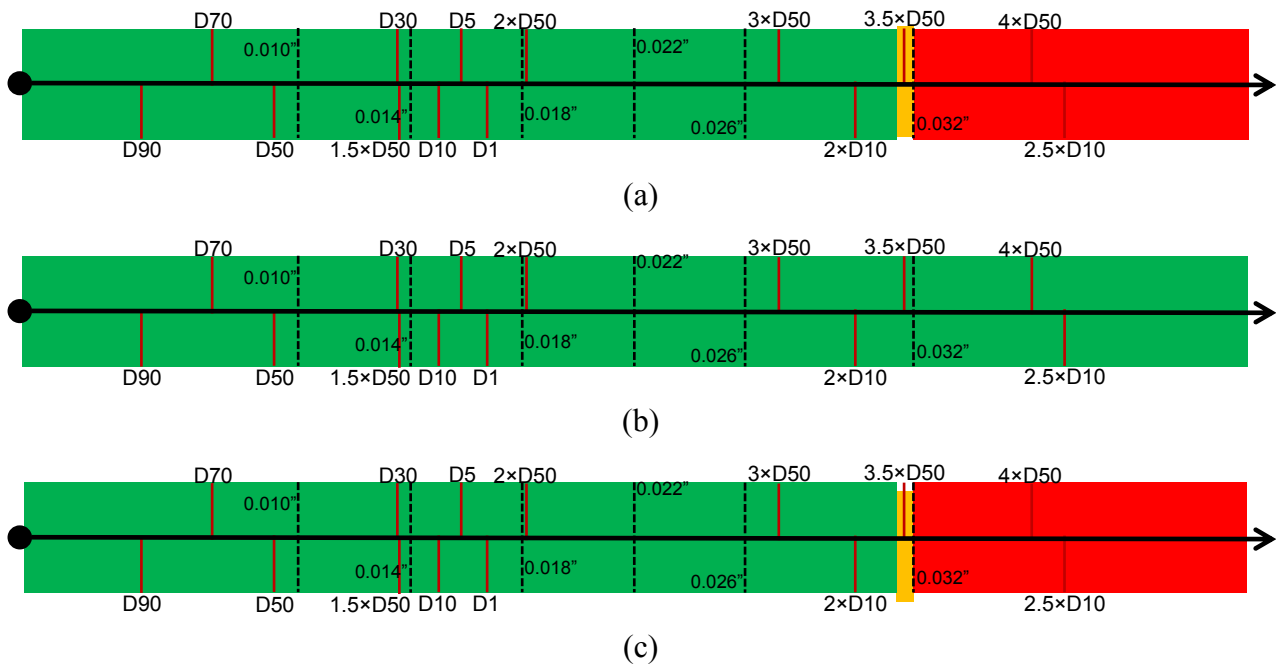


Figure 9-24. Slot window for DC-III and SPC=54 for low low flow rate (<0.8 bbl/day), (a) sanding performance, (b) flow performance, (c) overall design window

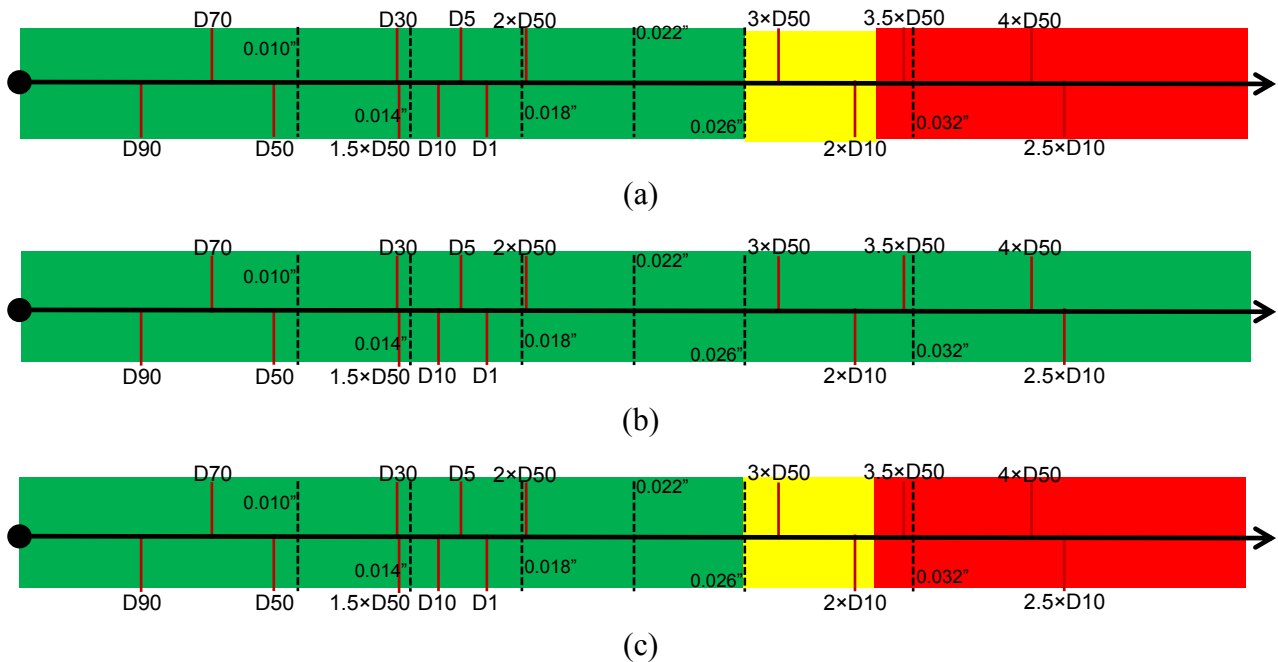


Figure 9-25. Slot window for DC-III and SPC=54 for moderate flow rate ( $0.8 \text{ bbl/day} < Q < 1.5 \text{ bbl/day}$ ), (a) sanding performance, (b) flow performance, (c) overall design window

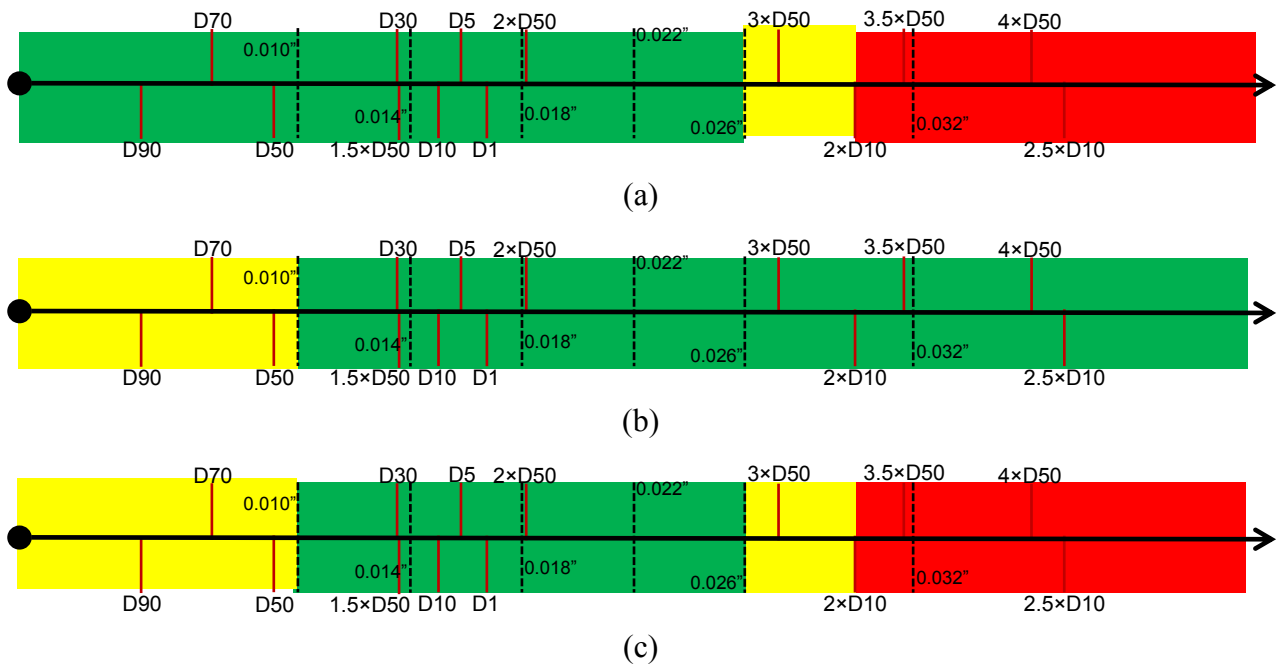


Figure 9-26. Slot window for DC-III and SPC=54 for aggressive flow rate ( $>1.5 \text{ bbl/day}$ ), (a) sanding performance, (b) flow performance, (c) overall design window

## CHAPTER TEN: CONCLUSIONS AND FUTURE WORKS

### 10.1 Main results

This thesis describes a detailed large-scale experimental procedure to assess the role of slot width and slot density on the performance of slotted liners in SAGD operations. The procedure is used to develop a set of criteria for the design of slotted liners in SAGD wells.

The research began by characterizing oil sand samples from the McMurray Formation and replicating the PSD, particle shape, and particle composition of oil sands with a commercial mix of sands and fines. Next, a series of mechanical tests were performed to verify the agreement between the mechanical properties of replicated and corresponding real oil sands samples.

The replicated sand packs were used in large-scale sand retention tests to assess the performance of slotted liners. Testing results clarify the role of slot width and slot density on sand production, retained permeability and plugging tendency. It was found that the produced sands from slotted liners are slightly finer than the original sand pack. This finding is important to consider in those experimental efforts that use bailed samples or separator sands for the liner design. Further, shape analysis of produced sands showed that the produced sands from narrower slots have a slightly different shape than the original sand pack. Observations indicate, however, the shape of produced sand becomes closer to the shape of the original sand pack as the slots become wider. Results from both PSDs indicate spherical particles are more prone to be produced.

An important outcome of this research is the observed modes of sand production. This thesis classifies the sanding mode to three. In Mode-I (initial sanding/spurt sanding), there is an initial occurrence of sanding at the start of the test at low flow rates. Mode II is flow rate dependent transient sanding. For each increase in flow rate, sanding rate is observed to spike and then start a declining trend to zero with the formation of stable sand bridges behind the slots. It is noted that the spike in sanding rate is higher with each increase in the flow rate for equal steps of flow rate increase. Mode III consists of continuous sanding beyond a critical flow rate. No stable sand bridges can form for Mode III sanding. It is evident that fluid flow rate, through seepage drag force, plays a critical role in forming and destabilizing the sand bridge and sand production. However, the literature has been silent on the combined role of slot width and density on the amount and mode of sanding.

Testing observations also indicate the important role of slot width and density on fines migration, production, and accumulation behind the slots. Fines accumulation behind the slots is seen to decrease for wider slots and lower slot densities. Results, however, indicate a higher sensitivity for the fines migration, accumulation, and production to the slot width than the slot density.

Another observation is the inverse effect of flow rate on retained permeability. Results also indicate the influence of slot density and width on retained permeability. Higher slot width and slot density result in the highest retained permeability for the same flow rate. Again, retained permeability is seen to be more sensitive to the slot width than density.

By combining the effects of slot density, slot width, flow rate, and sanding mode, this thesis presents a new set of graphical design criteria for slotted liners in SAGD. The design criteria are PSD-, slot density-, and flow rate-specific. This is a considerable improvement over existing criteria which do not account for the PSD shape, slot density, and flow rate.

## **10.2 Main contributions**

This research started with designing and building a new sand retention test (SRT) facility to study the role of slot density and slot size on screen performance indicators in sand production, retained permeability. Testing results improve the physical understanding of several field observations and can be used for improved sand control design in SAGD projects.

### ***10.2.1 Sand production***

Test results show the dependency of bridge stability, hence sanding, on seepage drag forces. This explains excessive sand production observed in the field when exercising aggressive production practices which result in Mode-II or Mode-III sanding, excessive sanding after a period of well cool down (at lower temperature the crude will have higher viscosity, which increases the drag forces at the same flow rate), and steam breakthrough. Sudden increase in pump speed also affects the drawdown in the pump vicinity leading to excessive drag forces, hence, increased level of sanding.

### ***10.2.2 Plugging***

Testing results indicate narrower slots lead to more pore plugging than wider slots, hence, lower wellbore productivity. Evidently, a drastic increase in fines concentration above the screen can

lead to a drastic decrease in retained permeability. On the contrary, fines accumulation, hence reduced productivity, can be negligible for wider slots.

It is evident that fluid flow rate and ionic composition of the producing fluid (pH and salinity) play a critical role in mobilizing and transporting the fines. However, the role of slot width and density seems to also be crucial. The concentration and size of produced fines are highly affected by the slot size and density.

As the slot width increases, the size and concentration of produced fines increase and the concentration of the fines above the slotted liner reduces. As the slot density increases, the concentration and size of produced fines decrease. The increase in slot density also reduces the concentration of the fines above the screen. This implies that for a given sand, increasing the slot width and slot density reduces the plugging tendency of the screen due to the fines migration.

### ***10.2.3 Sanding Criteria***

This thesis presents a new set of design criteria for slotted liners. Unlike the existing criteria which only specify a lower and upper bound for the slot width based on a certain D value (e.g. D50), the proposed criteria involve several factors into consideration, which have been neglected in the past. The proposed criteria are presented for different classes of PSD and relate to slot density, and fluid flow rate. The aim of the proposed criteria is to keep the plugging and produced sand within acceptable limits.

## **10.3 Recommendations for further research**

The following future research is recommended to further improve the design criteria for slotted liner design.

### ***10.3.1 Investigate the effect of multiphase flow***

It is evident the flow of multi-phase flow impacts the fines migration and sand production. Multiphase flow affects sanding due to capillarity (Bennion et al. 2008) and several other research in sanding from conventional wells (Vaziri et al. 2002; Han and Dusseault 2002). Also, the multi-phase flow will affect the fines mobilization and transport, hence, pore plugging in the screen vicinity.

### ***10.3.2 Effect of PSD curve on sand production and plugging***



The PSD of the sand pack highly affects the amount of produced sand as well as plugging. It has been found that PSD with higher uniformity coefficient produces more sand and possesses lower bridge stability. Two PSDs were used in this research; however, to generalize the design criteria, the testing program must include additional PSD curves.

### ***10.3.3 Effect of stress on sand production and plugging***

Stress buildup around the liner affects the frictional strength of the sand, hence, the stability of the bridge. Furthermore, the stress build up reduces the porosity and permeability, hence, affects the magnitude of fluid drag forces near the liner. Such changes affect the sanding, fines migration, and retained permeability.

### ***10.3.4 Effect of particle shape on sand production and plugging***

The testing in this research showed that the shape of produced particles is affected by the slot width. However, both PSDs used in the testing program possessed similar particle shapes, disallowing the study of the role of particle shape on sanding and plugging. Particle shape influences the inter-particle friction, hence, the sand bridge stability. Further, particle shape impact the sand compaction at higher stress, and also affect the porosity and permeability of the sand pack. The use of sand packs with different particle shapes can clarify this potential effect.

### ***10.3.5 Effect of clay composition on the pore plugging***

The characterization work showed the variability of the clay composition in the two studied wells. The testing program used sand packs with clay content with the composition of 80% kaolinite and 20% illite. However, there is a notable amount of smectite in the McMurray Formation. It is believed that smectite possesses a higher plugging potential than kaolinite and illite. Also, the sensitivity of smectite to pH and salinity is higher than kaolinite and illite, which lead to clay mobilization at lower pH and higher salinity.

## REFERENCES

- Abram, M., and Cain, G. 2014. Particle-Size Analysis for the Pike 1 Project, McMurray Formation. *J Can Pet Technol* , **53**(6): 339-354. SPE-173890-PA.
- Abrams, A. 1977. Mud Design to Minimize Rock Impairment Due to Particle Invasion. *J Pet Technol*, **29**(5): 587-892.
- Agbangla, C., Climent, E., and Bacchin, P. 2012. Experimental investigation of pore clogging by microparticles: Evidence for a critical flux density of particle yielding arches and deposits. *Sep Purif Technol*, **101**(13): 42-48.
- Alcorn, W., and Teague, U. 1937. Bottom-Hole Well-Completion Methods in the Gulf Coast. Presented at the spring meeting, Southern District, Division of Production, Dallas, Texas. API-37-030
- Al-Raoush, R. 2007. Microstructure Characterization of Granular Materials. *Physica A.*, **377**(2): 545-558.
- Asadi, M., Penny, S. 2000. Sand Control Screen Plugging and Cleanup. Presented at the SPE Asia Pacific Oil and Gas Conference and Exhibition held in Brisbane, Australia. 16-18 October. SPE 64413-MS
- ASTM D3080 / D3080M-11:2011. Standard Test Method for Direct Shear Test of Soils Under Consolidated Drained Conditions*, ASTM International, West Conshohocken, PA.
- Ballard, T. 2011. Controlling Sand, In and Out of the Laboratory. *J Pet Technol*, **63**(10):20-21.
- Ballard, T., and Beare, S. 2003. Media Sizing for Premium Sand Screens: Dutch Twill Weaves. Presented at the SPE European Formation Damage conference, Hague, Netherland, 13-14 May. SPE 82244-MS
- Ballard, T., and Beare, S. 2006. Sand Retention Testing: The More You Do, the Worse It Gets. Presented at SPE International Symposium and Exhibition on Formation Damage Control, Lafayette, LA, 15–17 February. SPE 98308.
- Ballard, T., and Beare, S. 2012. An Investigation of Sand Retention Testing With a View To Developing Better Guidelines for Screen Selection. Presented at the International Symposium

and Exhibition on Formation Damage, Lafayette, Louisiana, USA, 15–17 February 2012. SPE 151768.

Ballard, T., Beare, S., and Wigg, N. 2016. Sand Retention Testing: Reservoir Sand or Simulated Sand - Does it Matter? Presented at the SPE Formation Damage Control Symposium. Lafayette. Louisiana. USA. 25-27 February. SPE 178966-MS

Ballard, T., Kageson-Loc, N., and Mathison, A. M. 1999. The development and application of a method for the evaluation of sand screens. Presented at SPE European Formation Damage Conference, The Hague, 31 May-1 June. SPE 54745-MS.

Barkman, H., and Davidson, H. 1972. Measuring Water Quality and Predicting Well Impairment. *J Pet Technol*, 24(7): 865-873.

Bedrikovetsky, P., Tran, K., Van den Broek, T. et al. 2002 Damage characterization of deep bed filtration from pressure measurements. Presented at International Symposium and Exhibition on Formation Damage Control, 20-21 February, Lafayette, Louisiana. SPE- 73788-MS

Bedrikovetsky, P., Siqueira, P., Furtado, C. and Souza, A. 2010. Modified Particle Detachment Model for Colloidal Transport in Porous Media. *Transport Porous Med*, 86(2):1-31.

Bennion, B., Gittins, S., Gupta, S. et al. 2008. Protocols for Slotted Liner Design for Optimum SAGD Operation. Presented at the Canadian International Petroleum Conference/SPE Gas Technology Symposium Joint Conference, Calgary, Alberta, 17 -19 June. SPE 130441-MS

Bennion, B., Thomas, B., Bennion, D. et al. 1995. Underbalanced Drilling and Formation Damage-Is It a Total Solution? *J Can Pet Technol*, 34(9): 34-41.

Bernardo, F., Saraiva, P., and Pistikopoulos, E. 2000. The inclusion of Information Costs in Process Design Optimization Under Uncertainty. *J Computer and chem Eng*, 24(2000):1695-1701.

Bhattacharjee, S. 2011. *Oil Sands: A Bridge between Conventional Petroleum and a Sustainable Energy Future*, in *Towards Sustainable Clean Energy*, Ed. S. Basu, McGraw Hill.

Binbin Ding, B., Li, C. and Dong, X. 2015b. Percolation-based model for straining-dominant deep bed filtration. *Sep Purif Technol*, 147(2015): 82-89.

- Blott, S.J., and Pye, K. 2001. GRADISTAT: a Grain Size Distribution and Statistics Package for the Analysis of Unconsolidated Sediments. *Earth Surf Process Landf*, **26**, 1237-1248.
- Blunt, J. M., Bijeljic, B., Dong, et al. 2013. Pore-scale imaging and modeling. *Adv Water Resour*, **51**(2013):197-216.
- Boston, W.G., Brandner, C.F. and Foster, W.R. 1969. Recovery of Oil by Water flooding from an Argillaceous, Oil-Containing Subterranean Formation. US Patent 37409567 October.
- Bowden, P., Tabor, D. 1950. The friction and lubrication of solids, Part I. Clarendon Press, Oxford.
- Bowden, P., Tabor, D. 1964. The friction and lubrication of solids, Part II. Clarendon Press, Oxford.
- Bowman, E.T., Soga, K. and Drummond, T. W. 2000. Particle Shape Characterization Using Fourier Analysis. *Geotechnique*, **51**(6):545–554.
- Brown, M. 1998. Full Scale Attack Review. The BP Technology Magazine (October-December 1998): 30-32;
- Buckley, J.S. and Morrow, N.R. 2010. Improved Oil Recovery by Low Salinity Water- flooding: A Mechanistic Review. Presented at the 11<sup>th</sup> International Symposium on Reservoir Wettability. The university of Calgary, Calgary, Alberta, Canada, 6–9 September.
- CAPP (2011) The Facts on Oil Sands. Upstream Dialogue. Retrieved from: <http://www.capp.ca/Upstream Dialogue/Oilsands/Pages/default.aspx>.
- Carlson, M. 2003. SAGD and Geomechanics. *J Can Pet technol*, **42**(6):19-25.
- Carrigy, M. 1966. *Lithology of the Athabasca Oil Sands*. Bulletin. 18, Edmonton: Research Council of Alberta.
- Cerda, M. 1988. Mobilization of Quartz Fines in Porous Media. *Clays Clay Miner.*, **36**(6):491-497.
- Chanpura, R., Fidan, S., Mondal, S. et al. 2011b. Advancements in Screen Testing, Interpretation and Modeling for Standalone Screen Applications. Presented at the SPE European Formation Damage Conference, Noordwijk, The Netherland, 7-10 June. SPE 143731-MS

- Chanpura, R., Fidan, S., Sharma, M. et al. 2012a. New Analytical and Statistical Approach for Estimating and Analyzing Sand Production through Wire-Wrap Screens during a Sand-Retention Test. *SPE Drill & Compl*, **27**(3):416-426.
- Chanpura, R., Hodge, R., and Andrews, J. 2011a. A Review of Screen Selection for Standalone Applications and a New Methodology. *SPE Drill & Compl*, **26**(1): 84-95. SPE-127931-PA.
- Chanpura, R., Mondal, S., Andrews, S. et al. 2013. New Analytical and Statistical Approach for Estimating and Analyzing Sand Production Through Plain Square-Mesh Screens During a Sand-Retention Test. Presented at the SPE International symposium and Exhibition on Formation, 15-17 February, Lafayette, LA, USA. SPE 151637-MS
- Chanpura, R., Mondal, S., Sharma, M. et al. 2012b. Unraveling the Myths in Selection of Standalone Screens and a New Methodology for Sand Control Applications. Presented at the SPE Annual Technical Conference and Exhibition, 8-10 October, San Antonio, Texas, USA. SPE 158922-MS
- Chenault, L., 1938. Experiments on Fluid Capacity and Plugging of Oil-Well Screens. American Petroleum Institute. Presented at Eighth Mid-Year Meeting. Wichita, Kansas. API-38-293
- Cheng, C. and Chen, X. 2007. Evaluation of methods for determination of hydraulic properties on an aquifer-aquitard system hydrologically connected to river, *Hydrogeol J*, **15**(4): 669–678.
- Cho, G. Dodds, J. and Santamarina, C. 2006. Particle Shape Effects on Packing Density, Stiffness, and Strength; Natural and Crushed Sands. *J Geotech Geoenviron Eng.*, **132**(5):591-602.
- Civan, F. 2007. *Reservoir Formation Damage*. Second Edition, Burlington: Gulf Professional Publishing.
- Clayton, C. Xu, M., and Bloodworth, A. 2006. A Laboratory Study of the Development of Earth Pressures Behind Integral Bridge Abutments. *Geotechnique*. **56** (8):561–572.
- Coberly, C., 1937. Selection of Screen Opening for Unconsolidated Sands. *API Drilling and production Practice*, (1937):189-201
- Constien, V., and Skidmore, V. 2006. Standalone Screen Selection Using Performance Mastercurves. P at the International Symposium and Exhibition on Formation Damage Control, Lafayette, Louisiana, USA, 15-17 February. SPE- 98363-MS

- Corapcioglu, Y., Abboud, M., and Haridas, A. 1987. Governing equations for particle transport in porous media. *Adv in Trans Phenom in Porous Med*, **128**: 269-342.
- Cowie, B.R. 2013. *Stable Isotope and Geochemical Investigation into the Hydrogeology and Biogeochemistry of Oil Sands Reservoir Systems in Northeastern Alberta, Canada*, Doctoral Thesis, University of Calgary (2013 September).
- Dall'Acqua, D. Smith, T., and Kaiser, T. 2005. Post-Yield Thermal Design Basis for Slotted Liner. Presented at the International Thermal Operation and Heavy Oil Symposium, Calgary, Alberta, 1-3 November. SPE 97777-MS
- Dall'Acqua, D. Turconi, G., Monterrubio, I. et al. 2010. Development of an Optimized Tubular Material for Thermal Slotted Liner Completions. *J Can Pet Technol*, **49**(2):15-22. SPE 132640-PA
- Das, S., 2007. Application of thermal recovery processes in heavy oil carbonate reservoirs. Presented at the SPE Middle East Oil & Gas Show and Conference, Kingdom of Bahrain, 11–14 March. SPE 105392-MS
- De Zwart, A. 2007. Investigation of Clogging Processes in Unconsolidated Aquifers near Water Supply Wells. Delft University of Technology, Delft, The Netherland.
- Dean, J. 1938. Drilling and Production Problems in the Wilmington Field. Presented at spring meeting Pacific Coast District, Division of the Production, Los Angeles, California. API-38-267.
- Devere-Bennett, N. 2015. Using Prepack Sand-Retention Tests (SRT's) to Narrow Down Liner/Screen Sizing in SAGD Wells. Presented at the SPE Thermal Well Integrity and Design Symposium, Banff, Alberta, 23-25 November. SPE 178457-MS
- Diepenbroek, M., Bartholoma, A., and Ibbeken, H. 1992. How Round is Round? A New Approach to the Topic 'Roundness' by Fourier Grain Shape Analysis. *Sedimentology*, **39**:411-422.
- Ding, B., Li, C., Zhang, M. et al. 2015a. Effects of pore size distribution and coordination number on the prediction of filtration coefficients for straining from percolation theory. *Chem Eng. Sci*, **127**(2015):40-51.

- Doan, L., Baird, H., Doan, Q. et al. 1999. An Investigation of the Steam Assisted Gravity Drainage Process in the Presence of a Water Lag. Presented at the SPE Annual Technical Conference and Exhibition, Houston, TX, 3–6 October. SPE 56545-MS
- Dusseault, B., and Morgensten, R. 1979. Locked Sands. *Q J Eng. Geol*, **12**(2):117-131.
- El Mendili, Y., Abdelouas, A., Bardeau, J. 2014. The Corrosion Behavior of Carbon Steel in Sulfide Aqueous Media at 30° C. *J. of Mater Eng and Perform*, **23**(4):1350-1357.
- Endoh, S. 2006. *Particle Shape Characterization, Powder Technology Handbook* Third Edition. Boca Raton: Taylor and Francis.
- ERCB (2011) OilSands Fact sheets “talk about oil sands”, [www.oilsands.alberta.ca](http://www.oilsands.alberta.ca).
- Fattahpour, V., Moosavi, M., and Mehranpour, M. 2011. An Experimental Rock Mechanics Investigation for Sand Production in Oil Fields. Presented at 45th U.S. Rock Mechanics and Geomechanics Symposium, 26-29 June, San Francisco, California. ARMA-11-591
- Fattahpour, V., Moosavi, M., and Mehranpour, M. 2012a. An Experimental Investigation on the Effect of Rock Strength and Perforation Size on Sand Production. *J. Pet. Sci. Technol.* **86**(2012):172-189
- Fattahpour, V., Moosavi, M., and Mehranpour, M. 2012b. An Experimental Investigation on the Effect of Grain Size on Oil-Well Sand Production. *Pet Sci Technol*, **9** (3):343-353
- Fauré, H., Sardin, M. and Vitorge, P. 1997. Release of clay particles from an unconsolidated clay-sand core: experiments and modeling. *J of Contam Hydrol*, **26**(1-4): 169-178.
- Fermaniuk, B. 2013. *Sand Control in Steam Assisted Gravity Drainage (SAGD) Wellbores and Process of Slotted Liner Design and Process*. Master of Engineering thesis, University of Calgary.
- Fermaniuk, B., Claerhout, M., and Zhu, D. 2015. In-Situ SAGD Thermal-Chemical Effects and Metal-Bond Coated Slotted Liner Design for Enhanced Sand Control, Flow and Long Term Performance. Presented at SPE Thermal Well Integrity and Design Symposium, Banff, AB, 23-25 November. SPE 178465-MS
- Foct, F., Cabrera, J., Dridi, W. et al. 2004. Corrosion behavior of carbon steel in the Tournemire clay. Proceedings of the 2nd International workshop on Prediction of long-term corrosion behavior in nuclear waste systems, Nice, France, 10 p.

- Fonseca, J. 2011. *The Evolution of Morphology and Fabric of a Sand during Shearing*. Ph.D. Thesis, Imperial College London, University of London.
- Fonseca, J. O'Sullivan, C. Coop, M. et al. 2012. Non-invasive Characterization of Particle Morphology of Natural Sands. *Soils and Foundations*. **52**(4):712-722.
- Fountaine R. 1954. Investigation into the mechanism of soil adhesion. *J of Soil Sci*, 5(2):251-263.
- Fukagawa, R., Tamai, T., Tateyama, K. et al. 2002. Basic properties of adhesion between clays and solid surfaces. Proceedings of 2<sup>nd</sup> World Engineering Congress, Geotechnical Engineering & Transportation.
- Furgier, N., Viguerie, B., Aubry, E., et al. 2013. Stand Alone Screens: What Key Parameters are Really Important for a Successful Design? Presented at the European Formation Damage Conference, Scheveningen, The Netherlands, 5-7 June. SPE 165170-MS
- Furui, K. 2004. A Comprehensive Skin Factor Model for Well Completions Based on Finite Element Simulations. Ph.D. Dissertation, Austin, the University of Texas at Austin.
- Furui, K., Zhu, D., Hill, A. et al. 2007. Optimization of Horizontal Well-Completion Design With Cased/Perforated or Slotted Liner Completions. *SPE Prod & Oper*, **22**(2):248-253. *SPE 90579-PA*.
- Gaida, H., Kessel, V., Zimmerle, W. 1985. Geological Parameters of Reservoir Sandstones as Applied to Enhanced Oil Recovery. Presented at the International Symposium on Oilfield Chemistry, Phoenix, AZ, April, 9-11. SPE 13570-MS
- Gamache, D., Kus, J., and Minnich, K. 2012. Process for Solidifying Organic and Inorganic Constituents Contained in Produced Water from Heavy oil Operation. Patent number: WO 2012048217 A2.
- Gaudin, D., Bartier, L., Truche, E. et al. 2013. First corrosion stages in Tournemire claystone/steel interaction: In situ experiment and modeling approach. *Appl Clay Sci*, **83–84**(2013): 457-468.
- Gaudin, S., Gaboreau, E., Tinseau, D. et al. 2008. Mineralogical reactions in the Tournemire argillite after in-situ interaction with steels. *Appl Clay Sci*, **43**(2) :196-207.



- Ghidaglia, C., de Arcangelis, L., Hinch, J. et al. 1996. Transition in Particle Captures in Deep Bed Filtration. *Phys. Rev. E*, **53**: R3028.
- Goodman, W.H, Godfrey, M.R. and Miller, T.M. 2010. Scale and Deposit Formation in Steam Assisted Gravity Drainage (SAGD) Facilities. Presented at the International Water Conference in San Antonio, Texas, 24-28 October.
- Guariguata, A., Pascall, A., Gilmer, W., et al. 2012. Jamming of particles in a two-dimensional fluid-driven flow. *Phys. Rev. E*, **86**(6): 061311.
- Guo, P., and Su, X. 2007. Shear Strength, Interparticle Locking, and Dilatancy of Granular Materials. *Can Geotech J*, **44**(5): 579–591.
- Gupta, S., Fuerstenan, W. and Mika, S. 1975. An investigation of sieving in the presence of attrition. *Powder Technol*, **11**(3), 257-272, 227
- Hallman, T. Yung, B. and Albertson, A. 2015. Analysis of Wellbore Failures and Re-Design of Slotted Liners for Horizontal Wells Applied in a Heavy Oilfield. Presented at the SPE Western Regional Meeting, Garden Grove, California, USA, 27-30 April. SPE 174072-MS.
- Han, G. and Dusseault, M. 2002. Quantitative Analysis of Mechanisms for Water-Related Sand Production. Presented at SPE International Symposium and Exhibition on Formation Damage Control held in Lafayette, Louisiana, 20-21 February. SPE 73737-MS.
- Harris, C., and Odom, C. 1982. Effective Filtration in Completion and other Wellbore Operations Can be Good Investment. *Oil Gas J*, **80**:38-46.
- Head, K. H., and Epps, R. J., 2011. Manual of soil Laboratory testing. Volum II: Permeability, shear strength and compressibility test. 3rd edition. Whittles Publishing, Scotland, UK.
- Herzig, P., Leclerc, M., and Le Goff, P. 1970. Flow of suspension through porous media – application to deep filtration. *Ind Eng. Chem*, **62**(5): 8-35.
- Hill, R. 2012. Thermal in Situ Water Conservation Study, a Summary Report, Jacobs Consultancy.
- Hodge, R., Burton, R., Constien, V. et al. 2002. An Evaluation Method for Screen-Only and Gravel-Pack Completions. Presented at International Symposium and Exhibition on Formation Damage Control, 20-21 February, Lafayette, Louisiana. SPE-73772-MS.

- Holtz, D. Kovacs, D. and Sheahan, T. 2010. *An Introduction to Geotechnical Engineering*, 2<sup>nd</sup> edition. Prentice Hall.
- Holtz, R. D., and Kovacs, W. D., 1981. *Introduction to Geotechnical Engineering*. Prentice Hall.
- Illfelder, H. Forbes, E. McElhinney G. et al. 2011. A Systematic Approach for Wellbore Drilling and Placement of SAGD Well Pairs and Infill Wells. Presented at the World Heavy Oil Congress, Edmonton, Alberta, Canada, 14-17 March. WHOC11-503.
- Ives, J. 1987. Filtration of clay suspensions through sand. *Clay Miner*, **22** (1987) :49–61.
- Janda, A., Zuriguel, I., Garcimartian, A. 2008. Jamming and critical outlet size in the discharge of a two-dimensional silo. *Europhysics Letters*, **84**(4):44002.
- Jeannin, M., Calonnec, D., Sabot, R. et al. 2010. Role of a clay sediment deposit on the corrosion of carbon steel in 0.5 mol L<sup>-1</sup> NaCl solutions. *Corros Sci*, **52**(6):2026-2034.
- Jin, Y., Chen, J., Chen, M. et al. 2012. Experimental study on the performance of sand control screens for gas wells. *J Petr Explor and Prod Technol*, 2(1):37-47.
- Kaiser, T., Wilson, S., and Venning, L. 2000. Inflow Analysis and Optimization of Slotted Liners. Presented at the International Conference on Horizontal Well Technology, Calgary, Alberta, 6-8 November. SPE-65517-MS.
- Kenney, C., and Lau, D. 1985. Internal Stability of Granular Filters. *Can Geotech J*, **22**(2): 215–225.
- Khilar, C., Folger, S., and Ahluwalia, S. 1983. Sandstone Water Sensitivity: Existence of a Critical Rate of Salinity Decrease for Particle Capture. *Chem Eng Sci*, **38**(5):789-800.
- Khilar, C., Vaidya, N. and Folger, S. 1990. Colloidally-induced Fines Release in Porous Media. *J Pet Sci Eng*, **4**(3): 213-221.
- Khilar, K., and Fogler, H. 1984. The Existence of a Critical Salt Concentration for Particle Release. *J Coll Interface Sci*, **101**(1): 214–224.
- Khilar, K., and Fogler, H. 1998. *Migrations of Fines in Porous Media*. Dordrecht: Kluwer Academic Publishers.
- Kia, S.F., Fogler, H.S., Reed, M.G. and Vaidya, R.N. 1987. Effect of Salt Composition on Clay Release in Berea Sandstone. *SPE Prod Eng*, **2**(4): 277–283.

- Kobbe, H., 1917. Petroleum Connected with the Recovery of Petroleum from Unconsolidated Sands. Presented at the SPE NEW York Meeting, New York, New York, USA, February 1917. SPE 917799-G.
- Koch, K. Kemna, A. Irving, J. et al. 2011. Impact of Changes in Grain Size and Pore Space on the Hydraulic Conductivity and Spectral Induced Polarization Response of Sand. *Hydrol Earth Syst Sci*, **15**(6): 1785–1794.
- Kooistra, A., Verhoef, P., Broere, W. et al. 1998. Appraisal of stickiness of natural clays from laboratory tests. Proceedings of the National Symposium on Engineering Geology and Infrastructure, Delft, Netherland.
- Kovacs, G. 1981. *Seepage Hydraulics, Developments in Water Science*. Amsterdam: Elsevier Science Publishers.
- Krinsley, D.H., and Donahue, J., 1968. Environmental Interpretation of Sand Grain Surface Textures by Electron Microscopy. *Geological Society of America Bulletin*, **79**:743.
- Krinsley, D.H., and Takahashi, T., 1962. Applications of Electron Microscopy to Geology. *N. Y. Acad Sci Trans*, **25**:3-22.
- Krueger, R.F., Vogel, L.C., and Fischer, P.W. 1967. Effect of Pressure Drawdown on Clean-Up of Clay or Silt Blocked Sandstone. *J Pet Technol*, **19**:397-403.
- Krumbein, C., and Sloss, L. 1963. *Stratigraphy and Sedimentation*, 2<sup>nd</sup> edition, San Francisco: Freeman and Company.
- Ladd, S. 1978. Preparing Test Specimen Using Under Compaction, *Geotech Testing J*, **1**(1):16-23.
- Lafata, L., 2014. Effect of Particle Shape and Size on Compressibility Behavior of Dredged Sediment in a Geotextile Tube Dewatering Application. *Syracuse University Honors Program Capstone Projects*. Paper 757.
- Lafond, G., Gilmer, W., Koh, C. et al. 2013. Orifice jamming of fluid-driven granular flow. *Phys Rev. E* **87**(4): 042204.
- Lee, A., Wong, K., & Dudley, W. 2008. Evaluation of Screen Integrity in Horizontal Open-Hole Screen Completions-A Numerical Approach. This paper was prepared for presentation at the

42nd US Rock Mechanics Symposium and 2nd U.S.-Canada Rock Mechanics Symposium, held in San Francisco, June 29- July 2.

Leone, J.A., and Scott, M.E. 1988. Characterization and Control of Formation Damage During Water flooding of a High Clay-Content Reservoir. *SPE Reserv Eng*, **3**(4):1279-86.

Liu, J., Xu, Z., Masliyah, J. H. 2005. Interaction Forces in Bitumen Extraction from Oil Sands. *J Colloid Interface Sci*, **287**(2):507–520.

Louvet, N., Höhler, R. and Pitois, O. 2010. Capture of particles in soft porous media. *Phy. Rev.*, **82**(041405):1-5

Markestad, P., Christie, O., Espedal. A. et al. 1996. Selection of Screen Slot Width to Prevent Plugging and Sand Production. Presented at the SPE Formation Damage Control Symposium. Lafayette. Louisiana. USA. 14-15 February. SPE-31087-MS.

Mathisen, A.M, Aastveit, G.L., and Alteras, E. 2007. Successful Installation of Standalone Sand Screen in More Than 200 Wells-The Importance of Screen Selection Process and Fluid Qualification. Presented at the European Formation Damage Conference, Scheveningen, The Netherlands, 30 May-1 June. SPE 107539-MS

McDowell-Boyer, L., Hunt, J. and Sitar, N., 1986. Particle Transport Through Porous Media. *Water Resour. Res.*, **22**(13): 1901-1921.

McGuire, L., and Chatham, Jr. 2005. Low Salinity Oil recovery: An Exciting New Opportunity for Alaska's North Slope. Presented at the Western Regional Meeting. Irvine, California, 30 March–1 April. SPE93903

Meza, B., Tremblay, and B., Doan Q. 2003. Mechanisms of Sand Production through Horizontal Well Slots in Primary Production. *J Can Pet Technol*, **42**(10): 36-46

Meza, B., Tremblay, B., and Doan, Q. 2002. Visualization of Sand Structures Surrounding a Horizontal Well Slot During Cold Production. Presented at the SPE International Thermal Operations and Heavy Oil Symposium and International Horizontal Well Technology Conference, Calgary, AB, November 4-7. SPE 79025-MS

Mitchell, J. and Soga K. 2005. *Fundamentals of Soil Behavior*. Hoboken, NJ: John Wiley & Sons Inc.

Miura, K. Maeda, K. and Toki, S. 1997. Methods of Measurement for the Angle of Repose of Sands. *Soils and Found.* **37**(2): 89-96.

Mohan K.K. and H.S. Folger. 1997. Colloidally Induced Smectitic Fines Migration: - Existence of Microquakes. *AIChE J.* **43** (3): 556-576.

Mohan K.K., Vaidya R.N., Reed M.G. and Fogler H.S. 1993. Water Sensitivity of Sandstones Containing Swelling and Non-swelling Clays. *Colloids Surf A: Physicochem. Eng. Aspects.* **73** (1993):237-254.

Mondal, S. Sharma, M. Hodge, R. et al. 2011. Numerical simulation of Sand Screen Performance in Stand Alone Application. *SPE Drill and Compl.* **26**(4): 472-483. SPE- 134326-PA.

Mondal, S., Sharma, M., Hodge, R. et al. 2012. A new method for the Design and Selection of Premium/Woven Sand Screen. *SPE Drill and Compl.* **27**(3): 407-416. SPE- 146656-PA.

Mondal, S., Wu, H., Sharma, M. et al. 2014. Characterizing, Designing, and Selecting Metal Mesh Screens for Standalone Screen Applications. Presented at SPE Annual Technical Conference and Exhibition held in Amsterdam, The Netherland, 27-29 October. SPE 170935-MS

Muecke, T.W. 1979. Formation Fines and Factors Controlling Their Movement in Porous Media. *J Pet Technol*, **31**:144-150.

Mukunoki, T., Miyata, Y., Mikami, K. et al. 2016. X-ray CT analysis of pore structure in sand. *Solid Earth Discuss*, **7**(2016):929–942.

Mungan, N. 1965. Permeability Reduction through Changes in pH and Salinity. *J Petrol Technol*, **17**(12): 1449-53.

Nabawy, B., Géraud, Y. Rochette, P. et al. 2009. Pore-throat Characterization in Highly Porous and Permeable Sandstones, *AAPG Bull.*, **93**(6):719–739.

Narayan, R., Coury, R., Masliyah, H. et al. 1997. Particle capture and plugging in packed-bed reactors. *Ind Eng. Chem Res*, **36**(11): 4620-4627.

Nouri, A., Vaziri, H., Kuru, E. et al. 2005. A Comparison of Two Sanding Criteria in Physical and Numerical Modeling of Sand Production. *J Petrol Sci Eng*, **50**():55-70.

O'Hara, M. 2015. Thermal Operations in The McMurray; An Approach To Sand Control. Presented at SPE Thermal Well Integrity and Design Symposium, Banff, AB, 23-25 November. SPE 178446-MS

- Odong, J. 2008. Evaluation of Empirical Formulae for Determination of Hydraulic Conductivity Based on Grain-Size Analysis. *J Am Sci*, **3**(4): 105-113.
- Papamichos, E., Cerasi, P., Stenebraten, J.F. et al. 2010. Sand Production Rate Under Multiphase Flow and Water Breakthrough. Presented at 44th U.S. Rock Mechanics Symposium and 5th U.S.-Canada Rock Mechanics Symposium, 27-30 June, Salt Lake City, Utah. ARMA 10-340
- Papamichos, E., Stenebråten, J., Cerasi, P. et al. 2008. Rock Type and Hole Failure Pattern Effects on Sand Production. Presented at The 42nd U.S. Rock Mechanics Symposium (USRMS), 29 June-2 July, San Francisco, California. ARMA 08-217.
- Pedenaud, P., and Michaud, P. 2009. Silica Inhibition and Blowdown Evaporation Process. Patent number: WO 2009071981 A2.
- Peterson, D. 2007. Guidelines for Produced Water Evaporators, Presented at SAGD 68th Annual International Water Conference 2007, Orlando, Florida, USA, 21-25 October.
- PetroWiki. 2013. Slotted liners and wire wrapped screens. [http://petrowiki.org/Slotted\\_liners\\_and\\_wire\\_wrapped\\_screens](http://petrowiki.org/Slotted_liners_and_wire_wrapped_screens) (accessed 5 June 2016).
- Pittman, E.D. 1992. Relationship of Porosity and Permeability to Various Parameters Derived from Mercury Injection-Capillary Pressure Curves for Sandstone. *AAPG Bull.*, **76**(5):191-198.
- Pittman, E.D. 2001. Estimating Pore Throat Size in Sandstones from Routine Core-Analysis Data. Search and Discovery Article #40009.
- Porter, J.J., 1962. Electron Microscopy of Sand Surface Texture. *J Sediment Petrol*, **32**:124–135.
- Porubcan, A. and Xu, S. 2011. Colloid straining within saturated heterogeneous porous media. *Water Res*, **45**(4):1796-1806.
- Powers, M.C. 1953. A New Roundness Scale for Sedimentary Particles. *J Sediment. Res*, **23** (2): 117–119.
- Prins, J. 2003. *Suspended Material in Abstracted Groundwater in the Netherlands*. M.Sc. Thesis, Utrecht University, Utrecht.
- Procyk, A., Gou, X., Marti, S. et al. 2015. Sand Control Screen Erosion: Prediction and Avoidance. Presented at the SPE Annual Technical Conference and Exhibition, Houston, TX, 28-30 September. SPE 174837-MS

- Procyk, A., Whitlock, M., AIL S. 1998. Plugging-Induced Screen Erosion Difficult to Prevent, Oil and Gas Journal, July 20.
- Qi, G. 2004. *Study on sand controls mechanism and application of coated sand*. Ph.D. thesis, Southwest Petroleum University, Chengdu.
- Ramachandran, V., and Fogler, S. 1999. Plugging by hydrodynamic bridging during the flow of stable colloidal particles within cylindrical pores. *J. Fluid Mech*, **385**: 129-156.
- Rege, D. and Fogler, S. 1987. A network model for straining dominated particle entrapment in porous media. *Chem Eng Sci*, **42**(7):1553-1564.
- Retsch. 2005. Particle Analyzer CAMSIZER XT, Particle Size and Particle Shape Analysis with Dynamic Image Analysis. [www.retsch-technology.com](http://www.retsch-technology.com)
- Rodriguez, J. 2013. *Importance of the Particle Shape on Mechanical Properties of Soil Materials*. Ph.D. thesis, Luleå University of Technology, Sweden.
- Romanova, U., and Ma, T. 2013. An Investigation on the Plugging Mechanisms in a Slotted Liner from the Steam Assisted Gravity Operations. Presented at the SPE European Formation Damage Conference, Noordwijk, The Netherland, 5-7 June. SPE 165111-MS
- Romanova, U., Gillespie, G., Sladic, J. et al. 2014. A Comparative Study of Wire Wrapped Screens vs. Slotted Liners for Steam Assisted Gravity Drainage Operations. Presented at the World Heavy Oil Congress 2014, New Orleans, USA, March 5-7, 2014. Paper WHOC14-113
- Romanova, U., Ma T., Piwowar, M. et al. 2015b. Thermal Formation Damage and Relative Permeability of Oil Sands of the Lower Cretaceous Formations in Western Canada. Presented at SPE Canada Heavy Oil Technical Conference, 9-11 June, Calgary, Alberta, Canada. SPE-174449-MS.
- Romanova, U., Piwowar, M., and T., Ma. 2015. Sand Control for Unconsolidated Heavy Oil Reservoirs: A Laboratory Test Protocol and Recent Field Observation. Presented at the International Symposium of the Society of Core Analysts. St. John, New Founland, Canada, 16-21 August. SCA2015-055
- Sacramento, R., Yang, Y., You, Z. et al. 2015. Deep bed and cake filtration of two-size particle suspension in porous media. *J Petrol Sci Eng*, **126**(2015):201-210.

- Santamarina, C. 2002. Soil Behavior at the Microscale: Particle Forces. *Proc.*, ASCE Soil Behavior and Soft Ground Construction. **119**: 25–56.
- Santamarina, C. and Cho, C. 2004. Soil behavior: The role of particle shape. *Proc.*, Skempton Conference. London, 604-617.
- Santamarina, C., and Cascante, G. 1998. Effect of Surface Roughness on Wave Propagation Parameters. *Geotechnique*, **48**(1):129-136.
- Saraf, S. and Franklin, S. 2011. Power-law flow statistics in anisometric (wedge) hoppers. *Physical Review E*, **83**(3):1-4.
- Satomi, T., Nihei H. and Takahashi, H. 2012. Investigation on Characteristics of Soil Adhesion to Metallic Material Surface and Soil Animal's Cuticle. Proceedings of the 15th International Conference on Experimental Mechanics. Paper Ref: 2634
- Schulien, S., Ovsthus, J., Hestenes, A. et al. 1997. Scale Formation and Treatment in and around Sand Control Screens. Presented at the SPE International Symposium on Oilfield Chemistry, Houston, TX, 18-21 February. SPE 37305-MS
- Sharp, K.V., and, Adrian, R.J. 2005. On Flow-Blocking Particle Structures in Microtubes. *Microfluid Nanofluid*, **1**(4): 376-380.
- Sheng, J.J. 2014. Critical Review of Low-salinity Water Flooding. *J Pet Sci Eng*, **120**(2014): 216–224.
- Simon, D.E., McDaniel, B.W. and Coon, R.M. 1976. Evaluation of Fluid pH Effects on Low Permeability Sandstone. Presented at the 1976 SPE Annual Technical Conference and Exhibition, New Orleans, 3-6 October. SPE 6010
- Slack, W. Roggensack, D. Wilson, G. et al. 2000. Thermal-Deformation-Resistant Slotted-Liner Design for Horizontal Wells. Presented at the International Conference on Horizontal Well Technology, Calgary, Alberta, 6-8 November. SPE 65523-MS.
- Slyter, G. Byrne, T. McPhee, A. et al. 2008. Sand Control Design: What Are We Sure Of? Presented at SPE Asia Pacific Oil and Gas Conference and Exhibition, Perth October 2008. SPE 114781-MS.



Sparks, B. D., Kotlyar, L. S., O'Carroll, J. B., et al. 2003. Athabasca Oil Sands: Effect of Organic Coated Solids on Bitumen Recovery and Quality. *J Pet Sci Eng*, **39**(3-4):417-430.

Stahl, R., Smith, J., Hobbs, S. et al. 2014. Application of Intelligent Well Technology to an SAGD Producer: Firebag Field Trial. Presented at the SPE Heavy Oil Conference, Calgary, Alberta, 10-12 June. SPE 170153-MS.

Strobl, R. Fustic, M. Jablonski, B. et al. 2014. Production from SAGD pads vs. SAGD well pairs: the role of conductive heating and infill drilling on ultimate recovery. Presented at the Geoconvention, Calgary, Alberta.

Sukumaran, B., and Ashmawy, A.K. 2001. Influence of Inherent Particle Characteristics on the Strength Properties of Particulate Materials. Annual International Society of Offshore and Polar Engineering Conference, Oslo, Norway.

Suman, G., Ellis, R., and Snyder, R. 1985. Sand Control Handbook. *Houston: Gulf publishing company*.

Surmont Oil sand Project, 2013. Annual Surmont SAGD Performance Review Approvals 9426 and 11596 Surface Operations. Calgary, Alberta, Canada

Sympatec. 2009. Particle Size Analysis and Shape Evaluation with high-speed Dynamic Image Analysis (DIA). [www.sympatec.com](http://www.sympatec.com).

Tang, G.Q. and Morrow, N.R. 1999. Influence of Brine Composition and Fines Migration on Crude/oil/rock Interactions and Oil recovery. *J Pet Sci Eng*, **24**(2-4):99-111.

Tang, Y., Ozkan, E., Kelkar, M. et al. 2000. Performance of Horizontal Wells Completed with Slotted Liners and Perforations. Presented at the International Conference on Horizontal Well Technology, Calgary, Alberta, 6-8 November. SPE 65516-MS

Taniguchi, N., Honda, A. and Ishikawa, H. 1997. Experimental investigation of passivation behavior and corrosion rate of carbon steel in compacted bentonite. *Mat Res Soc Symp Proc*, **506**: 495-501.

Teeters, D., Andersen, M. A., and Thomas, D. C. 1989. Formation Wettability Studies that Incorporate the Dynamic Wilhelmy Plate Technique. In *Oil Field Chemistry*; Borhardt, J., Yen, T. F., Eds.; American Chemical Society: Washington, D.C., 1989; ACS Symposium Series, Vol. 396, Chapter 31, pp 560-576.

- Terzaghi, K., 1920. Old Earth Pressure Theories and New Test Results. *Engineering News Record*, **85**(14): 632-637.
- Tien, C., and Ramarao, B. 2011. Revisiting the laws of filtration: An assessment of their use in identifying particle retention mechanisms in filtration. *J of Membr Sci*, **383**(1-2):17-25.
- Tiffin, L., King, E., Larease, E. et al. 1998. New Criteria for Gravel and Screen Selection for Sand Control. Presented at the SPE Formation Damage Control Conference Lafayette, Louisiana, USA, 18–19 February. SPE 39437-MS
- To, K. and Lai, Y. 2002. Jamming pattern in a two-dimensional hopper. *Phys Rev E*, **66**(1):1-8.
- To, K., Pik-Yin, L. and K. Pak. 2001. Jamming of granular flow in a two-dimensional hopper. *Phys Rev Lett*, **86**(1):71-74.
- To, K. 2002 Gravity Driven Granular Steady State Flows in Two-Dimensional Hoppers and Silos. *Modern Phys Lett B*, **19**(30):1751-1766.
- Tran, V., Civan, F., and Robb, I. 2009. Correlating flowing time and condition for perforation
- Tronvoll, J., Kessler, N., Morita, N. et al. 1993. The Effect of Anisotropic Stress State on the Stability of Perforation Cavities. *Int J Rock Mech Min Sci*, **30** (7):1085–1089.
- Tronvoll, J., Skjaerstein, A., and Papamichos, E. 1997. Sand production: mechanical failure or hydrodynamic erosion. *Int J Rock Mech Min Sci*, **34** (3-4):291.
- Uno, T., Kamiya, K., and Tanaka, K. 1998. The Distribution of Sand Void Diameter by Air Intrusion Method and Moisture Characteristic Curve Method. *J Japan Society of Civil Eng*, **603**(III-44):35-44.
- Urios, L., Marsal, F., Pellegrini, D. et al. 2011. Microbial diversity of the 180 million-year-old Toarcian argillite from Tournemire, France. *Appl Geochem*, **27**(7): 1442-1450.
- Vaidya, N., and Fogler, S. 1992. Fines Migration and Formation Damage: Influence of pH and Ion Exchange. *SPE Prod Eng*, **7**(4): 325–330.
- Vaidya, R.N., and Fogler, H.S. 1990. Formation Damage due to Colloidally Induced Fine Migration. *Colloids and Surfaces*. **50**(1990): 215-229.
- Valdes, J. 2002. *Fines migration and formation damage-microscale studies*. Ph.D. dissertation, Georgia Institute of Technology, Atlanta, Ga.

- Valdes, J. and Santamarina, C. 2006. Particle clogging in radial flow: microscale mechanisms. *SPE J*, **11**(2): 193–198.
- Vallejo, L. E., 1995. Fractal Analysis of Granular Materials. *Geotechnique*, **45**(1):159-163.
- Van Oort, E., van Velzen, G., and Leerlooijer, K. 1993. Impairment by Suspended Solids Invasion: Testing and Prediction. *SPE Prod & Fac*, **8**(3): 178-184.
- Vaziri, H., Barree, B., Xiao Y. et al. 2002. What is the Magic of Water in Producing Sand?. Presented at SPE Annual Technical Conference and Exhibition held in San Antonio, Texas, 29 September. SPE 77683-MS.
- Veeken, C.A.M., Davies, D.R., Kenter, C.J. et al. 1991. Sand Production Prediction Review: Developing an Integrated Approach. Presented at the SPE Annual Technical Conference and Exhibition, 6-9 October, Dallas, Texas. SPE-22792-MS.
- Vitthal, S., and Sharma, M. 1992. A Stokesian Dynamics Model for Particle Deposition and Bridging in Granular Media. *J Colloid Interface Sci*, **153**(2): 314-336.
- Vukovic, M., and Soro, A. 1992. *Determination of Hydraulic Conductivity of Porous Media from Grain Size Composition*, Littleton, Colorado: Water Resources Publications.
- Wadell, H. 1932. Volume, shape and roundness of rock particles. *J Geol*, **40**: 443-451.
- Wakeman, R. 2007. The influence of particle properties on filtration. *Separation and Purification Technology*, **58**(2): 234-241.
- Wan, R., Wang, J. 2004. Analysis of Sand Production in Unconsolidated Oil Sand Using a Coupled Erosional-Stress-Deformation Model, *J Can Pet Technol*, **43**(2): 45-52.
- Weatherford International, 2010. Sand Screen Selector, [www.weatherford.com](http://www.weatherford.com)
- Wen, B. Aydin, A. and Aydin-Duzgoren, S. 2002. A Comparative Study of Particle Size Analysis by Sieve-hydrometer and Laser Diffraction Method. *Geotech. Test. J*, **25**(4):434-442.
- Wentworth, C., 1919. A Laboratory and Field Study of Cobble Abrasion. *J Geol*, **XXVII**:507.
- Wenzel, R. N. 1936. Resistance of Solid Surfaces to Wetting by Water. *Ind Eng. Chem Res*, **28**(1936):988.

Williams, F., Richard, M., and Horner, D. 2006. A New Sizing Criterion for Conformable and Nonconformable Sand Screens Based on Uniform Pore Structures. Presented at the SPE Formation Damage Control Symposium, Lafayette, Louisiana, USA. 15-17 February. SPE 98235-MS

Williamson, H., Babaganov, A., Romanova, U. 2016. Unlocking Potential of the Lower Grand Rapids Formation, Western Canada: The Role of Sand Control and Operational Practices in SAGD Performance. Presented at the SPE Canada Heavy Oil Technical Conference, 7-9 June, Calgary, Alberta, Canada, SPE-180700-MS.

Wu, B., and Tan, C. 2001. Effect of water-cut on sandstone strength and implications in sand production prediction. Presented at the 38th U.S. Rock Mechanics Symposium, Washington, D.C., USA, July 7-10. ARMA-01-0027

Wu, B., Tan, C., and Lu, N. 2005. Effect of Water-Cut on Sand Production - An Experimental Study. Presented at the SPE Asia and Pacific Oil and Gas Conference and Exhibition, Jakarta, Indonesia, 5-7 April. SPE 92715-MS

Wyss, M., Blair, L., Morris, F. et al. 2006. Mechanism for clogging of microchannels. *Phys. Rev. E* **74**: 061402.

Xie, J. 2015. Slotted Liner Design Optimization for Sand Control in SAGD Wells. Presented at the SPE Thermal Well Integrity and Design Symposium, Banff, Alberta, 23-25 November. SPE 178457-MS

Xie, J. Jones, C. Matthews, B. et al. 2006. Slotted Liner Design for SAGD Wells. Presented at the First World Heavy Oil Conference, Beijing, China, November 12-15.

Xie, Y., Chen, Z. and Sun, F. 2014. Particles migrating and plugging mechanism in loosen sandstone heavy oil reservoir and the strategy of production with moderate sanding. Presented in 5<sup>th</sup> International Conference on Porous Media and Their Applications in Science, Engineering, and Industry, June 22-27, Kona, Hawaii.

Yamamuro, J. and Wood, F. 2004. Effect of Depositional Method on the Undrained Behavior and Microstructure of Sand with Silt. *Soil Dyn Earthq Eng*, **24**:751–760.

Yan, M., Sun, C., Dong, J. et al. 2015. Electrochemical investigation on steel corrosion in iron-rich clay. *Corros Sci*, **97**(2015) :62-73.

Younessi, A., Rasouli, V., and Wu, B. 2012. Proposing a Sample Preparation Procedure for Sanding Experiments. Presented at Southern Hemisphere International Rock Mechanics Symposium, May 14-17, Sun City, South Africa.

Zamani, A., Brij, M. 2009. Flow of dispersed particles through porous media Deep bed filtration. *J Petrol Sci Eng*, **69**(1-2):71-88.

Zhang, K. Chanpura, A. Mondal, S. et al. 2014. Particle Size Distribution Measurement Techniques and Their Relevance or Irrelevance to Sand Control Design. Presented at SPE International Symposium and Exhibition on Formation Damage Control, 26-28 February, Lafayette, Louisiana, USA. SPE-168152-MS.

Zhuang, J., Jin, J., and Flury, M. 2004. Comparison of Hanford colloids and kaolinite transport in porous media. *Vadose Zone J*, **3**(2):395–402.

Zuriguel, I., Pagnaloni, L., Garcimartian, A. et al. 2003. Jamming during the discharge of grains from a silo described as a percolating transition. *Phys Rev E*, **68**(3):2-5.

Zuriguel, I., Garcimaein, A., Maza, A. et al. 2005. Jamming during the discharge of granular matter from a silo. *Phys Rev E*, **71**(5):051303.

## APPENDIX A: CURRENT INDUSTRIAL DESIGN PROCEDURES

Proposed slotted liner design model for slot size, density, and profile by Fermaniuk (2013) is outlined in this appendix.

### *A.1 Slot Width*

To illustrate the current industrial approach, we use the PSDs reported by Abram and Cain (2014) for Pike I project. These PSDs are based on the upper and lower limit for four PSD classes from the core samples obtained from wells in the McMurray Formation (**Figure A-1**). Class I is very fines sand to fine sand with high clay contents ranging from the lower limit (DC-I LL) with fines content of 37.5% (high content of silt size and clay size particles) to 8.5% for upper limit (DC-I UL). Such layers with PSD within DC-I class typically have lower oil contents and lower permeability (Carrigy, 1966). Class II is ranging from very fine sand to medium sand with less fines content. Class III is ranging from fine sand to medium sand with lower fines content and higher permeability. Class IV is ranging from medium sand to coarse sand with low fines content.

The necessary input data for the model include the D<sub>10</sub>, D<sub>40</sub>, D<sub>50</sub>, D<sub>70</sub>, D<sub>90</sub>, D<sub>95</sub>, the fines content (<44µm), and clay contents (<5µm). **Table A-1** summarizes the D values, fines content, and clay contents for the four classes of PSD in McMurray Formation.

Similar to the semi-empirical relationship developed by Markestad et al. (1996), a series of slot width was defined by Fermaniuk (2013) based on the field experience of RGL Reservoir Management Inc. which range from a maximum slot width to a minimum slot width as follow:

$$\text{Max. SW} = 3.5D_{50}$$

The minimum slot width:

$$\text{Min. SW} = 2.00D_{70}$$

The Average Slot Width (ASW) is defined as the estimate of the slot width required to prevent sand production from the reservoir. Fermaniuk (2013) proposed four values of the ASW:

$$\text{ASW}_1 = 2.00D_{10}$$

$$\text{ASW}_2 = 1.50D_{10}$$

$$\text{ASW}_3 = 1.36D_{10}$$

$$ASW3 = 2.29D_{50}$$

The model also uses the fines content (<44  $\mu\text{m}$ ) and clay content (<5  $\mu\text{m}$ ) to design the profile of the slot.

The values of these slot width are summarized in **Table A-2**. **Figure A-2** shows the slot window model for the four classes of McMurray formation; based on this slot window and the frequency and extent of each sand facies, one could define a series of slot widths that would be appropriate for the PSDs along the well. Solid horizontal lines in **Figure A-2** show the possible best-fit slot width for the slot window. The lower slot width is expected to result in less sand production and as the upper sand window is approached, there is a higher potential of sanding.

### ***A.2 Slot Profile***

Choosing between straight or seamed slot is based on the fines and clays contents within the reservoir sand samples. A seamed slot is required if the amount of fines and clays is larger than 5.5%. **Table A-2** shows the slot profile suggestion for the PSD classes in the McMurray Formation.

### ***A.3 Slot Density***

Fermaniuk (2013) suggested that there is an optimum ratio of slot density to produced fluids rate which is established by the balance between the inflow capability and inflow induced plugging. The optimum slot density depends on the length of the wellbore, production rate variability, plugging effects, and phases produced. From observations of slotted liners, the optimum slot density ( $SD_{opt.}$ ) at a given liquid production rate for a minimum flow velocity and volume of fluid to the slot defined by Fermaniuk (2013) as:

$$SD_{opt.} = 0.505 \frac{Q_{J_1}}{VLS_1}$$

where  $Q$  is the fluid production rate (bbl/day),  $J_1$  is the joint length (m),  $V$  is the volumetric flow rate per slot (L/hr/slot),  $L$  is the horizontal length (m), and  $S_1$  is the slotted portion per joint (m). A flow rate between 40-160 ml/hr/slot is identified by experimental tests as the optimum range for the flow in each slot that minimizes the pressure drop and plugging of the slot and near wellbore region.

To accommodate possible plugging of the slot over time, the optimum slot density is multiplied by a slot plugging factor, which is typically ranging from 2 to 9.

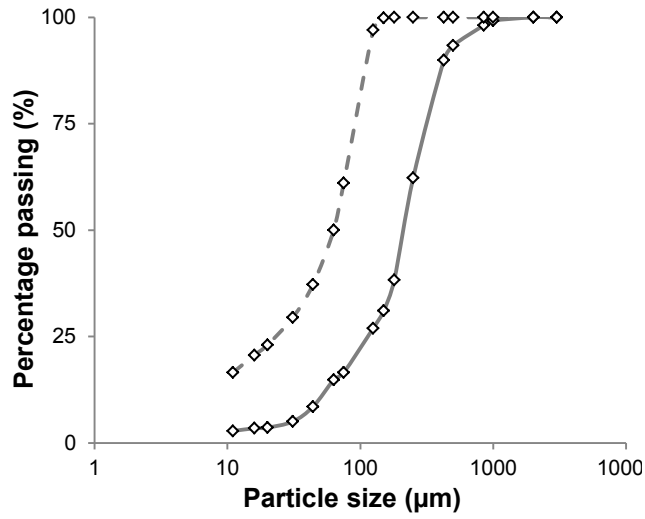


**Table A-1. Input parameters from the PSD curve into slot size model**

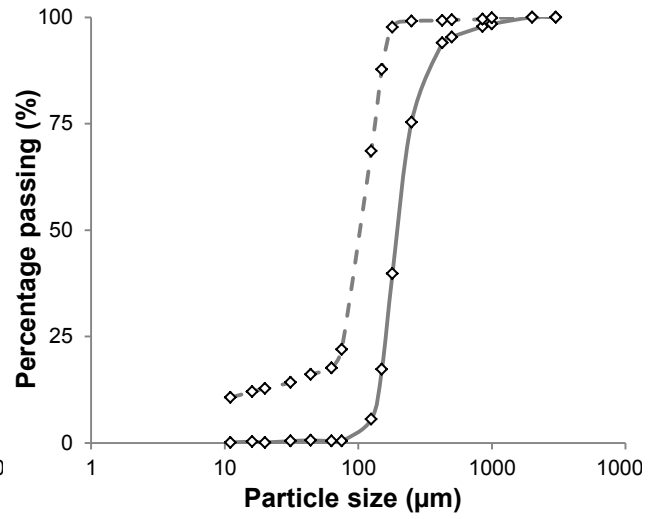
	DC-I LL	DC-I UL	DC-II LL	DC-II UL	DC-III LL	DC-III UL	DC-IV LL	DC-IV UL
<b>D10</b>	114.3	426.7	157.5	388.6	304.8	932.2	607.1	1785.6
<b>D40</b>	73.7	243.8	116.8	218.4	200.7	391.2	350.5	1140.5
<b>D50</b>	63.5	213.4	104.1	200.7	180.3	348.0	292.1	942.3
<b>D70</b>	33.0	142.2	83.8	167.6	134.6	264.2	134.6	652.8
<b>D90</b>	7.6	48.3	10.2	134.6	25.4	185.4	45.7	411.5
<b>D95</b>	5.1	38.1	5.1	68.6	15.2	68.6	38.1	375.9
<b>UC</b>	11.20	5.01	11.24	1.64	8.06	2.12	7.78	2.77
<b>SC</b>	23.06	11.39	27.02	5.62	21.55	13.49	16.00	4.76
<b>Fines content</b>	37.5%	8.5%	16.1%	0.6%	15.2%	0.4%	10.5%	0.5%
<b>Clays content</b>	17.5%	5.9%	8.8%	0.3%	7.8%	0.1%	5.5%	0.1%

**Table A-2. Slot model for the four class of sand of the McMurray Formation**

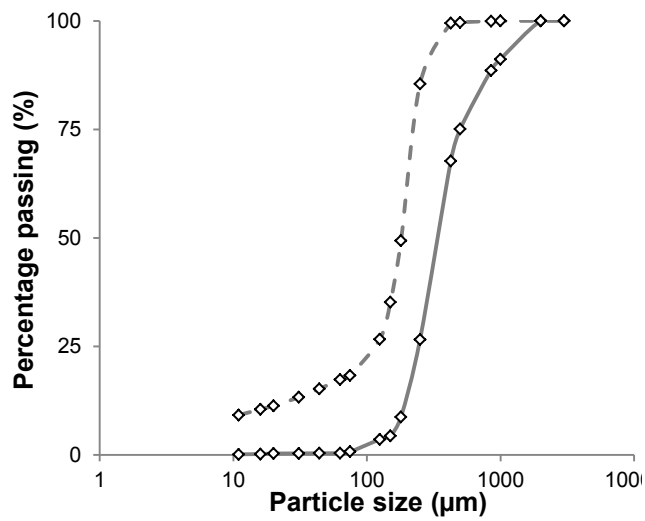
<b>Max. : 3.50D50</b>	0.009	0.029	0.014	0.028	0.025	0.040	0.040	0.040
<b>ASW1: 2.00D10</b>	0.009	0.034	0.012	0.031	0.024	0.040	0.040	0.040
<b>ASW2: 1.50D10</b>	0.007	0.025	0.009	0.023	0.018	0.040	0.036	0.040
<b>ASW3: 1.36D10</b>	0.006	0.023	0.008	0.021	0.016	0.040	0.033	0.040
<b>ASW4: 2.29D50</b>	0.006	0.019	0.009	0.018	0.016	0.031	0.026	0.040
<b>Min. : 2.00D70</b>	0.003	0.011	0.007	0.013	0.011	0.021	0.011	0.040
<b>Seaming required?</b>	Seamed slot required	Seamed slot required	Seamed slot required	Straight slot	Seamed slot required	Straight slot	Seamed slot required	Straight slot



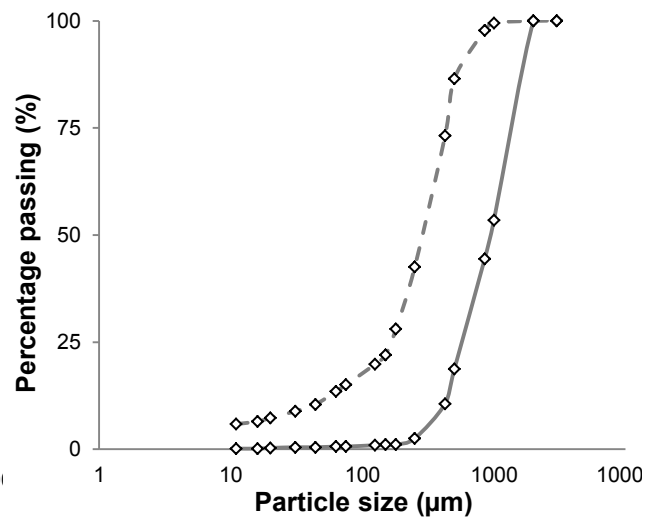
(a)



(b)



(c)



(d)

Figure A-1. Particle size distribution of oil sands categorized by Abram and Cain (2014); Solid lines show the upper limit of their set of PSD and dashed lines show the lower limit of their PSD in each class. Graphs show (a) the upper and lower ranges of DC-I, (b) the upper and lower range of DC-II, (c) the upper and lower range of DC-III, and (d) the upper and lower range of DC-IV

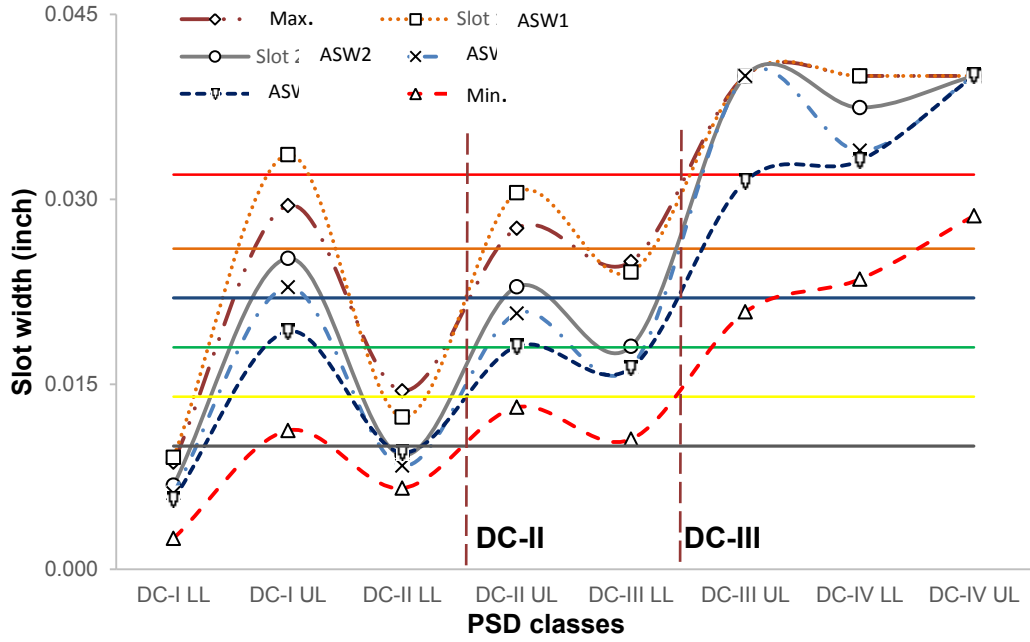


Figure A-2. Slot window model for the different classes proposed by Abram and Cain (2014)